Interfacial skew tunneling in group III-V and group IV semiconductors driven by exchange and spin-orbit interactions; Study in the frame of an extended k.p theory

Thi Huong Dang

NNT : 2016SACLX089

THESE DE DOCTORAT
DE
L'UNIVERSITE PARIS-SACLAY
PREPAREE A
L'ECOLE POLYTECHNIQUE
PREPARATION DE LA THESE"

ECOLE DOCTORALE INTERFACES N° 573

Spécialité de doctorat (Physique)

Par

Dang Thi Huong

Interfacial skew tunneling in group III-V and group IV semiconductors driven by exchange and spin-orbit interactions; Study in the frame of an extended k.p theory

Thèse présentée et soutenue au Laboratoire des Solides Irradiés, 09 Novembre 2016

Composition du Jury :

M. Amand Thierry	LPCNO CNRS-INSA Toulouse	Président
M. Jancu Jean-Marc	Universités INSA Rennes	Rapporteur
M. Bihlmayer Gustav	Forschungszentrum Jülich	Rapporteur
M. Fabian Jaroslav	University of Regensburg	Examinateur
M. Glazov Mikhail	Ioffe Physical-Technical Institute	Examinatrice
M. Drouhin Henri-Jean	Ecole Polytechnique	Directeur de thèse
M. Jaffrès Henri	Unité Mixte de Physique CNRS-Thales	Co-directeur de thèse

TABLE OF CONTENTS

ACKNOWLEDGEMENTS

First and foremost I would like to express my sincere gratitude to my advisors Prof. Drouhin Henri-Jean and Dr. Jaffrès Henri for the continuous support of my Ph.D. study and related research, and immense knowledge, for his patience, motivation, and encouragement. It has been an honor to be their Ph.D. student. Their guidance helped me in all the time of research and writing of this thesis.

Besides my advisors, I would like to thank the rest of my thesis committee Prof Amand Thierry, Prof. Jancu Jean-Mac, Dr. Bihlmayer Gustav, Prof. Fabian Jaroslav, Dr. Glazov Mikhail for their insightful comments and the hard question which incented me to widen my research from various perspectives. Specially, I would like to thank Prof. Jancu Jean-Marc and Dr. Bihlmayer Gustav for accepting to be reviewers of my thesis.

I gratefully acknowledge the funding source from Idex Paris-Saclay and Triangle de la Physique.

I would like to thank Dr. Nguyen Thi Lam Hoai, our collaboration at Institute of Physics in Vietnam, for her contribution in this thesis. She gave me a chance to meet my advisors and become a Ph.D. student in France.

My sincere thanks also go to Dr. Vander Beek Kees, the director of Laboratoir des Solides Irradiés, and Mrs. Taquin Isabelle, Mrs. Michelle Sylvie, Mrs. Marylène Raclot who helped me so much with admistrative procedure. I would like to thank the members of Physique et Chimie des Nano-Objets group, who were always kind with me.

I thank my very intelligent and friendly labmates. We shared together many experiences in research and life. I wish you have enough encouragement for your successful researching carriers.

Last but not the least, I would like to thank my family, my friend for supporting me spiritually throughout this thesis and my life in general.

SUMMARY

Effet Tunnel Hall Anormal à l'interface de semi-conducteurs contrôlé par les interactions d'échange et spin-orbite. Etude dans le cadre d'une approche k.p étendue

Nous avons étudié par des méthodes numériques et en théorie **k**.**p** avancée les propriétés tunnel d'électrons et de trous dans des systèmes modèles et hétérostructures composés de semi-conducteurs impliquant des interactions spin-orbite de volume. Nous démontrons que le couplage entre les interactions spin-orbite et d'échange à l'interface de jonctions tunnel résulte en un fort contraste de transmission de porteurs selon le signe de la composante de leur vecteur d'onde dans le plan de la jonction. Cet effet conduit à un effet tunnel anormal d'interface que nous appelons "Effet Hall Tunnel Anormal" (ATHE).

Dans un modèle 2 bandes (2×2) polarisé en spin par interaction d'échange, l'asymétrie du coefficient de transmission (A) pour des angles d'incidence respectivement positifs (+$k_{\|}$) et négatifs (-$k_{\|}$) est maximale à des points particuliers de la zone de Brillouin correspondant à une transmission strictement nulle pour un certain vecteur d'onde incident (A=100%). Plus généralement, nous démontrons le caractère universel de l'asymétrie A vis-à-vis des paramètres d'énergie cinétique réduite et du paramètre d'échange, A suivant une loi d'échelle universelle indépendant de l'interaction spin-orbite et des caractéristiques des matériaux. De façon similaire, des processus tunnel non-conventionnels se manifestant sur des isolants topologiques ont été prédits par d'autres auteurs. Alors que l'ensemble de ces effets Hall anormaux sont liés aux interactions spin-orbite, les effets tunnel anormaux diffèrent des effets Hall tunnel, des effets Hall et des effets Hall de spin par la forte amplitude prédite ainsi que par des phénomènes de chiralité. Ces propriétés possèdent un lien non-trivial avec la symétrie du système. L'ensemble de ces résultats démontre l'existence d'une nouvelle classe d'effets tunnel qui devaient être étudiés expérimentalement dans un futur proche.

En ce qui concerne la bande de valence, nous démontrons, en utilisant un Hamiltonien 14×14 prolongeant un modèle 2×2, que le calcul décrivant l'ATHE repose sur un traitement subtil des états dits "spurious" (états non-physiques) et nous donnons quelques éléments d'amélioration et de compréhension. Dans ce mémoire de thèse, nous développons deux méthodes numériques pour résoudre le problème des états spurious en développant en parallèle des méthodes **k**.**p** respectivement à 14 bandes et 30 bandes afin de décrire des matériaux semi-conducteurs à gap indirect. Les calculs menés

dans la bande de valence d'hétérostructures semi-conductrices incluant interfaces et barrières tunnel (approches 6×6 et 14×14) sans centre de symétrie d'inversion mettent en évidence des propriétés d'asymétrie équivalente à celles obtenues dans la bande de conduction. De tels effets sont interprétés, dans le cadre de calculs de perturbation en transport basés sur des techniques de fonctions de Green, par des effets chiraux orbitaux lors du branchement tunnel des fonctions évanescentes dans la barrière.

TABLE OF ACRONYMS

AHE: anomalous Hall effect
AP: anti-parallel
ARPES: angular-resolved photoelectron spectroscopy
ATHE: anomalous tunnel Hall effect
BDD: BenDaniel Duke
BZ: Brillouin zone
CB: conduction band
CIP: current in-plane
CPP: current perpendicular to plane
DMI: Dzyaloshinskii-Moriya interaction
DOS: density of states
DP: D'yaknov-Perel'
FMR: ferromagnetic resonance
GF: Green function
GMR: giant magnetoresistance
HH: heavy hole
ISHE: inverse spin Hall effect
KKR: Korringa–Kohn–Rostoker
LCAO: linear combination of atomic orbitals
LH: light hole
MFP: mean free path
PA: parallel
QW: quantum well
SHE: spin Hall effect
SIA: structure inversion asymmetry
SML: spin memory loss
SMR: spin Hall magnetoresistance
SO: spin-orbit
SOC: spin-orbit coupling
SOI: spin-orbit interaction
SOT: spin-orbit torque
STT: spin-transfer torque
TAMR: tunneling anisotropic magnetoresistance
THA: tunnel Hall angle
TI: topological insulator
USMR: unidirectional spin Hall magnetoresistance
VB: valence band

CHAPTER I

INTRODUCTION

The discovery of giant magnetoresistance in the end of the 80's at Orsay and Jülich by A. Fert [1] and P. Grünberg [2], who were awarded the 2007 Nobel prize, has kicked-off the field of spintronics. Spintronics is a science that merges both charge and spin degrees of freedom as well as their associated charge and spin currents in metallic systems, magnetic tunnel junctions [3], as well as in semiconducting heterostructures [4], to control the resistance of metallic multilayered devices using the so-called giant magnetoresistance (GMR) effects or magnetic tunnel junctions via the tunneling magnetoresistance effects. This is made possible via two different kinds of effects acting on the native spin currents, effects originating either from the bulk properties or from spin-dependent transmission at interfaces. In the first case, the generation of spin accumulation with current perpendicular-to-plane (CPP) (*e.g.* CPP geometry) is responsible for the CPP-GMR effect in metallic multilayers whereas the diffusion at each interface of the spin currents generated in the ferromagnetic materials is responsible for the current-in-plane GMR (CIP-GMR). More recently, the field of spinorbitronics in metals, which uses the electronic spin-orbit coupling (SOC), has emerged as a new route to create spin currents in the transverse direction of the current flow. This is made possible via the so-called intrinsic spin Hall effect (SHE) of heavy metals [5, 6] as well as the extrinsic SHE of metallic alloys [7, 8, 9]. Spin Hall effect borrows its concept from the well-established anomalous Hall effect (AHE) where the relativistic SOC promotes an asymmetric deflection of the electronic spin current depending on its spin-direction. Intrinsic SHE is at the base of magnetization commutation via spin-orbit torque (SOT) and spin-transfer torque (STT) operations in the ferromagnetic resonance regime (STT-FMR). Intrinsic SHE is also involved in the mechanism of domain-walls moving via SOT. However, from fundamental point of view, the exact anatomy of SOT between Rashba and Dzyaloshinskii-Moriya interactions at spin-orbit active interfaces, in particular involving the 5*d* heavy SOC material of low resistivity (*e.g.* Pt), seems to be of a high importance.

Since more than one decade (beginning 2000's), spintronics and spinorbitronics effects in semiconductors and related heterostructures and devices have firstly concerned the investigations of the intrinsic SHE in bulk materials (*e.g.* GaAs), the generation of (transverse) spin currents free of magnetization and magnetic field via related effects. The intense research led on the ferromagnetic semiconductor compounds (GaMnAs, GeMn) since the early 90's [4], and their integration in heterostructures and group IV

and III-V heterostructures, have boosted the development of new kind of spinorbitronics effects like tunneling anisotropic magnetoresistance (TAMR), Coulomb blockade TAMR, and spin-orbit assisted spin-transfer torques in III-V based magnetic tunneling devices. This was made possible due to the introduction of the natural core SOC of holes in the valence bands of the semiconducting host matrix which makes these ferromagnetic materials as state of the art templates for the investigation of a new class of physical effects. Another class of spinorbitronic effects naturally arises in semiconductors and their heterostructures presenting a lack of inversion symmetry or symmetry breaking, like in bulk group III-V, due to the particular T_d symmetry group (like GaAs). The bulk structural inversion asymmetry leads to the occurrence of supplementary Hamiltonian terms (*e.g.* Dresselhaus interaction) acting directly on the spin of carriers though the spin-orbit interactions [10]. The overall effective Hamiltonian models show that they are responsible for several important effects, that are spin-flip relaxation mechanism in bulk (D'yakonov-Perel') and spin filtering along the [001] crystallographic direction, and spin-dephasing along the [110] crystallographic direction for spin-polarized tunneling carriers. Significant investigations and contributions in this field have been performed since the beginning of the 2000's at IOFFE institute in Saint-Petersburg [11] and at the Ecole Polytechnique with the PhD thesis of Nguỹên Thị Lâm Hoài [12]. In detail, the spin filtering and spin-dephasing physical phenomena are related to the effect caused by the Dresselhaus interactions in tunneling barriers constituting a finite volume of interaction on both the spin polarization of carriers and their probability of transmission associated to this interaction. Like evidenced in a certain number of recent papers [11, 13, 14], this effect appears to be related to different effective masses in the tunneling barriers depending on the in-plane wavevector of the spin-polarized carriers within their characteristic Fermi surfaces.

However, some of the most exciting prospects in spinorbitronics also reside in the area of spin-orbit interaction (SOI) driven phenomena, which can manifest prominently at surfaces and interfaces in topological materials (topological insulators) and Rashba systems [15, 16]. This originates from the crystallographic symmetry breaking at interfaces, and generally responsible for the occurrence of a particular Rashba-split electronic structure appearing in both metallic and semiconductor structures. In the case of III-V heterostructures, this symmetry breaking is responsible for the reduction of the T_d symmetry group to a particular C_{2v} symmetry group leading to a number of exotic effects like optical Pockels effect, reflectance anisotropy (in-plane [110] *vs.* in-plane $[1\bar{1}0]$), linear gain anisotropy in semiconductor lasers and VECSELs as well as a class of spin filtering effects in [110]-grown structures.

In more detail, the electronic energy bands are split by SOI via the Rashba SOC which is odd and generally linear in the wavevector, **k**. The essential feature of any

SOC is that electrons moving in an electric field experience, even in the absence of an external magnetic field, an effective magnetic field in their frame of motion, called SO field, which couples to the electron magnetic moment. The odd parity of this coupling in the momentum enables a wide variety of phenomena (SHE, Inverse Edelstein effect, SOT) and the exploration of these new asymmetry effects is now at the heart of spinorbitronics. Charge carriers, electrons or holes, with asymmetric SOC terms then experience a momentum-dependent effective magnetic field, a spin-dependent correction to their velocity, as well as a geometric dephasing resulting from the SOC. Benefit can be taken of these features for the realization of concept devices in which the spin polarization is generated independently of the charge current or, inversely, absorbed in ferromagnetic layers for spin-torque operation. Among other research directions in the field of spinorbitronics, one can cite the so-called spin-galvanic effects which arises from the locking between the electron momentum and the angular momentum. It has for effect to generate a lateral charge current from spin-accumulation in a Rashba-interface gas. This concept of spin-to-charge conversion was originally developed in the context of optical manipulation of spins in semiconductors and observed in quantum wells or more recently in structures involving different topological insulators (TI) [17].

In the present work, we focused on a special class of physical phenomena dealing with spin-polarized-carriers deflection and generation of lateral charge currents promoted by pure exchange and spin-orbit-split interfaces involving evanescent states, and that we call anomalous (topological) tunnel Hall effects (ATHE) [18]. This effect arises at interfaces and (tunnel) junctions and manifests itself by a deviation of the charge (and also spin currents) resulting from the particular matching conditions of the spin-polarized spin-orbit-split electronic wave functions (pure contact effect). This effect, of significant size, which can even reach 100% in certain cases, also manifests itself by an asymmetry of transmission at interfaces for the carriers depending on their incident in-plane wavevectors. This has been the focus of similar recent studies [16] in III-V structures involving both interfacial Rashba and Dresselhaus contributions. Nonetheless, one important feature of our study is the numerical (**k**.**p** theory for spin-orbit and exchange-split transport) as well as analytical (**k**.**p** theory for matching, perturbative treatment through Green's function techniques) demonstration of an "intrinsic skew tunneling" effect derived from the interplay of pure exchange and Dresselhaus interactions without involving Rashba terms [19]. This departs from the "skew tunneling" with Dresselhaus field from the non-asymmetric behavior of the density of states (DOS) *vs.* the in-plane carrier wavevectors which makes the asymmetric "intrinsic" to the matching. We will prove, by perturbation techniques, that this asymmetry, occurring in both semiconductor conduction (CB) and valence band (VB), should be related to a pure chirality effect due to the mixing of both propagative (parallel wavevector) and evanescent

(tunneling currents) states. This leads to a pure 0-dimensional surface tunneling effect.

Beyond the analytical developments presented in this manuscript for describing the particular wave function matching at each interface, we have primarily chosen to develop numerical calculations using the robust **k**.**p** method for tunneling and adapted to any type of multilayers. Beyond the 2×2 CB and 6×6 VB models describing for instance the GaMnAs band structure and heterostructures [20], the simultaneous treatment of electrons and holes needs a 8-band **k**.**p** transport code whereas, the inclusion of odd parity symmetry effects requires at least a 14-band **k**.**p** treatment (including the Γ_{5C} upper CB in Koster's or Fishman's notations [21, 22]). However, the difficulty to treat a 14-band (as well as 8-band) spin-transport model is to get rid of some well-known unphysical "spurious" electronic states making the tunneling calculation unfeasible due to tunneling shortcuts within the first Brillouin zone (BZ). The adaptation of a derived 14×14 Hamiltonian including "healing terms" makes possible to treat spin transport over the whole structure with a satisfactory accuracy, at least in the neighborhood of the BZ center (Γ point) as required. The implementation of an effective 18-band tunneling code, involving supplementary electronic bands (anti-spurious or ghost bands), improves the fidelity further away from the Γ point. This makes a playground for future similar investigations towards a full 30-band treatment describing direct and indirect gaps materials belonging to group IV semiconductors and heterostructures.

One of the real peculiarity and difficulty is to treat correctly the tunneling elastic transport in heterostructures occurring at a constant energy, and not at a constant wavevector *k*. This generally involves non-orthogonal states and large *k*- states away from the first Brillouin zone (BZ), states that can admit a *spurious* or unphysical character being away from the validity zone of the **k**.**p** treatment. This makes the tunneling problem much more complex than the electronic band structure calculations as well as band-to-band optical-transition estimations.

This work provides one of the first advanced implementation of numerical **k**.**p** tunneling transport codes (14- and 30-band) and then one of the first playground platform devoted to the investigation of spin-orbit field effects in carrier transport in a new class of spintronics interfaces.

CHAPTER II

SOME EXAMPLES OF SPINORBITRONICS FUNCTIONALITIES WITH SEMICONDUCTORS BELONGING TO THE T_D SYMMETRY GROUP

In this chapter, as an introduction, we will consider the case of electron spin-polarized transport in tunnel barriers and devices made of semiconductors belonging to the T_d symmetry group. The phenomenon of electron tunneling has been known since the advent of quantum mechanics like described in pioneering papers by Bardeen and Harrison in the beginning in the 60's [23, 24] and afterward by Slonczewski [25] for the case of spin-polarized transport. Electron tunneling continues to enrich our understanding of many fields of physics, as well as spin-dependent tunneling. In that frame, one of the major issues of general interest is the possibility of spin injection into semiconductors aside of optical pumping. A natural way to achieve spin orientation in experiments is the injection of spin-polarized carriers from magnetic materials through a tunnel junction (3*d* ferromagnetic materials) or from ferromagnetic semiconductors like GaMnAs with a III-V host [26, 27]. However, only in the last decade, it was realized that the process of electron tunneling in semiconductors could be spin and orbital dependent due to the SOI. It was shown that the Rashba SOC at interfaces as well as the Dresselhaus coupling in the bulk of the barrier make the barrier tunnel transmission dependent on the spin orientation and on the wavevector of the incident electrons [11, 28, 29, 30].

The first important problem and issue which have been raised since the beginning of the 2000's is the one of electron tunneling through thin III-V barriers, seat of Dresselhaus interactions and leading to spin filtering effects. In the case of Rashba and Dresselhaus coupling in [001]-grown barriers between bulk semiconductors, the spin polarization of transmitted electrons linearly scales with the lateral component $\mathbf{k}_{\|}$ of the electron wavevector and is of opposite sign for the wavevectors $\mathbf{k}_{\|}$ and $-\mathbf{k}_{\|}$ [28, 11]. A spin polarization efficiency, P, was then introduced to determine the difference of transmission coefficients ($T_{\uparrow}$ and $T_{\downarrow}$) between up- ($\uparrow$) and down- ($\downarrow$) spin states and then the overall efficiency of the process according to the following relationship:

$$P = \frac{T_{\uparrow} - T_{\downarrow}}{T_{\uparrow} + T_{\downarrow}}. \tag{1}$$

The spin polarization efficiency can reach a fraction of unity (about twenty percents) for very large SOC (*e.g.* GaSb), with a reasonable width of the barriers to keep a sizable

transmission. This effect, which is referred to as spin filtering effect, leads to a significant spin polarization of the carriers for an incoming non-zero parallel flux (in-plane current) leading to preferential $\mathbf{k}_{\|}$ of a given sign. On the other hand, the tunneling of electrons through a [110]-oriented single barrier in a heterostructure made of T_d semiconductor compounds, with combined Dresselhaus SOC in the barrier and Rashba SOC at the barrier interfaces, has recently been considered [15]. These couplings, arising concurrently, do not only generate electron spin polarization after tunneling but also lead to spin dephasing and spin rotation along the [110] direction.

The basic theory of the spin filtering effect through a [001]-grown barrier is introduced in Sec. 2.1.2 following two distinct point of views [11, 31]. Then, in Sec. 2.1.3 we consider the effect in extended ferromagnetic-based structures which include electrodes made of ferromagnetic semiconductors. Finally, the spin injection via [110]-grown semiconductor barriers will be considered in Sec. 2.2 as a state of the art result.

2.1 Spin filtering effect through [001]-grown barriers

2.1.1 Dresselhaus interactions in T_d symmetry group materials

Semiconductor crystals of diamond and zinc blende structures are constructed by two face-centered cubic (fcc) sublattices (A) and (B), shifted by one forth of the cube main diagonal. The atoms are placed at the nodes of each sublattice. If we take the O_x, O_y, and O_z axes parallel to the cubic crystallographic axes, respectively [100], [010], and [001], an atom of sublattice (A) at the point $\mathbf{R}'_j = \mathbf{R}_j + \mathbf{a}$ where $\mathbf{a} = a\,[1/4, 1/4, 1/4]$ has four nearest neighbors set at the point $\mathbf{R}_j + \mathbf{a}_n,\ (n \in \{0,\ 1,\ 2,\ 3\ \})$ where $a_0 = 0$, $a_1 = a\,[1/2, 1/2, 0]$, $a_2 = a\,[1/2, 0, 1/2]$, $a_3 = a\,[0, 1/2, 1/2]$ with a being the length of the unit cell.

If the two atoms in the two sublattices are identical, we obtain the diamond structure. An inversion center exists in the middle of the segment joining these two atoms. These semiconductors belong to the O_h group, *e.g.* silicon, gemanium, and carbon (see Fig. 1 a).

If the two atoms in the two sublattices are different, we obtain the zinc blende structure. These semiconductors, *e.g.* GaAs and GaSb, belong to the T_d symmetry group, where the inversion center symmetry no longer exists (see Fig. 1 b).

The Bravais lattice of this structure is the body-centered cubic lattice (bcc). The first Brillouin zones of the O_h and T_d groups are described in Fig. 1 c; characteric points are:

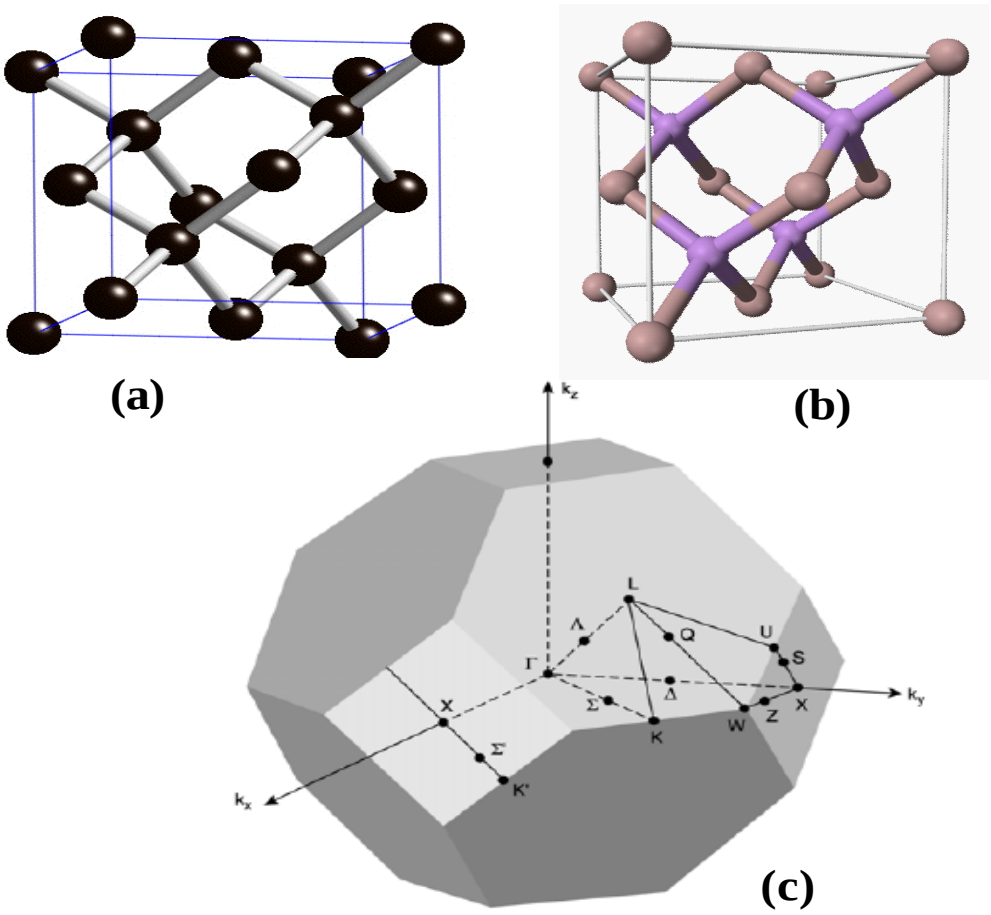

Figure 1: (a): Diamond crystal; (b) zinc blende structure; (c) common Brillouin zone of diamond and zinc blende structure.

Γ	$(2\pi/a)\,(0,0,0)$	K'	$(2\pi/a)(1,1/4,-1/4)$
X	$(2\pi/a)\,(1,0,0)$	U	$(2\pi/a)(1,1/4,1/4)$
L	$(2\pi/a)(1/2,1/2,1/2)$	W	$(2\pi/a)(1,1/2,0)$
K	$(2\pi/a)(3/4,3/4,0)$		

Group theory shows that for the O_h group the lattice potential displays a perfect inversion symmetry, whereas the lack of inversion center leads to a small potential asymmetry in the T_d group, $V_d = V_{sym} + V_{antisym}$, where $V_{antisym}$ can be considered as a perturbation [22]. When the SOI is included, the lack of inversion center can create an effective internal magnetic field, felt by electrons in the CB and referred to as Dresselhaus terms $\hat{H}_D$ [10]

$$\hat{H}_D = \gamma \left[\sigma_x k_x \left(k_y^2 - k_z^2\right) + \sigma_y k_y \left(k_z^2 - k_x^2\right) + \sigma_z k_z \left(k_x^2 - k_y^2\right)\right], \tag{2}$$

where $\boldsymbol{\sigma}$ is Pauli's operator and γ represents the strength of the SOI which will be largely discussed in this manuscript. This is the so-called D'yakonov-Perel' Hamiltonian known to lead to a spin relaxation mechanism of the conduction electrons [32]. When the $[001]$ axis is the quantization direction, the two terms $\sigma_x k_x \left(k_y^2 - k_z^2\right)$ and $\sigma_y k_y \left(k_z^2 - k_x^2\right)$ are called in-plane Dresselhaus components, and the term $\sigma_z k_z \left(k_x^2 - k_y^2\right)$ is the out-of-plane Dresselhaus component. In almost all previous work concerning the spin filtering effect, the Dresselhaus Hamiltonian in Eq. 2 is simplified, getting rid of the out-of plane component [11]**:**

$$\hat{H}_D = \gamma \left[\sigma_x k_x - \sigma_y k_y\right] \frac{\partial^2}{\partial z^2}, \tag{3}$$

for a perfect two-dimensional electron gas (2D electron gas) or at the limit of a grazing incidence. Up to now, this reduced Dresselhaus form has been used to study the spin-dependent tunneling [13, 14, 15, 16]. Note that, in Eq. 3, the out-of-plane Dresselhaus component has been totally neglected. In Chapter 5, we will show that the out-of plane Dresselhaus component plays an important role in the ATHE and is connected to a new type of chiral phenomena.

The orientations of $\uparrow$- and $\downarrow$-spins for various directions of the in-plane electron wavevectors $\mathbf{k}_{\|}$ are shown in Fig. 2. If $\mathbf{k}_{\|}$ is directed along a cubic crystal axis ([100] or [010]) then the spins are parallel (or antiparallel) to $\mathbf{k}_{\|}$, while the spin directions are perpendicular to $\mathbf{k}_{\|}$ if the in-plane wavevector is directed along the $[1\bar{1}0]$ or [110] axes.

2.1.2 Spin filtering effect without ferromagnetism

In this section, we consider the case of spin-dependent tunneling transmission in presence of a spin-orbit Dresselhaus field (Fig. 2) localized within a "thin" tunnel barrier, (Fig. 3).

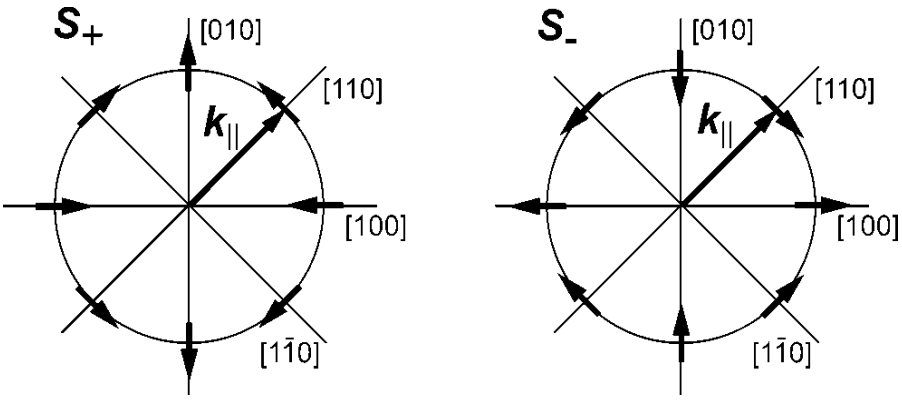

Figure 2: Spin orientation of ↑- and ↓- spins versus the in-plane wavevector [11].

The transmission of electrons with an initial wavevector $\mathbf{k} = (\mathbf{k}_{\|}, k_z)$ through a rectangular barrier grown along the $z\|[001]$ direction is studied. We assume that the inversion symmetry is broken only inside the barrier.

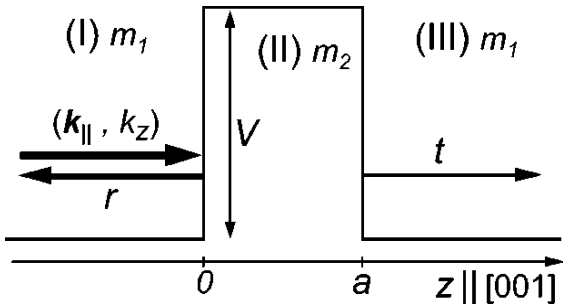

Figure 3: Transmission of electron though a rectangular barrier with the wavevector $\mathbf{k} = (\mathbf{k}_{\|}, k_z)$, barrier height V, barrier thickness a; m_1, m_2 electron effective mass outside and inside the barrier [11].

The Hamiltonian $\hat{H}_D$ given in Eq. 3 is diagonalized by spinors

$$\chi_{\pm} = \frac{1}{\sqrt{2}} \begin{pmatrix} 1 \\ \mp e^{i\varphi} \end{pmatrix},$$

where $\mathbf{k} = (k_x \cos\varphi, k_y \sin\varphi, k_z)$. This introduces a correction to the effective mass of ↑- and ↓- spins in the barrier according to

$$m_{\pm} = m_2 (1 \pm \frac{2\gamma k_{\|} m_2}{\hbar^2})^{-1},$$

where m_2 is the electron effective mass in the barrier with no SOI included.

The energy and in-plane wavevector are conserved upon electron tunneling. The wave functions of electrons are,

$$\Psi_{\pm}(\mathbf{r}) = u_{\pm}(z) \exp(i\mathbf{k}_{\|}\boldsymbol{\rho}),$$

where $\mathbf{k}_{\parallel} = \mathbf{k}_x + \mathbf{k}_y$, and $\boldsymbol{\rho} = (\mathbf{x}, \mathbf{y})$. The functions $u_{\pm}(z)$ are solutions of the Schrödinger equations in each layer: left electrode, barrier, and right electrode according to:

$$\begin{aligned} u_{\pm}^{(I)}(z) &= \exp(ik_z z) + r_{\pm}\exp(ik_z z), \\ u_{\pm}^{(II)}(z) &= A_{\pm}\exp(-q_{\pm}z) + B_{\pm}\exp(q_{\pm}z), \\ u_{\pm}^{(III)}(z) &= t_{\pm}\exp(ik_z z), \end{aligned}$$

where $q_{\pm}$ are wavevectors in the barrier:

$$\begin{aligned} q_{\pm} &= \sqrt{\frac{2m_{\pm}V}{\hbar^2} - k_z^2\frac{m_{\pm}}{m_1} - k_{\parallel}^2\left(\frac{m_{\pm}}{m_1} - 1\right)}, \\ q_{\pm} &= \sqrt{\left(\frac{2m_2V}{\hbar^2} - k_z^2\frac{m_2}{m_1}\right)(1 \pm \frac{2\gamma k_{\shortparallel} m_2}{\hbar^2})^{-1} - k_{\parallel}^2\left(\frac{m_2}{m_1}(1 \pm \frac{2\gamma k_{\shortparallel} m_2}{\hbar^2})^{-1} - 1\right)}. \end{aligned}$$

In the limit where $\left(2\gamma k_{\parallel} m_2/\hbar^2\right) \ll 1$, we get:

$$\begin{aligned} q_{\pm} &\approx \sqrt{\left(\frac{2m_2V}{\hbar^2} - k_z^2\frac{m_2}{m_1}\right)(1 \pm \frac{2\gamma k_{\shortparallel} m_2}{\hbar^2})^{-1} - k_{\parallel}^2\left(\frac{m_2}{m_1} - 1\right)(1 \pm \frac{2\gamma k_{\shortparallel} m_2}{\hbar^2})^{-1}}, \\ q_{\pm} &\approx \sqrt{\left(\frac{2m_2V}{\hbar^2} - k_z^2\frac{m_2}{m_1}\right) - k_{\parallel}^2\left(\frac{m_2}{m_1} - 1\right)}(1 \pm \frac{2\gamma k_{\shortparallel} m_2}{\hbar^2})^{-1/2} = q_0(1 \pm \frac{2\gamma k_{\shortparallel} m_2}{\hbar^2})^{-1/2}, \end{aligned}$$

where $q_0 = \sqrt{\left(\frac{2m_2V}{\hbar^2} - k_z^2\frac{m_2}{m_1}\right) - k_{\parallel}^2\left(\frac{m_2}{m_1} - 1\right)}$ is the wavevector in the barrier when the Dresselhaus term is neglected.

To anticipate discussions on the matching conditions needed for the description of interface crossing, the BenDaniel Duke (BDD) [33] matching conditions are used here in the case of the CB: u and $(1/m)\,(\partial u/\partial z)$ are continuous at the interface. Note that the small spin-dependent renormalization of the effective mass induced by the Dresselhaus Hamiltonian can be neglected in the boundary conditions, since it produces only a small correction to the pre-exponential factor in the final expressions, thus leading to

$$\begin{aligned} t_{\pm} &= -4i\frac{m_2}{m_1}\frac{k_z q_{\pm}}{(q_{\pm} - ik_z m_2/m_1)}\exp(-q_{\pm}a - ik_z a) \\ &\approx -4i\frac{m_2}{m_1}\frac{k_z q_0}{(q_0 - ik_z m_2/m_1)}\exp(-q_0 a - ik_z a)\exp\left(\pm\frac{\gamma k_{\shortparallel} m_2}{\hbar^2}\right) \\ &\approx t_0\exp\left(\pm\frac{\gamma k_{\shortparallel} m_2}{\hbar^2}\right), \end{aligned} \tag{4}$$

where

$$t_0 = -4i\frac{m_2}{m_1}\frac{k_z q_0}{(q_0 - ik_z m_2/m_1)^2}\exp(-q_0 a - ik_z a),$$

is the transmission amplitude when the SOI is neglected in the barrier. Equation. 4 presents the difference of transmission between $\uparrow$- and $\downarrow$- spin electrons. The spin

polarization defined in Eq. 1 is then:

$$P = \frac{|t_+|^2 - |t_-|^2}{|t_+|^2 + |t_-|^2} = \tanh(2\gamma \frac{m_2 k_{\shortparallel}}{\hbar^2} a q_0). \tag{5}$$

It clearly depends on the barrier thickness. It is plotted for some T_d materials in Fig. 4 (upper) and compared to the numerical calculations performed for GaAs within a 2-band effective model (Eq. 2), and within 14-band **k**.**p** (Fig. 4 lower).

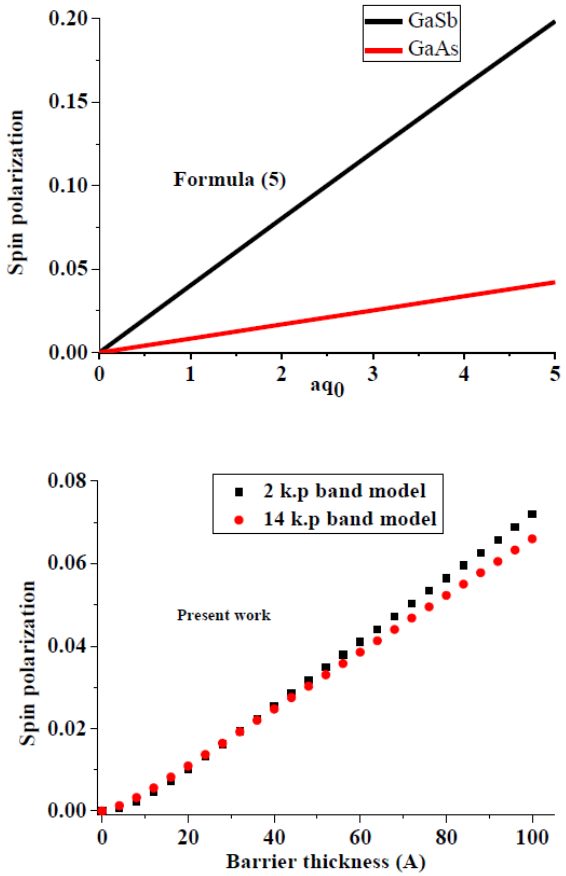

Figure 4: (Upper) Spin polarization *vs.* aq_0 for GaAs with $m^* = 0.067\ m_0$, and $\gamma = 24$ eVÅ^3 (red line), and GaSb with $m^* = 0.041\ m_0$, and $\gamma = 187$ eVÅ^3(black line). (Lower) Spin polarization *vs.* barrier thickness within a 2-band effective model (black line), $m^* = 0.067\ m_0$, and $\gamma = 24$ eVÅ^3, and 14 band **k**.**p** model with parameters close the parameters given in Ref [34], barrier height 1 eV, $k_{\|} = 0.02$ Å^{-1}, and $\mathcal{E}$ =81 meV.

In an other point of view [31], the authors considered that Dresselhaus terms do not renomalize the effective masses of ↑- and ↓- spinors in the barrier but alter their wavevectors. In the limit of a small in-plane wavevector they recovered Eq. 5.

From these results, it is possible to say that the in-plane Dresselhaus components play a very important role for spin filtering, whereas the out-of-plane component may be neglected in this particular case; in contrast, latter one will make the specificity of the tunnel Hall effect (transmission asymmetry of opposite in-plane wavevectors) via a new type of chiral phenomena, that we will discuss in Chapter 5.

2.1.3 Spin filtering effect in zinc blende structure with ferromagnetic electrodes (present work)

One of the most important aspects in the present work is the study of extended spintronics phenomena in electrons and holes tunneling (computed by a single tunneling **k**.**p** code - this work). In the related structures, two different physical effects may be considered: the spin filtering effect with spin injection and potentially new spin orbital chiral transport via tunneling (due to the interplay of propagative and evanescent wave functions). In the simplest case, all the calculations are done with identical materials in the layers, so that the Dresselhaus constant γ remains unchanged at the interfaces. Therefore, the continuity of the current wave reduces to the continuity of derivative of the wave function.

*2.1.3.1 **Exchange interactions***

We now introduce important notions of ferromagnetism that we will need throughout the manuscript. Let us consider as an example the case of ferromagnetic semiconductors made of zinc blende III-V materials.

The discovery of ferromagnetism in zinc blende III-V [35, 36] and II-VI [37, 38] Mn-based compounds allows one to explore the physics of previously unavailable combinations of quantum structures and ferromagnetism in semiconductors. Let us consider zinc blende semiconductor compounds in which the cations are partly substituted with magnetic ions, such as Mn. The Mn ions provide localized $5/2$ spins and, in the case of III-V semiconductors, act as acceptors. These Mn acceptors compensate the deep antisite donors commonly present in GaAs grown by low-temperature molecular beam epitaxy, and produce a p-type conduction with metallic resistance for the Mn concentration x in the range $0.04 < x < 0.06$ [39, 40, 41, 42].

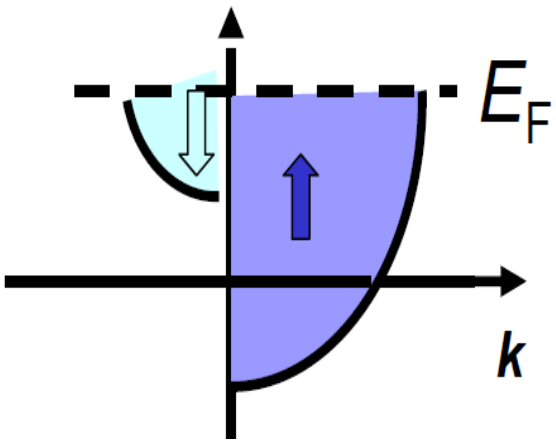

Figure 5: A schematic band structure for the Stoner model of ferromagnetism. An exchange interaction has split the energy of states with different spins, and states near the Fermi level are spin-polarized.

In the picture given by Dietl [26], the exchange interaction between hole and $p-d$ hybridization is described in a **k**.**p** model as:

$$\hat{H}_{exc} = \frac{\beta \mathbf{s}.\mathbf{M}}{g\mu_B} = 6B_G \mathbf{s}.\mathbf{m} \tag{6}$$

where β is the average exchange integral, $\mathbf{s}$ is the electron spin, $\mathbf{M}$ is a localized spin, g is the Landé factor for hole, and μ_B is the Borh magneton, $6B_G = \frac{\beta|\mathbf{M}|}{g\mu_B}$ represents the average interaction energy among holes, $\mathbf{m}$ is a unit vector along the exchange direction. For the sake of simplicity, we will assume that Eq. 6 can be applied to the exchange interaction between electron and localized magnetic moments, and the Landé factor for electron instead of the factor for hole.

2.1.3.2 *In-plane incident wavevector parallel to the magnetization direction ($\overrightarrow{k_\parallel} \parallel \overrightarrow{M}$)*

We consider here the spin filtering effect with magnetic electrodes in both cases: either for parallel or antiparallel magnetic configurations. The magnetization is parallel to the in-plane wavevector.

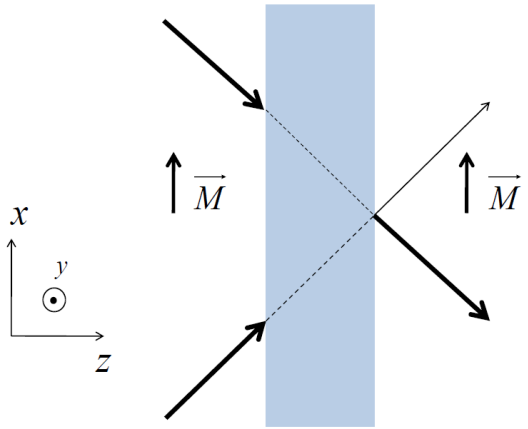

Figure 6: Schema of transmission process through a tunnel junction grown along z direction, PA magnetizations **M** along x. In-plane wavevector $\mathbf{k}_\parallel = (\xi,\ 0)$. Carriers with +$\xi$ in-plane wavevector component are more easily transmitted than those carrying -ξ.

Parallel (PA) magnetic configuration (↑↑) The exchange potential is modeled via Dietl's picture [26] $\hat{H}_{exc} = \mathbf{B}.\mathbf{S} = w\mathbf{m}.\boldsymbol{\sigma}$, where w is the exchange constant. The x component of the exchange potential is $\hat{H}_{exc} = w\sigma_x$. The electron possesses the initial in-plane wavevector $\mathbf{k}_\parallel = (\xi, 0)$ and an energy ε smaller than the barrier height. The electron Hamiltonian writes (see Fig. 6)

$$\hat{H}_\xi = \begin{cases} \gamma_c\left(\xi^2+k^2\right)+w\sigma_x+\gamma\xi k^2\sigma_x & \text{if } z<0 \text{ or } z>a, \\ \gamma_c\left(\xi^2+k^2\right)+\gamma\xi k^2\sigma_x\ +V & \text{if } 0<z<a, \end{cases} \tag{7}$$

where γ_c is related to the effective electron mass in the crystal. The SOI has the simple form given in Eq. 3, without the out-of-plane component.

We consider the limiting case of small SOI, $\gamma\xi k^2 \ll w$, so that it can be neglected in the magnetic contacts.

In the electrodes: The upper energy level is $\mathcal{E}=\gamma_c\left(\xi^2+k^2\right)+w$, with the respective eigenvector $\binom{1}{1}=|\uparrow\rangle$; whereas the lower one is $\mathcal{E}=\gamma_c\left(\xi^2+\tilde{k}^2\right)-w$, with the respective eigenvector $\binom{1}{-1}=|\downarrow\rangle$.

In the barrier: The upper energy is $\mathcal{E}=\gamma_c\left(\xi^2+q^2\right)+\gamma\xi q^2+V$, with the eigenvector $\binom{1}{1}=|\uparrow\rangle$; whereas the lower one is $\mathcal{E}=\gamma_c\left(\xi^2+\tilde{q}^2\right)-\gamma\xi\tilde{q}^2+V$, with the eigenvector $\binom{1}{-1}=|\downarrow\rangle$.

We assume that the electrons come with $\downarrow$-spin and with energies lying within the exchange step, $-w<\mathcal{E}<w$. It means that there is one propagative wave $\tilde{k}$ and one evanescent wave k. The wave functions then write:

$$\Psi = \begin{cases} |\downarrow\rangle e^{i\tilde{k}z}+A_1'|\downarrow\rangle e^{-i\tilde{k}z}+B_1'|\uparrow\rangle e^{-ikz} & \text{if } z<0, \\ A_2|\downarrow\rangle e^{i\tilde{q}z}+A_2'|\downarrow\rangle e^{-i\tilde{q}z}+B_2|\uparrow\rangle e^{iqz}+B_2'|\uparrow\rangle e^{-iqz} & \text{if } 0<z<a, \\ A_3|\downarrow\rangle e^{i\tilde{k}z}+B_3|\uparrow\rangle e^{ikz} & \text{if } z>a. \end{cases} \tag{8}$$

The wave function and its derivative are continuous at the interfaces. According to the BDD matching conditions for the $\downarrow$ spin states, we obtain:

$$\begin{cases} |\downarrow\rangle+A_1'|\downarrow\rangle=A_2|\downarrow\rangle+A_2'|\downarrow\rangle, \\ \tilde{k}|\downarrow\rangle-\tilde{k}A_1'|\downarrow\rangle=\tilde{q}A_2|\downarrow\rangle-\tilde{q}A_2'|\downarrow\rangle, \\ A_2|\downarrow\rangle e^{i\tilde{q}a}+A_2'|\downarrow\rangle e^{-i\tilde{q}a}=A_3|\downarrow\rangle e^{i\tilde{k}a}, \\ \tilde{q}A_2|\downarrow\rangle e^{i\tilde{q}a}-\tilde{q}A_2'|\downarrow\rangle e^{-i\tilde{q}a}=\tilde{k}A_3|\downarrow\rangle e^{i\tilde{k}a}. \end{cases} \tag{9}$$

Solving Eq. 9, we find:

$$A_3=\frac{4\tilde{q}\tilde{k}e^{-i\tilde{q}a}}{(\tilde{k}-\tilde{q})^2-(\tilde{k}+\tilde{q})^2e^{-2i\tilde{q}a}},$$

where the wavevectors in the barrier are purely imaginary, $\tilde{q}=i\tilde{Q}$. Here, we have assumed that $(\tilde{k}-\tilde{Q})^2 \ll (\tilde{k}+\tilde{Q})^2e^{2\tilde{Q}a}$. The $\uparrow$-spin wavevectors are pure imaginary inside and outside the barrier. Therefore, they do not contribute to the transmission coefficient. The total transmission coefficient is equal to the $\downarrow$-spin one:

$$T_+=|A_3|^2 \approx \left|\frac{4\tilde{Q}\tilde{k}e^{-\tilde{Q}a}}{\tilde{Q}-i\tilde{k}}\right|^2=\frac{16\tilde{Q}^2\tilde{k}^2e^{-2\tilde{Q}a}}{\tilde{Q}^2+\tilde{k}^2}. \tag{10}$$

When the in-plane wavevector changes its sign, the spinors in barrier are exchanged so that the transmission coefficient becomes:

$$T_- \approx \left| \frac{4Q\tilde{k}e^{-Qa}}{Q - i\tilde{k}} \right|^2 = \frac{16Q^2\tilde{k}^2 e^{-2Qa}}{Q^2 + \tilde{k}^2}, \tag{11}$$

where $q = iQ$.

The asymmetry of the transmission coefficients A, for opposite in-plane wavevectors, $k_\parallel$ and -$k_\parallel$ is:

$$A = \frac{T_+ - T_-}{T_+ + T_-} \approx \tanh a\delta Q, \tag{12}$$

where $\delta Q = \tilde{Q} - Q$. The formula yielding the spin filtering efficiency derived in previous work is recovered in Eq. 12. The asymmetry of the transmission coefficients in single-spin channel with opposite in-plane wavevectors parallel to the magnetization direction should be considered as a spin filtering effect.

Figure 7 a shows the different transmission coefficients for opposite in-plane wavevectors calculated by Eqs. 10, 11 and using our 2-band **k.p** effective Hamiltonian transport code (present work), which are in good agreement. The respective asymmetry transmission for pairs of opposite in-plane wavevectors, *i.e.*, the spin filtering efficiency, is displayed in Fig. 7 b. The transmission coefficient dependence on the in-plane wavevector is plotted in Fig. 7 c. We can see that the spin filtering effect occurs along k_x and not along k_y. The results discussed in the next part will explain why the effect vanishes along k_y in the PA magnetic configuration along the x direction.

The tunneling of spin polarized carriers, as well as the "tunneling spin-galvanic" effect, through a single barrier with no inversion symmetry for pairs of opposite in-plane wavevectors is expected to generate an in plane electric current $j_\parallel$ at the scale of the electron mean free path [13]. These authors found $j_\parallel \sim 10^{-7}$ A/cm for a GaAs barrier in structures with barrier transparency $|t_0|^2 \sim 10^{-5}$ and taking a momentum scattering time $\tau_p \sim 10^{-12}$ s.

Anti-parallel (AP) magnetic configuration (↑↓) The electron Hamiltonian is (see Fig. 8):

$$\hat{H}_\xi = \begin{cases} \gamma_c\left(\xi^2 + k^2\right) + w\sigma_x + \gamma\xi k^2\sigma_x & \text{if } z < 0 \\ \gamma_c\left(\xi^2 + k^2\right) + \gamma\xi k^2\sigma_x + V & \text{if } 0 < z < a \\ \gamma_c\left(\xi^2 + k^2\right) - w\sigma_x + \gamma\xi k^2\sigma_x & \text{if } z > a \end{cases} \tag{13}$$

This is similar to the PA magnetic configuration except that the spinors in the right electrode are exchanged.

$$\Psi = \begin{cases} |\downarrow\rangle e^{i\tilde{k}z} + A_1' |\downarrow\rangle e^{-i\tilde{k}z} + B_1' |\uparrow\rangle e^{-ikz} & \text{if } z < 0 \\ A_2 |\downarrow\rangle e^{i\tilde{q}z} + A_2' |\downarrow\rangle e^{-i\tilde{q}z} + B_2 |\uparrow\rangle e^{iqz} + B_2' |\uparrow\rangle e^{-iqz} & \text{if } 0 < z < a \\ A_3 |\uparrow\rangle e^{i\tilde{k}z} + B_3 |\downarrow\rangle e^{ikz} & \text{if } z > a \end{cases} \tag{14}$$

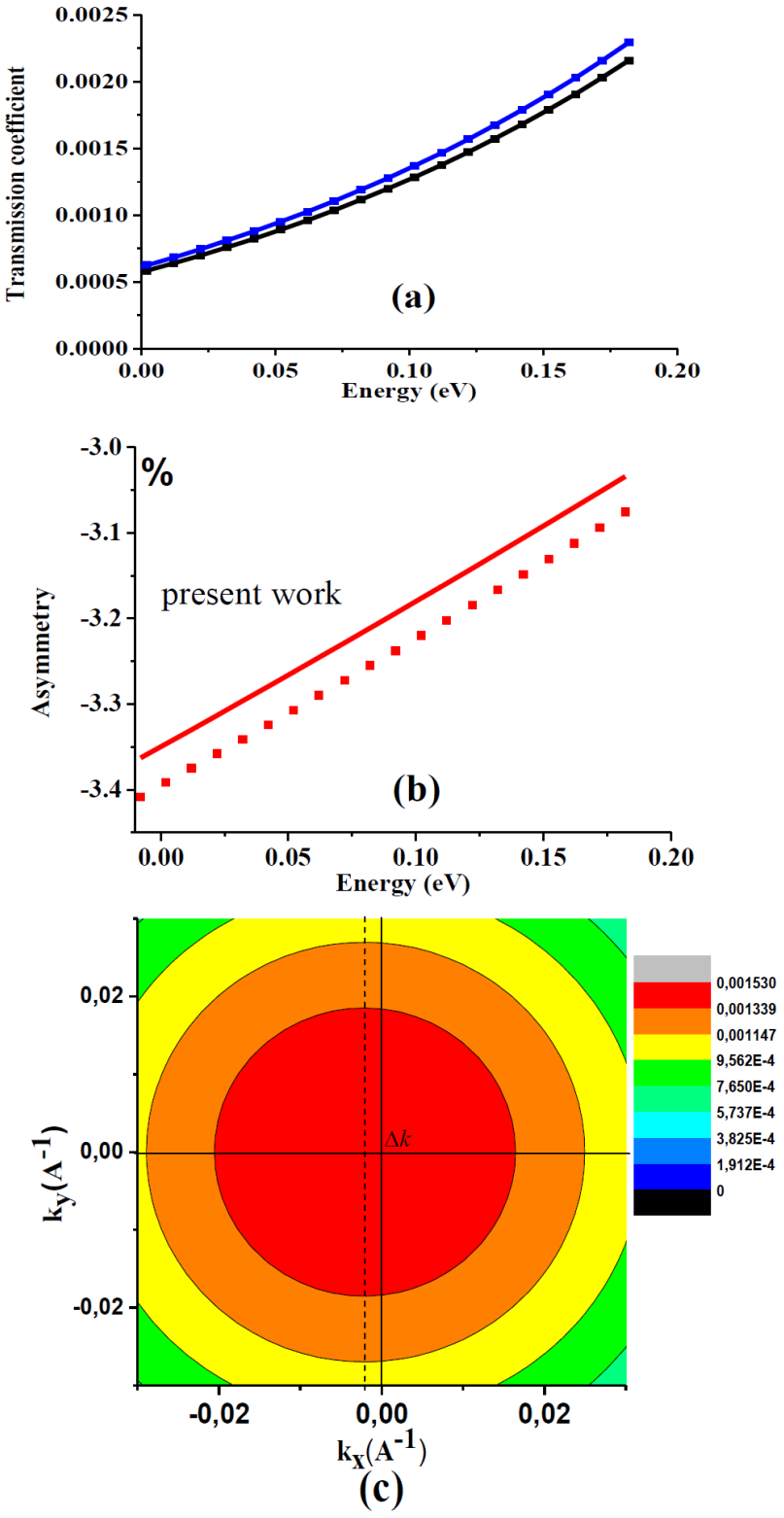

Figure 7: (a) Transmission coeffcient *vs.* incident energy through a single GaAs barrier, barrier thickness 3 nm, barrier height 1 eV, calculated by our numerical 2-band **k**.**p** code (present work) (solid lines) and from Eqs. 10, 11 (dotted lines) wavevectors $k_x = -0.02$ Å^{-1} (blue lines), and $k_x = 0.02$ Å^{-1} (black lines); (b) Respective asymmetry transmission coefficient of opposite in-plane wavevectors calculated by our numerical 2-band **k**.**p** code (solid line) and from Eq. 12 (dotted line); (c) Transmission coefficient dependence on the in-plane wavevector, the displacement Δk from the center of the spherical transmission coefficient along k_x corresponds to the spin filtering effect along k_x.

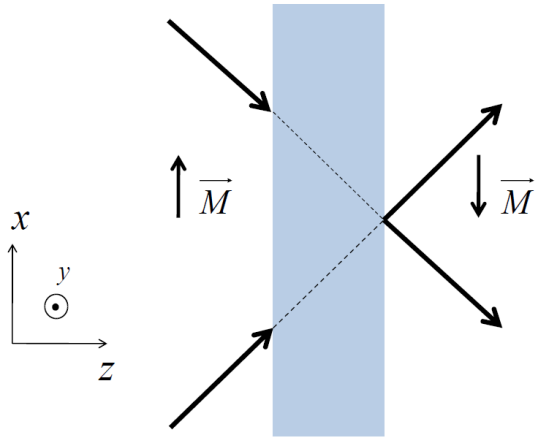

Figure 8: Schema of transmission process through a tunnel junction grown along z direction, AP magnetizations **M** and -**M** along x, in-plane wavevector $\mathbf{k}_{\parallel} = (\xi,\ 0)$. Carriers with $+\xi$ and -ξ in-plane wavevector components have equal transmission coefficients.

Note that an electron possessing an energy within the exchange step, $-w < \mathcal{E} < w$, cannot tunnel from the pure $\downarrow$- (or $\uparrow$-) spin to the pure $\uparrow$- (or $\downarrow$-) spin state. Only electrons with energies overcoming the exchange step can be transmitted from one side to the other, *i.e.*, with $\mathcal{E} > w$, with an non-zero transmission coefficient. Using the continuity of the wave function and of its derivative at the barrier interfaces, the total transmission coefficient (sum of the transmission coefficients of $\uparrow$- and $\downarrow$-incoming spins) is found to be:

$$T = \frac{16\tilde{Q}^4 e^{-2\tilde{Q}a}}{(\tilde{k}^2+\tilde{Q}^2)(k^2+\tilde{Q}^2)} + \frac{16Q^4 e^{-2Qa}}{(\tilde{k}^2+Q^2)(k^2+Q^2)} \tag{15}$$

When the sign of the in-plane wavevector is changed $\xi \longrightarrow -\xi$, the spins in the barrier are also exchanged, *i.e.*, $Q \longleftrightarrow \tilde{Q}$. Eventually, Eq. 15 does not change when the sign of the in-plane wavevector is changed. The spin filtering effect does not exist in this configuration.

2.1.3.3 ***In-plane wavevector perpendicular to magnetization ($\overrightarrow{k} \perp \overrightarrow{M}$)***

The exchange potential is still along the x direction and the in-plane wavevector is taken parallel to the y direction, $\mathbf{k}_{\parallel} = (\xi,\ 0)$.

Parallel magnetic configuration ($\uparrow\uparrow$) The Hamiltonian in the layers is now, (see Fig. 9):

$$\hat{H}_{\xi} = \begin{cases} \gamma_c\left(\xi^2+k^2\right) + w\sigma_x + \gamma\xi k^2\sigma_y & \text{if } z<0 \text{ or } z>a \\ \gamma_c\left(\xi^2+k^2\right) + \gamma\xi k^2\sigma_y + V & \text{if } 0<z<a \end{cases}$$

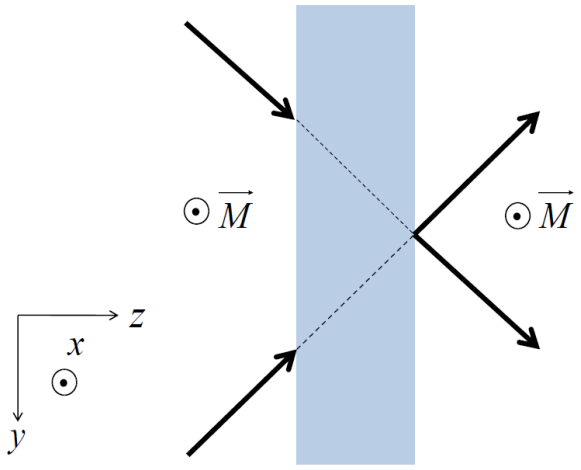

Figure 9: Schema of transmission process through a tunnel junction grown along z direction, PA magnetization **M** along x. In-plane waveveccotor $\mathbf{k}_{\parallel} = (0,\, \xi)$. Carriers with $+\xi$ and $-\xi$ in-plane wavevector components have equal transmission coefficients.

In this case, we obtain the relation $\hat{H}_{-\xi} = \hat{H}^*_{+\xi}$. This relation leads to:

$$t\,(-\xi) = t^*\,(+\xi)\,, \tag{16}$$

where $t(\pm\xi)$ is the transmission amplitude for an electron with the in-plane wavevectors $\pm\xi$. Therefore,

$$\begin{aligned} |t(-\xi)|^2 &= |t^*(+\xi)|^2\,, \\ \text{or } T_- &= T_+. \end{aligned} \tag{17}$$

Equation 17 shows that the transmission coefficient is independent of the sign of in-plane wavevector so that the spin filtering effect naturally disappears like proven by the symmetry argument developed hereafter. This means that the spin filtering effect disappears together with the generation of the in-plane current. This is the reason why in Fig. 7 c the transmissions calculated for opposite values of k_y are equal.

Anti-parallel magnetic configuration (↑↓) The electron Hamiltonian writes (see Fig. 11):

$$\hat{H}_{\xi} = \begin{cases} \gamma_c\left(\xi^2 + k^2\right) + w\sigma_x + \gamma\xi k^2\sigma_y & \text{if } z < 0\,, \\ \gamma_c\left(\xi^2 + k^2\right) + \gamma\xi k^2\sigma_y \; + V & \text{if } 0 < z < a, \\ \gamma_c\left(\xi^2 + k^2\right) - w\sigma_x + \gamma\xi k^2\sigma_y & \text{if } z > 0\,. \end{cases} \tag{18}$$

In this case, we also obtain $\hat{H}_{-\xi} = \hat{H}^*_{+\xi}$. For the same reason as discussed in the case of PA configuration, there is either no spin filtering in this case, as can be shown by simple symmetry arguments [11].

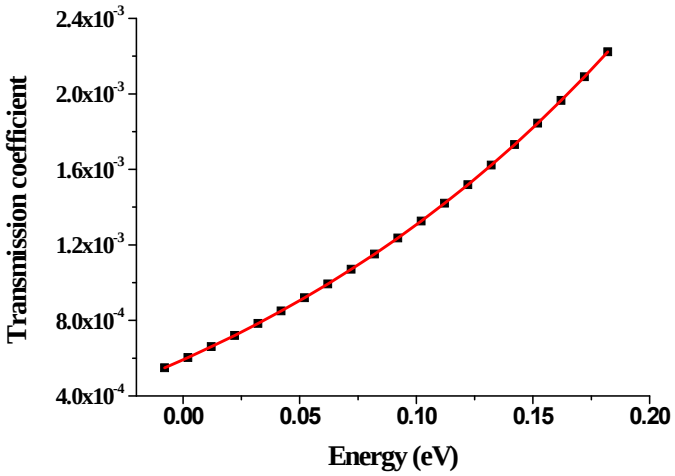

Figure 10: Electron transmission coeffcient *vs.* incident energy calculated using a 2-band **k.p** code (present work), PA magnetizations **M** along x, $k_y = 0.02$ Å^{-1} (solid line), $k_y = -0.02$ Å^{-1} (dotted line), exchange potential in electrodes 0.3 eV, barrier thickness 3 nm, barrier height 1 eV.

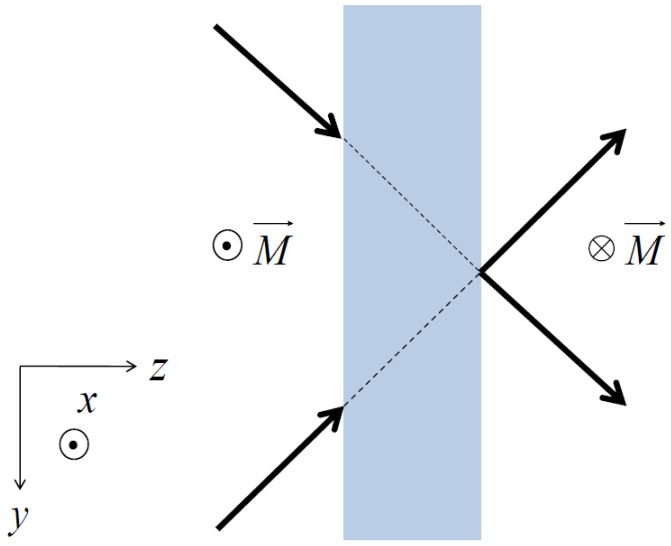

Figure 11: Schema of transmission process through a tunnel junction grown along z direction, AP magnetizations **M** and **-M** along x, in-plane waveveccor $\mathbf{k}_{\|} = (0,\, \xi)$. Carriers with $+\xi$ and $-\xi$ in-plane wavevector components have equal transmission coefficients.

For coordinate axes x, y, and z parallel to the cubic crystallographic axes, a conclusion is that the spin filtering effect only arises through the in-plane components of the Dresselhaus terms. This effect exits in the case where the wavevector is parallel to the spin direction of the incident electrons but it vanishes in the AP magnetic configuration. In the case of an in-plane wavevector perpendicular to the incoming spin direction, the spin filtering effect does not exist.

2.1.4 Spin filtering effect viewed from a 14-band k.p model (present work)

In a 14-band **k**.**p** approach, the lack of inversion symmetry is introduced by **k**.**p** matrix elements coupling the first conduction band (Γ_6) and the higher conduction bands (Γ_{5C}), P', and by supplementary spin-orbit terms coupling the valence bands (Γ_5) and higher conduction bands, Δ'. The Dresselhaus term is obtained by the projection of the 14-band **k**.**p** Hamiltonian on the first conduction band defining an effective Hamiltonian of reduced dimension [43, 44] in a Löwdin or Rayleigh-Schrödinger approach [22]:

$$\gamma = \gamma_3 + \gamma_4,$$

$$\gamma_3 = \frac{4}{9} P_X P P' \frac{\Delta \left(E^G + 2E^\Delta\right) + \Delta^C \left(E_G + 2E_\Delta\right)}{E_G E_\Delta E^G E^\Delta},$$

$$\gamma_4 = -\frac{4}{9} P_X \Delta' \frac{P^2 \left(2E^G + E^\Delta\right) + P'^2 \left(E_G + 2E_\Delta\right)}{E_G E_\Delta E^G E^\Delta},$$

γ_3 is obtained via third-order perturbation, whereas γ_4 is obtained via fourth-order perturbation series.

The energies of $\uparrow$- and $\downarrow$-spin states in the first CB in a 2-band effective model can then be evaluated according to:

$$\mathcal{E}_\pm = \gamma_C k^2 \pm \gamma \sqrt{k^2 \left(k_x^2 k_y^2 + k_y^2 k_z^2 + k_z^2 k_x^2\right) - 9 k_x^2 k_y^2 k_z^2}.$$

For a fixed energy and in-plane wavevector, the $\uparrow$- and $\downarrow$-spin states are associated to different wavevectors along the tunneling direction (z direction in this case).

Besides, we checked the validity of our numerical 14-band tunneling code. We have checked the value of the electron effective mass calculated in the 14-band **k**.**p** model by comparing the transmission coefficient *vs.* barrier thickness between the 14-band **k**.**p** (red line) and the 2-band **k**.**p** effective models (black line) (see Fig. 12 upper panel). The electron effective mass in the 2-band **k**.**p** model was taken to be $m^* = 0.067 m_0$; an exchange potential $2w = 0.3$ eV in PA configuration is considered in the electrodes; the barrier height is taken to be 1 eV, $k_\parallel = 0.02$ Å^{-1}, incident energy is -0.119 eV. The low incident energy is chosen to describe tunneling near the Γ point. The parameters used in the 14-band **k**.**p** code are chosen to be very close to the values given by J.-M. Jancu *et al*.

in Ref. [34]. From this set of results, we observe that the GaAs electron effective mass is close to the one given in the literature. Figure 12 (lower panel) displays the spin filtering effect, defined as in Eq. 12, calculated through the 14-band **k**.**p** tunneling code (red line) and the 2-band effective model (black line). In this case, the Dresselhaus coefficient in the barrier was fixed at $\gamma = 23,5$ eVÅ^3. The spin filtering effect strongly depends on the barrier thickness. We observe a very good agreement between these results which proves the validity of our 14-band **k**.**p** approach (detailed hereafter). Besides, we will show in the next chapter that ATHE very weakly depends on the barrier thickness.

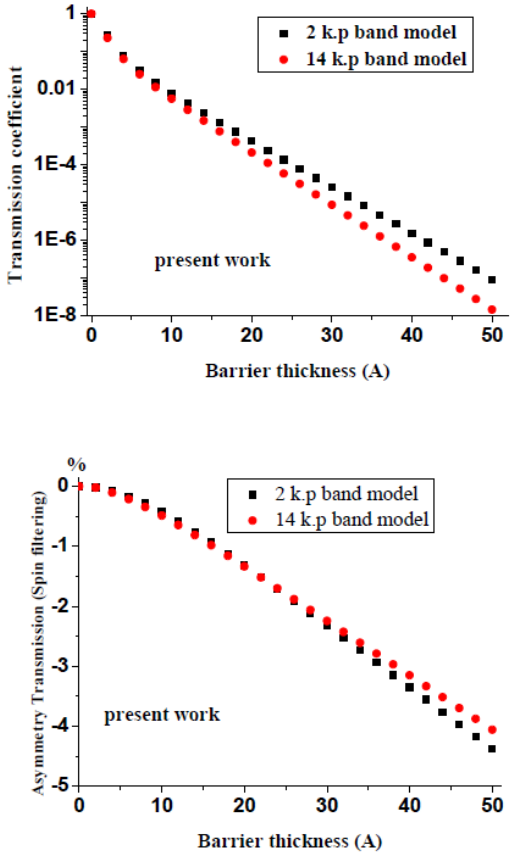

Figure 12: Upper (present work): Transmission coefficient through a GaAs barrier *vs.* barrier thickess calculated in a 2-band effective model (black lines), and in 14-band **k.p (**red lines**).** The parameters are: parallel magnetization in electrode with exchange potential $2w$=0.3 eV, barrier height 1 eV, $\mathcal{E} = -0.119$ eV; $k_{\|} = 0.02$ Å^{-1}; $m^* = 0.067m_0$, $\gamma = 23.5$ eVÅ^3; and band parameters of 14- band **k.p** taken from Ref [34]; Lower (present work): Respective transmission asymmetry coefficient *vs.* barrier thickness.

2.1.4.1 ***Double-barrier resonant transmission***

In order to derive the effective Dresselhaus interactions in a more subtle way, we have considered the case of double-barrier resonant structures where the inversion symmetry

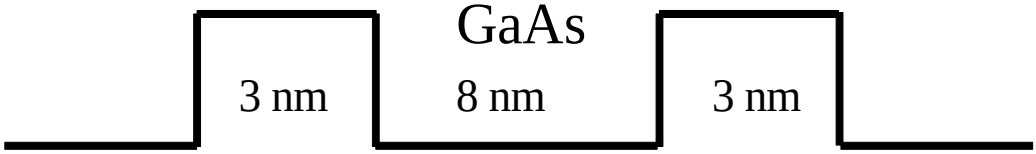

Figure 13: Double barrier structure, QW is made of materials belonging to T_d symmetry group like GaAs; barrier thickness 3 nm, QW width 8 nm, barrier height 1 eV.

is broken only in the QW, *i.e.*, $P' \neq 0$ and $\Delta' \neq 0$ in the QW whereas their values are zero outside the QW. To simplify, we assume that the electron effective masses coincide in all layers. These calculations yield the splitting of the resonant peaks and also allow us to check the robustness of our 14-band **k.p** tunneling code. The electron transmission coefficient, with $k_{\|} = k_y = 0.02$ Å^{-1}, in the structure shown in Fig. 13 is evaluated. The transmission coefficient as a function of energy is displayed in Fig. 14, in a 14-band **k**.**p** tunneling model (lower) and 2-band effective model (upper).

We call $\mathcal{E}_1$ is the peak energy for $\uparrow$-spin

$$\mathcal{E}_1 = \gamma_c \left(k_{1,z}^2 + k_{\|}^2\right) - \gamma \sqrt{k_1^2 \left(k_x^2 k_y^2 + k_y^2 k_{1,z}^2 + k_{1,z}^2 k_x^2\right) - 9 k_x^2 k_y^2 k_{1,z}^2}, \qquad (19)$$

and $\mathcal{E}_2$ is the peak energy for $\downarrow$-spin

$$\mathcal{E}_2 = \gamma_c \left(k_{2,z}^2 + k_{\|}^2\right) + \gamma \sqrt{k_2^2 \left(k_x^2 k_y^2 + k_y^2 k_{2,z}^2 + k_{2,z}^2 k_x^2\right) - 9 k_x^2 k_y^2 k_{2,z}^2}. \qquad (20)$$

The Dresselhaus terms in the QW split the $\uparrow$- and $\downarrow$-spin subbands by $\Delta\mathcal{E} = 0.7$ meV for the 2-band effective model with $m^* = 0.067 m_0$, $\gamma = 23.5$ eVÅ^3, and by $\Delta\mathcal{E} = 0.68$ meV for the 14-band **k**.**p** model.

We have extracted the value of the Dresselhaus coefficient in the bulk and of the effective mass in the 14-band **k**.**p** model. From the 14-band code we have: $\mathcal{E}_1 = 0.089$ eV, respective out-of plane wavevectors $k_{z1} = 0.036$ Å^{-1} and $k'_{z1} = 0.035$ Å^{-1}; $\mathcal{E}_2 = 0.088$ eV, for the out-of-plane wavevector $k_{z2} = 0.0355$ Å^{-1} and $k'_{z2} = 0.035$ Å^{-1}. Solving Eqs. 19 and 20, and using the above values, we obtain $m^* \approx 0.067 m_0$ and $\gamma = 23.5$ eVÅ^3. These values perfectly agree with the data from previous works [34].

Moreover, we have considered the in-plane dispersion of a QW in the valence band for holes. Figure. 15 displays the hole dispersion $\mathcal{E}(k_{\|})$ in a 8 nm-wide GaAs QW calculated in a 14-band **k.p** model. Our results are similar to those obtained by Hayden *et al*. [45] with a specific inverted effective hole mass for the third heavy hole band (HH3). The agreement between the experimental dispersion of $\mathcal{E}(k)$ and the calculated one is perfect up to HH2. Afterwards, above HH2 the quantization energy does not fit any more simply because of the electronic leakage through the barrier at small barrier thickness.

Eventually, from our numerical results we have calculated the electron effective

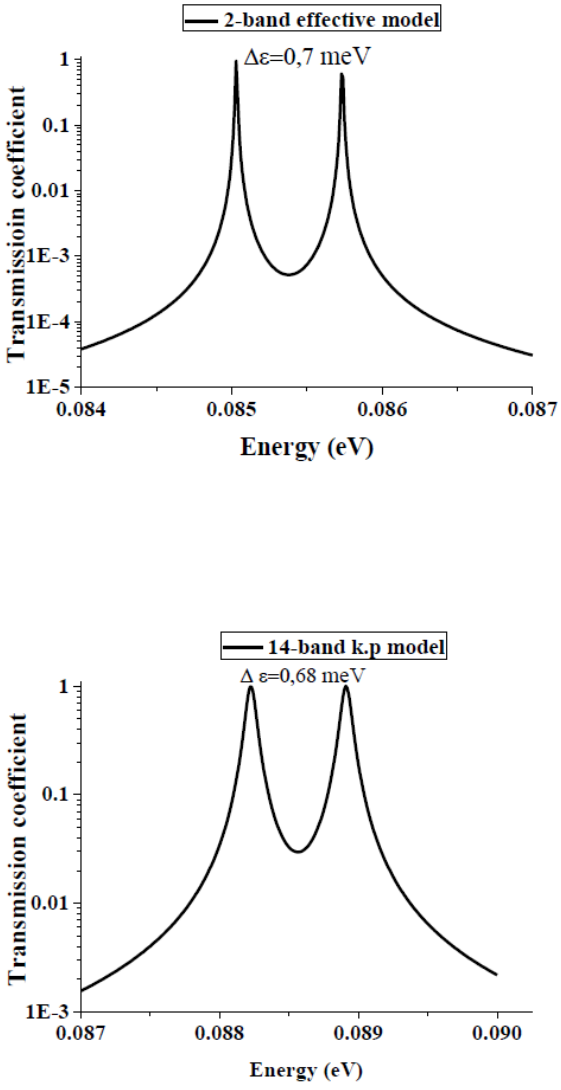

Figure 14: Electron transmission coefficient *vs.* incident energy through double barriers GaAs/ GaAs /GaAs/ GaAs/ GaAs (3 nm/8 nm/3 nm); barrier thickness 1 eV; $k_{\|} = k_y = 0.02$ Å^{-1} for the 2-band effective model; (Upper) with fixed $m^* = 0.067m_0$ and $\gamma = 23.5$ eVÅ^3; (Lower) 14-band **k.p** model with parameters close to the values given in Ref. [34].

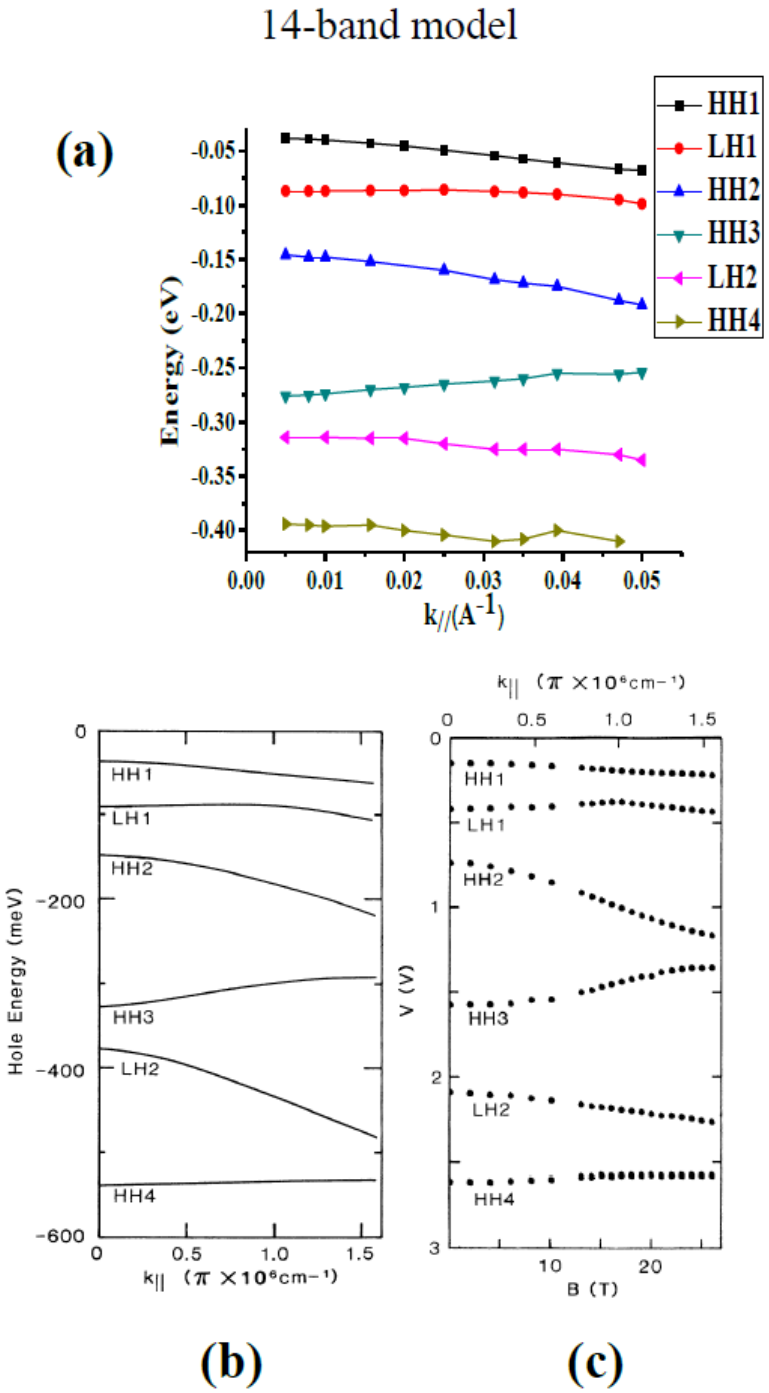

Figure 15: (a) Hole subband dispersion *vs.* in-plane wavevector for 8 nm GaAs QWs grown along the [001] direction, calculated by 14-band **k**.**p** model; Hole dispersion *vs.* in-plane wavevector for 4.2 nm GaAs QWs [45]: (b) calculation, (c) experiment.

masses and the Dresselhaus bulk coefficients for some materials which are listed in Fig. 16. They perfectly agree with the values given in Refs. [11, 46, 34].

γ	*Exp. 7 I. Vurgaftman et al., J. Appl. Phys. 89, 5815 (2001).*	*Jancu et al. PRB 72, 193201 (2005)*	*Perel et al. PRB 67, 201304 (R), 2003*	*Present work (T.H. Dang et al. 2015)*	**Effective mass** *Perel et al. PRB 67, 201304 (R) 2003*	**Effective mass (current work's parameters)**
GaAs	17.4-26	24.4	24	23.5	0.067	0.067
GaSb	185	176	187	180	0.043	0.0381
InAs	-	48.6	130	130	0.023	0.023
InSb	226	465	220	335	0.013	0.0136
AlAs	-	11.2	11.4	17	0.16	0.15

Figure 16: Electron effective mass (present work) and Dresselhaus constant in bulk extracted from our 14-band **k.p** code compared to previous work.

2.2 Spin injection along the [110] crystallographic direction and spin-galvanic effect

The detail of the calculations can be found in Ref. [15].

A particular property of the Dresselhaus interaction is its dependence on the crystallographic direction. The net spin polarization in the structure in Eq. 5

$$P = \frac{|t_+|^2 - |t_-|^2}{|t_+|^2 + |t_-|^2} = \tanh(2\gamma \frac{m_2 k_{\shortparallel}}{\hbar^2} a q_0)$$

cancels because of the equal population of $k_{\|}$ and $-k_{\|}$ states. The spin injection along the [110] direction emerges due to the combined action of the Dessellhaus SOC in the barrier and the Rashba SOC at the barrier interfaces [15]. The Rashba coupling can be considered as an effective magnetic field $\mathbf{\Omega}_R$ lying in the interface plane which rotates the spin direction. The authors consider a zinc blende semiconductor heterostructure with a symmetric potential barrier grown along the $z \parallel [110]$ axis, and an in-plane wavevector $\mathbf{k}_{\|} = (k_x, k_y)$ where $x \parallel [1\bar{1}0]$ and $y \parallel [00\bar{1}]$. The electron effective Hamiltonian is:

$$\hat{H} = \hat{H}_0 + \hat{H}_D + \hat{H}_R,$$

where $\hat{H}_0$ is the Hamiltonian without SOI, $\hat{H}_R$ describes the Rashba SOC at the barrier interface

$$\hat{H}_R = \alpha \left[\delta\left(z-a\right) - \delta\left(z\right)\right]\left(\sigma_x k_y - \sigma_y k_x\right),$$

where a is the barrier thickness, α is the Rashba coefficient and $\delta(z)$ the Dirac distribution; $\hat{H}_D$ is the Dresselhaus Hamiltonian presented as the sum of four terms

$$\begin{aligned}
\hat{H}_{D1} &= i\frac{\sigma_x}{2}\left\{\gamma(z), \frac{\partial^3}{\partial z^3}\right\} \\
\hat{H}_{D2} &= \frac{\sigma_z k_x}{2}\frac{\partial}{\partial z}\gamma(z)\frac{\partial}{\partial z} \\
\hat{H}_{D3} &= i\left[\sigma_x\left(\frac{k_x^2}{2}+k_y^2\right) - 2\sigma_y k_x k_y\right]\left\{\gamma(z), \frac{\partial}{\partial z}\right\} \\
\hat{H}_{D4} &= \sigma_z k_x\left(\frac{k_x^2}{2}-k_y^2\right)\gamma(z)
\end{aligned}$$

$\gamma(z)$ is the bulk Dresselhaus coefficient. The kinetic energy of electrons is assumed substantially smaller than the barrier height, therefore, they neglect $\hat{H}_{D3}$ and $\hat{H}_{D4}$ in comparison with $\hat{H}_{D1}$ and $\hat{H}_{D2}$, respectively. The calculations demonstrate that the term $\hat{H}_{D1}$ does not lead to spin injection to the first order [15, 31]. In Ref. [15], the authors focused on the combined effect of the term $\hat{H}_{D2}$ and the Rashba term. The mechanism of spin injection along the [110] direction can be viewed in Fig. 17. They assume that the electrons impinging the barrier are unpolarized and that their distribution in the interface plane is isotropic. The incident electrons are transmitted with different in-plane wavevectors k_x. As in the case of the spin filtering effect described in Sec. 2.1.3.2, a spin polarized current is generated. In the case where the Rashba term is absent, the equal population of the k_x and $-k_x$ states makes that the net spin polarization goes to zero. The Rashba coupling is considered as an effective Hamiltonian with $\mathbf{\Omega}_R$ proportional to k_x, leading to a rotation with opposite axes for electron with positive and negative k_x. The spin injection is analyzed by using the spin-dependent transfer matrix technique. They assume that the effective masses inside and outside the barrier are the same (m) and neglect the spin-orbit coupling outside the barrier.

The conclusion is that the spin distribution of the transmitted electrons is an even function of the in-plane wavevector ,

$$S_{k,x} = 2\frac{\alpha\gamma m^2 k_x^2 k_z a}{\hbar^4 q},$$

where q is the electron wavevector in the barrier when SOI is neglected. Therefore spin injection along the [110] direction occurs even for an isotropic distribution of the incident electrons in the interface plane.

Beside the spin injection, the authors consider the emergence of a direct electric current j_z, through the barrier in the presence of spin polarization, which is possible

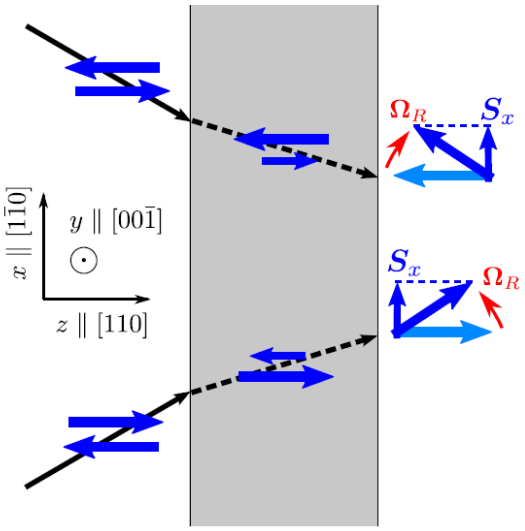

Figure 17: The model of spin injection via a $[110]$-grown barrier. The spin component $S_x > 0$ of electrons transmitted through the barrier with different in-plane wavevectors emerges due to (i) anisotropic spin filtering caused by the Dresselhaus SOC in the barrier interior followed by (ii) spin rotation in the interface-included Rashba magnetic field $\mathbf{\Omega}_R$ [15].

in the [110] direction. Taking into account that the transmission coefficients for the electrons incident upon the barrier from left and from right, the tunneling current density is

$$j_z = e\sum_k Tr\left[T_k(a)\rho_l T_k^+(a)\right] v_z\Theta(v_z) + e\sum_k Tr\left[T_k(-a)\rho_r T_k^+(-a)\right] v_z\Theta(-v_z)$$

where ρ_l (ρ_r) is the spin density matrix on the left (right), e is the electron charge, $T_k(a)$ and $T_k(-a)$ are matrices of transmission amplitude for an electron propagating from the left to the right and from the right to left. The calculation yields the tunnel current

$$j_z = \frac{64ep_s}{105\pi^2}\frac{\alpha\gamma mak_F^9}{\hbar^3k^3}\exp(-2\sqrt{2mV/\hbar^2})$$

where k_F is the Fermi wavevector, p_s is the spin polarization along the x axis, V is barrier height.

2.2.1 Spin rotation along the [110] direction

The spin filtering effect in heterostructures grown along the [110] direction without ferromagnetism was considered in Ref. [31]. It was shown that, in the simplest case, under normal incidence, no solution can be calculated in the usual way assuming that the wave function and its derivative are continuous. The energies of the electrons along

the [110] axis with normal incidence $\mathbf{k} = k(1/\sqrt{2})[110]$ are

$$\text{for} \quad \uparrow \quad \text{-spin } \mathcal{E}_\uparrow = \gamma_c k^2 + \frac{1}{2}\gamma k^3,$$
$$\text{for} \quad \downarrow \quad \text{-spin } \mathcal{E}_\downarrow = \gamma_c k^2 - \frac{1}{2}\gamma k^3.$$

Respectively, their eigenvectors satisfy two equations in parallel

$$\left[-\gamma_c \frac{\partial^2}{\partial z^2} + \frac{1}{2} i\gamma \frac{\partial^3}{\partial z^3}\right] \Psi_\uparrow = \left[\mathcal{E} - V(z)\right] \Psi_\uparrow, \tag{21}$$

$$\left[-\gamma_c \frac{\partial^2}{\partial z^2} - \frac{1}{2} i\gamma \frac{\partial^3}{\partial z^3}\right] \Psi_\downarrow = \left[\mathcal{E} - V(z)\right] \Psi_\downarrow, \tag{22}$$

where $V(z) = V$ when $0 \leq z \leq a$ and $V(z) = 0$ outside.

If the in-plane wavevector in the barrier is purely imaginary, $\pm iK$, the respective energy $-\gamma_c K^2 \mp \frac{1}{2} i\gamma K^3$ will be not real. Therefore, the wavevectors in the barrier are complex quatities, *i.e.*, $Q \pm iK$. Let us write $\Uparrow = \uparrow e^{iQz}$ and $\Downarrow = \downarrow e^{iQz}$.

We first try to deal with this situation according to the usual procedure. The wave function writes

$$\Psi = \begin{cases} \Psi_I(z) = (A_1 e^{iqz} + B_1 e^{-iqz}) \uparrow + \tilde{B}_1 e^{-iqz} \downarrow \ (z < 0), \\ \Psi_{II}(z) = \left(A_2 e^{-Kz} + B_2 e^{Kz}\right) \Uparrow + \left(\tilde{A}_2 e^{-Kz} + \tilde{B}_2 e^{Kz}\right) \Downarrow \ (0 \leq z \leq a), \\ \Psi_{III}(z) = A_3 e^{iqz} \uparrow + \tilde{A}_3 e^{iqz} \downarrow \ (z > a). \end{cases}$$

Applying the BDD [33] matching conditions for $\downarrow$- spin states, we find:

$$\begin{cases} \tilde{B}_1 = \tilde{A}_2 + \tilde{B}_2, \\ q\tilde{B} = (Q - iK)\,\tilde{A}_2 + (Q + iK)\,\tilde{B}_2, \\ \tilde{A}_2 e^{-i(Q-iK)a} + \tilde{B}_2 e^{-i(Q+iK)a} = \tilde{A}_3 e^{iqa}, \\ (Q - iK)\tilde{A}_2 e^{-i(Q-iK)a} + (Q + iK)\tilde{B}_2 e^{-i(Q+iK)a} = -q\tilde{A}_3 e^{iqa}. \end{cases} \tag{23}$$

These equations have a (non zero) solution when

$$\left(q^2 - Q^2 - K^2\right) \sinh Ka + 2iKq \cosh Ka = 0.$$

The only solution is $K = 0$ but it is not relevant to our problem.

As introduced above, the DP term was obtained by perturbation method, so that we will look for a solution of the effective Schrödinger equation to the first order in γ only, *e.g.* for $\uparrow$- spin $\Psi_\uparrow = \Psi^{(0)} + \Psi^{(1)}_\uparrow$ where $\Psi^{(0)}$ is solution when Dresselhaus terms are neglected.

The Schrödinger equation for $\uparrow$- spin in Eq. 21 becomes

$$\left[-\gamma_c \frac{\partial^2 \Psi_\uparrow}{\partial z^2} + \frac{1}{2} i\gamma \frac{\partial^3 \Psi^{(0)}}{\partial z^3}\right] = \left[\mathcal{E} - V(z)\right] \Psi_\uparrow.$$

Integrating this equation from one side of the interface to the other, the authors obtain

$$\lim_{\varepsilon \longrightarrow 0} \left[-\gamma_c \frac{\partial \Psi_\uparrow}{\partial z}\Big|_{z_0-\varepsilon}^{z_0+\varepsilon} + \frac{1}{2} i\gamma \frac{\partial^2 \Psi^{(0)}}{\partial z^2}\Big|_{z_0-\varepsilon}^{z_0+\varepsilon}\right] = 0. \tag{24}$$

Note that, in the electrodes, if the incident wave has a wavevector q, the reflected wave will have wavevector $-q'$, where $\gamma_c q^2 + \frac{1}{2}\gamma q^3 = \gamma_c q'^2 - \frac{1}{2}\gamma q'^3$. It leads to $\delta q = q' - q$ being a second order term in γ so that this term can be neglected. This means there is no spin splitting in the electrode.

In the case of free electrons, it can be shown that:

$$\frac{\partial^2 \Psi^{(0)}}{\partial z^2}\Big|_{z_0-\varepsilon}^{z_0+\varepsilon} = \left(K^2 + q^2\right) \Psi^{(0)}\left(z_0\right). \tag{25}$$

From Eqs. 24 and 25

$$\lim_{\varepsilon \longrightarrow 0} \left(\frac{\partial \Psi_\uparrow}{\partial z}\Big|_{z_0-\varepsilon}^{z_0+\varepsilon}\right) = \frac{i\gamma}{2\gamma_c} \left(K^2 + q^2\right) \Psi^{(0)}\left(z_0\right) \approx 2iQ_\uparrow \Psi^{(0)}\left(z_0\right). \tag{26}$$

Equation. 26 clearly shows the discontinuity of the derivative of the wave function at an interface grown along the [110] direction in the presence of DP field.

Now, the solutions of the Schrödinger equation have to satisfy the new matching condition, *e.g.* for ↑-spin that are:

$$\text{The continuity of the wave function } \Psi, \text{ and } \lim_{\varepsilon \longrightarrow 0} \left(\frac{\partial \Psi_\uparrow}{\partial z}\Big|_{z_0-\varepsilon}^{z_0+\varepsilon}\right) = 2iQ_\uparrow \Psi^{(0)}\left(z_0\right). \tag{27}$$

We write $Q_\uparrow = Q$ for ↑-spin and $Q_\downarrow = -Q$ for ↓-spin.

The solution of the Schrödinger equation is calculated to the first order in γ in the form

$$\Psi = \varphi^s + \varphi^{\hat{s}},$$

where

$$\varphi^s = \begin{cases} \varphi^s_I(z) = a_1 e^{iqz} + b_1 e^{-iqz} & (z < 0), \\ \varphi^s_{II}(z) = \left(a_2 e^{-Kz} + b_2 e^{Kz}\right) e^{iQz} & (0 < z < a), \\ \varphi^s_{III}(z) = a_3 e^{iqz} e^{iQz} & (a < z). \end{cases}$$

and

$$\varphi^{\hat{s}} = \begin{cases} \varphi^{\hat{s}}_I(z) = \beta_1 Q e^{-iqz} & (z < 0), \\ \varphi^{\hat{s}}_{II}(z) = Q\left(\alpha_2 e^{-Kz} + \beta_2 e^{Kz}\right) e^{iQz} & (0 < z < a), \\ \varphi^{\hat{s}}_{III}(z) = \alpha'_3 Q e^{iqz} & (a < z). \end{cases}$$

The new matching conditions state that

(i) φ^s and $\varphi^{\hat{s}}$ are continuous at the interfaces,

(ii) $\lim_{\varepsilon \longrightarrow 0} \left(\frac{\partial \left(\varphi^s + \varphi^{\hat{s}} \right)}{\partial z} \Big|_{z_0 - \varepsilon}^{z_0 + \varepsilon} \right) = iQ\Psi_{II}^{(0)}(z_0).$

The detail of the calculations can be found in Ref. [31]; in that work it is found that $\alpha_3' = 0$ and the amplitudes of the transmission coefficients are $a_3 e^{iQz}$ for $\uparrow$-spin and $a_3 e^{-iQz}$ for $\downarrow$-spin. Therefore, $\uparrow$- and $\downarrow$-spins are transmitted equivalently: there is no spin filtering effect for normal incidence along the [110] direction.

The conclusion of this section is that it is very difficult to find the exact analytical solution for electron tunneling through a heterostructure grown along [110] direction. In the simplest model, the normal incoming electron was treated to the first order in γ. Even though along the [110] direction the spin spliting is maximum. There is not necessary a spin filtering effect. The difficulties do not only come from the mathematical techniques but also from the physical point of view; the discontinuity of the derivative of the wave function caused by the **k** cubic term highlight the crucial the role of the matching conditions. The consequence is that numerical computational techniques, *e.g.* using advanced **k**.**p** methods, like 14-band or 30-band tunneling codes, become mandatory in order to analyse the new properties brought by spin-orbit effects over the BZ. The techniques we have employed and developed beyond the state of the art, will also appear to be perfect numerical tools to check some analytical developments based on perturbation technique approaches.

CHAPTER III

DESCRIPTION OF THE K.P METHODS FOR SEMICONDUCTORS AND HETEROSTRUCTURES

In this chapter, we will present in some detail the principles and methods in the **k**.**p** framework to describe the electronic band structure and (spin-polarized) transport in the semiconductor heterostructures which are considered in the present manuscript. The **k**.**p** approach [47, 48, 49, 50, 51, 52, 53] is known to be very efficient to accurately describe the properties of the electronic structure near the Γ point using a 2-band model for the conduction sates, a 6-band Luttinger model for the only VB of p-symmetry in an effective Hamiltonian approach using the Luttinger parameters γ_i in a multi-orbital band description [54, 55]. However a 8-band **k**.**p** model is needed to describe the coupling between the CB and VB, whereas a 14-band **k**.**p** model is necessary to deal properly with the absence of inversion symmetry with the Dresselhaus SOI [44]. This had never been adressed in the frame of a **k**.**p** model for transport in a multi-layered structure. One can presently cite the recent work performed at IOFFE institute [56] for the numerical analysis of the matching conditions required by the effective Dresselhaus parameters of a III-V QW embedded between thick tunnel barriers in a 4-band approach derived from a larger 14-band model. Nonetheless, the effect and physics of spin as well as the spin-orbit assisted injection from a ferromagnetic reservoir within a 14-band **k**.**p** code have never been addressed before. The present work represents a real advance for our community.

Beyond, an extended 30-band **k**.**p** tunneling approach [22, 57, 58] is mandatory to describe the spin-injection properties in a full-BZ approach, as required for indirect band gap group IV semiconductors like Si, Ge, their compounds, and related heterostructures. Their treatment requires to include remote bands in the Hamiltonian representation. The description of spin-dependent tunneling transport in a 14-band or 30-band **k**.**p** approach requires to unpin the unsolved issue of the spurious bands inherent to band truncation in the **k**.**p** approach [58, 59, 60]. We will discuss that particular point in the present chapter.

Note that, in recent work [61, 62] concerning spin-orbit assisted transport in group IV semiconductors as well as metallic interface Ag/Bi [111] involving Rasha interaction at the interfaces, the **k.p** framework has been shown to represent a valid and relevant approach to describe unusual spin splittings in interface states.

3.1 Principle of the k.p method

The details can be found in Refs. [12, 22].

Taking into account the SOI, the electron Hamiltonian in the crystal is written:

$$\begin{aligned}\hat{H}_{SC} &= \frac{\mathbf{p}^2}{2m_0} + \mathfrak{U} + \frac{\hbar}{4m_0^2c^2}\left(\boldsymbol{\nabla}\mathfrak{U}\times\mathbf{p}\right).\boldsymbol{\sigma} \\ &= \hat{H}_{\mathfrak{U}} + \hat{H}_{SO},\end{aligned} \tag{28}$$

where

$$\hat{H}_{\mathfrak{U}} = \frac{\mathbf{p}^2}{2m_0} + \mathfrak{U}, \tag{29}$$

$$\hat{H}_{SO} = \frac{\hbar}{4m_0^2c^2}\left(\boldsymbol{\nabla}\mathfrak{U}\times\mathbf{p}\right).\boldsymbol{\sigma}, \tag{30}$$

$\mathfrak{U} = \mathfrak{U}(\mathbf{r})$ is the lattice periodic potential, m_0 is the free electron mass, $\boldsymbol{\sigma} = \{\sigma_x, \sigma_y, \sigma_z\}$ is the Pauli operator, c is speed of light. The wave function is the solution of the Schrödinger equation $\hat{H}_{SC}\Psi = \mathcal{E}\Psi$, with the Bloch form $\Psi_{n,\mathbf{k}}(\mathbf{r}) = e^{i\mathbf{k}.r}\varphi_{n\mathbf{k}}(\mathbf{r})$.

The term $\hat{H}_{SO} = \frac{\hbar}{4m_0^2c^2}\left(\boldsymbol{\nabla}\mathfrak{U}\times\mathbf{p}\right).\boldsymbol{\sigma} = \frac{\hbar}{4m_0^2c^2}\left(\boldsymbol{\sigma}\times\boldsymbol{\nabla}\mathfrak{U}\right).\mathbf{p}$ represents the SOI.

$$\begin{aligned}\hat{H}_{SO}\Psi &= \left\{\frac{\hbar^2}{4m_0^2c^2}\left(\boldsymbol{\sigma}\times\boldsymbol{\nabla}\mathfrak{U}\right).\mathbf{p}\right\}\left[e^{i\mathbf{k}.r}\varphi_{n\mathbf{k}}(\mathbf{r})\right] \\ &= e^{i\mathbf{k}.r}\left\{\frac{\hbar^2}{4m_0^2c^2}\left(\boldsymbol{\sigma}\times\boldsymbol{\nabla}\mathfrak{U}\right)\right\}.\left[\hbar\mathbf{k}+\mathbf{p}\right]\varphi_{n\mathbf{k}}(\mathbf{r}) \\ &= e^{i\mathbf{k}.r}\left\{\frac{\hbar^2}{4m_0^2c^2}\left(\boldsymbol{\nabla}\mathfrak{U}\times\mathbf{p}\right).\boldsymbol{\sigma}+\frac{\hbar^2}{4m_0^2c^2}\left(\boldsymbol{\nabla}\mathfrak{U}\times\mathbf{k}\right).\boldsymbol{\sigma}\right\}\varphi_{n\mathbf{k}}(\mathbf{r}),\end{aligned} \tag{31}$$

so that

$$\hat{H}_{SC}\Psi = e^{i\mathbf{k}.r}\left[\hat{H}_{SC} + \breve{k}^2 + \frac{\hbar}{m_0}\,\mathbf{k}.\mathbf{p} + \frac{\hbar^2}{4m_0^2c^2}\left(\boldsymbol{\nabla}\mathfrak{U}\times\mathbf{k}\right).\boldsymbol{\sigma}\right]\varphi_{n\mathbf{k}}(\mathbf{r}).$$

The Schrödinger equation becomes:

$$\left[\hat{H}_{SC} + \breve{k}^2 + \frac{\hbar}{m_0}\,\mathbf{k}.\mathbf{p} + \frac{\hbar^2}{4m_0^2c^2}(\boldsymbol{\nabla}\mathfrak{U}\times\mathbf{k}).\boldsymbol{\sigma}\right]\varphi_{n\mathbf{k}} = \mathcal{E}_{n\mathbf{k}}\,\varphi_{n\mathbf{k}}, \tag{32}$$

where $\breve{k}^2 = (\hbar^2/2m_0)k^2$ is the free-electron energy.

The last term $\hat{H}^{\mathbf{k}}_{SO} = \frac{\hbar^2}{4m_0^2c^2}(\boldsymbol{\nabla}\mathfrak{U}\times\mathbf{k}).\boldsymbol{\sigma}$ is zero in the O_h group. In the T_d group, it does not introduce new splittings. Furthermore its influence is negligible [22, 47]. Finally we obtain,

$$\left[\hat{H}_{SC} + \breve{k}^2 + \frac{\hbar}{m_0}\,\mathbf{k}.\mathbf{p}\right]\varphi_{n\mathbf{k}} = \mathcal{E}_{n\mathbf{k}}\,\varphi_{n\mathbf{k}}, \tag{33}$$

The functions $\varphi_{n\mathbf{k}}(\mathbf{r})$ at $\mathbf{k} = \mathbf{0}$ are supposed to be known through their symmetry properties. We denote $\varphi_n = \varphi_{n(\mathbf{k}=0)}(\mathbf{r})$ and $\mathcal{E}_n = \mathcal{E}_{n(\mathbf{k}=0)}$ with $\hat{H}_{SC}\varphi_n = \mathcal{E}_n\varphi_n$. The functions at $\mathbf{k} \neq 0$ can be expanded as series of φ_n

$$\varphi_{n\mathbf{k}}(\mathbf{r}) = \sum_{\mathbf{k}} C_{n\mathbf{k}}\varphi_n.$$

Multiplying Eq. 33 with φ_m^* and integrating over the unit cell, we obtain the equations determining the C_{nk} coefficients:

$$\left[\langle\varphi_m|\left(\hat{H}_{SC}+\frac{\hbar}{m_0}\mathbf{k}.\mathbf{p}\right)|\varphi_n\rangle+\breve{k}^2\delta_{mn}-\mathcal{E}_{nk}\delta_{mn}\right]C_{nk}=0, \tag{34}$$

$\{\varphi_n\}$ is a relevant set of basis functions, $\langle\varphi_m|A|\varphi_n\rangle=(1/\Omega)\int_\Omega\varphi_m^*(\mathbf{r})A\varphi_n(\mathbf{r})d\mathbf{r}$ where Ω is the crystal volume. The energy $\mathcal{E}$ is the solution of the secular equation

$$\det\left(\hat{H}_{\mathbf{k}.\mathbf{p}}-\mathcal{E}\,\hat{\mathbb{I}}\right)=0,$$

$\hat{\mathbb{I}}$ being the identity matrix and

$$\hat{H}_{\mathbf{k}.\mathbf{p}}=\langle\varphi_m|\left(\hat{H}_{SC}+\frac{\hbar}{m_0}\mathbf{k}.\mathbf{p}\right)|\varphi_n\rangle+\breve{k}^2\delta_{mn}. \tag{35}$$

3.2 A 2-band k.p toy model for the conduction and valence band

We first consider a 2-band **k**.**p** toy model which has only one CB, U_C, and one VB, U_V, in order to give an insight in the band coupling in the **k**.**p** approach and in the appearance of spurious states. The simple **k**.**p** toy Hamiltonian then writes:

$$\hat{H}=\begin{array}{c}\begin{array}{cc}|U_C\rangle & |U_V\rangle\end{array}\\\begin{bmatrix}E_G+\breve{k}^2 & Pk\\ Pk & \breve{k}^2\end{bmatrix}\end{array},$$

where E_G is the energy difference between the CB and the VB at the Γ point, and $P=(\hbar/m_0)\langle U_C|\,p\,|U_V\rangle$.

Solving the secular equation

$$\det(\hat{H}-\mathcal{E}\hat{\mathbb{I}})=0,$$

we obtain the relationship between the eigenenergy and wavevector according to

$$\mathcal{E}=\breve{k}^2+\frac{E_G\pm\sqrt{E_G^2+4E_P\breve{k}^2}}{2}, \tag{36}$$

with $E_P=(2m_0/\hbar^2)\,P^2$.

For very small wavevectors, we have $P^2k^2\ll E_G^2$ and the energies in Eq. 36 become:

$$\begin{aligned}\mathcal{E} &= \breve{k}^2\left(1+\frac{E_P}{E_G}\right)+E_G \text{ for electron,}\\ \mathcal{E} &= \breve{k}^2\left(1-\frac{E_P}{E_G}\right) \text{ for hole.}\end{aligned}$$

The ratio E_P/E_G is of the order of 10 so that the electron effective mass $m_e^* = (1 + E_P/E_G)^{-1}$ is positive and the hole effective mass $m_h^* = (1 - E_P/E_G)^{-1}$ is negative as we expected. However, at large scale, k^2 increases faster than $\sqrt{E_G^2 + 4E_P\breve{k}^2}$ which makes the energy in the VB increasing and crossing the band gap (see Fig. 18). Considering then a characteric carrier energy in the band gap (*e.g.* considering tunneling effect through a barrier), propagative states with a very large real wavevector k appear in the electronic structure diagram as well as in the tunneling transport. These unphysical states are called "*spurious states*" and appear as a natural consequence of the truncation of the remote bands necessary to recover the Bloch periodicity. The important point is that the **k**.**p** method was built to describe the electronic structure near the Γ point but not the electronic structure at arbitrary large wavevectors. Spurious states with large imaginary wavevector components are rapidly decaying and therefore they are harmless [63, 64]. Spurious states with large real wavevectors [65, 66] are more problematic because they mix and interact with real states, making it difficult to identify and remove them in numerical calculations.

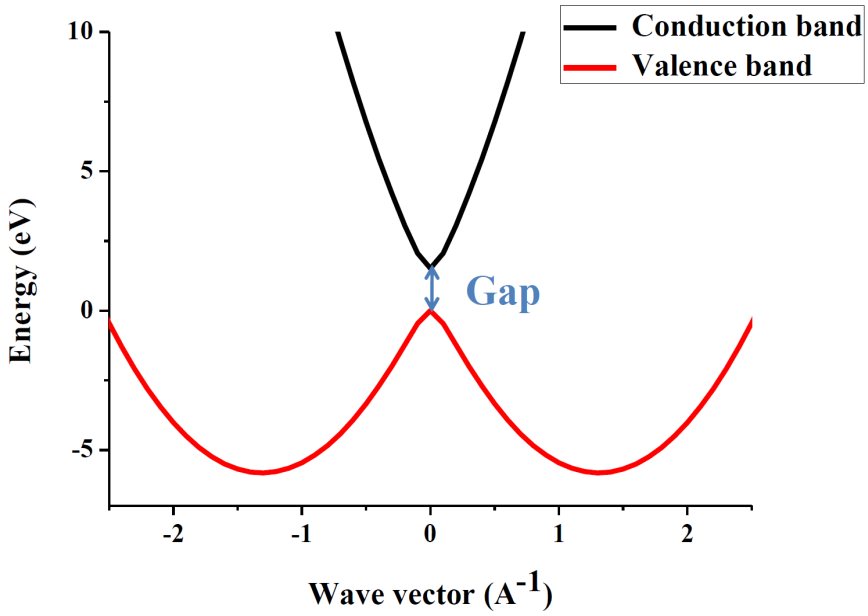

Figure 18: Energy *vs.* wavevector in Eq. 36, with E_P/E_G=10, and $E_g = 1.519$ eV.

In a realistic description of the electronic band structure, the spurious states are well-recognized in 8-band **k**.**p** models [65, 66, 67, 68] and certainly in the larger **k**.**p** models, *e.g.* 14-band **k**.**p** [34], and 30-band **k**.**p** [58, 69]. So far, treating the spurious sates has been a pragmatic recipe. In our work, we managed to treat spurious states far away from the Γ point to remove their influence on our results near the center of BZ. The method to eliminate spurious states will be discussed here in Sec. 3.7.

3.3 14-band k.p matrix

A general overview of the 14-band **k**.**p** basis is displayed in Fig. 19. As mentioned

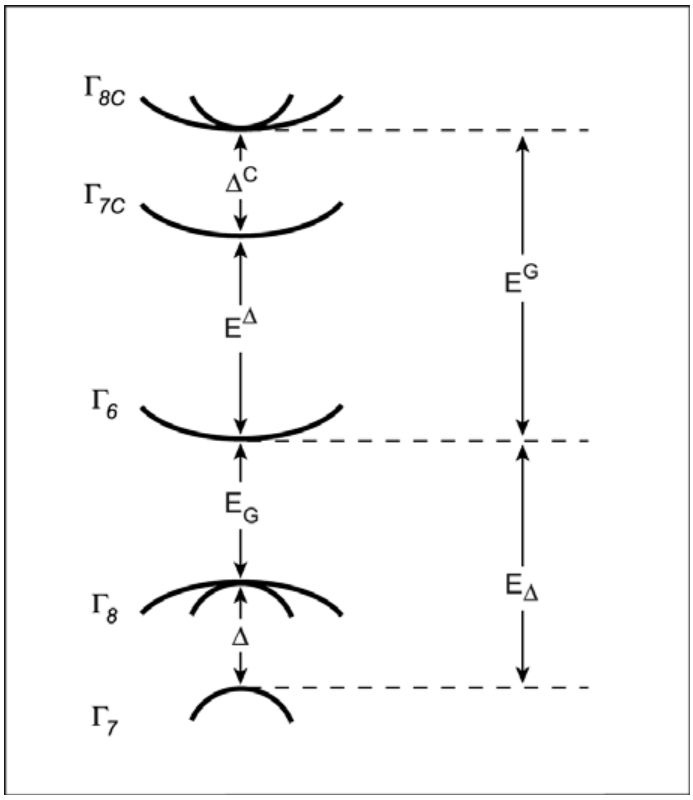

Figure 19: Band schema used in the 14-band **k**.**p** model

before, we need an Hamiltonian which describes the properties of the CB and of the VB when the SOI is taken into account, the smallest possible Hamiltonian being the 14×14 matrix. This Hamiltonian is built in the $\{\Gamma_{8C}, \Gamma_{7C}, \Gamma_6, \Gamma_7, \Gamma_8\}$ irreducible representations like described in Ref. [22]. Its elements will be introduced hereafter. The following basis is chosen to construct the 14×14 **k**.**p** matrix according to Ref. [22].

$$\left.\begin{array}{c}
\left|\frac{3}{2},\frac{3}{2}\right\rangle_{\Gamma_{8C}} = \left|i\left[-\left(1/\sqrt{2}\right)(X_C+iY_C)\uparrow\right]\right\rangle, \\
\left|\frac{3}{2},\frac{1}{2}\right\rangle_{\Gamma_{8C}} = \left|i\left[\sqrt{2/3}Z_C\uparrow -1/\sqrt{6}\,(X_C+iY_C)\downarrow\right]\right\rangle, \\
\left|\frac{3}{2},\frac{-1}{2}\right\rangle_{\Gamma_{8C}} = \left|i\left[1/\sqrt{6}\,(X_C-iY_C)\uparrow +\sqrt{2/3}Z_C\downarrow\right]\right\rangle, \\
\left|\frac{3}{2},\frac{-3}{2}\right\rangle_{\Gamma_{8C}} = \left|i\left[\left(1/\sqrt{2}\right)(X_C-iY_C)\downarrow\right]\right\rangle, \\
\left|\frac{1}{2},\frac{1}{2}\right\rangle_{\Gamma_{7C}} = \left|i\left[1/\sqrt{3}Z_C\uparrow +\sqrt{2/3}\,(X_C+iY_C)\downarrow\right]\right\rangle, \\
\left|\frac{1}{2},\frac{-1}{2}\right\rangle_{\Gamma_{7C}} = \left|i\left[1/\sqrt{3}\,(X_C-iY_C)\uparrow -1/\sqrt{3}Z_C\downarrow\right]\right\rangle,
\end{array}\right\} \quad p\text{-type symmetry}$$

$$\left.\begin{array}{l} |+\rangle = |S\uparrow\rangle\,, \\ |-\rangle = |S\downarrow\rangle\,, \end{array}\right\} \quad s\text{-type symmetry} \tag{37}$$

$$\left.\begin{array}{c} \left|\frac{3}{2},\frac{3}{2}\right\rangle_{\Gamma_8} = \left|i\left[-\left(1/\sqrt{2}\right)(X+iY)\uparrow\right]\right\rangle, \\ \left|\frac{3}{2},\frac{1}{2}\right\rangle_{\Gamma_8} = \left|i\left[\sqrt{2/3}Z\uparrow -1/\sqrt{6}\,(X+iY)\downarrow\right]\right\rangle, \\ \left|\frac{3}{2},\frac{-1}{2}\right\rangle_{\Gamma_8} = \left|i\left[1/\sqrt{6}\,(X-iY)\uparrow +\sqrt{2/3}Z\downarrow\right]\right\rangle, \\ \left|\frac{3}{2},\frac{-3}{2}\right\rangle_{\Gamma_8} = \left|i\left[\left(1/\sqrt{2}\right)(X-iY)\downarrow\right]\right\rangle, \\ \left|\frac{1}{2},\frac{1}{2}\right\rangle_{\Gamma_7} = \left|i\left[1/\sqrt{3}Z\uparrow +\sqrt{1/3}\,(X+iY)\downarrow\right]\right\rangle, \\ \left|\frac{1}{2},\frac{-1}{2}\right\rangle_{\Gamma_7} = \left|i\left[1/\sqrt{3}\,(X-iY)\uparrow -1/\sqrt{3}Z\downarrow\right]\right\rangle. \end{array}\right\} \quad p\text{-type symmetry}$$

In the O_h group, the functions S, X_C, Y_C, and Z_C are antisymmetric; the functions X, Y, and Z are symmetric. In the T_d group, the lack of inversion center destroys the strictly antisymmetric nature of S, X_C, Y_C, and Z_C and strictly symmetrical nature of X, Y, and Z. But, anyway, we keep these notations for the T_d group.

This basis of functions consists of pairs of Kramers' conjugates

$$\begin{aligned} \hat{K}\left|\frac{3}{2},\pm\frac{3}{2}\right\rangle &= \pm\left|\frac{3}{2},\mp\frac{3}{2}\right\rangle, \\ \hat{K}\left|\frac{3}{2},\pm\frac{1}{2}\right\rangle &= \mp\left|\frac{3}{2},\mp\frac{1}{2}\right\rangle, \\ \hat{K}\left|\frac{1}{2},\pm\frac{1}{2}\right\rangle &= \pm\left|\frac{1}{2},\mp\frac{1}{2}\right\rangle. \end{aligned}$$

or

$$\hat{K}\,|j,m\rangle = (-1)^{j-m}\,|j,-m\rangle\,.$$

3.3.1 k.p coupling term

Note that $\hat{H}_{SC} = \hat{H}_{\mathfrak{U}} + \hat{H}_{SO}$ and $\langle\varphi_n|\,\hat{H}_{\mathfrak{U}}\,|\varphi_m\rangle = E_n\delta_{nm}$, particularly in this case

$$\begin{aligned} {}_{\Gamma_{8C}}\left\langle\frac{3}{2},M\right|\hat{H}_{\mathfrak{U}}\left|\frac{3}{2},M\right\rangle_{\Gamma_{8C}} &= {}_{\Gamma_{7C}}\left\langle\frac{1}{2},M\right|\hat{H}_{\mathfrak{U}}\left|\frac{1}{2},M\right\rangle_{\Gamma_{7C}} = E_{5C}, \\ \langle\pm|\,\hat{H}_{\mathfrak{U}}\,|\pm\rangle &= E_1, \\ {}_{\Gamma_{8}}\left\langle\frac{3}{2},M\right|\hat{H}_{\mathfrak{U}}\left|\frac{3}{2},M\right\rangle_{\Gamma_{8}} &= {}_{\Gamma_{7}}\left\langle\frac{1}{2},M\right|\hat{H}_{\mathfrak{U}}\left|\frac{1}{2},M\right\rangle_{\Gamma_{7}} = E_5, \end{aligned}$$

with $M = \left\{\pm\frac{3}{2},\pm\frac{1}{2}\right\}$ for Γ_{8C} and Γ_8, $M = \left\{\pm\frac{1}{2}\right\}$ for Γ_{7C} and Γ_7, so that we need to describe two terms $\langle\varphi_m|\,(\hbar/m_0)\,\mathbf{k}.\mathbf{p}|\varphi_n\rangle$, called $\mathbf{k}.\mathbf{p}$ term, and $\langle\varphi_m|\hat{H}_{SO}|\varphi_n\rangle$ called spin-orbit term to find all the matrix elements in Eq. 35.

By essence, these **k.p** coupling terms are closely linked to the *k*-dependent optical transitions between initial and final excited states through a dipolar Hamiltonian of the type $\hat{H}_D = \overrightarrow{A}.\overrightarrow{p}$ with $\overrightarrow{A}$ is vector potential or equivalently $\hat{H}_D = \overrightarrow{E}.\overrightarrow{r}$ with $\overrightarrow{E}$ is electric field.

Let $U_{n\sigma}$ be the set of functions $\{X_C, Y_C, Z_C, S, X, Y, Z\} \otimes \{\uparrow, \downarrow\}$; the basis functions in Eq. 37 are linear combinations of $U_{n\sigma}$. This allows us to calculate $\langle U_{n\sigma}| \left(\hbar/m_0\right) \mathbf{k}.\mathbf{p} \left|U_{n'\sigma'}\right\rangle$.

$$\langle U_{n\sigma}| \frac{\hbar}{m_0}\mathbf{k}.\mathbf{p} \left|U_{n'\sigma'}\right\rangle = \langle U_n| \frac{\hbar}{m_0}\mathbf{k}.\mathbf{p} \left|U_{n'}\right\rangle \delta_{\sigma\sigma'} \tag{38}$$

This term is possibly non-zero only when the spin remains unchanged ($\sigma = \sigma'$).

In summary, the non-zero **k**.**p** terms are:

(i) the coupling terms between Γ_6 and $\{\Gamma_7, \Gamma_8\}$ representations

$$\langle S| p_x \left|iX\right\rangle = \langle S| p_y \left|iY\right\rangle = \langle S| p_z \left|iZ\right\rangle = \varpi;$$

(ii) the coupling terms between Γ_6 and the second CBs $\{\Gamma_{7C}, \Gamma_{8C}\}$ in the case of lack of inversion center

$$\langle S| p_x \left|iX_C\right\rangle = \langle S| p_y \left|iY_C\right\rangle = \langle S| p_z \left|iZ_C\right\rangle = \varpi',$$

(iii) and the coupling terms between $\{\Gamma_7, \Gamma_8\}$ and $\{\Gamma_{7C}, \Gamma_{8C}\}$

$$\begin{aligned}\langle X| p_y \left|iZ_C\right\rangle &= \langle X| p_z \left|iY_C\right\rangle = \langle Y| p_x \left|iZ_C\right\rangle \\ &= \langle Y| p_z \left|iX_C\right\rangle = \langle Z| p_x \left|iY_C\right\rangle = \langle Z| p_y \left|iX_C\right\rangle = -\varpi_X\end{aligned}$$

where w, w', and w_X are real. In the O_h group, we have $w' = 0$.

The natural $\mathbf{k}.\mathbf{p}$ parameters are introduced according to:

$$P = \frac{\hbar}{m_0}\varpi, \qquad P' = \frac{\hbar}{m_0}\varpi', \qquad P_X = \frac{\hbar}{m_0}\varpi_X;$$

with the characteristic energy

$$E_P = \frac{2m_0}{\hbar^2}P^2, \qquad E'_P = \frac{2m_0}{\hbar^2}P'^2\,, \qquad E_{PX} = \frac{2m_0}{\hbar^2}P_X^2.$$

3.3.2 Spin-orbit coupling

The SOC terms were evaluated using the book of Koster *et al.* [21]. We resume here the couplings which may differ from zero:

(i) The core spin-orbit in the second CB

$$\Delta^C = \left(\frac{3\hbar^2}{4m_0^2c^2}\right) \langle X_C| \frac{\partial \mathfrak{U}}{\partial x}p_y - \frac{\partial \mathfrak{U}}{\partial y}p_x \left|iY_C\right\rangle .$$

(ii) The core spin-orbit in the VB

$$\Delta = \left(\frac{3\hbar^2}{4m_0^2c^2}\right) \langle X| \frac{\partial \mathfrak{U}}{\partial x}p_y - \frac{\partial \mathfrak{U}}{\partial y}p_x \left|iY\right\rangle .$$

(iii) And the spin-orbit caused by the lack of inversion center in the T_d group

$$\Delta' = \left(\frac{3\hbar^2}{4m_0^2c^2}\right) \langle X| \frac{\partial \mathfrak{U}}{\partial x}p_y - \frac{\partial \mathfrak{U}}{\partial y}p_x \left|iY_C\right\rangle .$$

In the O_h group, $\Delta' = 0$.

3.3.3 The 14×14 k.p matrix

The supplementary perturbations originate from remote bands, out of the 14-band subset, *i.e.*, the bands lower than $\{\Gamma_7, \Gamma_8\}$ or upper than $\{\Gamma_6, \Gamma_{7C}, \Gamma_{8C}\}$. They are introduced through the terms:

$$\begin{aligned}
K' &= \frac{2}{m_0}\sum_{n\neq 5C,1,5}\frac{\langle S|\,p_x\,|n\rangle\,\langle n|\,p_x\,|S\rangle}{E_1-E_n},\\
L' &= \frac{2}{m_0}\sum_{n\neq 5C,1,5}\frac{\langle X|\,p_x\,|n\rangle\,\langle n|\,p_x\,|X\rangle}{E_5-E_n},\\
M' &= \frac{2}{m_0}\sum_{n\neq 5C,1,5}\frac{\langle X|\,p_y\,|n\rangle\,\langle n|\,p_y\,|X\rangle}{E_5-E_n},\\
N' &= \frac{2}{m_0}\sum_{n\neq 5C,1,5}\frac{\langle X|\,p_x\,|n\rangle\,\langle n|\,p_y\,|X\rangle+\langle X|\,p_y\,|n\rangle\,\langle n|\,p_x\,|X\rangle}{E_5-E_n}.
\end{aligned}$$

The full 14×14 **k.p** matrix, including perturbations of all remote bands, can be expressed through the measurable effective Luttinger parameters γ_C, γ_j, $\gamma_{\Delta j}$ $(j=1,2,3)$ in both the CB and VB:

$$\begin{aligned}
\gamma_C &= 1-\frac{E'_P}{3}\left(\frac{2}{E_{8C-6}}+\frac{1}{E_{7C-6}}\right)+\frac{E_P}{3}\left(\frac{2}{E_{6-8}}+\frac{1}{E_{6-7}}\right)+K',\\
\gamma_1 &= -1+\frac{E_{PX}}{3}\left(\frac{1}{E_{8C-8}}+\frac{1}{E_{7C-8}}\right)-\frac{L'+2M'}{3}+\frac{E_P}{3E_{6-8}},\\
\gamma_2 &= -\frac{1}{6}\frac{E_{PX}}{E_{7C-8}}-\frac{L'-M'}{6}+\frac{E_P}{6E_{6-8}},\\
\gamma_3 &= \frac{1}{6}\frac{E_{PX}}{E_{7C-8}}-\frac{N'}{6}+\frac{E_P}{6E_{6-8}},\\
\gamma_{\Delta 1} &= -1+\frac{2}{3}\frac{E_{PX}}{E_{8C-7}}-\frac{L'+2M'}{3}+\frac{E_P}{3E_{6-7}},\\
\gamma_{\Delta 2} &= -\frac{E_{PX}}{12}\left(\frac{1}{E_{8C-8}}+\frac{1}{E_{8C-7}}\right)-\frac{L'-M'}{6}+\frac{E_P}{12}\left(\frac{1}{E_{6-8}}+\frac{1}{E_{6-7}}\right),\\
\gamma_{\Delta 3} &= \frac{E_{PX}}{12}\left(\frac{1}{E_{8C-8}}+\frac{1}{E_{8C-7}}\right)-\frac{N'}{6}+\frac{E_P}{12}\left(\frac{1}{E_{6-8}}+\frac{1}{E_{6-7}}\right);
\end{aligned}$$

together with the notations

$E^H_{8C} = E'_{8C} - \gamma'_{C1}\breve{k}^2 + \mathfrak{U}'_C;$
$E^L_{8C} = E'_{8C} - \gamma'_{C1}\breve{k}^2 - \mathfrak{U}'_C;$
$E^k_{7C} = E'_{7C} - \gamma'_{C\Delta 1}\breve{k}^2;$
$E^k_6 = E_6 + \gamma'_C\breve{k}^2;$
$E^H_8 = E'_8 - \gamma'_1\breve{k}^2 + \mathfrak{U}';$
$E^L_8 = E'_8 - \gamma'_1\breve{k}^2 - \mathfrak{U}';$

$E_7^k = E_7' - \gamma_{\Delta 1}' \breve{k}^2$;
$\mathfrak{U}_C' = \gamma_{C2}' \left(2\breve{k}_z^2 - \breve{k}_\rho^2 \right)$;
$\mathfrak{U}_{C\Delta}' = \gamma_{C\Delta 2}' \left(2\breve{k}_z^2 - \breve{k}_\rho^2 \right)$;
$\mathfrak{B}_C' = 2\sqrt{3}\gamma_{C3}' \breve{k}_z \breve{k}_-$;
$\mathfrak{B}_{C\Delta}' = 2\sqrt{3}\gamma_{C\Delta 3}' \breve{k}_z \breve{k}_-$;
$\mathfrak{C}_C' = \sqrt{3} \left[\gamma_{C2}' \left(\breve{k}_x^2 - \breve{k}_y^2 \right) - 2i\gamma_{C3}' \breve{k}_x \breve{k}_y \right]$;
$\mathfrak{C}_{\Delta C}' = \sqrt{3} \left[\gamma_{\Delta C2}' \left(\breve{k}_x^2 - \breve{k}_y^2 \right) - 2i\gamma_{\Delta C3}' \breve{k}_x \breve{k}_y \right]$;
$\mathfrak{U}' = \gamma_2' \left(2\breve{k}_z^2 - \breve{k}_\rho^2 \right)$;
$\mathfrak{U}_\Delta' = \gamma_{\Delta 2}' \left(2\breve{k}_z^2 - \breve{k}_\rho^2 \right)$;
$\mathfrak{B}' = 2\sqrt{3}\gamma_3' \breve{k}_z \breve{k}_-$;
$\mathfrak{B}_\Delta' = 2\sqrt{3}\gamma_{\Delta 3}' \breve{k}_z \breve{k}_-$;
$\mathfrak{C}' = \sqrt{3} \left[\gamma_2' \left(\breve{k}_x^2 - \breve{k}_y^2 \right) - 2i\gamma_3' \breve{k}_x \breve{k}_y \right]$;
$\mathfrak{C}_\Delta' = \sqrt{3} \left[\gamma_{\Delta 2}' \left(\breve{k}_x^2 - \breve{k}_y^2 \right) - 2i\gamma_{\Delta 3}' \breve{k}_x \breve{k}_y \right]$;

where $\breve{k}_\pm = \breve{k}_x \pm i\breve{k}_y$, $\breve{k}_\rho^2 = \breve{k}_x^2 + \breve{k}_y^2$. E_{8C}', E_{7C}', E_8 , and E_7 would, respectively, be the energies $E\left(\Gamma_{8C}\right)$, $E\left(\Gamma_{7C}\right)$, $E\left(\Gamma_8\right)$, and $E\left(\Gamma_7\right)$ at **k**=0 if the interband spin-orbit coupling Δ' were equal to zero.

Furthermore,

$$\gamma_C' = \gamma_C - \frac{E_P}{3}\left(\frac{2}{E_{6-8}} + \frac{1}{E_{6-7}}\right) + \frac{E_P'}{2}\left(\frac{2}{E_{8C-6}} + \frac{1}{E_{7C-6}}\right),$$

$$\gamma_1' = \gamma_1 - \frac{E_P}{3E_{6-8}} - \frac{E_{PX}}{3}\left(\frac{1}{E_{7C-8}} + \frac{1}{E_{8C-8}}\right),$$

$$\gamma_2' = \gamma_2 - \frac{E_P}{6E_{6-8}} + \frac{E_{PX}}{6E_{7C-8}},$$

$$\gamma_3' = \gamma_3 - \frac{E_P}{6E_{6-8}} - \frac{E_{PX}}{6E_{7C-8}},$$

$$\gamma_{C1}' = \gamma_{C1} + \frac{E_P'}{3E_{8C-6}} + \frac{E_{PX}}{3}\left(\frac{1}{E_{8C-8}} + \frac{1}{E_{8C-7}}\right),$$

$$\gamma_{C2}' = \gamma_{C2} + \frac{E_P'}{6E_{8C-6}} - \frac{E_{PX}}{6E_{8C-7}},$$

$$\gamma_{C3}' = \gamma_{C3} + \frac{E_P'}{6E_{8C-6}} + \frac{E_{PX}}{6E_{8C-7}},$$

$$\gamma_{\Delta j}' \simeq \gamma_j';\ \ \gamma_{C\Delta j}' \simeq \gamma_{Cj}',$$

We would like to stress on the particular point that the lack of inversion center does not contribute to the parameters in the VB. We take here the Hamiltonian in a 14×14 **k**.**p** model and plot the following band structure along three characteric directions with parameters close to the values introduced in Ref. [34].

We consider here the overall 14×14 **k**.**p** Hamiltonian with the perturbation of all remote bands which includes linear or quadratic k_i terms but no cubic terms.

$$
\begin{array}{c}
\begin{array}{cccccccccccccc}
\left|c\frac{3}{2}\right\rangle & \left|c\frac{1}{2}\right\rangle & \left|c\frac{-1}{2}\right\rangle & \left|c\frac{-3}{2}\right\rangle & \left|c\frac{7}{2}\right\rangle & \left|c\frac{-7}{2}\right\rangle & |+\rangle & |-\rangle & \left|\frac{3}{2}\right\rangle & \left|\frac{1}{2}\right\rangle & \left|\frac{-1}{2}\right\rangle & \left|\frac{-3}{2}\right\rangle & \left|\frac{7}{2}\right\rangle & \left|\frac{-7}{2}\right\rangle
\end{array}
\\
\left[\begin{array}{cccccccccccccc}
E_{8C}^{H} & \mathfrak{B}'_{C} & \mathfrak{C}'_{C} & 0 & \frac{1}{\sqrt{2}}\mathfrak{B}'_{C\Delta} & \sqrt{2}\mathfrak{C}'_{C\Delta} & \frac{-1}{\sqrt{2}}P'^{-} & 0 & \frac{1}{3}\Delta' & \frac{1}{\sqrt{3}}P_X^{+} & \frac{1}{\sqrt{3}}P_X^{z} & 0 & \frac{1}{\sqrt{6}}P_X^{+} & \sqrt{\frac{2}{3}}P_X^{z} \\
\mathfrak{B}'^{*}_{C} & E_{8C}^{L} & 0 & \mathfrak{C}'_{C} & -\sqrt{2}\mathfrak{A}'_{C\Delta} & -\sqrt{\frac{3}{2}}\mathfrak{B}'_{C\Delta} & \sqrt{\frac{2}{3}}P'^{z} & \frac{-1}{\sqrt{6}}P'^{-} & \frac{-1}{\sqrt{3}}P_X^{-} & \frac{1}{3}\Delta' & 0 & \frac{1}{\sqrt{3}}P_X^{z} & 0 & \frac{-1}{\sqrt{2}}P_X^{+} \\
\mathfrak{C}'^{*}_{C} & 0 & E_{8C}^{L} & -\mathfrak{B}'_{C} & -\sqrt{\frac{3}{2}}\mathfrak{B}'^{*}_{C\Delta} & \sqrt{2}\mathfrak{A}'_{C\Delta} & \frac{-1}{\sqrt{6}}P'^{+} & \sqrt{\frac{2}{3}}P'^{z} & \frac{-1}{\sqrt{3}}P_X^{z} & 0 & \frac{1}{3}\Delta' & \frac{-1}{\sqrt{3}}P_X^{+} & \frac{1}{\sqrt{2}}P_X^{-} & 0 \\
0 & \mathfrak{C}'^{*}_{C} & -\mathfrak{B}'^{*}_{C} & E_{8C}^{H} & -\sqrt{2}\mathfrak{C}'^{*}_{C\Delta} & \frac{1}{\sqrt{2}}\mathfrak{B}'^{*}_{C\Delta} & 0 & \frac{1}{\sqrt{2}}P'^{+} & 0 & \frac{-1}{\sqrt{3}}P_X^{z} & \frac{1}{\sqrt{3}}P_X^{-} & \frac{1}{3}\Delta' & \sqrt{\frac{2}{3}}P_X^{z} & \frac{-1}{\sqrt{6}}P_X^{-} \\
\frac{1}{\sqrt{2}}\mathfrak{B}'^{*}_{C\Delta} & -\sqrt{2}\mathfrak{A}'_{C\Delta} & -\sqrt{\frac{3}{2}}\mathfrak{B}'_{C\Delta} & -\sqrt{2}\mathfrak{C}'_{C\Delta} & E_{7C}^{k} & 0 & \frac{1}{\sqrt{3}}P'^{z} & \frac{1}{\sqrt{6}}P'^{-} & \frac{-1}{\sqrt{6}}P_X^{-} & 0 & \frac{-1}{\sqrt{2}}P_X^{+} & -\sqrt{\frac{2}{3}}P_X^{z} & \frac{-2}{3}\Delta' & 0 \\
\sqrt{2}\mathfrak{C}'^{*}_{C\Delta} & -\sqrt{\frac{3}{2}}\mathfrak{B}'^{*}_{C\Delta} & \sqrt{2}\mathfrak{A}'_{C\Delta} & \frac{1}{\sqrt{2}}\mathfrak{B}'_{C\Delta} & 0 & E_{7C}^{k} & \frac{1}{\sqrt{3}}P'^{+} & \frac{-1}{\sqrt{3}}P'^{z} & -\sqrt{\frac{2}{3}}P_X^{z} & \frac{1}{\sqrt{2}}P_X^{-} & 0 & \frac{1}{\sqrt{6}}P_X^{+} & 0 & \frac{-2}{3}\Delta' \\
\frac{-1}{\sqrt{2}}P'^{+} & \sqrt{\frac{2}{3}}P'^{z} & \frac{1}{\sqrt{6}}P'^{-} & 0 & \frac{1}{\sqrt{3}}P'^{z} & \frac{1}{\sqrt{3}}P'^{-} & E_{6}^{k} & 0 & \frac{-1}{\sqrt{2}}P^{+} & \sqrt{\frac{2}{3}}P^{z} & \frac{1}{\sqrt{6}}P^{-} & 0 & \frac{1}{\sqrt{3}}P^{z} & \frac{1}{\sqrt{3}}P^{-} \\
0 & \frac{-1}{\sqrt{6}}P'^{+} & \sqrt{\frac{2}{3}}P'^{z} & \frac{1}{\sqrt{2}}P'^{-} & \frac{1}{\sqrt{3}}P'^{+} & \frac{-1}{\sqrt{3}}P'^{z} & 0 & E_{6}^{k} & 0 & \frac{-1}{\sqrt{6}}P^{+} & \sqrt{\frac{2}{3}}P^{z} & \frac{1}{\sqrt{2}}P^{-} & \frac{1}{\sqrt{3}}P^{+} & \frac{-1}{\sqrt{3}}P^{z} \\
\frac{1}{3}\Delta' & \frac{-1}{\sqrt{3}}P_X^{+} & \frac{-1}{\sqrt{3}}P_X^{z} & 0 & \frac{-1}{\sqrt{6}}P_X^{+} & -\sqrt{\frac{2}{3}}P_X^{z} & \frac{-1}{\sqrt{2}}P^{-} & 0 & E_{8}^{H} & \mathfrak{B}' & \mathfrak{C}' & 0 & \frac{1}{\sqrt{2}}\mathfrak{B}'_{\Delta} & \sqrt{2}\mathfrak{C}'_{\Delta} \\
\frac{1}{\sqrt{3}}P_X^{-} & \frac{1}{3}\Delta' & 0 & \frac{-1}{\sqrt{3}}P_X^{z} & 0 & \frac{1}{\sqrt{2}}P_X^{+} & \sqrt{\frac{2}{3}}P^{z} & \frac{-1}{\sqrt{6}}P^{-} & \mathfrak{B}'^{*} & E_{8}^{L} & 0 & \mathfrak{C}' & -\sqrt{2}\mathfrak{A}' & -\sqrt{\frac{3}{2}}\mathfrak{B}'_{\Delta} \\
\frac{1}{\sqrt{3}}P_X^{z} & 0 & \frac{1}{3}\Delta' & \frac{1}{\sqrt{3}}P_X^{+} & \frac{-1}{\sqrt{2}}P_X^{-} & 0 & \frac{1}{\sqrt{6}}P^{+} & \sqrt{\frac{2}{3}}P^{z} & \mathfrak{C}'^{*} & 0 & E_{8}^{L} & -\mathfrak{B}' & -\sqrt{\frac{3}{2}}\mathfrak{B}'^{*}_{\Delta} & \sqrt{2}\mathfrak{A}'_{\Delta} \\
0 & \frac{1}{\sqrt{3}}P_X^{z} & \frac{-1}{\sqrt{3}}P_X^{-} & \frac{1}{3}\Delta' & -\sqrt{\frac{2}{3}}P_X^{z} & \frac{1}{\sqrt{6}}P_X^{-} & 0 & \frac{1}{\sqrt{2}}P^{+} & 0 & \mathfrak{C}'^{*} & -\mathfrak{B}'^{*} & E_{8}^{H} & -\sqrt{2}\mathfrak{C}'^{*}_{\Delta} & \frac{1}{\sqrt{2}}\mathfrak{B}'^{*}_{\Delta} \\
\frac{1}{\sqrt{6}}P_X^{-} & 0 & \frac{1}{\sqrt{2}}P_X^{+} & \sqrt{\frac{2}{3}}P_X^{z} & \frac{-2}{3}\Delta' & 0 & \frac{1}{\sqrt{3}}P^{z} & \frac{1}{\sqrt{3}}P^{-} & \frac{1}{\sqrt{2}}\mathfrak{B}'^{*}_{\Delta} & -\sqrt{2}\mathfrak{A}' & -\sqrt{\frac{3}{2}}\mathfrak{B}'_{\Delta} & -\sqrt{2}\mathfrak{C}'_{\Delta} & E_{7}^{k} & 0 \\
\sqrt{\frac{2}{3}}P_X^{z} & \frac{-1}{\sqrt{2}}P_X^{-} & 0 & \frac{-1}{\sqrt{6}}P_X^{+} & 0 & \frac{-2}{3}\Delta' & \frac{1}{\sqrt{3}}P^{+} & \frac{-1}{\sqrt{3}}P^{z} & \sqrt{2}\mathfrak{C}'^{*}_{\Delta} & -\sqrt{\frac{3}{2}}\mathfrak{B}'^{*}_{\Delta} & \sqrt{2}\mathfrak{A}'_{\Delta} & \frac{1}{\sqrt{2}}\mathfrak{B}'_{\Delta} & 0 & E_{7}^{k}
\end{array}\right]
\end{array}
\tag{39}
$$

where $P_\alpha^z = P_\alpha k_z$, $P_\alpha^\pm = P_\alpha k_\pm$ with $P_\alpha = P$ or P' or P_X. In Eq. 39 we keep the notations of Ref. [22], $|cM\rangle$ instead of $\left|\frac{3}{2}, M\right\rangle_{\Gamma_{8C}}$ with $M = \left\{\pm\frac{3}{2}, \pm\frac{1}{2}\right\}$; $\left|c \pm \frac{7}{2}\right\rangle$ instead of $\left|\frac{1}{2}, \pm\frac{1}{2}\right\rangle_{\Gamma_{7C}}$; $|M\rangle$ instead of $\left|\frac{3}{2}, M\right\rangle_{\Gamma_8}$; and $\left|\pm\frac{7}{2}\right\rangle$ instead of $\left|\frac{1}{2}, \pm\frac{1}{2}\right\rangle_{\Gamma_7}$.

In Fig. 20, it is easy to recognize the appearance of the spurious states in the VB.

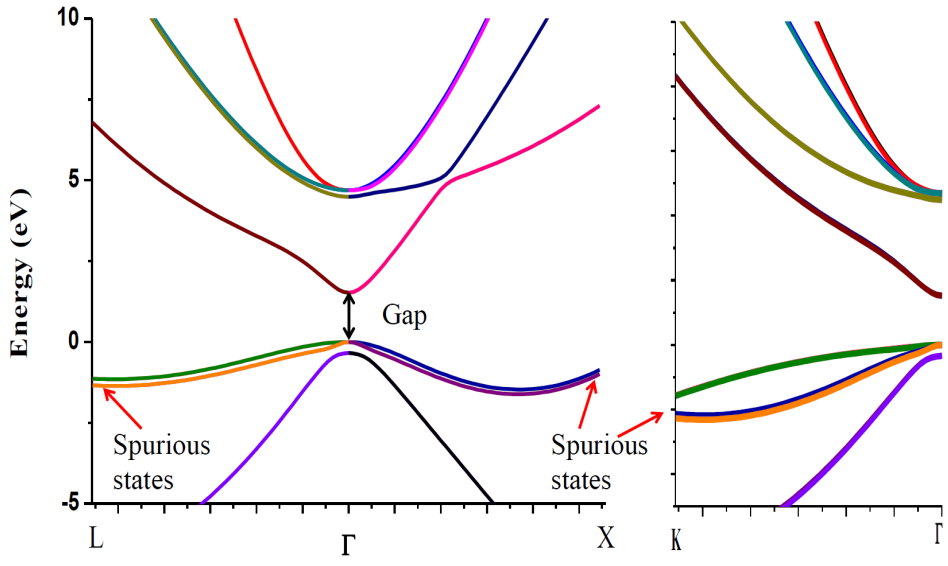

Figure 20: GaAs band structure along [111], [100], and [110] directions calculated from matrix in Eq. 39 with the parameters given by Ref. [34]

3.4 The effective Hamiltonian in the conduction band

In this part, we will explain how we can find the Dresselhaus terms responsible for the spin-splitting in an effective model which is often used for electrons in the CB band of zinc blende semiconductors, like described in Chapter 2. For projecting the 14×14 **k**.**p** matrix in Eq. 39 on the first CB $\Gamma_6 = \{S\uparrow, S\downarrow\}$, Löwdin's perturbation theory is applied at the third and fourth order. We obtain the effective Hamiltonian for electrons in the first CB:

$$\hat{H}_C = \frac{\hbar^2}{2m^*}k^2\hat{\mathbb{I}} + \hat{H}_D, \tag{40}$$

where m^* is the electron effective mass in the crystal, $\hat{\mathbb{I}}$ is the unity matrix, $\hat{H}_D$ is known as D'yakonov- Perel' Hamiltonian or Dresselhaus Hamiltonian like detailed in Chapter 2,

$$\hat{H}_D = \gamma \begin{bmatrix} k_z(k_x^2 - k_y^2) & k_x(k_y^2 - k_z^2) - ik_y(k_z^2 - k_x^2) \\ k_x(k_y^2 - k_z^2) + ik_y(k_z^2 - k_x^2) & -k_z(k_x^2 - k_y^2) \end{bmatrix}, \tag{41}$$

$$\gamma = \gamma^{(3)} + \gamma^{(4)}, \tag{42}$$

$$\gamma^{(3)} = \frac{4}{9}P_X P P' \frac{\Delta\left(E^G + 2E^\Delta\right) + \Delta^C\left(E_G + 2E_\Delta\right)}{E_G E_\Delta E^G E^\Delta}, \tag{43}$$

$$\gamma^{(4)} = -\frac{4}{9}P_X \Delta' \frac{P^2\left(2E^G + E^\Delta\right) + P'^2\left(E_G + 2E_\Delta\right)}{E_G E_\Delta E^G E^\Delta}, \tag{44}$$

where $\gamma^{(3)}$ represents the Dresselhaus coefficient obtained to third-order perturbation series, whereas $\gamma^{(4)}$ corresponds to fourth-order contribution. Both terms originate from antisymmetric P' and Δ' couplings which are zero in the O_h group (*e.g.* Si, Ge). With the parameters in the literature [34], $\left|\gamma^{(4)}\right|$ is much larger than $\left|\gamma^{(3)}\right|$, which means that the contribution of the fourth-order term is larger than the third order one. This non trivial property makes then difficult to anticipate the consequence of a truncature, possible higher-order development could give significant Dresselhaus contributions. From Eqs. 43, and 44, we show that SOI in effective models originates from core spin-orbit (Δ, and Δ^C) and the lack of inversion center (Δ', and P'). In the O_h group, $\Delta' = P' = 0$ so that the Dresselhaus Hamiltonian identically vanishes.

The electron energies in the CB are eigenvalues of the Hamiltonian $\hat{H}_D$,

$$\mathcal{E} = \frac{\hbar^2}{2m^*}k^2 \pm \gamma\sqrt{\left[k_z(k_x^2 - k_y^2)\right]^2 + \left[k_x(k_y^2 - k_z^2)\right]^2 + \left[k_y(k_z^2 - k_x^2)\right]^2}. \tag{45}$$

The degeneracy of the conduction band is lifted in all directions but not along the [001] and [111] directions. In the [110] direction, $\mathcal{E} = \frac{\hbar^2}{2m^*}k^2 \pm \gamma k^3$, the spin splitting is maximum.

The effective model is known as a convenient model for analytical calculations but this is not always true, sometimes it introduces the difficult physical questions due to the appearance of higher-order momentum terms. For example, if one considers tunneling through the [110] direction, the appearance of k cubic terms lead to the discontinuity of the envelope function and requires a redefinition of the current operator and current flux at the interface as introduced in Chapter 2, as well as emphasized in Ref. [31]. The conclusion is that it is not easy to find the new relevant matching conditions for electron tunneling along the [110] direction in the general case.

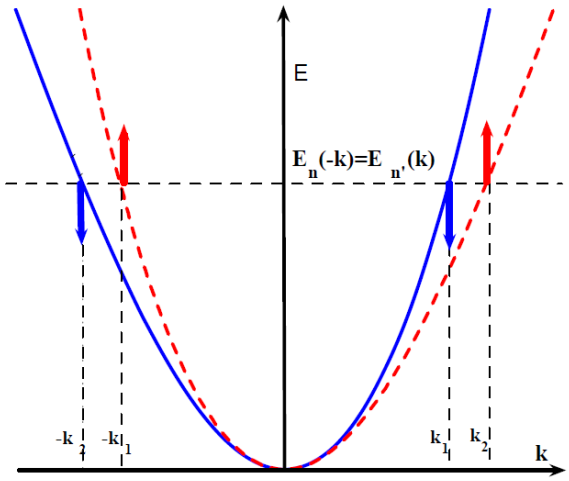

Figure 21: Energies of ↑-spin (red line) and ↓-spin (blue line) states generated by Dresselhaus terms.

3.5 The effective model in the valence band

Now projecting the 14×14 **k**.**p** Hamiltonian in Eq. 39 on the $\{\Gamma_7, \Gamma_8\}$ subspace through second-order Lowdin's perturbation method, we obtain the 6×6 **k**.**p** effective Hamiltonian for the VB.

$$\begin{array}{c} \left|\tfrac{3}{2},\tfrac{3}{2}\right\rangle_{\Gamma_8} \quad \left|\tfrac{3}{2},\tfrac{1}{2}\right\rangle_{\Gamma_8} \quad \left|\tfrac{3}{2},\tfrac{-1}{2}\right\rangle_{\Gamma_8} \quad \left|\tfrac{3}{2},\tfrac{3}{2}\right\rangle_{\Gamma_8} \quad \left|\tfrac{1}{2},\tfrac{1}{2}\right\rangle_{\Gamma_7} \quad \left|\tfrac{1}{2},\tfrac{-1}{2}\right\rangle_{\Gamma_7} \\ \left[\begin{array}{cccccc} -\gamma_1\breve{k}^2+\mathfrak{A} & \mathfrak{B} & \mathfrak{C} & 0 & \frac{1}{\sqrt{2}}\mathfrak{B}_\Delta & \sqrt{2}\mathfrak{C}_\Delta \\ cc & -\gamma_1\breve{k}^2-\mathfrak{A} & 0 & \mathfrak{C} & -\sqrt{2}\mathfrak{A}_\Delta & -\sqrt{\frac{3}{2}}\mathfrak{B}_\Delta \\ cc & 0 & -\gamma_1\breve{k}^2-\mathfrak{A} & -\mathfrak{B} & -\sqrt{\frac{3}{2}}\mathfrak{B}^*_\Delta & \sqrt{2}\mathfrak{A}_\Delta \\ 0 & cc & cc & -\gamma_1\breve{k}^2+\mathfrak{A} & -\sqrt{2}\mathfrak{C}^*_\Delta & \frac{1}{\sqrt{2}}\mathfrak{B}^*_\Delta \\ cc & cc & cc & cc & -\Delta-\gamma_{\Delta 1}\breve{k}^2 & 0 \\ cc & cc & cc & cc & 0 & -\Delta-\gamma_{\Delta 1}\breve{k}^2 \end{array}\right] \end{array}, \tag{46}$$

where the Luttinger parameters in the 6×6 **k**.**p** matrix in Eq. 46, γ_j and $\gamma_{\Delta j}$ were introduced in Sec.3.3.3, and

$$\gamma_{\Delta(j=1,2,3)} \approx \gamma_{(j=1,2,3)}.$$

The Luttinger parameters in the VB have no contribution arising from the lack of inversion center. It means that this Hamiltonian applies for the O_h and T_d groups as well. In that picture, the SOI in VB is introduced through the core spin-orbit parameter Δ. This particular shape of the 6×6 projected Hamiltonian was firstly proposed by Luttinger-Kohn from general arguments of invariant theory [55].

3.6 Exchange interactions (Ferromagnetism)

The $p-d$ exchange interactions occurring in the VB are introduced through the Hamiltonian matrix as proposed by Dietl *et al.* [26] as well as in Ref. [70] in a different approach

$$H_{exc} = 6B_G \mathbf{s}.\mathbf{m}, \tag{47}$$

where $6B_G$ represents the average interaction energy among holes, $\mathbf{s}$ is spin of the hole and $\mathbf{m}$ is a unit vector along the magnetization of the localized spins.

Here, we expand this model for electrons in the first and second CB with different values of B_G like classically considered. Using the basis defined in Eq. 37, we write the exchange Hamiltonian in the 14-band **k**.**p** model as:

$$H_{exc} = \begin{bmatrix} H_{exc}^{\Gamma_{5C}} & 0 & 0 \\ 0 & H_{exc}^{\Gamma_1} & 0 \\ 0 & 0 & H_{exc}^{\Gamma_5} \end{bmatrix}$$

where $H_{exc}^{\Gamma_{5C}}$ is the block exchange Hamiltonian in the Γ_{5C} subspace, $H_{exc}^{\Gamma_1}$ is the block exchange Hamiltonian in the Γ_1 subspace, and $H_{exc}^{\Gamma_5}$ is the block exchange Hamiltonian in the Γ_5 subspace.

We write

$$\mathbf{s}.\mathbf{m} = [(s_- m_+ + s_+ m_-) + s_z m_z]$$

after having defined $s_\pm = (s_x \pm i s_y)/2$ and $m_\pm = (m_x \pm i m_y)$.

The Hamiltonian in the $\{\Gamma_8, \Gamma_7\}$ representations is written:

$$H_{exc}^{\Gamma_5} = B_G^{\Gamma_5} \begin{array}{c} \begin{array}{cccccc} \left|\frac{3}{2},\frac{3}{2}\right\rangle_{\Gamma_8} & \left|\frac{3}{2},\frac{1}{2}\right\rangle_{\Gamma_8} & \left|\frac{3}{2},\frac{-1}{2}\right\rangle_{\Gamma_8} & \left|\frac{3}{2},\frac{-3}{2}\right\rangle_{\Gamma_8} & \left|\frac{1}{2},\frac{1}{2}\right\rangle_{\Gamma_7} & \left|\frac{1}{2},\frac{-1}{2}\right\rangle_{\Gamma_7} \end{array} \\ \begin{bmatrix} 3m_z & \sqrt{3}m_- & 0 & 0 & -\sqrt{6}m_- & 0 \\ \sqrt{3}m_+ & m_z & 2m_- & 0 & 2\sqrt{2}m_z & -\sqrt{2}m_- \\ 0 & 2m_+ & -m_z & \sqrt{3}m_- & \sqrt{2}m_+ & 2\sqrt{2}m_z \\ 0 & 0 & \sqrt{3}m_+ & -3m_z & 0 & \sqrt{6}m_+ \\ -\sqrt{6}m_+ & 2\sqrt{2}m_z & \sqrt{2}m_- & 0 & -m_z & -m_- \\ 0 & -\sqrt{2}m_+ & 2\sqrt{2}m_z & \sqrt{6}m_- & -m_+ & m_z \end{bmatrix} \end{array}, \tag{48}$$

whereas the exchange Hamiltonian in Γ_6 is

$$H_{exc} = 3B_G^{\Gamma_1} \begin{array}{c} \begin{array}{cc} |S\uparrow\rangle & |S\downarrow\rangle \end{array} \\ \begin{bmatrix} m_z & m_- \\ m_+ & -m_z \end{bmatrix} \end{array}. \tag{49}$$

The Hamiltonian in the second CB is similar to Eq. 48 but with $B_G^{\Gamma_{5C}}$ instead of $B_G^{\Gamma_5}$.

3.7 k.p Hamiltonian without spurious states

Spurious states naturally arise at large k when considering a 2-band toy **k**.**p** model coupling the CB and VB. Whereas the spurious states simply need to be omitted in the electronic structure at large k for the calculation of the density of states, or of the effective mass as well as for the calculation of optical transitions (at constant *k*), these states have to be fully included in transport properties (*e.g.* tunneling) at constant energy $\mathcal{E}_c$ and $\mathcal{E}_h$. The general matching conditions connect continuity / discontinuity conditions of the components of the wave function to the corresponding current wave. In this sense the number of matching conditions should be equal to ensure that every k state (at constant energy) is considered, including the unphysical spurious states. This particular point was perfectly described in the paper of Foreman [59]. In the present work, we proposed two different solutions in order to remove the spurious states and "cure" their effects, based on previous propositions [60].

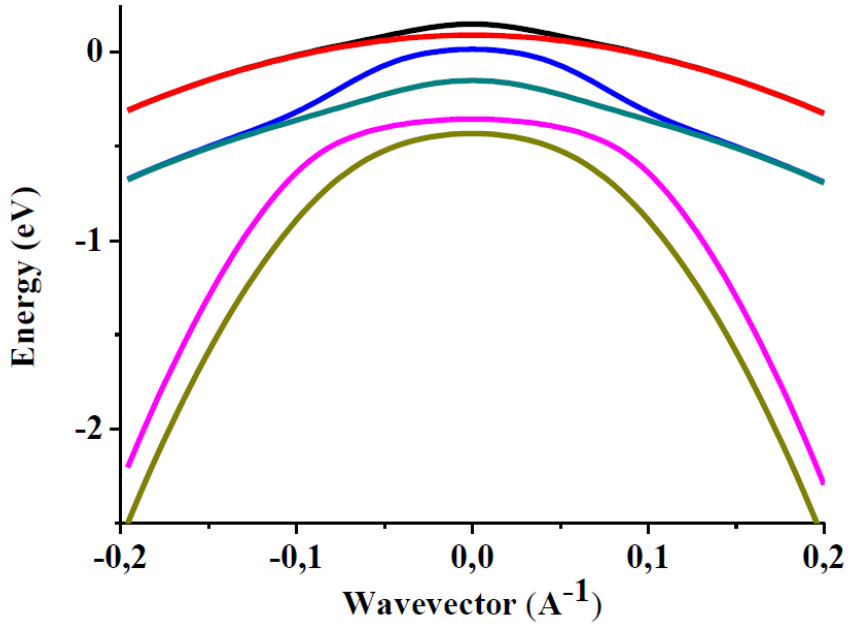

Figure 22: GaMnAs valence band structure with $\overrightarrow{M} \perp \overrightarrow{k}$.

3.7.1 Off-diagonal term method

The first method consists in adding supplementary off-diagonal matrix elements; these are terms of the form $P_{off} = i\alpha k_z^2$ parameterized by a parameter α where k_z is the wavevector along the current flow (z). This approach is the extension of the method given by Kolokolov [60] and first applied to the 8- and 14-band Hamiltonians. The main issues of this method lies in five main points:

(i) The unphysical spurious states characterized by large real k, making impossible the development of transport theory, have to disappear.

(ii) The Hamiltonian has to be fully unchanged at the Γ point.

(iii) The current operator $(1/\hbar)\,(\partial\hat{H}/\partial k_z)$ has to be fully unchanged at the Γ point.

Provided that conditions (ii) and (iii) are fulfilled, the electronic structure and (spin-polarized) transport properties are kept unchanged at the Γ point and close to it, in particular, in terms of symmetry properties (O_h,T_d). The symmetry of the crystal is unchanged at the Γ point.

(iv) The supplementary term $P_{off} = i\alpha k_z^2$ allows us to invert the concavity of the electronic states and their dispersion beyond a certain k value away from the Γ point. The inversion of the concavity parameterized by the α parameter leads to the disappearance of the spurious states.

(v) The electronic and transport properties are only weakly affected when increasing k_z from zero (far away from the BZ center). We will calculate in the following the errors made in the energy and components of the wave function introduced by the supplemental terms, P_{off}.

3.7.1.1 *2-band k.p toy model*

To have a preview of this method, we first consider the 2×2 toy **k**.**p** Hamiltonian. The energies were given in Eq. 36.

$$\begin{aligned} \text{for the CB} \qquad \mathcal{E} &= \breve{k}^2 + \frac{\sqrt{E_G^2 + 4E_P\breve{k}^2}}{2} + \frac{E_G}{2}, \\ \text{for the VB} \qquad \mathcal{E} &= \breve{k}^2 - \frac{\sqrt{E_G^2 + 4E_P\breve{k}^2}}{2} + \frac{E_G}{2}. \end{aligned}$$

Ideally, to pull down the VB at large wavevector scale, one needs to increase the value of $E_G^2 + 4E_P\breve{k}^2$ by adding a positive term α^2k^4 which can be compared to the $\breve{k}$ term. This is the role of the supplementary terms $i\alpha k^2$ in the off-diagonal term in the toy **k**.**p** Hamiltonian

$$\hat{H} = \begin{array}{c} \begin{array}{cc} |U_C\rangle & |U_V\rangle \end{array} \\ \left[\begin{array}{cc} E_G + \breve{k}^2 & Pk - i\alpha k^2 \\ Pk + i\alpha k^2 & \breve{k}^2 \end{array} \right] \end{array} \tag{50}$$

We assume that $E_G^2 + 4E_P\breve{k}^2 \ll \alpha^2k^4$ at the large wavevector scale. The energy for the VB becomes $\mathcal{E} = (\hbar^2/2m_0 - \alpha)\,k^2$. If $\alpha > \hbar^2/2m_0$, the hole effective mass is always negative like expected. With the supplemental terms we obtained from the energy, the electron effective mass for small wavevectors becomes:

$$\begin{aligned} \mathcal{E}_{electron} &= \breve{k}^2 + \frac{\sqrt{E_G^2 + 4E_P\breve{k}^2 + \alpha^2k^4}}{2} + \frac{E_G}{2} \\ &\approx \breve{k}^2 + \frac{E_G}{2}\left(1 + \frac{4E_P\breve{k}^2 + \alpha^2k^4}{E_G^2}\right)^{1/2} + \frac{E_G}{2} \\ &= E_G + \breve{k}^2 + \frac{E_P\breve{k}^2}{E_G} + \frac{\alpha^2k^4}{4E_G}. \end{aligned}$$

One observes that as $\alpha^2k^4/E_G \ll k^2$, the electron effective mass weakly depends on the supplementary terms. We have similar results for the hole band. This method was improved to remove spurious states within the 8-band **k**.**p** model [60].

3.7.1.2 *14-band k.p model*

In the present contribution, we develop this method for a 14-band **k**.**p** Hamiltonian approach. As introduced in Fig. 20, far away from the Γ point the VBs go up and leads to real spurious states in the band gap. Our idea is similar to the method described in the 2-band **k**.**p** toy model: we modify the coupling terms between the VB and the CB

by adding terms $i\alpha k^2$ pulling down the VBs far away from the Γ point. The pairs of states selected for coupling are: $\left|\frac{3}{2},\pm\frac{3}{2}\right\rangle_{\Gamma_{8C}}$ and $\left|\frac{1}{2},\pm\frac{1}{2}\right\rangle_{\Gamma_7}$; $\left|\frac{1}{2},\pm\frac{1}{2}\right\rangle_{\Gamma_{7C}}$ and $\left|\frac{3}{2},\mp\frac{3}{2}\right\rangle_{\Gamma_8}$; $|\ \pm\rangle$ and $\left|\frac{3}{2},\pm\frac{1}{2}\right\rangle_{\Gamma_{8C}}$. Then, we need to find the critical value for the α parameter. Let us consider the simplest case, the band structure of the O_h group along the [001] direction. It means that in the 14×14 **k.p** matrix (Eq. 39) we consider $P' = \Delta' = 0$, and $k_x = k_y = 0$. In this case, the 14×14 matrix can be expressed in the following block form:

$$\hat{H} = \begin{bmatrix} H_1 & 0 \\ 0 & H_2 \end{bmatrix},$$

where $H_1 = H_2$. The basis chosen to express the H_1 matrix is

$$\left\{\left|\frac{3}{2},\frac{1}{2}\right\rangle_{\Gamma_{8C}},\ \left|\frac{3}{2},\frac{-3}{2}\right\rangle_{\Gamma_{8C}},\ \left|\frac{1}{2},\frac{1}{2}\right\rangle_{\Gamma_{7C}},\ |+\rangle,\ \left|\frac{3}{2},\frac{1}{2}\right\rangle_{\Gamma_8},\ \left|\frac{3}{2},\frac{-3}{2}\right\rangle_{\Gamma_8},\ \left|\frac{1}{2},\frac{1}{2}\right\rangle_{\Gamma_7}\right\},$$

and the basis for the H_2 matrix is

$$\left\{\left|\frac{3}{2},\frac{-1}{2}\right\rangle_{\Gamma_{8C}},\ \left|\frac{3}{2},\frac{3}{2}\right\rangle_{\Gamma_{8C}},\ \left|\frac{1}{2},\frac{-1}{2}\right\rangle_{\Gamma_{7C}},|-\rangle,\ \left|\frac{3}{2},\frac{-1}{2}\right\rangle_{\Gamma_8},\ \left|\frac{3}{2},\frac{-3}{2}\right\rangle_{\Gamma_8},\ \left|\frac{1}{2},\frac{-1}{2}\right\rangle_{\Gamma_7}\right\}.$$

$$H_1 = \begin{bmatrix}
E_{8C}^L & 0 & 0 & 0 & 0 & \frac{1}{\sqrt{3}}P_X^z & 0 \\
0 & E_{8C}^H & 0 & 0 & \frac{-1}{\sqrt{3}}P_X^z & 0 & \sqrt{\frac{2}{3}}P_X^z \\ & & & & & & +i\alpha k^2 \\
0 & 0 & E_{7C}^k & 0 & 0 & -\sqrt{\frac{2}{3}}P_X^z & 0 \\ & & & & & -i\alpha k^2 & \\
0 & 0 & 0 & E_6^k & \sqrt{\frac{2}{3}}P^z & 0 & \frac{1}{\sqrt{3}}P^z \\ & & & & -i\alpha k^2 & & \\
0 & \frac{-1}{\sqrt{3}}P_X^z & 0 & \sqrt{\frac{2}{3}}P^z & E_8^L & 0 & -\sqrt{2}U' \\ & & & +i\alpha k^2 & & & \\
\frac{1}{\sqrt{3}}P_X^z & 0 & -\sqrt{\frac{2}{3}}P_X^z & 0 & 0 & E_8^H & 0 \\ & & +i\alpha k^2 & & & & \\
0 & \sqrt{\frac{2}{3}}P_X^z & 0 & \frac{1}{\sqrt{3}}P^z & -\sqrt{2}U' & 0 & E_7^k \\ & -i\alpha k^2 & & & & &
\end{bmatrix} \tag{51}$$

Because of the time reversal properties, if k is a solution of $\det(H_1 - \mathcal{E}\hat{\mathbb{I}}) = 0$, $-k$ will also satisfy this equation. Therefore, we can write

$$\det(H_1 - \mathcal{E}\hat{\mathbb{I}}) = 0 \Longleftrightarrow R_{14}k^{14} + R_{12}k^{12} + R_{10}k^{10} + R_8k^8 + R_6k^6 + R_4k^4 + R_2k^2 + R_0 = 0 \tag{52}$$

where R_i is a function of $\{\alpha, \mathcal{E}\}$. If real spurious states appear, Eq. 52 will possess solutions with real k at energy $\mathcal{E}$ in the band gap. To remove the spurious states, we

try to find possible values of α making Eq. 52 with no real solution k in the gap. The simplest way is to chose the value of α making all of R_i negative at energy $\mathcal{E}$ in the band gap, this is our critical value of α. The critical value depends on the material, *e.g.* $\alpha = 5.32$ for GaAs, $\alpha = 6.42$ for GaSb, $\alpha = 5.26$ for InAs,...

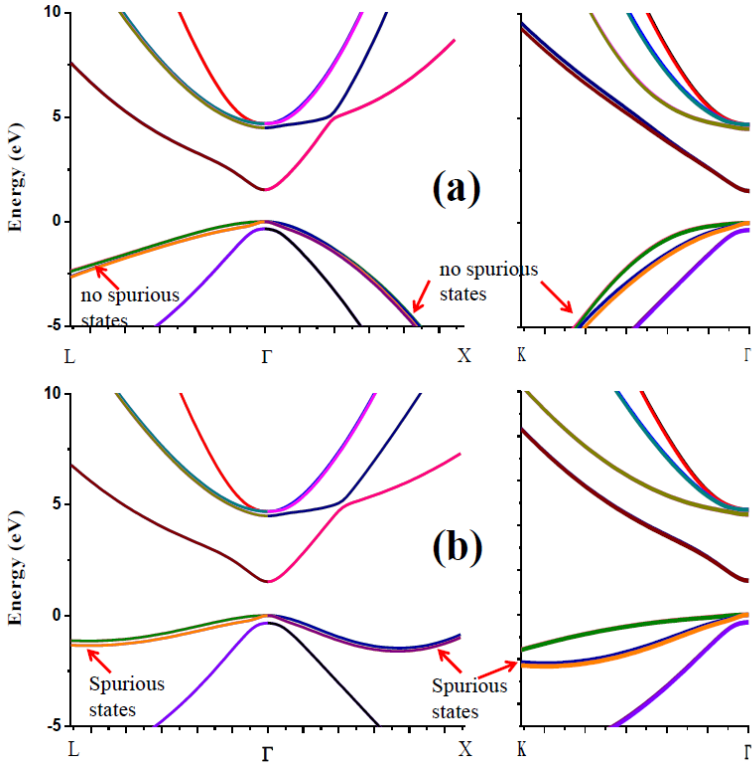

Figure 23: GaAs band structures: (a) after adding the supplementary terms in the matrix, Eq. 39; (b) before treatment of the spurious states.

In Fig. 23, we can observe that, after this treatment, the spurious states totally disappear in the band gap.

3.7.1.3 ***Estimation of Errors***

Figure. 24 displays the energy difference in GaAs between the original 14-band **k**.**p** Hamiltonian (with spurious states) and treated 14-band **k**.**p** Hamiltonian after adding off-diagonal terms. The difference in the relevant eigenfunctions is given by the formula:

$$\Delta\Psi = \sqrt{\|\Psi_0 - \Psi_{off-diagonal}\|^2},$$

where Ψ_0 is the eigenvector of the original 14×14 Hamiltonian, and $\Psi_{off-diagonal}$ is the respective eigenvector of the Hamiltonian with supplemental terms at the same point. This expression is plotted in Fig. 25 for Γ_6 and $\{\Gamma_7, \Gamma_8\}$ subsets along the [001] axis.

Within 20% of the BZ, the calculated energy and wave functions differences are observed to be small. We also carefully checked that the supplementary terms do not contribute to the k-cubic term: the spin-splitting of the first CB in the bulk is zero in the

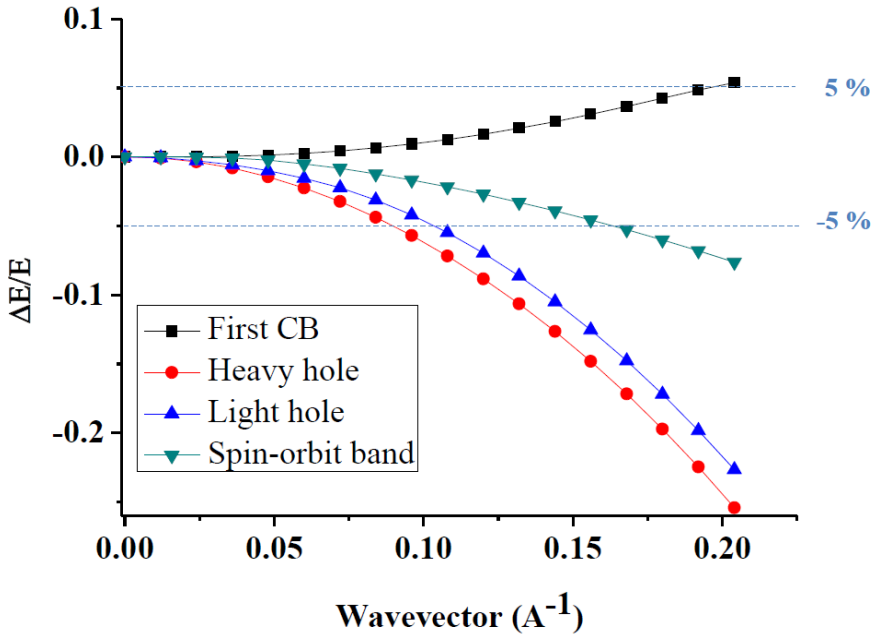

Figure 24: Difference in energies in GaAs along the [001] axis between the original 14-band **k**.**p** Hamiltonian with spurious states and 14-band **k**.**p** Hamiltonian treated by adding off-diagonal terms (no spurious states) corresponding to the first CB and VBs *vs*. wavevector. The edge of the BZ is located at 1 $Å^{-1}$.

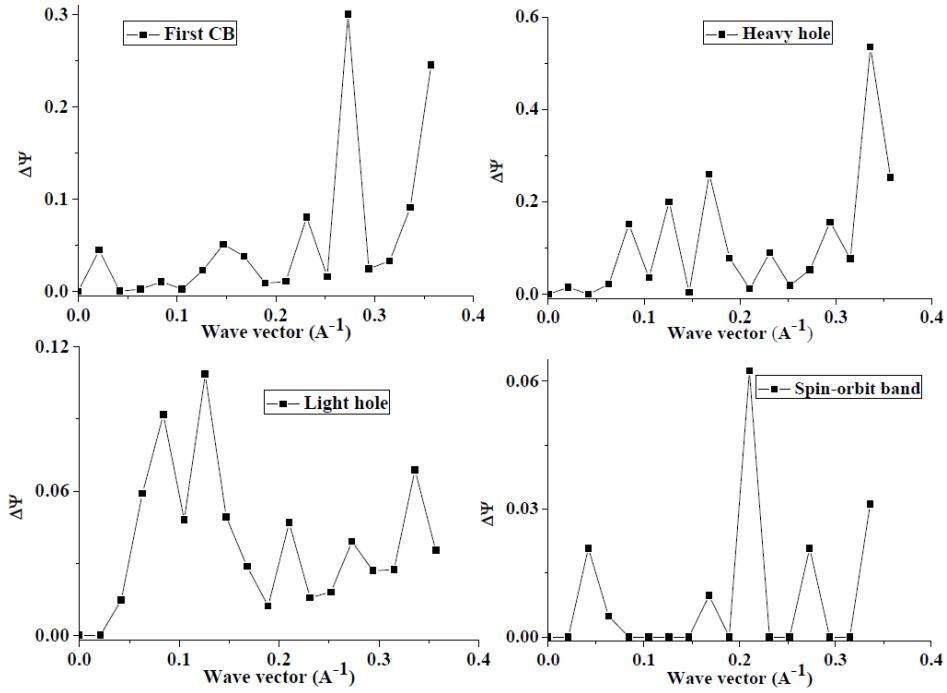

Figure 25: Difference of wave functions in GaAs along the [001] direction for the first CB and VBs before and after treatment of the spurious states by adding off-diagonal supplementary terms. The edge of the BZ is located at 1 $Å^{-1}$.

O_h group and, in addition, we used the 14-band treated Hamiltonian with supplementary terms for all our calculations, *e.g.* the results related to the 14-band calculation in Chapter 2 represented again in Fig. 26. We obtained a good agreement between the 14-band and 2-band effective tunneling models. The 14-band code demonstrated to be very robust.

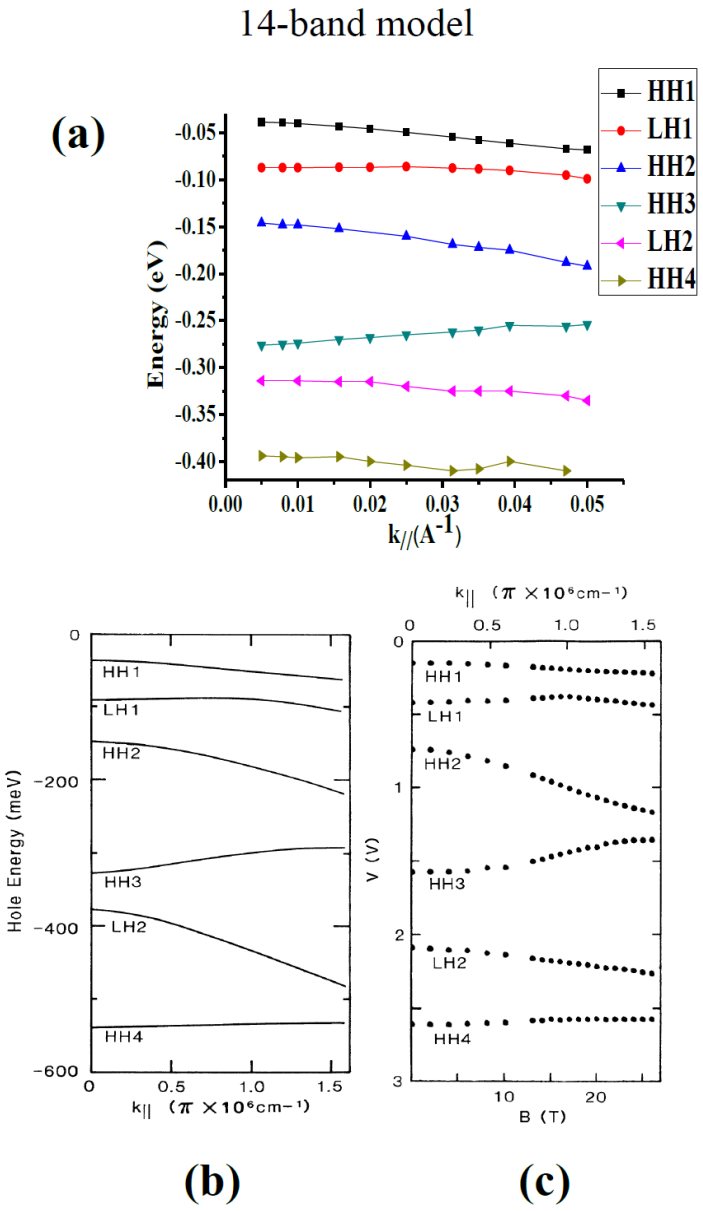

Figure 26: (a) Hole subband dispersion *vs.* in-plane wavevector for 8 nm GaAs QWs grown along the [001] direction, calculated by 14-band **k**.**p** model; Hole dispersion *vs.* in-plane wavevector for 4.2 nm GaAs QWs [45]: (b) calculation, (c) experiment.

However, one of the main drawbacks of the present method of supplementary off-diagonal k^2 term is its inadequation to remove the spurious states in the vicinity of the indirect gap of group IV semiconductors like in the L valleys of Ge, or near the X valleys of Si. We then propose another solution which can be able to remove the

spurious states of Si and Ge (and their alloys).

3.7.2 Novel "ghost-band" approach

In order to extend the treatment of the spurious states to a wider region of the BZ (not only close to the Γ point, at $k < 0.2$ Å), we propose a so-called "ghost-band method". The idea is to use the same trick as previously, that is adding "off-diagonal" $i\alpha k^2$ squared coupling terms, but much closer in the k space to the point where the spurious band starts to possess an inverted effective mass. The properties of these supplementary terms are the same:

(i) The Hamiltonian is strictly unchanged at the Γ point.

(ii) The (spin) current-operator is also unchanged at the Γ point.

Therefore, the physical properties remain exactly unchanged at the Γ point and in particular the symmetry of the crystal.

3.7.2.1 ***Details of the method***

In order to minimize the perturbation of the electronic structure and transport properties due to the spurious-band treatment, one must minimize the perturbation at specific k points (A) where are operating the supplementary $P_{off} = i\alpha k^2$ off-diagonal terms. This implies that:

(i) One must introduce new fictitious supplementary bands (the so-called ghost-bands) of arbitrary or adequate symmetry on which the P_{off} coupling acts in order to leave unchanged the properties of the true (physical) CB (free of supplementary couplings). These ghost-bands introduced hereafter (the 14-band model becomes a 18-band model because there are 4 spurious states in the VB (see Fig. 20)), mimic on the average the other physical bands that are necessarily truncated by the **k**.**p** method. The mean energy positions of these ghost-bands have to be set by optimization according to a trial and error procedure (components of the envelope function and energy).

(ii) In order to minimize the effect of the spurious states on the top VB, one needs to apply the supplementary coupling in the basis where the Hamiltonian is purely diagonal at a given A point in the *k*-space (see Eq. 53) in order to leave other bands uncoupled.

$$H = \begin{array}{|c|c|} \hline \text{Conduction band } \{\Gamma_6, \Gamma_{7C}, \Gamma_{8C}\} & 0 \\ \hline 0 & \begin{array}{|c|c|} \hline \text{Valence band } \{\Gamma_7, \Gamma_8\} & P_{off} \\ \hline P_{off} & \text{Ghost band} \\ \hline \end{array} \\ \hline \end{array} \tag{53}$$

The philosophy is then as follows:

- The electronic and transport properties are not affected at the Γ point (BZ center) for all CB, VB, HH, LH, and SO bands.

- The electronic and transport properties are not affected at the A point where P_{off} is introduced (away from Γ point), see Eq. 53, for the CB (see Fig. 27).

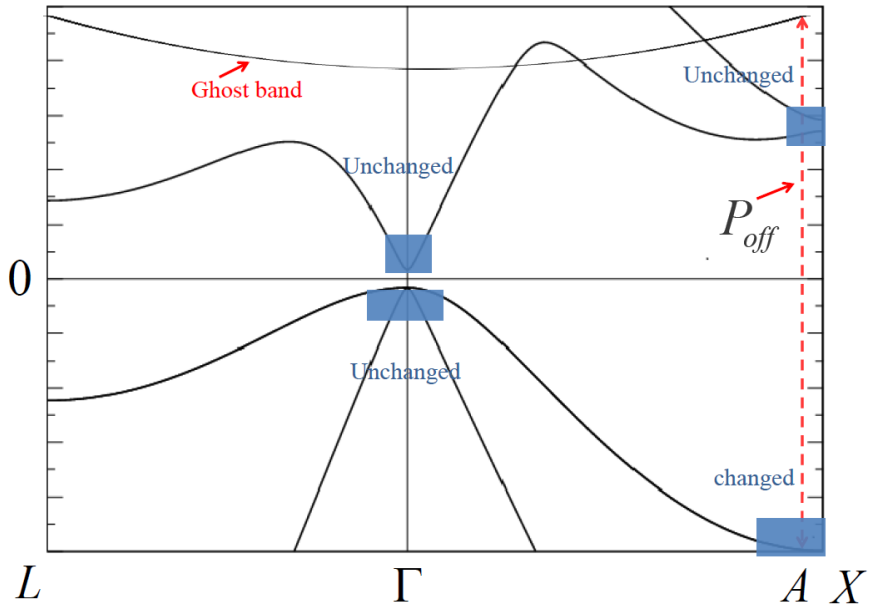

Figure 27: Band structure diagram of Eq. 53. The ghost bands are included at higher energy than the first conduction band. At the A point, the ghost bands only couple with the VB. At the Γ and A points, the CBs are not affected.

- We can expect that the tunneling transport properties (evanescent states from the bottom of the CB to the top of the VB (Γ point)) will be only weakly affected which is the case and particularly in the 30-band model.

Then, the interest of this procedure is that one can readily transpose the method to a full 30-multiband approach where spurious states originating from the VB arise at the first BZ boundary (the L valley of Ge [58]) or approximately for the X valleys of Si. The symmetry of the corresponding states at the first BZ boundary generally admits a well-defined character which can make the correction more convenient. Note that the Hamiltonian in the CB is unchanged at the A point (see Eq. 53).

The price to pay for the method is the necessity to introduce at least two different coupling points at $+\mathbf{k}$ (A^+) and $-\mathbf{k}$ (A^-) (instead of a single one for the BZ center treatment) because of the different symmetry of the eigenvectors corresponding to $+\mathbf{k}$ and $-\mathbf{k}$.

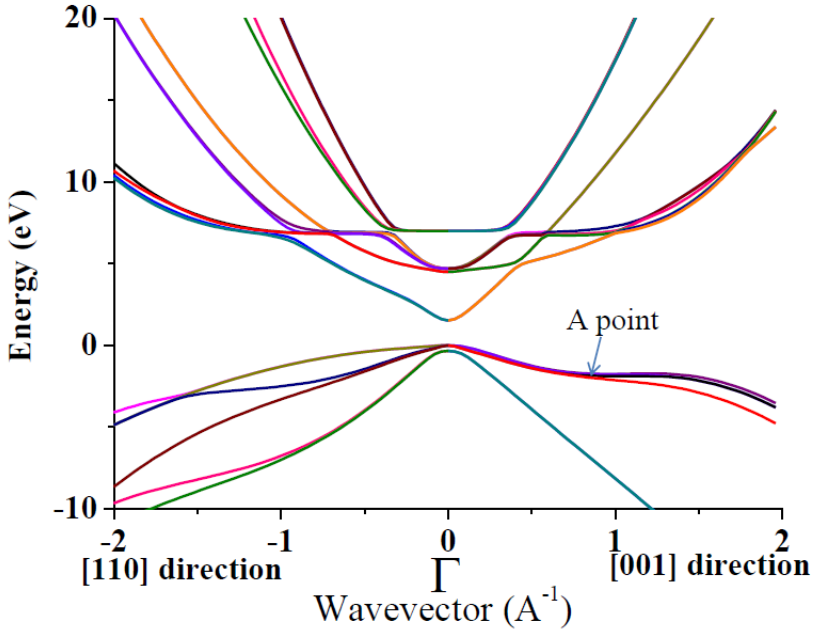

Figure 28: GaAs band structure along the [110] and [001] directions treated by the ghost-band method at large scale using parameters close to the values introduced in Ref. [34]

In Fig. 28, we plot the GaAs band structure along the [110] and the [001] directions at large scale after treatment by the ghost-band method. It is easy to see that the spurious states in the hole bands are pushed away. In addition, near the Γ point the VBs and the first CB are almost nearly unperturbed when compared to the ones before treatment (see Fig. 29). The method must satisfy these conditions in order that the physical properties near the Γ point are not changed.

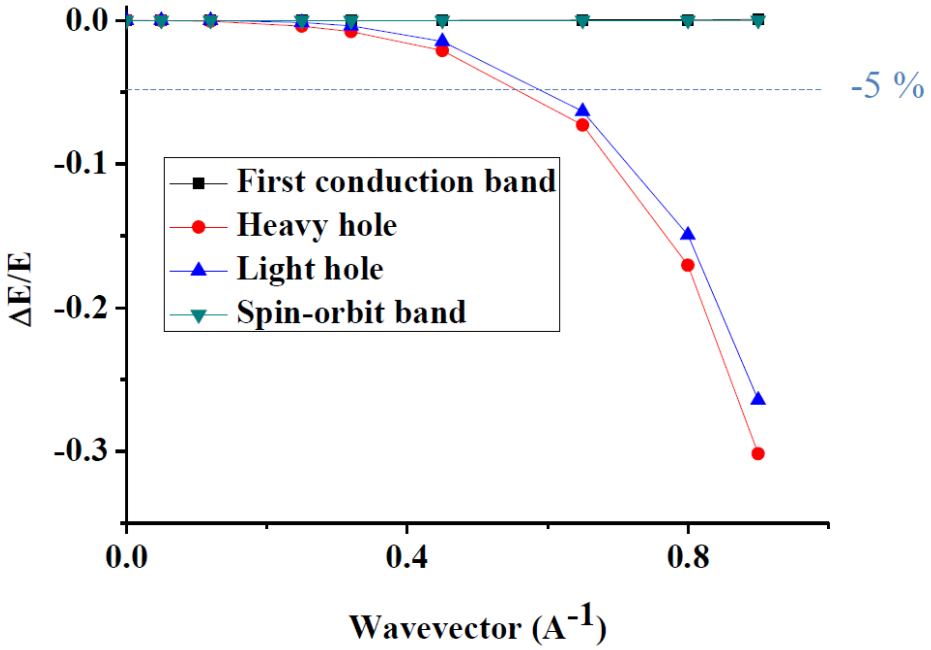

Figure 29: Difference between energies of 14×14 **k.p** matrix in GaAs without healing spurious states and after treatment based on the 18×18 ghost-band method along the [001] direction. The edge of the BZ is located at 1 $Å^{-1}$.

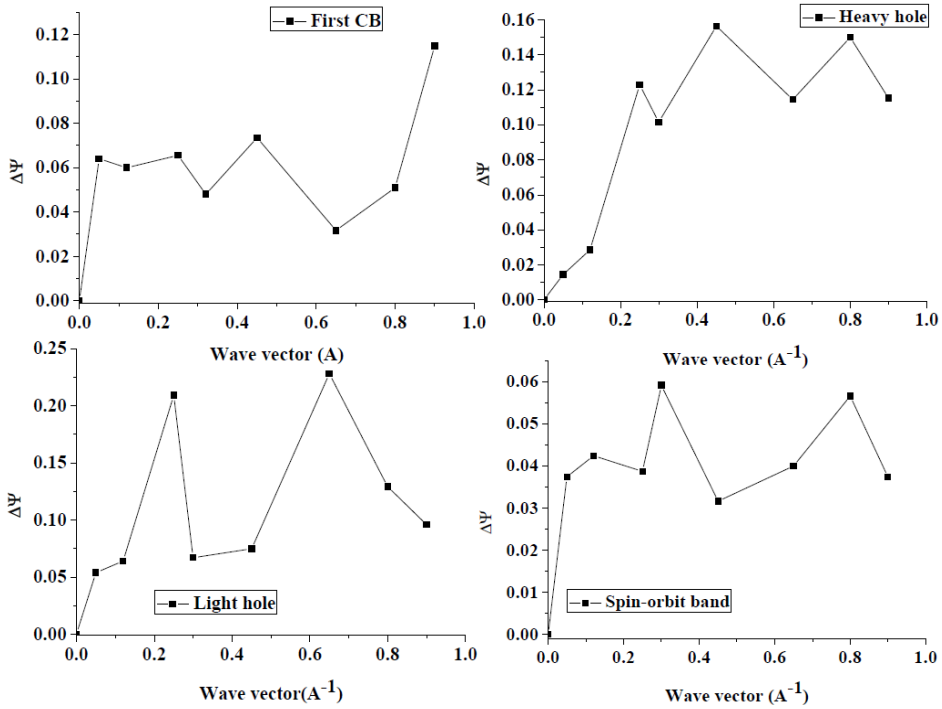

Figure 30: Difference of wave functions in GaAs for the first CB and VBs before and after treatment of the spurious states by ghost-band method along the [001] direction. The edge of the BZ is located at 1 $Å^{-1}$.

3.7.2.2 *Estimation of Errors*

We decompose the wave function Ψ into a form

$$\Psi_T = \begin{pmatrix} \Psi_P \\ \bar{\Psi}_G \end{pmatrix},$$

where Ψ_T is over all the full wave function of the complete Hamiltonian, Ψ_P refers to the physical components and $\bar{\Psi}_G$ to the unphysical ghost part. The difference of the wave function between the 14-band **k**.**p** matrix without ghost-band treatment in Eq. 39 and the physical wave function Ψ_P after treatment with the ghost-band method is defined by:

$$\Delta\Psi = \sqrt{\frac{\|\Psi_0 - \Psi_P\|^2}{\|\Psi_P\|^2}}.$$

These calculations for the CB and VBs are showed in Fig. 30; the differences near the Γ point are small.

3.7.2.3 *Matching conditions*

To anticipate the discussions on the matching conductions given in Chapter 4, we adopt here the continuity of the wave function and wave current (the BDD conditions extended to the multiband case) to study the consequence of the ghost-band treatment. Our conclusion will be that, through standard matching conditions, the ghost-band treatment is truly relevant to describe the full (spin-dependent) transport properties in the main conduction valleys: *i.e.*, Γ valley for direct-gap semiconductors for both electrons and holes, L valleys for the CB in the case of indirect-gap semiconductors (*e.g.* AlAs). We have already checked (without formal proofs) that the symmetry of both the wave function and the wave current remain almost unchanged at the relevant valleys following the ghost-band approach. What about the (spin-dependent) current flux?

Like in the last part, we decompose the wave function Ψ into a form

$$\Psi_T = \begin{pmatrix} \Psi_P \\ \bar{\Psi}_G \end{pmatrix},$$

(i) The continuity of the wave function means that Ψ_T is continuous at each interface indicating that both of the Ψ_P and $\bar{\Psi}_G$ parts are continuous. Ψ_P is then continuous (necessary condition) at each interface and at each energy.

(ii) The continuity of the wavecurrent means that $\hat{J}(\Psi_T)$ is continuous at each interface which, however, it does not necessary imply that $\hat{J}\Psi_P$ and $\hat{J}\bar{\Psi}_G$ are both continuous separately at each energy.

However this important property remains true near the extrema of the valleys involved in the transport because the symmetry is conserved for both wave function and wave current in these regions.

Let us write the current operator in the form:

$$\hat{J} = \hat{J}_P + \hat{J}_G,$$

where $\hat{J}_P$ is a 18×18 matrix which has 14×14 non-zero components concerning to the original 14×14 **k**.**p** Hamiltonian, and all the ones concerning ghost-band being zero; whereas 18×18 matrix, $\hat{J}_G$, has only ones concerning to ghost-band being non-zero.

The (spin-dependent) current flux is written:

$$\begin{aligned} \mathrm{Re}\left\langle \Psi_T \right| \hat{J} \left| \Psi_T \right\rangle &= \mathrm{Re}\left\langle \begin{array}{cc} \Psi_P & \bar{\Psi}_G \end{array} \middle| \hat{J} \middle| \begin{array}{c} \Psi_P \\ \bar{\Psi}_G \end{array} \right\rangle \\ &= \mathrm{Re}\left\langle \begin{array}{cc} \Psi_P & 0 \end{array} \middle| \hat{J}_P \middle| \begin{array}{c} \Psi_P \\ 0 \end{array} \right\rangle + \mathrm{Re}\left\langle \begin{array}{cc} 0 & \bar{\Psi}_G \end{array} \middle| \hat{J}_G \middle| \begin{array}{c} 0 \\ \bar{\Psi}_G \end{array} \right\rangle, \end{aligned} \tag{54}$$

By principle (matching conditions), $\mathrm{Re}\langle\Psi_T| \hat{J} |\Psi_T\rangle$ is continuous over the multilayer structure which means that the sum of the two terms are continuous but not necessary each term separately.

However the current of evanescent states are zero Refs. [71, 72, 73], the supplementary ghost-bands (evanescent states) lead to:

$$\mathrm{Re}\left\langle \begin{array}{cc} 0 & \bar{\Psi}_G \end{array} \middle| \hat{J}_G \middle| \begin{array}{c} 0 \\ \bar{\Psi}_G \end{array} \right\rangle = 0,$$

so that we obtain

$$\mathrm{Re}\left\langle \Psi_T \right| \hat{J} \left| \Psi_T \right\rangle = \mathrm{Re}\left\langle \Psi_P \right| \hat{J}_P \left| \Psi_P \right\rangle.$$

The proof is based on the current vanishing of evanescent states given in Ref. [71, 72], and is valid for the 14-band as well as for the 30-band ghost methods. The proof for the spin-dependent tunneling current can be considered but, by simple arguments, one can estimate that the result is equivalent so that one neglects the evanescent current contribution originating from the lower spurious VBs, which is generally the case.

3.8 30-band k.p model

The details can be found in Refs. [57, 22].

As introduced above, the 14-band **k**.**p** model is pretty relevant within 20% of the BZ near the Γ point. It is necessary to extend the **k**.**p** model to describe the band diagram of indirect band gap semiconductors. Cardona and Pollak [43] used a 15-function basis (without spin) to describe the dispersion curve throughout the whole Brillouin zone. They reproduced the band structure of silicon and germanium without adding perturbation involving states outside the 15-function basis: Luttinger-like parameters are not

needed anymore and, in this sense, the Cardona-Pollak basis is self-contained. This 15-band method leads to a 30-band method if the spin is taken into account. This is the reason why Cavassilas *et al.* [74] used a 20-function basis (with spin) and introduced two bands named s^* and pseudo-Luttinger parameters to mimic d levels following the idea developed by Vogl *et al.* in Ref. [75] for linear combination of atomic orbitals (LCAO) calculations. With this 20-band **k**.**p** Hamiltonian model, the valleys useful for transport (Γ, L, and X valleys in $GaAs$, Δ and L valleys in Si) were described but this model contains ten adjustable parameters to describe the s^* bands, nine interaction energies between bands for T_d group semiconductors (only six for O_h group semiconductors) and six pseudo-Luttinger parameters, *i.e.*, 25 adjustable parameters. Moreover, this 20-band Hamiltonian gave valid results up to 3.5 eV above the top of the VB but did not give access to the L valley of the second CB. Therefore, Richard *et al.* [57] proposed a 30-band **k**·**p** Hamiltonian which allowed to calculate the band diagram of bulk materials for T_d or O_h group semiconductors with SOI. The 15 states of the real crystal which are taken into account correspond to [000], $(2\pi/a)[1\ 1\ 1]$, and $(2\pi/a)[2\ 0\ 0]$ plane-wave states of free electrons in the "empty" germanium lattice. The large gap between $(2\pi/a)[2\ 0\ 0]$, and $(2\pi/a)[2\ 2\ 0]$ plane waves (more than 15 eV) suggests that these 15 states are enough to obtain a correct energy band diagram.

Simple group			Double group	
Ref. 5	O_h	T_d	O_h	T_d
$\Gamma^u_{2'}$	Γ^-_{2u}	Γ_{1q}	Γ^-_{7q}	Γ_{6q}
$\Gamma^u_{25'}$	Γ^+_{5d}	Γ_{5d}	$\Gamma^+_{8d}/\Gamma^+_{7d}$	Γ_{8d}/Γ_{7d}
$\Gamma_{12'}$	Γ^-_3	Γ_3	Γ^-_{8d}	Γ_{8-3}
Γ^u_1	Γ^+_{1u}	Γ_{1u}	Γ^+_{6u}	Γ_{6u}
Γ_{15}	Γ^-_4	Γ_{5C}	Γ^-_8/Γ^-_6	Γ_{8C}/Γ_{7C}
$\Gamma^l_{2'}$	Γ^-_2	Γ_1	Γ^-_7	Γ_6
$\Gamma^l_{25'}$	Γ^+_5	Γ_5	Γ^+_8/Γ^+_7	Γ_8/Γ_7
Γ^l_1	Γ^+_1	Γ_{1v}	Γ^+_6	Γ_{6v}

Figure 31: Notation in group theory for simple and double group.

For O_h group semiconductors (Si and Ge), the ten **k**·**p** matrix elements of interest are: $P = \langle S|\, p_x\, |iX\rangle$, $P_d = \langle S|\, p_x\, |iX_d\rangle$, $P_X = \langle X_C|\, p_y\, |iZ\rangle$, $P_{Xd} = \langle X_C|\, p_y\, |iZ_d\rangle$, $P_3 = \langle D_1|\, p_x\, |iX\rangle$, $P_{3d} = \langle D_1|\, p_x\, |iX_d\rangle$, $P_2 = \langle S_2|\, p_x\, |iX\rangle$, $P_{2d} = \langle S_2|\, p_x\, |iX_d\rangle$, $P_S = \langle S_v|\, p_x\, |iX_C\rangle$, $P_U = \langle S_U|\, p_x\, |iX_C\rangle$ (see Fig. 32).

The lack of inversion center causes eight additionnal couplings in the T_d group: $P' = \langle S|\, p_x\, |iX_C\rangle$, $P'_d = \langle X_d|\, p_x\, |iZ\rangle$, $P'_3 = \langle D_1|\, p_x\, |iX_C\rangle$, $P'_2 = \langle S_2|\, p_x\, |iX_C\rangle$, $P'_S = \langle S_v|\, p_x\, |iX\rangle$, $P'_{Sd} = \langle S_v|\, p_x\, |iX_d\rangle$, $P'_U = \langle S_U|\, p_x\, |iX\rangle$, $P'_{Ud} = \langle S_U|\, p_x\, |iX_d\rangle$,

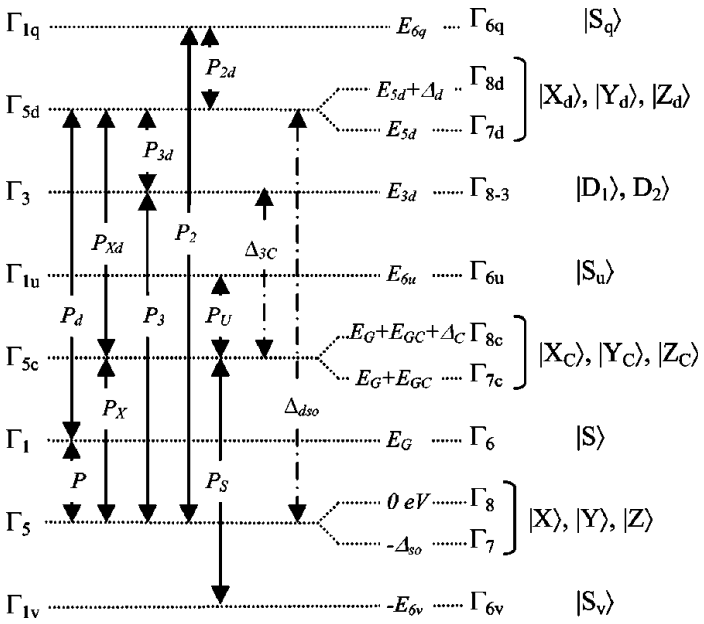

Figure 32: Wave functions in the 30-band **k**.**p** model at **k**=0 for O_h group [57].

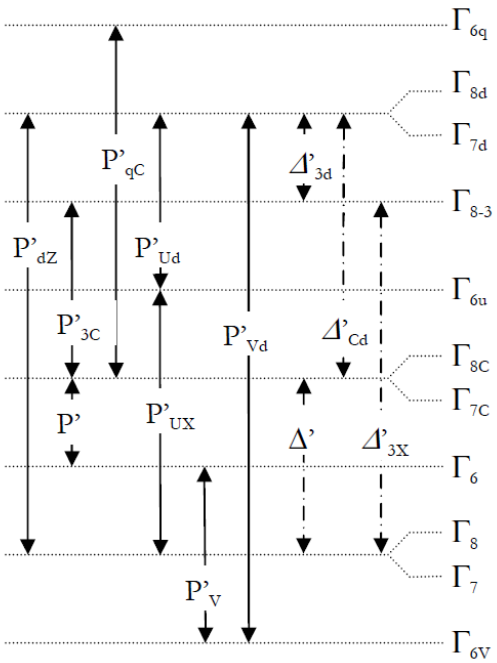

Figure 33: T_d group: Additional matrix elements and SOC due to the lack of symmetry in T_d group [57].

$P_S = \langle S_v | \, p_x \, | iX_C \rangle$, $P_U = \langle S_U | \, p_x \, | iX_C \rangle$, (see Fig. 33).

The spin-orbit interaction is introduced by the following couplings:

(i) The core SOI

$$\Delta_{so} = \frac{3\hbar}{4m_0^2c^2} \langle X | \, \frac{\partial V}{\partial x} p_y - \frac{\partial V}{\partial y} p_x \, | iY \rangle \, ,$$

$$\Delta_C = \frac{3\hbar}{4m_0^2c^2} \langle X_C | \, \frac{\partial V}{\partial x} p_y - \frac{\partial V}{\partial y} p_x \, | iY_C \rangle \, ,$$

$$\Delta_d = \frac{3\hbar}{4m_0^2c^2} \langle X_d | \, \frac{\partial V}{\partial x} p_y - \frac{\partial V}{\partial y} p_x \, | iY_d \rangle \, ,$$

(ii) The coupling between the two different multiplets the (Γ_7, Γ_8) and the $(\Gamma_{7d}, \Gamma_{8d})$

$$\Delta_{dso} = \frac{3\hbar}{4m_0^2c^2} \langle X_d | \, \frac{\partial V}{\partial x} p_y - \frac{\partial V}{\partial y} p_x \, | iY \rangle \, ,$$

(iii) The coupling between the $(\Gamma_{7C}, \Gamma_{8C})$ multiplet and the $(\Gamma_{7d}, \Gamma_{8d})$ multiplet which stems from Γ_{5C} levels and the Γ_8 level which stems from the Γ_3

$$\Delta_{3C} = \frac{3\hbar}{4m_0^2c^2} \langle D_1 | \, \frac{\partial V}{\partial x} p_z - \frac{\partial V}{\partial y} p_y \, | iX_C \rangle \, .$$

For the T_d group, there are some additional SOCs:

(i) The coupling inside the (Γ_7, Γ_8) multiplets

$$\Delta' = \frac{3\hbar}{4m_0^2c^2} \langle X_C | \, \frac{\partial V}{\partial x} p_y - \frac{\partial V}{\partial y} p_x \, | iY \rangle \, ,$$

$$\Delta'_{Cd} = \frac{3\hbar}{4m_0^2c^2} \langle X_d | \, \frac{\partial V}{\partial x} p_y - \frac{\partial V}{\partial y} p_x \, | iY_C \rangle \, ,$$

(ii) The coupling inside the (Γ_7, Γ_8) which stems from the Γ_{5C} levels and the Γ_8 level which stems from the Γ_3

$$\Delta'_3 = \frac{3\hbar}{4m_0^2c^2} \langle D_1 | \, \frac{\partial V}{\partial x} p_y - \frac{\partial V}{\partial y} p_x \, | iX \rangle \, ,$$

$$\Delta'_{3d} = \frac{3\hbar}{4m_0^2c^2} \langle D_1 | \, \frac{\partial V}{\partial x} p_z - \frac{\partial V}{\partial y} p_y \, | iX_d \rangle \, ,$$

(iii) The Luttinger parameters:

$$\begin{aligned} \gamma_1 \;\; = \;\; & -1 + \frac{E_P}{3E_G} + \frac{E_{PX}}{3} \left(\frac{1}{E_G + E_{GC}} + \frac{1}{E_G + E_{GC} + \Delta_C} \right) + \frac{2E'_{Pd}}{3E_{5d}} \\ & + \frac{4}{3} \frac{E_{P3}}{E_3} + \frac{E_{P2}}{3E_{6q}} - \frac{E'_{PS}}{3E_{6v}} + \frac{E'_{PU}}{3E_{6v}}, \end{aligned}$$

$$\gamma_2 = \frac{1}{6} \left(\frac{E_P}{E_G} + \frac{E_{P2}}{E_{6q}} + \frac{E'_{PU}}{E_{6u}} - \frac{E'_{PS}}{3E_{6v}} \right) - \frac{E_{PX}}{6 \left(E_G + E_{GC} \right)} - \frac{E'_{Pd}}{6E_{5d}} + \frac{2}{3} \frac{E_{P3}}{E_{3d}},$$

$$\gamma_3 = \frac{1}{6}\left(\frac{E_P}{E_G} + \frac{E_{P2}}{E_{6q}} + \frac{E'_{PU}}{E_{6u}} - \frac{E'_{PS}}{3E_{6v}}\right) + \frac{E_{PX}}{6\left(E_G + E_{GC}\right)} + \frac{E'_{Pd}}{6E_{5d}} - \frac{E_{P3}}{3E_{3d}},$$

$$\gamma_C = \frac{m}{m_C} = 1 + \frac{E_P}{3}\left(\frac{1}{E_G + \Delta} + \frac{2}{E_G}\right) - \frac{E'_P}{3}\left(\frac{1}{E_{GC}} + \frac{2}{E_{GC} + \Delta_C}\right) - \frac{E_{Pd}}{E_{5d} - E_G}.$$

The ghost-band method is applied to remove the spurious states in 30-band models. The electronic band structures of GaAs at large scale before (blue) and after (red) treatment of spurious states are plotted in Fig. 34. The spurious states are removed, enabling possible tunneling transport calculations in a 30-band framework.

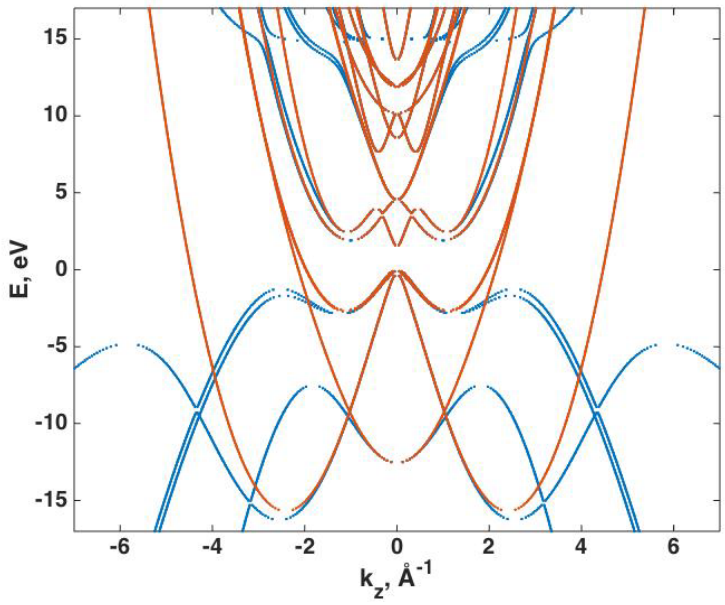

Figure 34: GaAs band structure before (red) and after (blue) spurious treatment by ghost band method, with the parameters introduced in [57].

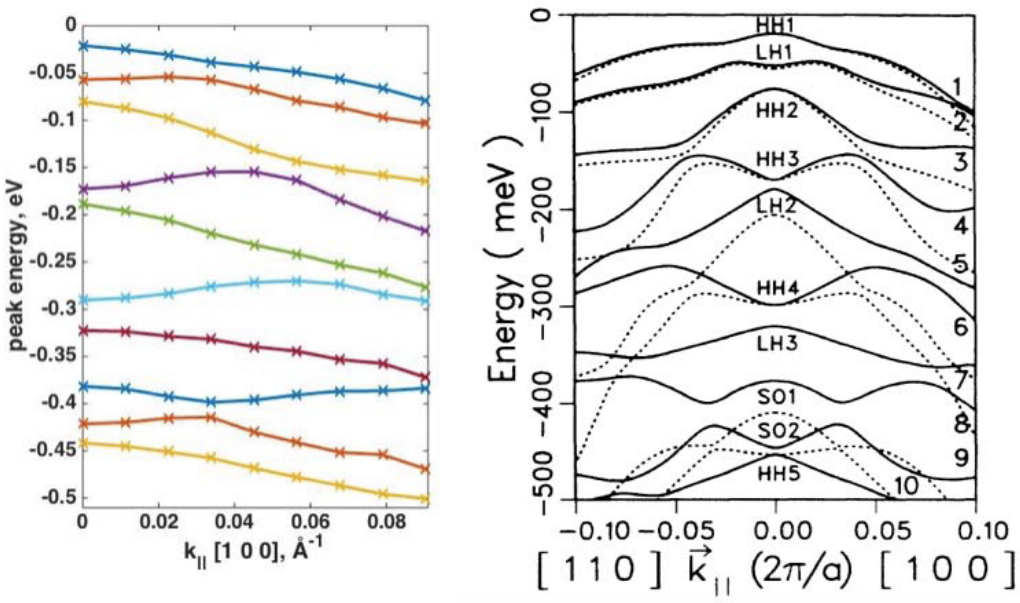

Figure 35: Comparison between the in-plane hole energy dispersion for a AlAs/ GaAs/AlAs QW 6.21 nm derived from our 30-band tunnel **k**.**p** code (left) along the $[001]$ direction of the BZ and the one derived from Ref. [66] obtained with a 6-band model along both $[001]$ and $[110]$ directions.

CHAPTER IV

THE MATCHING CONDITIONS FOR TRANSPORT WITHIN THE K.P FRAMEWORK

In this chapter, we consider the general rules defining the matching conditions for the wave functions at single interfaces or in multilayered structures. These will be adopted for electrons in effective-mass models or holes using Luttinger parameters in multiband transport with different engineered interfaces. Respectively, we consider in the same way the propagation of spin current waves and their profiles throughout the heterostructures in a multiband approach. The set of matching conditions arises from the resolution of the Schrödinger equation in each layer with correct boundary conditions depending on the interface properties and related symmetries (*e.g.* Rashba interface, T_d, or C_{2v} reduction) [53]. In some special cases, the need of perturbative methods adapted to the whole heterostructure (or single interface) is mandatory to get a physical insight in the new physical properties we calculate. This is often the case when one considers the effect of SOI in the diffusion processes (*e.g.* tunneling) from pure numerical and analytical developments. In particular, we adopt the formalism of spin-dependent scattering in the **k.p** frame, including SOI to study the effect of scattering asymmetry (topological Hall effect like investigated throughout the present thesis) in the VB of semiconductors in an improved Kane model. On the other hand, the electron transport through interfaces which is a location of spin-orbit phenomena (*e.g.* Rashba interactions) can lead to the same kind of interfacial transverse Hall effect. It can also lead to a discontinuity of the longitudinal spin current due to local interface dephasing phenomena which are important to consider in a general way. This could constitute a natural extension of the present work.

More generally, the integration of possible Rashba, spin-orbit and/or exchange interactions at interfaces in Dirac-like interaction potentials (δ-potentials) becomes, nowadays, a systematic way to consider the properties of electrons crossing ferromagnetic/ heavy-metal interfaces. These properties of electron crossing, scattering off interfaces by reflection/transmission processes, are very important when one considers, *e.g.* the issue of STT by SHE or Rashba processes from a heavy metal to a thin ferromagnetic film. These particular issues are largely developed in recent papers [76, 78, 79] when considering the absorption of the respective longitudinal and transverse parts of the spin current relevant from both Rashba and SHE in the case of Co/Pt systems. The calculation of the spin current transmissivity at the specific interfaces leads to the correct

determination and anatomy of the STT with possible relaxation to the lattice (by the SO term) or directly transferred to the local magnetization (through the exchange interactions). This is made possible *via* the determination of the extended spin-mixing conductance integrating spin-orbit and exchange at interfaces.

These physical issues of wave function matching are, presently, of a primary importance, because the properties of interface crossing for carriers (electrons or holes) is a problem encountered more generally in the physical model of the spin-resolved Boltzmann diffusion equations for both in-plane (*e.g.* CIP-GMR) and out-of-plane (CPP-geometry) diffusion transport, like in recent spin-Hall magnetoresistance (SMR) or unidirectional spin-Hall magnetoresistance (USMR) experiments [77, 80, 81, 82]. More generally, the particular matching conditions to adopt, and generalized to the spin-orbit case, enter into the relevant boundary conditions to adopt *e.g.* from a 2×2 spinor approach, for the out-of-equilibrium distributions responsible for the spin currents, for the magnetoresistances and for the spin-torque and for SMR. The reason is that interface crossing or scattering derives from a pure quantum-mechanical process where spin-polarized electrons or carriers mainly behave like both wave and particles. These observations partly explain the choice to dedicate a full-chapter to the matching conditions.

For the case of semiconducting heterostructures, largely developed here, we have chosen to consider the standard multiband matching conditions possibly involving *extrinsic SO surface potentials* although, in the particular case of T_d compounds, interfaces break the bulk symmetry group into the C_{2v} symmetry responsible for example of mixing between heavy hole and light holes. These particular matching condition for the C_{2v} symmetry have been proposed at the IOFFE institute in 1996 [83] in a first 4-band and 6-band approach before their generalization to a 14-band treatment very recently [56]. These particular matching conditions could be very easily implemented in a short future in our 14- and 30-band codes without large complexity.

In this chapter, we first describe the matching conditions for unpolarized electrons in the CB before generalizing to the case of the spin-polarized multiband applicable in both the CB and VB of semiconductors, in a full BZ approach (30-band calculation) and allowing the exact determination of both currents and spin currents in the whole heterostructures.

4.1 Example for free electron

Tunneling transport is a very basic problem in fundamental quantum physics and its applications. An electron can be transmitted through barrier of higher energy than the electron energy. Let us consider for instance free electron tunneling in one dimension,

for which the Hamiltonian in whole space writes:

$$\hat{H} = \frac{\hat{p}_x^2}{2m_0} + V_0\Theta(x) = -\frac{\hbar^2}{2m_0}\frac{\partial^2}{\partial x^2} + V_0\Theta(x), \tag{55}$$

where m_0 is free electron mass, V_0 a certain constant, $\Theta(x)$ is Heaviside function.

An alternative approach is first to establish the continuity of the wave function derivative by integration of the Schrödinger equation:

$$\begin{aligned} \int_{-\varepsilon}^{+\varepsilon} \left[-\frac{\hbar^2}{2m_0}\frac{\partial^2}{\partial x^2} + V_0\Theta(x) \right] \Psi(x)dx &= \int_{-\varepsilon}^{+\varepsilon} \mathcal{E}\Psi(x)dx \\ \int_{-\varepsilon}^{+\varepsilon} -\frac{\hbar^2}{2m_0}\frac{\partial^2}{\partial x^2}\Psi(x)dx &= \int_{-\varepsilon}^{+\varepsilon} \left[\mathcal{E} - V_0\Theta(x)\right] \Psi(x)dx. \end{aligned} \tag{56}$$

Taking the limit when $\varepsilon \longrightarrow 0$, because the term $\mathcal{E} - V_0\Theta(x)$ is bounded, we obtain:

$$\lim_{\varepsilon \longrightarrow 0} \int_{-\varepsilon}^{+\varepsilon} \left[\mathcal{E} - V_0\Theta(x)\right] \Psi(x)dx = 0.$$

Therefore, Eq. 56 becomes:

$$\lim_{\varepsilon \longrightarrow 0} \left[\frac{\partial}{\partial x}\Psi(x) \right]_{-\varepsilon}^{+\varepsilon} dx = 0.$$

Physically, the probability current has to be continuous, *i.e.*,

$$\mathbf{J}^f\left[\Psi\right] = \mathrm{Re}\left[\Psi^* \frac{\hat{p}}{m_0}\Psi\right] = \frac{\hbar}{m_0}\,\mathrm{Im}\left[\Psi^*\frac{\partial}{\partial x}\Psi\right] = 0. \tag{57}$$

So that a sufficient condition is $\left[\Psi\right]_{x=0} = 0$ which provides us the standard matching condition, namely the continuity of the envelope function and of its derivative.

4.2 The BenDaniel-Duke condition

The problem becomes more complex when an electron propagates through a heterostructure made of different materials, where in each bulk medium, the system is described by its own relevant Hamiltonian. We then need to define the proper matching conditions at each boundary. In this situation, the BDD approach is known to be the simplest one [33] to be considered. Let us introduce the BDD ideas for the matching conditions in one dimension. Suppose that an electron tunnels through an interface delimiting two different media at $x < 0$ and $x > 0$. As mentioned before, each medium is characterized by its own Hamiltonian and one must find a solution of Schrödinger's equation, made of eigenvectors of relevant bands in the two bulk materials, ensuring the continuity of the probability current at the origin. In this sense, the problem is analogous to a scattering problem, where the wave functions are determined only at some distance of the scattering potential. Proper matching conditions rely on the extension of the bulk

envelope function over the whole space. In an effective mass point of view, the BDD proposed to write the Hamiltonian in the whole space as:

$$\hat{H}(x) = \frac{\hat{p}_x^2}{2m(x)} + V(x) = \hat{p}_x \left[\frac{1}{2m(x)}\hat{p}_x\right] + V(x) = \frac{1}{2}\hat{p}_x \frac{\partial \hat{H}}{\partial \hat{p}_x} + V(x), \tag{58}$$

where $m(x)$ is the effective position-dependent mass and $V(x)$ is the potential in each medium. This procedure yields an Hermitian Hamiltonian. The integration of the Hamiltonian in Eq. 58 around the boundary automatically ensures the continuity of the probability current, provided that both $\Psi(x)$ and current wave $\left(\partial \hat{H}/\partial \hat{p}_x\right)\Psi$ are continuous. The BDD matching conditions are known as standard matching conditions for electrons in the CB and have been applied with success to a variety of situations. But one must note that these are not valid in the systems characterized by an Hamiltonian including terms with momentum operator power of orders larger than two along the flux direction [31].

For more complex systems including, *e.g.* k^3 terms, corresponding to Dresselhaus interactions in an effective Hamiltonian approach, it is no longer possible to treat the transport in the standard way. A solution is to increase the number of bands to express to the Hamiltonian so that each matrix element of the Hamiltonian only involves k terms with power strictly lower than three.

4.3 Standard matching condition for the multiband transport

In this part, we consider the matching conditions in the structures possibly including SOI and exchange interactions. This particular issue raises when one considers the crossing of ferromagnetic/spin-orbit couples in semiconductor as well as metallic spintronics systems like recently emphasized in papers dealing with the problematic of STT via the SHE or SMR. As mentioned before, the SOI associated the the lack of inversion center leads to the occurrence of the cubic terms, *i.e.*, Dresselhaus terms, in the electron effective model. It makes us modify the standard matching conditions [31] or consider the cubic terms as perturbation terms [15]. Another solution, which is adopted in the present work, is to work within a larger basis function to decrease the order of momentum terms, *e.g.* using a 14-band **k**.**p** model instead of a 2-band effective model. In this point of view, it becomes necessary to redefine the matching conditions for multiband transport [84, 85]. Let us start with the Hamiltonian without exchange interaction:

$$\hat{H} = \frac{\mathbf{p}^2}{2m_0} + \mathfrak{U} + \frac{\hbar}{4m_0^2c^2}\left(\boldsymbol{\nabla}\mathfrak{U} \times \mathbf{p}\right).\boldsymbol{\sigma}.$$

As introduced before in Sec.3.1, the Hamiltonian can be written in the form:

$$\hat{H} = \sum_{j,k} a_j \hat{p}_j + \sum_{j,k} b_{jk} \hat{p}_j \hat{p}_k, \tag{59}$$

where $\hat{p}_j$, $\hat{p}_k$ are the components of momentum $\mathbf{p}$; a_j and b_{jk} (j, k refer to Cartesian coordinates) are 14×14 Hermitian matrices operating on the spin and space components and invariant under permutation of j, k. To describe the potentials independent of the momentum, *e.g.* the exchange potential or external magnetic field, we introduce $\hat{H}_0$ as a supplemental term in Eq. 59.

We have intentionally chosen to give the exact derivation for the current and spin current operators from the general Schrödinger equation in multilayers. The Schrödinger equation writes:

$$\begin{aligned} i\hbar \frac{\partial |\Psi\rangle}{\partial t} &= \hat{H} |\Psi\rangle \\ i\hbar \frac{\partial |\Psi\rangle}{\partial t} &= \sum_j a_j \hat{p}_j |\Psi\rangle + \sum_{j,k} b_{jk} \hat{p}_j \hat{p}_k |\Psi\rangle + \hat{H}_0 |\Psi\rangle . \end{aligned}$$

Taking the adjoint, we obtain:

$$-i\hbar \frac{\partial \langle\Psi|}{\partial t} = \sum_j \langle \hat{p}_j \Psi| \, a_j + \sum_{j,k} \langle \hat{p}_j \hat{p}_k \Psi| \, b_{jk} + \langle\Psi| \, \hat{H}_0 .$$

The conservation equation related to the density of probability (*i.e.*, the so-called "continuity equation") can be straightforward defined:

$$\begin{aligned} i\hbar \frac{\partial \langle\Psi| \, \Psi\rangle}{\partial t} &= i\hbar \left[\langle\Psi| \, \frac{\partial \Psi}{\partial t} \right\rangle + \left\langle \frac{\partial \Psi}{\partial t} \right| \, \Psi\rangle \Bigg] \\ &= \sum_j \langle\Psi| \, a_j \hat{p}_j |\Psi\rangle + \sum_{j,k} \langle\Psi| \, b_{jk} \hat{p}_j \hat{p}_k |\Psi\rangle \\ &\quad - \sum_j \langle \hat{p}_j \Psi| \, a_j \, \Psi\rangle - \sum_{j,k} \langle \hat{p}_j \hat{p}_k \Psi| \, b_{jk} \, \Psi\rangle \\ &= \left[\sum_j \langle\Psi| \, a_j \hat{p}_j |\Psi\rangle - \sum_j \langle \hat{p}_j \Psi| \, a_j \, \Psi\rangle \right] \\ &\quad + \left[\sum_{j,k} \langle\Psi| \, b_{jk} \hat{p}_j \hat{p}_k |\Psi\rangle - \sum_{j,k} \langle \hat{p}_j \hat{p}_k \Psi| \, b_{jk} \, \Psi\rangle \right] . \end{aligned}$$

Because $\langle \hat{p}_j \Psi| \, a_j \, \Psi\rangle = \langle\Psi| \, a_j \hat{p}_j |\Psi\rangle^*$, $\langle \hat{p}_j \hat{p}_k \Psi| \, b_{jk} \, \Psi\rangle = \langle\Psi| \, b_{jk} \hat{p}_j \hat{p}_k |\Psi\rangle^*$, we observe:

$$\frac{\partial \langle\Psi| \, \Psi\rangle}{\partial t} = \frac{2}{\hbar} \, \mathrm{Im} \left[\sum_j \langle\Psi| \, a_j \hat{p}_j |\Psi\rangle + \sum_{j,k} \langle\Psi| \, b_{jk} \hat{p}_j \hat{p}_k |\Psi\rangle \right] . \tag{60}$$

Let us demonstrate that

$$\frac{2}{\hbar}\,\mathrm{Im}\left[\sum_j \langle\Psi|\, a_j\hat{p}_j\,|\Psi\rangle + \sum_{j,k}\langle\Psi|\, b_{jk}\hat{p}_j\hat{p}_k\,|\Psi\rangle\right] = -\sum_j \boldsymbol{\nabla}_j\left(\mathrm{Re}\,\langle\Psi|\,\hat{\mathbf{J}}_j\,|\Psi\rangle\right),$$

where $\hat{\mathbf{J}}_j$ is the j component of the wave current operator $\hat{\mathbf{J}}$,

$$\hat{\mathbf{J}}_j = \frac{\partial\hat{H}}{\partial\hat{p}_j} = a_j + 2\sum_k b_{jk}\hat{p}_k.$$

One obtains,

$$\mathrm{Re}\,\langle\Psi|\,\hat{\mathbf{J}}_j\,|\Psi\rangle = \sum_k\langle\Psi|\,\frac{a_j}{2} + b_{jk}\hat{p}_k\,|\Psi\rangle + \sum_k\left\langle\left(\frac{a_j}{2}+b_{jk}\hat{p}_k\right)\Psi\right|\,|\Psi\rangle\,. \tag{61}$$

Note $\nabla_j = (i/\hbar)\,\hat{p}_j$, and $(a_j)^+ = a_j$, $(b_{jk})^+ = b_{jk}$.

We first consider the derivation of the first-order components in Eq. 61,

$$\begin{aligned} A_1 &= \frac{i}{\hbar}\hat{p}_j\left\{\langle\Psi|\,\frac{a_j}{2}\Psi\right\rangle + \left\langle\frac{a_j}{2}\Psi\right|\,\Psi\rangle\right\} \\ &= \frac{i}{\hbar}\hat{p}_j\left\{\langle\Psi|\,a_j\Psi\rangle\right\} \\ &= \frac{i}{\hbar}\left\{\langle\Psi|\,a_j\hat{p}_j\Psi\rangle - \langle\hat{p}_j\Psi|\,a_j\Psi\rangle\right\} \\ &= \frac{-2}{\hbar}\,\mathrm{Im}\,\langle\Psi|\,a_j\hat{p}_j\Psi\rangle\,. \end{aligned} \tag{62}$$

And the derivation of the second-order components in Eq. 61,

$$\begin{aligned} A_2 &= \frac{i}{\hbar}\sum_k\hat{p}_j\left\{\langle\Psi|\,b_{jk}\hat{p}_k\Psi\rangle + \langle b_{jk}\hat{p}_k\Psi|\,\Psi\rangle\right\} \\ &= \frac{i}{\hbar}\sum_k\left\{\begin{array}{c}\langle\Psi|\,b_{jk}\hat{p}_j\hat{p}_k\Psi\rangle - \langle\hat{p}_j\Psi|\,b_{jk}\hat{p}_k\Psi\rangle \\ -\langle b_{jk}\hat{p}_j\hat{p}_k\Psi|\,\Psi\rangle + \langle b_{jk}\hat{p}_k\Psi|\,\hat{p}_j\,\Psi\rangle\end{array}\right\}. \end{aligned} \tag{63}$$

We have $\langle b_{jk}\hat{p}_k\Psi|\,\hat{p}_j\,\Psi\rangle = \langle\hat{p}_k\Psi|\,b_{jk}\hat{p}_j\,\Psi\rangle = \langle\hat{p}_j\Psi|\,b_{jk}\hat{p}_k\Psi\rangle$ so that Eq. 63 becomes

$$\begin{aligned} A_2 &= \frac{i}{\hbar}\sum_k\left\{\langle\Psi|\,b_{jk}\hat{p}_j\hat{p}_k\Psi\rangle - \langle b_{jk}\hat{p}_j\hat{p}_k\Psi|\,\Psi\rangle\right\} \\ A_2 &= \frac{-2}{\hbar}\sum_k\mathrm{Im}\,\langle\Psi|\,b_{jk}\hat{p}_j\hat{p}_k\Psi\rangle\,. \end{aligned} \tag{64}$$

From Eqs. 62 and 64, we obtain

$$\boldsymbol{\nabla}_j\left\{\mathrm{Im}\,\langle\Psi|\,\hat{\mathbf{J}}_j\,|\Psi\rangle\right\} = \frac{-2}{\hbar}\sum_k\mathrm{Im}\,\langle\Psi|\,\left(a_j\hat{p}_j + b_{jk}\hat{p}_j\hat{p}_k\right)\Psi\rangle\,. \tag{65}$$

According to Eqs. 60 and Eq. 65

$$\frac{\partial\,\langle\Psi|\,\Psi\rangle}{\partial t} = -\sum_j\boldsymbol{\nabla}_j\left(\mathrm{Re}\,\langle\Psi|\,\hat{\mathbf{J}}_j\,|\Psi\rangle\right).$$

Under stationary regime, we obtain

$$0 = \boldsymbol{\nabla}_j \left\{ \mathrm{Re} \left\langle \Psi \right| \hat{\mathbf{J}}_j \left| \Psi \right\rangle \right\}.$$

This equation demonstrates that the current $\left\langle \Psi \right| \hat{\mathbf{J}}_j \Psi \Big\rangle$ is conserved, at least in each layer of the heterostructure separately. We will show, in the next section, that this is also true within the whole heterostructure under the conditions that the correct current operator is defined from the Hamiltonian and the correct boundary conditions from the surface potential terms. Concerning the exchange potential, if this is to be considered (*e.g.* appearing in the ferromagnetic semiconductor structures), the corresponding exchange Hamiltonian, $\hat{H}_0$, is independent of momentum and position. Therefore, it is not necessary to redefine the components of the current operator $\hat{\mathbf{J}}$.

Finally, the continuity of the wave function Ψ and the continuity of the wave current $\hat{\mathbf{J}}_i \Psi$ are sufficient conditions which ensure that the probability current is continuous at an interface. These are the matching conditions which we use in the present work. And we will show that the charge current remains constant throught the heterostructure.

4.4 Definition of the spin current with the standard matching conditions

With the standard matching conditions for multiband transport introduced in Sec.4.3, respectively we consider the spin current.

$$\begin{aligned} i\hbar \frac{\partial \left\langle \Psi \right| \hat{\sigma}_\alpha \left. \Psi \right\rangle}{\partial t} &= i\hbar \left[\left\langle \Psi \right| \hat{\sigma}_\alpha \frac{\partial \Psi}{\partial t} \Big\rangle + \left\langle \frac{\partial \Psi}{\partial t} \right| \hat{\sigma}_\alpha \left. \Psi \right\rangle \right] \\ &= \left\langle \Psi \right| \hat{\sigma}_\alpha \hat{H} \Psi \Big\rangle - \left\langle \hat{\sigma}_\alpha \hat{H} \Psi \right| \left. \Psi \right\rangle, \end{aligned} \tag{66}$$

where $\hat{\sigma}_\alpha$ is spin operator, $\hat{\sigma}_\alpha = \{\sigma_x,\ \sigma_y, \sigma_z\}$.

For symmetry properties, the operator $\hat{\sigma}_\alpha \hat{H}$ can be written as:

$$\frac{\hat{\sigma}_\alpha \hat{H} + \hat{H}^+ \hat{\sigma}_\alpha^+}{2} = \frac{\hat{\sigma}_\alpha \hat{H} + \hat{H} \hat{\sigma}_\alpha}{2},$$

because the spin operator and the Hamiltonian are Hermitian matrices.

The conservation equation expressed by Eq. 66 becomes:

$$\begin{aligned} \frac{\partial \left\langle \Psi \right| \hat{\sigma}_\alpha \left. \Psi \right\rangle}{\partial t} &= \frac{1}{i\hbar} \left(\begin{array}{c} \left\langle \Psi \right| \frac{\hat{\sigma}_\alpha \hat{H} + \hat{H} \hat{\sigma}_\alpha}{2} \Psi \Big\rangle - \left\langle \frac{\hat{\sigma}_\alpha \hat{H} + \hat{H} \hat{\sigma}_\alpha}{2} \Psi \right| \left. \Psi \right\rangle \\ + \left\langle \Psi \right| \left[\hat{\sigma}_\alpha, \hat{H}_0 \right] \left| \Psi \right\rangle \end{array} \right) \\ &= \frac{2}{\hbar} \mathrm{Im} \left\langle \Psi \right| \frac{\hat{\sigma}_\alpha \hat{H} + \hat{H} \hat{\sigma}_\alpha}{2} \Psi \Big\rangle + \frac{1}{i\hbar} \left\langle \Psi \right| \left[\hat{\sigma}_\alpha, \hat{H}_0 \right] \left| \Psi \right\rangle. \end{aligned} \tag{67}$$

Let us introduce $\hat{\mathbf{J}}_j^\alpha$ which is the α, $(\alpha = \{x,\ y,\ z\})$, component of spin current operator, along the j direction $(j = \{x,\ y,\ z\})$ of charge current,

$$\hat{\mathbf{J}}_j^\alpha = \frac{\hat{\sigma}_\alpha}{2}\frac{\partial \hat{H}}{\partial \hat{p}_j} + \frac{\partial \hat{H}}{\partial \hat{p}_j}\frac{\hat{\sigma}_\alpha}{2}.$$

We will demonstrate that

$$\frac{2}{\hbar}\,\mathrm{Im}\left\langle \Psi\right| \left(\frac{\hat{\sigma}_\alpha \hat{H} + \hat{H}\hat{\sigma}_\alpha}{2}\right) \Psi \Big\rangle = -\sum_j \boldsymbol{\nabla}_j \left(\mathrm{Re}\left\langle \Psi\right| \hat{\mathbf{J}}_j^\alpha\ \Psi\right\rangle\right),$$

The spin operator is independent of the momentum so that we can write,

$$\begin{aligned}
\boldsymbol{\nabla}_j \left(\frac{\hat{\sigma}_\alpha}{2}\frac{\partial \hat{H}}{\partial \hat{p}_j} + \frac{\partial \hat{H}}{\partial \hat{p}_j}\frac{\hat{\sigma}_\alpha}{2}\right) &= \frac{\hat{\sigma}_\alpha}{2}\boldsymbol{\nabla}_j\frac{\partial \hat{H}}{\partial \hat{p}_j} + \boldsymbol{\nabla}_j\frac{\partial \hat{H}}{\partial \hat{p}_j}\frac{\hat{\sigma}_\alpha}{2} \\
&= \frac{i}{\hbar}\sum_k \left\{\frac{\hat{\sigma}_\alpha}{2}\left(a_j\hat{p}_j + 2b_{jk}\hat{p}_{kj}\hat{p}_j\right) + \left(a_j\hat{p}_j + 2b_{jk}\hat{p}_{kj}\hat{p}_j\right)\frac{\hat{\sigma}_\alpha}{2}\right\} \\
&= 2\frac{i}{\hbar}\left(\frac{\hat{\sigma}_\alpha \hat{H} + \hat{H}\hat{\sigma}_\alpha}{2}\right).
\end{aligned}$$

Therefore, we have

$$\left\langle \Psi\right| \hat{\mathbf{J}}_j^\alpha\ \Psi\right\rangle = 2\frac{i}{\hbar}\left\langle \Psi\right| \left(\frac{\hat{\sigma}_\alpha \hat{H} + \hat{H}\hat{\sigma}_\alpha}{2}\right) \Psi\Big\rangle.$$

One obtains,

$$\begin{aligned}
\mathrm{Re}\left\langle \Psi\right| \hat{\mathbf{J}}_j^\alpha\ \Psi\right\rangle &= \frac{1}{2}\left(\left\langle \Psi\right| \hat{\mathbf{J}}_j^\alpha\ \Psi\right\rangle + c.c\right) \\
&= \frac{i}{\hbar}\left\langle \Psi\right| \left(\frac{\hat{\sigma}_\alpha \hat{H} + \hat{H}\hat{\sigma}_\alpha}{2}\right) \Psi\Big\rangle + c.c \\
&= -2\,\mathrm{Im}\left\langle \Psi\right| \left(\frac{\hat{\sigma}_\alpha \hat{H} + \hat{H}\hat{\sigma}_\alpha}{2}\right) \Psi\Big\rangle.
\end{aligned}$$

We observe and conclude that the conservation equation for the spin current writes:

$$\frac{\partial \left\langle \Psi\right| \hat{\sigma}_\alpha\ \Psi\right\rangle}{\partial t} = -\sum_j \boldsymbol{\nabla}_j \left(\mathrm{Re}\left\langle \Psi\right| \hat{\mathbf{J}}_j^\alpha\ \Psi\right\rangle\right) + \frac{1}{i\hbar}\left\langle \Psi\right| \left[\hat{\sigma}_\alpha, \hat{H}_0\right] \left|\Psi\right\rangle.$$

In the case, when the Hamiltonian is time independent, we obtain the continuity equation for the spin current according to the following form:

$$0 = \boldsymbol{\nabla}_j \left(\mathrm{Re}\left\langle \Psi\right| \hat{\mathbf{J}}_j^\alpha\ \Psi\right\rangle\right) + \frac{1}{i\hbar}\left\langle \Psi\right| \left[\hat{\sigma}_\alpha, \hat{H}_0\right] \left|\Psi\right\rangle. \tag{68}$$

which means that, unlike the charge current which is always conserved, the spin current is conserved on the condition that the Hamiltonian in the bulk and at the interface (see

the following section) commutes with the corresponding spinor. On this unique condition, the spin current is conserved within the whole heterostructure. If one considers, for example, the case of a spin-orbit coupling of the form $\hat{H}_{S.O} = \mathbf{L}.\mathbf{S}$, one can easily observe that its commutator with the spin physical observable $\mathbf{S}$ is not zero but includes the orbital-moment operator $\mathbf{L}$, playing the role of a non-zero external magnetic field acting on the spin. By reciprocity, the orbital current (not defined here, see for instance Ref. [86]) will be neither conserved due to the action of the spin $\mathbf{S}$. Note however, that the total angular-momentum ($\mathbf{J} = \mathbf{L} + \mathbf{S}$) is conserved at least in the case of a pure spherical symmetry because it commutates with the spin-orbit Hamiltonian term.

Another example is the one of an exchange field in a ferromagnet, which is a general problem for the issue of the spin-transfer phenomena. The presence of an exchange field in the ferromagnetic layer to be switched, by STT or by SHE, makes the spin current nonuniform in the layer but modulated by a precession of the local spin-polarized carriers around the local magnetic field. This precession, which is shortly described below, is responsible for the mixing between the damping-like and field-like torques within the film thickness, as largely emphasized in the case of spin-torques through a tunnel barrier [87, 145, 88].

Let us consider an example where $\hat{H}_0$ is the exchange Hamiltonian $\hat{H}_0 = 6B_G\overrightarrow{m}.\hat{\sigma}$, where we observe

$$\begin{aligned}\frac{1}{i\hbar}\left\langle\Psi\right|\left[\hat{\sigma}_\alpha, \hat{H}_0\right]\left|\Psi\right\rangle &= \frac{1}{i\hbar}\left\langle\Psi\right|\left[\hat{\sigma}_\alpha, 6B_G\overrightarrow{m}.\hat{\sigma}\right]\left|\Psi\right\rangle \\ &= \frac{1}{\hbar}\left\langle\Psi\right|\left(6B_G\overrightarrow{m}\times\hat{\sigma}\right)_\alpha\left|\Psi\right\rangle.\end{aligned}$$

This equation describes the physics of STT in tunnel junctions where the precession term (second term) results in a strong mixing between the damping-like and field-like symmetries of the torque.

Equation. 68 becomes

$$0 = \boldsymbol{\nabla}_j\left(\mathrm{Re}\left\langle\Psi\right|\frac{\hat{\sigma}_\alpha}{2}\frac{\partial\hat{H}}{\partial\hat{p}_j} + \frac{\partial\hat{H}}{\partial\hat{p}_j}\frac{\hat{\sigma}_\alpha}{2}\ \Psi\right\rangle\right) + \frac{1}{\hbar}\left\langle\Psi\right|\left(6B_G\overrightarrow{m}\times\hat{\sigma}\right)_\alpha\left|\Psi\right\rangle.$$

4.5 Matching conditions with structure inversion asymmetry (SIA) at interface

We consider now, the case where a surface potential of a particular symmetry possibly involving either spin-orbit and/or surface exchange terms at interfaces or in interface states is rapidly damped in the layer on a typical length scale given by the electronic evanescent wave, that is a few nanometers. We will call it SIA-like structure inversion asymmetry, even if these terms may gather different meanings, *e.g.* if exchange

terms are included due to the proximity effect of the exchange interactions within the ferromagnet. This case corresponds to the interface properties between two different materials involving generally several interfaces which can be the seat of strong asymmetric potential effects (Rashba-Dresselhaus supplementary in-plane terms breaking symmetry).

We consider the SIA spin-splitting given by a Rashba interface term along the j direction,

$$\hat{H}_R = \sum_j V_j \delta(x_j - x_0),$$

where V_j is a matrix which is independent of the j component of the momentum.

The total Hamiltonian is:

$$\hat{H}_{total} = \hat{H} + \hat{H}_R, \tag{69}$$

where $\hat{H}$ was introduced in the last Sec. 4.3,

$$\hat{H} = \sum_j a_j \hat{p}_j + \sum_{j,k} b_{jk} \hat{p}_j \hat{p}_k \ .$$

The Schrödinger equation is:

$$\begin{aligned} i\hbar \frac{\partial \left|\Psi\right\rangle}{\partial t} &= \hat{H}_{total} \left|\Psi\right\rangle \\ i\hbar \frac{\partial \left|\Psi\right\rangle}{\partial t} &= \hat{H} \left|\Psi\right\rangle + \sum_j V_j \delta(x_j - x_0) \left|\Psi\right\rangle . \end{aligned}$$

Taking the adjoint of this equation, one gets

$$-i\hbar \frac{\partial \left\langle\Psi\right|}{\partial t} = \left\langle \hat{H}\Psi \right| + \sum_j \left\langle V_j \Psi\right| \delta(x_j - x_0).$$

4.5.1 Definition of the charge current and new matching condition

We are now going to generalize the definition of the charge current operator, as well as the matching conditions to use for a given interface. The equation of conservation for the present Hamiltonian, can now be written as:

$$\begin{aligned} \frac{\partial \left\langle\Psi\right| \left.\Psi\right\rangle}{\partial t} &= \left\langle\Psi\right| \left.\frac{\partial \Psi}{\partial t}\right\rangle + \left\langle \frac{\partial \Psi}{\partial t} \right| \left.\Psi\right\rangle \\ &= \frac{1}{i\hbar} \left(\left\langle\Psi\right| \left.\hat{H}\Psi\right\rangle - \left\langle \hat{H}\Psi \right| \left.\Psi\right\rangle \right) \\ &\quad + \frac{1}{i\hbar} \left[\sum_j \left\langle\Psi\right| V_j \delta(x_j - x_0) \left|\Psi\right\rangle - \sum_j \left\langle V_j \Psi\right| \delta(x_j - x_0) \left|\Psi\right\rangle \right] . \end{aligned}$$

As we did before,

$$\begin{aligned} & \frac{1}{i\hbar}\left(\langle\Psi|\,\hat{H}\Psi\Big\rangle - \Big\langle\hat{H}\Psi\Big|\,\Psi\rangle\right) \\ = & -\sum_j \boldsymbol{\nabla}_j \,\mathrm{Re}\,\langle\Psi|\,\frac{\partial\hat{H}}{\partial\hat{p}_j}\,|\Psi\rangle\,. \end{aligned}$$

We obtain

$$\begin{aligned} \frac{1}{i\hbar}\left[\sum_j \langle\Psi|\,V_j\delta(x_j-x_0)\,|\Psi\rangle - \sum_j \langle V_j\Psi|\,\delta(x_j-x_0)\,|\Psi\rangle\right] &= \sum_j \frac{-i}{\hbar}\,\langle\Psi|\,V_j\delta(x_j-x_0)\,|\Psi\rangle + c.c \\ &= \mathrm{Re}\,\langle\Psi|\,\frac{(-2i)}{\hbar}V_j\delta(x_j-x_0)\,|\Psi\rangle\,. \end{aligned}$$

We know that $\delta(x_j - x_0)$ is equal to $\frac{\partial\Theta(x_j-x_0)}{\partial x_j}$, where Θ is the Heaviside function. The continuity equation for the current-operator becomes:

$$\begin{aligned} \frac{\partial\,\langle\Psi|\,\Psi\rangle}{\partial t} &= \sum_j \boldsymbol{\nabla}_j \,\mathrm{Re}\left[-\langle\Psi|\,\frac{\partial\hat{H}}{\partial\hat{p}_j} - \frac{2i}{\hbar}V_j\Theta(x_j-x_0)\,|\Psi\rangle\right] \\ &= -\frac{1}{\hbar}\sum_j \boldsymbol{\nabla}_j \,\mathrm{Re}\left[\langle\Psi|\,\frac{\partial\hat{H}}{\partial\hat{k}_j} + 2iV_j\Theta(x_j-x_0)\,|\Psi\rangle\right]. \end{aligned}$$

In the case where the Hamiltonian is time independent like one considers here, one obtains:

$$\begin{aligned} 0 &= \sum_j \nabla_j \,\mathrm{Re}\left[\langle\Psi|\,\frac{\partial\hat{H}}{\partial\hat{k}_j} + 2iV_j\Theta(x_j-x_0)\,|\Psi\rangle\right], \\ \text{or } 0 &= \sum_j \nabla_j \,\mathrm{Re}\left[\langle\Psi|\,\hat{\mathbf{J}}_j\,|\Psi\rangle\right], \end{aligned}$$

where $\hat{\mathbf{J}}_j = \frac{\partial\hat{H}}{\partial\hat{k}_j} + 2iV_j\Theta(x_j - x_0)$ is the j component of the current operator to be matched at interfaces. This important relationship allows us to give a formal definition of the current operator to use in each media and, in this sense, provides a generalization of the correct expression to use in the case of a general surface potential possibly involving Rashba, Dresselhaus, exchange interactions, and of all other types.

This development then provides us the new matching conditions to use as far as:

$$\mathrm{Re}\left[\langle\Psi|\,\hat{\mathbf{J}}_j\,|\Psi\rangle\right] \text{ is continuous at the interface.}$$

4.5.2 Definition of the spin current

Now, let us consider the spin current in heterostructures involving surface potential terms.

According to Eq. 68 with $\hat{H}_0 = \hat{H}_R$, we obtain:

$$0 = \boldsymbol{\nabla}_j \left(\frac{1}{\hbar} \mathrm{Re} \left\langle \Psi \right| \frac{\hat{\sigma}_\alpha}{2} \frac{\partial \hat{H}}{\partial \hat{k}_j} + \frac{\partial \hat{H}}{\partial \hat{k}_j} \frac{\hat{\sigma}_\alpha}{2} \left. \Psi \right\rangle \right) + \frac{1}{i\hbar} \left\langle \Psi \right| \left[\hat{\sigma}_\alpha, \hat{H}_R \right] \left| \Psi \right\rangle_j . \tag{70}$$

We calculate $\frac{1}{i\hbar} \left\langle \Psi \right| \left[\hat{\sigma}_\alpha, \hat{H}_R \right] \left| \Psi \right\rangle_j$,

$$\begin{aligned} \frac{1}{i\hbar} \left\langle \Psi \right| \left[\hat{\sigma}_\alpha, \hat{H}_R \right] \left| \Psi \right\rangle_j &= \frac{1}{i\hbar} \left\langle \Psi \right| \hat{\sigma}_\alpha V_j \delta(x_j - x_0) - V_j \delta(x_j - x_0) \hat{\sigma}_\alpha \left| \Psi \right\rangle \\ &= \frac{1}{\hbar} \boldsymbol{\nabla}_j \left\langle \Psi \right| - i\hat{\sigma}_\alpha V_j \delta(x_j - x_0) + i V_j \delta(x_j - x_0) \hat{\sigma}_\alpha \left| \Psi \right\rangle . \end{aligned} \tag{71}$$

Equation. 70 becomes:

$$0 = \boldsymbol{\nabla}_j \left\{ \mathrm{Re} \left\langle \Psi \right| \left(\frac{\hat{\sigma}_\alpha}{2} \frac{\partial \hat{H}}{\partial \hat{k}_j} + \frac{\partial \hat{H}}{\partial \hat{k}_j} \frac{\hat{\sigma}_\alpha}{2} \right) \left| \Psi \right\rangle + \left\langle \Psi \right| - i\hat{\sigma}_\alpha V_j \Theta(x_j - x_0) + i V_j \Theta(x_j - x_0) \hat{\sigma}_\alpha \left| \Psi \right\rangle \right\} . \tag{72}$$

Therefore, we observe:

$$\mathrm{Re} \left\langle \Psi \right| \left\{ \left(\frac{\hat{\sigma}_\alpha}{2} \frac{\partial \hat{H}}{\partial \hat{k}_j} + \frac{\partial \hat{H}}{\partial \hat{k}_j} \frac{\hat{\sigma}_\alpha}{2} \right) \right\} \left| \Psi \right\rangle = \left\{ \begin{array}{cc} const + i \left\langle \Psi \right| \left[\hat{\sigma}_\alpha, V_j \right] \left| \Psi \right\rangle & \text{if } x_j > x_0 \\ const & \text{if } x_j < x_0 \end{array} \right. . \tag{73}$$

This equation shows the discontinuity of the spin current at the interface for a SIA spin splitting given by Rashba interface term, and will be discussed in the next chapter concerning transport in heterostructures.

4.6 Current in heterostructures

In this section, we will demonstrate that the use of the matching conditions derived previously in the preceding sections and applied to each interface within a given heterostructure, simple interfaces, tunnel junctions, quantum wells, double-barrier structures, are always associated to a conservative charge-current profile within the transport direction. The demonstration will be made taking into account the properties of the S-scattering matrix for the contact interface. On the other hand, the same conclusions cannot be generalized to the case of the spin current profile if either bulk or interface potentials admit an Hamiltonian term responsible for local spin decoherence (linear or cubic Rashba interactions, Dresselhaus for the C_{2v} symmetry interface) responsible for spin current discontinuities in the longitudinal direction (what is called spin-memory loss) or in the two-transverse directions (spin decoherence). This effect should lead to in the re-examination of the calculations of the spin-mixing conductance (real part and imaginary part) for systems involving Rashba interactions at interfaces.

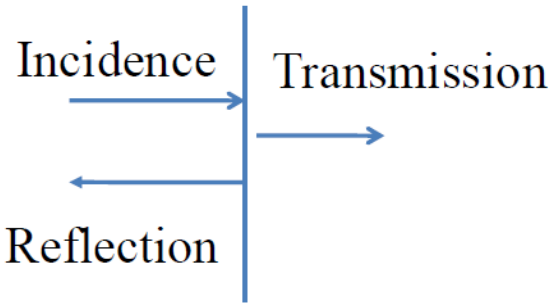

Figure 36: The continuity of the flux current at the interface

We demonstrate here the continuity of the charge current. The wave function at the left interface is written as:

$$\Psi_L = \Phi_{in}(\overrightarrow{r}) + \sum_n r_{in,n}\Phi_r^n(\overrightarrow{r}),$$

whereas the wave function at the right interface is:

$$\Psi_R = \sum_n t_{in,n}\Phi_r^n(\overrightarrow{r}).$$

Let assume that the matching conditions at the interfaces are the continuity of the wave function Ψ and of the wave current $\mathrm{Re}\left\langle\Psi\right|\hat{\mathbf{J}}\left|\Psi\right\rangle$ where $\hat{\mathbf{J}} = \partial\hat{H}/\partial\hat{\mathbf{p}}$. These are the matching conditions that we consider through the present work.

The probability current at the left of the interface is:

$$\begin{aligned}\mathrm{Re}\left\langle\Psi_L\right|\hat{\mathbf{J}}\left|\Psi_L\right\rangle &= \mathrm{Re}\left\langle\Phi_{in} + \sum_n r_{in,n}\Phi_r^n\right|\hat{\mathbf{J}}\left|\Phi_{in} + \sum_{n'} r_{in,n'}\Phi_r^{n'}\right\rangle \\ &= \mathrm{Re}\left\langle\Phi_{in}\right|\hat{\mathbf{J}}\left|\Phi_{in}\right\rangle + \sum_n \left|r_{in,n}\right|^2 \mathrm{Re}\left\langle\Phi_r^n\right|\hat{\mathbf{J}}\left|\Phi_r^n\right\rangle \\ &\quad + \sum_n \mathrm{Re}\left\langle r_{in,n}\Phi_r^n\right|\hat{\mathbf{J}}\left|\Phi_{in}\right\rangle + \sum_n \mathrm{Re}\left\langle\Phi_{in}\right|\hat{\mathbf{J}}\left|r_{in,n}\Phi_r^n\right\rangle.\end{aligned} \tag{74}$$

The interference term,

$$\left\langle r_{in,n}\Phi_r^n\right|\hat{\mathbf{J}}\left|\Phi_{in}\right\rangle = \left\langle\hat{\mathbf{J}}^+ r_{in,n}\Phi_r^n\right|\left.\Phi_{in}\right\rangle = \left\langle\Phi_{in}\right|\hat{\mathbf{J}}\left|r_{in,n}\Phi_r^n\right\rangle^* = -\left\langle\hat{\mathbf{J}}\Phi_{in}\right|\left.r_{in,n}\Phi_r^n\right\rangle^*. \tag{75}$$

From Eq. 75, one has:

$$\mathrm{Re}\left\langle r_{in,n}\Phi_r^n\right|\hat{\mathbf{J}}\left|\Phi_{in}\right\rangle = 0. \tag{76}$$

Equations 75 and 76 show that the interference terms in Eq. 74 are canceled

$$\sum_n \mathrm{Re}\left\langle r_{in,n}\Phi_r^n\right|\hat{\mathbf{J}}\left|\Phi_{in}\right\rangle + \sum_n \mathrm{Re}\left\langle\Phi_{in}\right|\hat{\mathbf{J}}\left|r_{in,n}\Phi_r^n\right\rangle = 0.$$

Therefore, we obtain

$$\langle\Psi_L|\,\hat{\mathbf{J}}\,|\Psi_L\rangle = \langle\Phi_{in}|\,\hat{\mathbf{J}}\,|\Phi_{in}\rangle + \sum_n |r_{in,n}|^2\,\langle\Phi_r^n|\,\hat{\mathbf{J}}\,|\Phi_r^n\rangle\,.$$

The probability current at the right of the interface is:

$$\begin{aligned}\mathrm{Re}\,\langle\Psi_R|\,\hat{\mathbf{J}}\,|\Psi_R\rangle &= \left\langle \sum_n t_{in,n}\Phi_r^n \middle|\, \hat{\mathbf{J}} \,\middle| \sum_{n'} t_{in,n'}\Phi_r^{n'} \right\rangle \\ &= \sum_n |t_{in,n}|^2\,\langle\Phi_r^n|\,\hat{J}\,|\Phi_r^n\rangle\,.\end{aligned}$$

The continuity of the probability current gives:

$$\begin{aligned}\langle\Phi_{in}|\,\hat{\mathbf{J}}\,|\Phi_{in}\rangle + \sum_n |r_{in,n}|^2\,\langle\Phi_r^n|\,\hat{\mathbf{J}}\,|\Phi_r^n\rangle &= \sum_n |t_{in,n}|^2\,\langle\Phi_r^n|\,\hat{\mathbf{J}}\,|\Phi_r^n\rangle\,, \\ 1 + \sum_n |r_{in,n}|^2\,\frac{\langle\Phi_r^n|\,\hat{\mathbf{J}}\,|\Phi_r^n\rangle}{\langle\Phi_{in}|\,\hat{\mathbf{J}}\,|\Phi_{in}\rangle} &= \sum_n |t_{in,n}|^2\,\frac{\langle\Phi_r^n|\,\hat{\mathbf{J}}\,|\Phi_r^n\rangle}{\langle\Phi_{in}|\,\hat{\mathbf{J}}\,|\Phi_{in}\rangle}, \\ 1 + \sum_n R_{in,n}\frac{\left\langle\hat{\mathbf{J}}_L\right\rangle_n}{\left\langle\hat{\mathbf{J}}_L\right\rangle_{in}} &= \sum_n T_{in,n}\frac{\left\langle\hat{\mathbf{J}}_R\right\rangle_n}{\left\langle\hat{\mathbf{J}}_L\right\rangle_{in}}\end{aligned}$$

$R_{in,n}$, $T_{in,n}$ are reflection and transmission coefficients from in channel to n channel.

4.7 Scattering matrix formalism

The detail can be found in Refs. [89, 90].

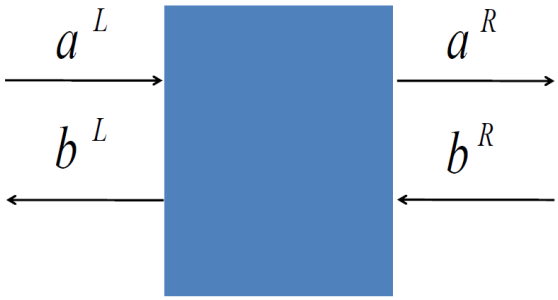

Figure 37: Schema of tunneling electron

We assume that the electrons/holes tunnel through a heterostructure grown along the z axis, each medium being characterized by its own Hamiltonian. Suppose that the incident energy $\mathcal{E}$ and the in-plane wavevector $\mathbf{k}_{\|} = (k_x, k_y)$ are conserved during the transport. Then we can find the relevant out-of-plane wavevectors k_z and eigenvectors of the Hamiltonian in each medium.

Because of the time reversal properties, if $\Phi(k_n)$ is a solution of the Schrödinger equation, $\Phi(-k_n)$ will also satisfy this equation. The solution of the Schrödinger equation in the j^{th} layer has the form

$$\Psi^{(j)} = \sum_{n=1}^{m} a_n^{(j)} \Phi^{(j)}(k_n) \exp(ik_n z) + b_n^{(j)} \Phi^{(j)}(-k_n) \exp(-ik_n z)$$

where m is the band index in the **k**.**p** model, *i.e.*, $m = 6$ in 6-band **k**.**p** model, $m = 14$ in 14-band **k**.**p** model ; k_n is the respective value of k_z in the n^{th} band; $\Phi^{(j)}(k_n)$ is the eigenvector of the Hamiltonian in the j^{th} layer at incident energy ε. Applying the standard matching conditions for multiband transport, Φ and $\hat{J}_z\Phi$ are continuous. We first consider a three-layer structure. It is convenient to write $-k_n = k_{n+m}$.

The matching condition between the left (L) region and the barrier (B) (i.e., for $z = 0$) can be written:

$$\begin{bmatrix} \Phi_1^L(k_1) & .... & \Phi_1^L(k_{2n}) \\ . & . & . \\ . & . & . \\ . & . & . \\ \Phi_n^L(k_1) & ... & \Phi_n^L(k_{2n}) \\ J_z\Phi_1^L(k_1) & .... & J_z\Phi_1^L(k_{2n}) \\ . & . & . \\ . & . & . \\ . & . & . \\ J_z\Phi_n^L(k_1) & .... & J_z\Phi_n^L(k_{2n}) \end{bmatrix} \begin{bmatrix} a_1^L \\ . \\ . \\ . \\ a_2^L \\ b_1^L \\ . \\ . \\ . \\ b_2^L \end{bmatrix} = \begin{bmatrix} \Phi_1^B(k_1) & .... & \Phi_1^B(k_{2n}) \\ . & . & . \\ . & . & . \\ . & . & . \\ \Phi_n^B(k_1) & ... & \Phi_n^B(k_{2n}) \\ J_z\Phi_1^B(k_1) & .... & J_z\Phi_1^B(k_{2n}) \\ . & . & . \\ . & . & . \\ . & . & . \\ J_z\Phi_n^B(k_1) & .... & J_z\Phi_n^B(k_{2n}) \end{bmatrix} \begin{bmatrix} a_1^B \\ . \\ . \\ . \\ a_2^B \\ b_1^B \\ . \\ . \\ . \\ b_2^B \end{bmatrix}, \tag{77}$$

or equivalently,

$$M_L \begin{bmatrix} a^L \\ b^L \end{bmatrix} = M_B \begin{bmatrix} a^B \\ b^B \end{bmatrix}.$$

The matching conditions between barrier and right region (R):

$$M_B Q_B \begin{bmatrix} a^B \\ b^B \end{bmatrix} = M_R \begin{bmatrix} a^R \\ b^R \end{bmatrix}, \tag{78}$$

$$Q_B = \begin{bmatrix} e^{-ik_1 d} & ... & 0 \\ . & . & . \\ . & . & . \\ . & . & . \\ 0 & 0 & e^{-ik_{2n} d} \end{bmatrix},$$

$$M_R = \begin{bmatrix} \Phi_1^R(k_1) & .... & \Phi_1^R(k_{2n}) \\ . & . & . \\ . & . & . \\ . & . & . \\ \Phi_n^R(k_1) & ... & \Phi_n^R(k_{2n}) \\ J_z\Phi_1^R(k_1) & .... & J_z\Phi_1^R(k_{2n}) \\ . & . & . \\ . & . & . \\ . & . & . \\ J_z\Phi_n^R(k_1) & .... & J_z\Phi_n^R(k_{2n}) \end{bmatrix},$$

$$\begin{bmatrix} a^L \\ b^L \end{bmatrix} = M_L^{-1} M_B Q_B^{-1} M_B^{-1} M_R \begin{bmatrix} a^R \\ b^R \end{bmatrix},$$

$M = M_L^{-1} M_B Q_B^{-1} M_B^{-1} M_R = \begin{bmatrix} M_{11} & M_{12} \\ M_{21} & M_{22} \end{bmatrix}$ is the transfer matrix.

$$\begin{bmatrix} a^L \\ b^L \end{bmatrix} = \begin{bmatrix} M_{11} & M_{12} \\ M_{21} & M_{22} \end{bmatrix} \begin{bmatrix} a^R \\ b^R \end{bmatrix}, \tag{79}$$

In the scattering theoretical point of view we relate the coefficients according to a different criterion. We consider the outgoing amplitudes, corresponding to b^L and a^R and define the S-matrix which relates them to the incoming ones, a^L and b^R. Thus

$$\begin{bmatrix} b^L \\ a^R \end{bmatrix} = \begin{bmatrix} S_{11} & S_{12} \\ S_{21} & S_{22} \end{bmatrix} \begin{bmatrix} a^L \\ b^L \end{bmatrix}. \tag{80}$$

From Eqs. 79 and 80, we obtain the relationship between the scattering matrix and the transfer matrix

$$\begin{aligned} S_{11} &= M_{21}.M_{11}^{-1}, \\ S_{12} &= M_{22} - M_{21}.M_{11}^{-1}.M_{12}, \\ S_{21} &= M_{11}^{-1}, \\ S_{22} &= -M_{11}^{-1}.M_{12}. \end{aligned} \tag{81}$$

The scattering matrix can be easily related to some phenomenological coefficients. If we set $b^R = 0$ in Eq. 80, then we describe an experiment in which a wave propagating from the left, a^L, b^L is partly reflected with reflection amplitude r and partly transmitted, a_R, with transmission amplitude t. Likewise, for incidence from the right, $a^L = 0$, the respective transmission and reflection amplitudes are noted t' and r'. Then, the S-matrix can be cast in a more physical form.

Usually the scattering matrix entries are denoted as

$$S = \begin{bmatrix} r & t' \\ t & r' \end{bmatrix}. \tag{82}$$

We have to note that the reference to incoming and outgoing amplitudes does not necessarily mean that the above analysis is restricted to a basis of propagating states only. As is well-known by appropriate analytical continuation, wavevectors change from real to complex, *i.e.*, change from waves propagating to the right/ left into waves decaying to the right/ left and the same formal analysis holds for bound states, if there are any.

We will show that in order to ensure current conservation, the S-matrix must be unitary. We assume that the incoming and outgoing currents in a particular mode m are proportional to the squared magnitudes of the corresponding mode amplitudes in_m and out_m respectively. Current conservation then requires that

$$\sum_m |in_m|^2 = \sum_m |out_m|^2 , \tag{83}$$

that is

$$\{in\}^+ \{in\} = \{out\}^+ \{out\} .$$

Since

$$\{out\} = [S] \{in\} ,$$

we can write

$$\{out\}^+ \{out\} = \{in\}^+ [S]^+ [S] \{in\} = \{in\}^+ \{in\} .$$

Hence

$$[S]^+ [S] = I = [S] [S]^+ , \tag{84}$$

so that in terms of the elements of the S-matrix we obtain

$$\sum_{k=1}^{2m} |S_{kn}|^2 = \sum_{k=1}^{2m} |S_{nk}|^2 , \tag{85}$$

or equivalenty,

$$\begin{aligned} \sum_{k=1}^{m} |r_{kn}|^2 + \sum_{k=1}^{m} |t'_{kn}|^2 &= \sum_{k=1}^{m} |r_{nk}|^2 + \sum_{k=1}^{m} |t_{nk}|^2 , \\ \text{and } \sum_{k=1}^{m} |t_{kn}|^2 + \sum_{k=1}^{m} |r'_{kn}|^2 &= \sum_{k=1}^{m} |t'_{nk}|^2 + \sum_{k=1}^{m} |r'_{nk}|^2 . \end{aligned} \tag{86}$$

As a consequence of Eq. 86, we obtain

$$\sum_{k=1,n=1}^{k=m,n=m} |t_{kn}|^2 = \sum_{k=1,n=1}^{k=m,n=m} |t'_{kn}|^2 . \tag{87}$$

Equation 87 shows that the total transmission coefficients of the left and right incoming waves are equal.

CHAPTER V

PRINCIPLE OF GIANT SCATTERING ASYMMETRY AND TUNNELING HALL EFFECT AT SEMICONDUCTOR INTERFACES OF T_D SYMMETRY

Spintronics functionalities require efficient spin current injection at ferromagnet-non magnetic interfaces as well as efficient STT and possibly efficient SHE [91] with heavy materials for magnetic commutation without external field. In that context, investigations of SOI in solids, interfaces, as well as tunnel junctions are of a prime importance [92, 93, 94]. Moreover, SOI at an interface with a broken inversion symmetry can lead to the observation of Bychkov-Rashba-split states [95] for carriers propagating along surface or interface states. Such a splitting, if well controlled, can be used to convert a perpendicular spin current into a lateral charge current by Inverse-Rashba or Inverse Edelstein effect [17, 96, 97]. Alternatively, SOI can lead to inherent spin-memory loss (SML) [78, 79, 98] or spin current discontinuities [99] when electrons cross interfaces. In that context, investigations of SOI in solids and at interfaces are of prime importance for basic physics and today's technology. No much attention has been paid to the particular anatomy of the electronic spin-polarized transport at SOI-magnetic interfaces where exchange-split interface states may be observed [100, 101, 102].

In this work, we show that the interplay of SOI and exchange interactions at interfaces and tunnel junctions may result in a large difference of transmission for carriers, depending on the sign of their incident in-plane wavevector: this leads to interfacial skew-tunneling effects that we refer to as anomalous tunnel Hall effect (ATHE) [18] or tunnel anomalous Hall effect like proposed by other international groups [16]. In a 2×2 exchange-split band model, the transmission asymmetry ($\mathcal{A}$) between incidence angles related to $+k_{\|}$ and $-k_{\|}$ wavevector components, is shown to be maximal at peculiar points of the Brillouin zone corresponding to a totally quenched transmission ($\mathcal{A}$ = 100%) making the transmission difference from the standard tunneling case.

As an example of reference systems without SOI effects, we provide here the transmission coefficient mapping for the case of fully-epitaxial Fe/MgO/Fe magnetic tunnel junctions, majority and minority spin channels, calculated within 2-dimensional BZ incoming channels in the respective PA and AP states [103]. Figure. 38 calculated by Korringa–Kohn–Rostoker method (KKR) displays a clear symmetry *vs.* the BZ center

in both PA and AP states without involving large SOI in the barrier.

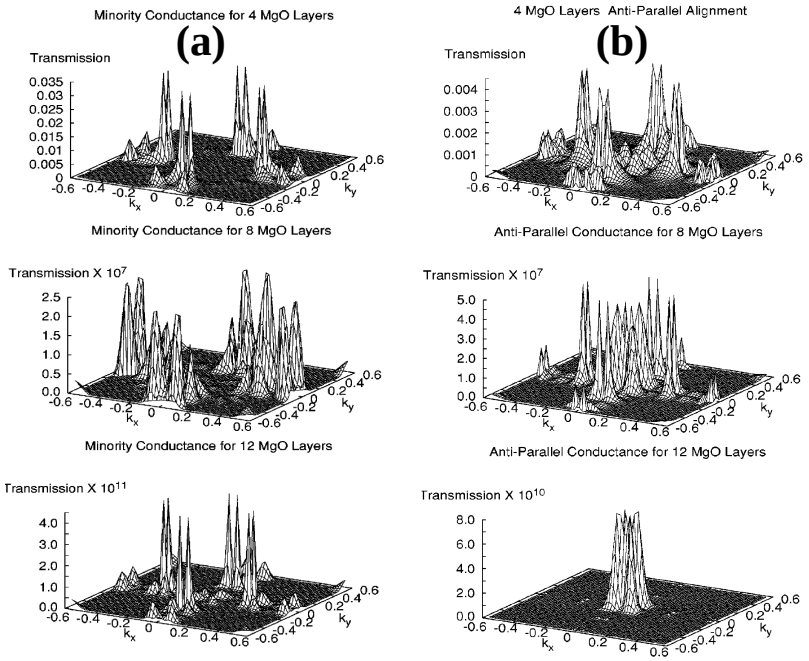

Figure 38: Conductance for PA (a) and AP (b) alignment of the moments in the electrodes [103].

More generally by inclusion of SOI, we demonstrate the universal character of the transmission asymmetry $\mathcal{A}$ *vs.* in-plane wavevector component, for given reduced kinetic energy and exchange parameter, $\mathcal{A}$ being universally scaled by a unique function, independent of the spin-orbit strength and of the material parameters. Similarly, striking tunneling phenomena arising in topological insulators have just been predicted. While they all are related to the spin-orbit directional anisotropy, ATHE differs from the tunneling planar Hall effect [104], spontaneous anomalous and spin Hall effects [105], or spin-galvanic effect [106], previously reported for electron transport, by its giant forward asymmetry and chiral nature. These features have non-trivial connection with the symmetry properties of the system. All these results show that a new class of tunneling phenomena can now be investigated and experimentally probed.

5.1 Giant universal transport asymmetry and anomalous tunnel Hall effect in the conduction band

In this part, we will describe the main properties of transmission or scattering asymmetry including large SOI which is at the core of the present manuscript like also proposed recently by the Buffalo and Regensburg groups [16]. In order to address the issue in a simple way, we first consider a heterojunction made of two identical magnetic semiconductors of zinc blende symmetry, with opposite in-plane magnetizations: this structure

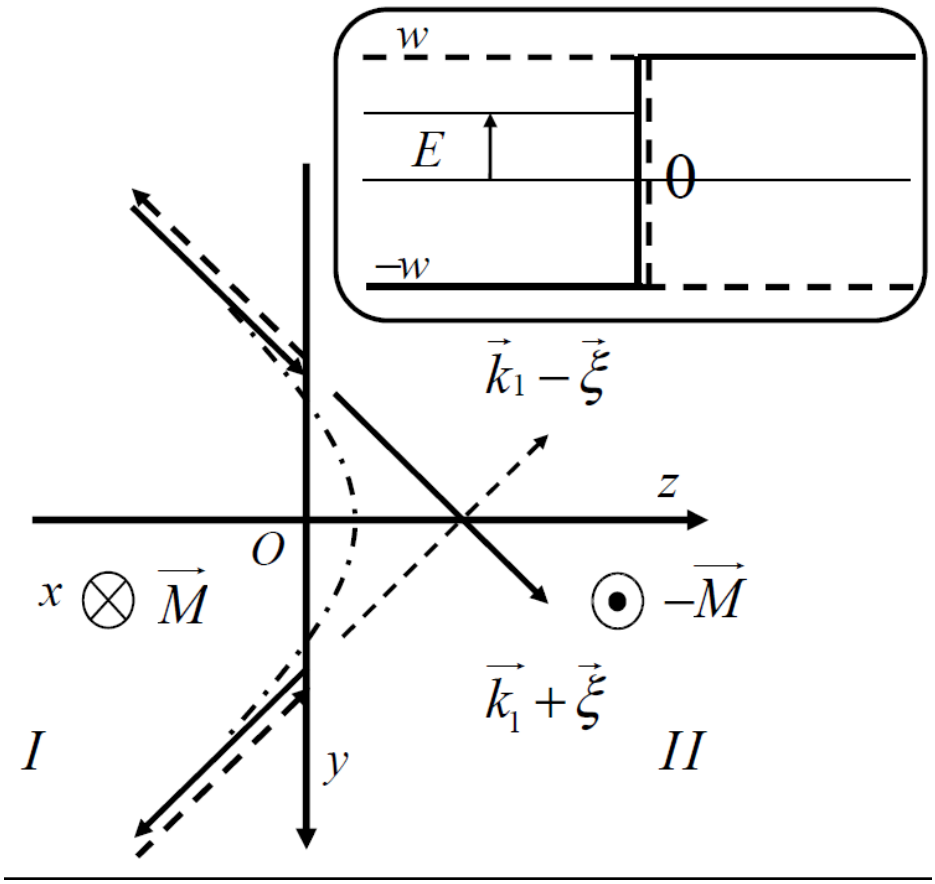

Figure 39: Scheme of transmission process at an exchange-SOI step with AP magnetizations $\mathbf{M}$ and $-\mathbf{M}$ along the x cubic crystal axis. The propagation direction of carriers (straight arrow) is along z with propagative wavevector k_1 whereas the in-plane incident component $+\xi$ (heavy line) or $-\xi$ (dashed line) is along y; $\mathbf{xyz}$ forms a direct frame. The dash-dot curve denotes the evanescent waves, either reflected or transmitted. Carriers with $+\xi$ in-plane wavevector component are more easily transmitted than those carrying $-\xi$.(Top right inset): Energy profile of the exchange step; E is the longitudinal kinetic energy along z and $2w$ is the exchange splitting in the magnetic materials.

(Fig. 39) constitutes an ideal exchange step and is a paradigm for exchange-engineered heterostructures, similarly to the symmetrical spin-valve structure in giant magnetoresistance [107, 108]. Indeed, due to the axial character of the magnetization, the AP configuration breaks the symmetry with respect to the reflection plane, and also some possible rotation and time conjugation invariances existing in the parallel (PA) magnetic arrangement [109]. The result is that two states with opposite in-plane incident wavevectors $\pm\mathbf{k}_{\|}$ may be differently transmitted through exchange-SOI interactions.

We first consider the Dresselhaus interaction in the conduction band of bulk materials [10]. For readers who are interested in the Appendix A we consider the geometry of the scattering matrix, which is the more systematic and simple way to consider the interplay of SOI and exchange interactions in bulk semiconductors. The second possibility would be to investigate the particular Rashba SOC term with either 3D bulk properties

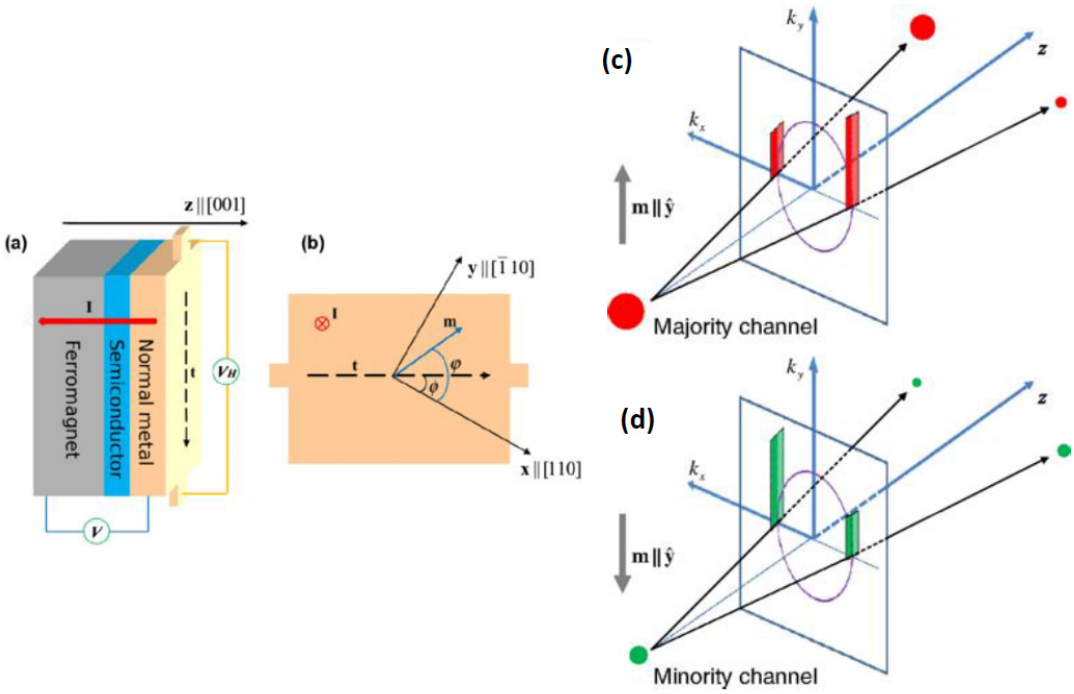

Figure 40: (a) Schematic of a ferromagnet-semiconductor-normal metal tunnel junction. The tunneling current flowing in the z direction generates the anomalous Hall voltage (VH) in the nonmagnetic electrode. (b) Side view of (a).Taking the [110] axis as a reference, the magnetization direction (m) and the direction along which the Hall voltage is measured (t) are determined by the angles φ and ϕ, respectively. Spin-dependent momentum filtering resulting from tunneling through a barrier with Bychkov-Rashba SOC for majority channel (c), and minority chanel (d) [16].

(electric field) or in tunnel junctions. This case, departing from Dresselhaus from the point of view of symmetry because of the appearance of a potential profile within the barrier itself, will be considered in the second part of this chapter. The third interesting system is the one studied recently by A. Matos-Abigue and J. Fabian, namely a pure Rashba interface term [16]. In one sense, the present contribution generalizes the work of Fabian and Matos-Abiague to the case of finite barrier thickness. This could correspond to the SOI assisted transmission of carriers at FM/SOI interfaces like involved in Co/Pt systems prepared for STT experiments [76, 78, 79] in the regime of interfacial tunneling transmission.

5.1.1 System investigated

In the following analytical calculations, the lack of inversion symmetry is needed to introduce spin-orbit effects in the pure s-type CB near the Γ point in a 2×2 model [47]. Hereafter, we refer the structure to the cubic axes and we assume that electron transport occurs along the $[001]$ axis (z axis), whereas the magnetization lies along $[100]$ (x axis). We study the transmission asymmetry when the wavevector component along $[010]$ (y axis) is changed from ξ to $-\xi$. Electrons are injected from the first CB of material I to the left ($\epsilon = 1$) into the first CB of material II to the right ($\epsilon = -1$). Then, the relevant 2×2 Hamiltonians write respectively:

$$\begin{aligned} \widehat{H}_{I,II} &= \gamma_c \left(k^2+\xi^2\right)\widehat{I} + w\mathbf{m}\cdot\widehat{\boldsymbol{\sigma}} + (\widehat{\gamma}\boldsymbol{\chi})\cdot\widehat{\boldsymbol{\sigma}} \\ &= \begin{bmatrix} \gamma_c(k^2+\xi^2) - \tilde{\gamma}\xi^2 k & -i\gamma\xi k^2 + \epsilon w \\ i\gamma\xi k^2 + \epsilon w & \gamma_c(k^2+\xi^2) + \tilde{\gamma}\xi^2 k \end{bmatrix}, \end{aligned} \tag{88}$$

where $(0,\xi,k)$ is the electron wavevector. $\widehat{I}$ is the identity matrix, γ_c accounts for the conduction effective mass, $\mathbf{m}$ is the unit magnetization vector, $2w$ the exchange splitting (assumed to be positive), $\widehat{\boldsymbol{\sigma}}$ the Pauli operator, and $\boldsymbol{\chi} = \left[0, \xi k^2, -\xi^2 k\right]$ is the DP internal field responsible for the spin splitting [8, 10]. For the subsequent discussion, we introduce the tensor $\widehat{\gamma} = (\gamma_i \delta_{ij})$ which characterizes the DP-field strength, with $\gamma_x = \gamma_y = \gamma$, $\gamma_z = \tilde{\gamma}$, and δ_{ij} the Kronecker symbol. We will consider the two cases $\tilde{\gamma} = \gamma$ and $\tilde{\gamma} = 0$, switching on and off the diagonal ξ^2 perturbation.

5.1.2 Eigenvectors and density of states

To first order in γ, the two energies in the exchange and spin-orbit-split subbands are given by $\mathcal{E}_1 = \gamma_c\left(k_1^2+\xi^2\right) - w$ and $\mathcal{E}_2 = \gamma_c(k_2^2+\xi^2) + w$, where k_1 (k_2) is the z-component of the wavevector in the lower (upper) subband. These expressions are correct up to first order in γ provided $\left|\tilde{\gamma}\xi^2 k/w\right| << 1$ and $|\gamma\xi k^2/w| << 1$, where $k =$

k_1 or $k = k_2$. The respective eigenvectors write:

$$\mathbf{u}_{\epsilon,1}(\xi, k_1) = \left[1 - 2\epsilon i\mu k_1^2, -\epsilon(1 - 2\tilde{\mu}\xi k_1)\right]/\sqrt{2}, \quad (89)$$

$$\mathbf{u}_{\epsilon,2}(\xi, k_2) = \left[1 - 2\epsilon i\mu k_2^2, \epsilon(1 + 2\tilde{\mu}\xi k_2)\right]/\sqrt{2}, \quad (90)$$

where $\mu = \gamma\xi/(2w)$ and $\tilde{\mu} = \tilde{\gamma}\xi/(2w)$ are reduced spin-orbit parameters. Note that the norm of $\mathbf{u}_{\epsilon,\ell}$ ($\ell = 1$ or 2) only involves even powers of ξ likewise the direct overlap $|\langle \mathbf{u}_{\epsilon,\ell} | \mathbf{u}_{-\epsilon,\ell} \rangle|^2$ between incoming and outgoing states, so that no transmission asymmetry between waves with opposite $k_\parallel$ can be expected in usual tunneling models, *e.g.* based on interface density of states [3, 23, 25]. The asymmetry appears in full-quantum treatments involving matching conditions at interfaces and may be correctly described by embedding methods [71, 72] in a future work.

5.1.3 The matching properties

The corresponding wave functions in Regions I and II can be written in a compact form:

$$\begin{aligned}\Psi_I(z) &= \alpha\mathbf{u}_{1,2}(\xi, k_2)\ e^{ik_2 z} + \beta\mathbf{u}_{1,1}(\xi, k_1)\ e^{ik_1 z} \\ &\quad + A\mathbf{u}_{1,2}(\xi, -k_2)\ e^{-ik_2 z} + B\mathbf{u}_{1,1}(\xi, -k_1)\ e^{-ik_1 z}, \\ \Psi_{II}(z) &= C\mathbf{u}_{-1,1}(\xi, k_1)\ e^{ik_1 z} + D\mathbf{u}_{-1,2}(\xi, k_2)\ e^{ik_2 z}, \end{aligned} \quad (91)$$

where the α and β (resp. A and B) amplitudes stand for incident waves (resp. reflected waves) in Region I, and C and D for transmitted waves in Region II. Because $k_\parallel$ is conserved in the transport process, we are dealing with states with the same *longitudinal* kinetic energy E along z axis and a total kinetic energy $\mathcal{E} = E + \gamma_c\xi^2$. The proper matching conditions are, as usual, the continuity of the wave function and of the current operator $\widehat{J} = (1/\hbar)\ \partial\widehat{H}_{I,II}/\partial k$ because $\widehat{H}_{I,II}$ contains no more than quadratic k terms [31, 85, 110, 111, 112] and because the two regions are made of the same material ($\hat{\gamma}/\gamma_c$ is continuous).

5.1.4 Transmission and asymmetry of transmission

The average transmission coefficient $T(\xi, k_1, k_2)$ upon positive and negative incidences we have found is related to the amplitude of the transmitted wave $C(\xi, k_1, k_2)$ calculated with the initial conditions $\alpha = 0$ and $\beta = 1$ through:

$$T(\xi, k_1, k_2) = \frac{|C(\xi, k_1, k_2)|^2 + |C(-\xi, k_1, k_2)|^2}{2}, \quad (92)$$

and we define the transmission asymmetry as:

$$\mathcal{A}(\xi, k_1, k_2) = \frac{|C(\xi, k_1, k_2)|^2 - |C(-\xi, k_1, k_2)|^2}{|C(\xi, k_1, k_2)|^2 + |C(-\xi, k_1, k_2)|^2}. \quad (93)$$

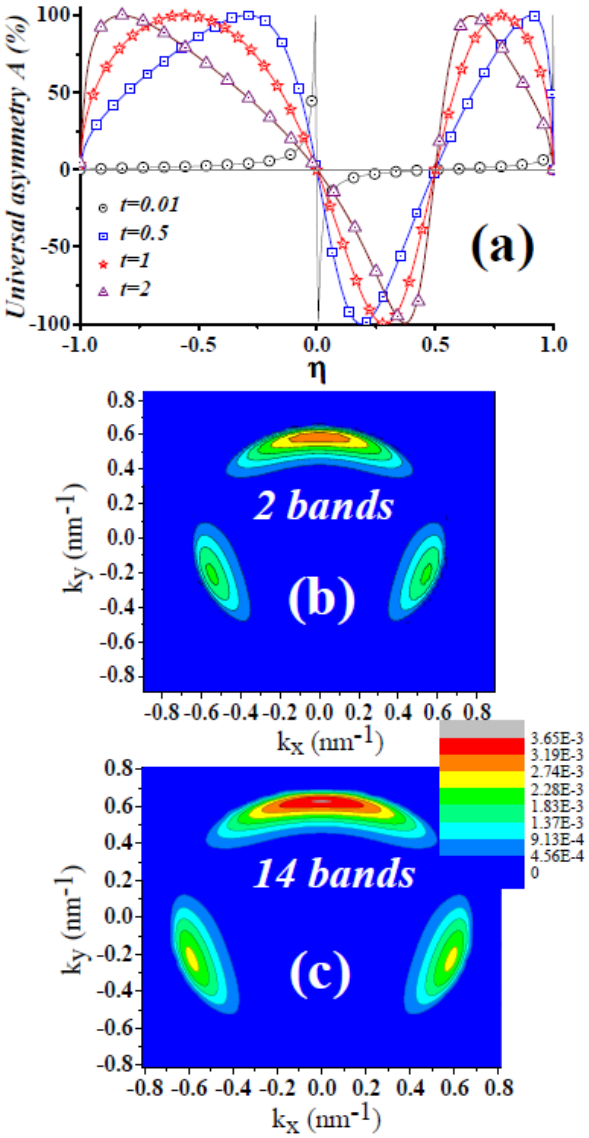

Figure 41: (a) Universal asymmetry coefficient $\mathcal{A}$ *vs.* reduced energy $\eta = E/w$ obtained for different values of the incidence parameter $t = \xi/K$ [$t = 0.01$ (black; circles), $t = 0.5$ (blue; squares), $t = 1$ (red; stars), and $t = 2$ (purple; triangles) by 2-band analytical (full line) and numerical (symbols) calculations. Two-dimensional map of the transmission coefficient T in 2×2 (b) and 14×14 (c) $\mathbf{k}.\mathbf{p}$ band models for the exchange-SOI step schematized in Fig. 39; the parameters are: exchange energy $2w = 0.3$ eV, *total* kinetic energy $\mathcal{E} = 0.08$ eV counted from the middle of the conduction step, and DP strength $\gamma = -24$ eV Å^3; band parameters of the 14-band $\mathbf{k}.\mathbf{p}$ model taken from Ref [34]**.**

It can be checked that, when $\tilde{\gamma} = 0$, $\mathcal{A}(\xi, k_1, k_2)$ vanishes when α and β are real, which is a non trivial result. **The transmission of a pure spin-up incident electron from left into a pure spin-down state with the same group velocity at right is only possible under oblique incidence via SOI** which introduces off-diagonal matrix elements. Moreover, a non-vanishing diagonal part of the SOI is also necessary to obtain a non-zero asymmetry although the related component of the DP field along the z axis does not depend on the sign of $k_{\|}$. Then, from now on, we take $\tilde{\gamma} = \gamma$. The wavevector k_1 in the lower subband has to be real so that we can define $K = k_1$. We introduce the parameter λ with $k_2 = i\lambda K$, the reduced energy $\eta = \left(1-\lambda^2\right)/\left(1+\lambda^2\right)$ with $\eta = E/w$, as well as the incidence parameter $t = \xi/K$. After a lengthy calculation, one obtains:

$$C(\xi, K, \lambda) = \left(\frac{\gamma K^2 \xi}{w}\right) \frac{\left[(\xi/K)\left(3\lambda^2 - 1\right) + 2\lambda\left(\lambda^2 - 1\right)\right]}{(\lambda - i)^2}. \tag{94}$$

From Eq. 94, it is straightforward to check that $\mathcal{A}(\xi, k_1, k_2) = 0$ if λ is purely imaginary; **the asymmetry appears when the lower-energy band carries a propagative state whereas the upper one acts as a barrier sustaining an evanescent state**. Transport is then described in a two-k-channel model, a propagative channel (k_1) and an evanescent channel (k_2). One obtains:

$$T(t, \eta) = \frac{\gamma^2}{\gamma_c^3} w t^2 (1+\eta)^2 \left\{\left[t\ (2\eta - 1)\right]^2 + 4\eta^2(1-\eta)\right\}, \tag{95}$$

as well as the asymmetry

$$\mathcal{A}(t, \eta) = \frac{4t\eta\sqrt{1-\eta^2}\,(2\eta - 1)}{4\eta^2(1-\eta) + t^2(1+\eta)(2\eta-1)^2}. \tag{96}$$

This is the main result we expect from the derivation of properties of transmission corresponding to Dresselhaus SOI for a magnetic-step contact.

5.1.5 Properties of the transmission asymmetry

The expression for $T(t, \eta)$ emphasizes the increase of the carrier transmission with t and γ. The range of validity defined above can be written $|t^2(\gamma K^3/\gamma_c K^2)| << 1$, a condition easily fulfilled as $|\gamma K^3/\gamma_c K^2|$ is expected to be small. The asymmetry $\mathcal{A}$ is plotted in Fig. 41 for several values of t and $1/t$ (full lines), where the symbols refer to the 2×2 numerical calculations showing an excellent agreement. It can be seen that the curves related to t and $1/t$ are located at almost symmetrical positions with respect to the $t = 1$ curve. They admit four zeros in the energy range considered: *i*) two at the two ends of the energy step when either the propagative or the evanescent state disappears and *ii*) one in the middle of the energy barrier and one for an energy equal to $3/4$ of the energy step, which is particular to the Dresselhaus interaction. It is a remarkable result

that $\mathcal{A}(t,\eta)$ does not depend either on the material parameters or on the sign of γ, thus conferring to $\mathcal{A}$ a universal character. Reversing the magnetization (changing w into $-w$) makes transport occur in the k_2 channel and it can be seen that this changes $\mathcal{A}(t,\eta)$ to $-\mathcal{A}(t,\eta)$ [116]. Another striking feature is that an arbitrarily small perturbation is able to produce a 100% transport asymmetry with, accordingly, a total quenching of transmission for some given incidences. Figs. 41 b-41 c display the 2-dimensional map of the electron transmission in the reciprocal space calculated using both a 2×2 effective Hamiltonian (Fig. 41 b) and a full 14×14 band $\mathbf{k}.\mathbf{p}$ treatment (Fig. 41 c) involving odd-potential coupling terms $P^{'}$ and $\Delta^{'}$ [34, 44, 117]. These calculations are based on the multiband transfer matrix technique developed in Refs. [20, 85]. We have checked that transport asymmetry also arises for a tunnel junction where a thin tunneling barrier is inserted between the two magnetic layers.

5.1.6 Tunnel Hall effect (THE) and tunnel Hall angle (THA)

We want to point out that the scattering asymmetry demonstrated in this chapter is associated to the generation of a lateral interfacial charge current at the length scale of the mean free path (MFP) in the magnetic or non magnetic collector. However, we also want to show that it strongly differs by nature from the well known extrinsic or intrinsic SHE [6, 91, 126, 127] by several aspects.

(i) The property of THE we describe is of a pure interfacial nature (exchange step, extended to tunnel devices) originating from the exact matching of spin polarized waves. In that sense, it describes a pure 0-dimensional (0-D) effect which does not require any bulk effect in the electrodes (intrinsic SHE) or alloying with impurities embedded in a given host (extrinsic SHE). Its 0-D nature is clearly new and can be understood in the next chapter by a new type of chirality phenomena.

(ii) The property of THE that we describe originates from a forward scattering asymmetry property and not from skew-scattering phenomena during the diffusion (case of skew scattering SHE [127]).

(iii) Its nature will be explained by chirality arguments which come into play when the transport mixes both propagative and evanescent waves for ingoing and outgoing waves.

We can calculate the total transmitted current, $\mathbf{J}[t,\eta]=\mathbf{J}_{\xi}[\Psi_{II}(z)]+\mathbf{J}_{-\xi}[\Psi_{II}(z)]$, originating from incident waves of equal amplitude with opposite $k_{\parallel}$. To the lowest order in γ, we find

$$\mathbf{J}_{y,z}[t,\eta]=\frac{4(\gamma_c w)^{1/2}}{\hbar}(1+\eta)^{1/2}T(t,\eta)\left[\mathcal{A}(t,\eta)\,t\widehat{y}+\widehat{z}\right]. \tag{97}$$

resulting of two incident waves of equal amplitude with opposite parallel wavevectors. This is connected to the non-diagonal σ_{xy} tunnel conductivity [127, 126].

Thus, the asymmetrical transmission gives rise to a transverse momentum and then to a tunneling surface current (per unit length) $\mathbf{j}_y = \mathbf{J}_y \times \ell$ (ℓ is the MFP) which can lead to an anomalous tunnel Hall effect under steady state regime. This effect could be experimentally investigated at a scale where the thickness of the channel collecting the current is comparable to ℓ, *i.e.*, not exceeding a few nm [120]. The ratio of the (surface) transverse to the longitudinal current $j_y\left[t,\eta\right]/J_z\left[t,\eta\right] = t\mathcal{A}\left(t,\eta\right)\ell$ then defines the THE length in the spirit of a recent work dealing with Inverse Edelstein phenomenon [17, 122]. An incident beam in Region I with a given isotropic angular dispersion with respect to the normal to the barrier gives rise, after angular averaging, to a tilted beam bearing a transverse current. Hereafter, we take an isotropic angle distribution for the incident beam of electrons with a total energy $\mathcal{E}$ within an incidence cone defined by the half angle θ_M so that $t_M = \tan\theta_M$. Then, using the relation $\eta = \left(-t^2 + \mathcal{E}/w\right)/\left(1+t^2\right)$ which relates η to the reduced total energy $\mathcal{E}/w$, the mean transmitted current writes [121]

$$\mathbf{J}\left[\mathcal{E}\right] = \frac{1}{\theta_M}\int_0^{\theta_M}\mathbf{J}\left[t,\eta\right]d\theta = \frac{1}{\theta_M}\int_0^{t_M}\frac{\mathbf{J}\left[t,\mathcal{E}\right]}{1+t^2}dt. \tag{98}$$

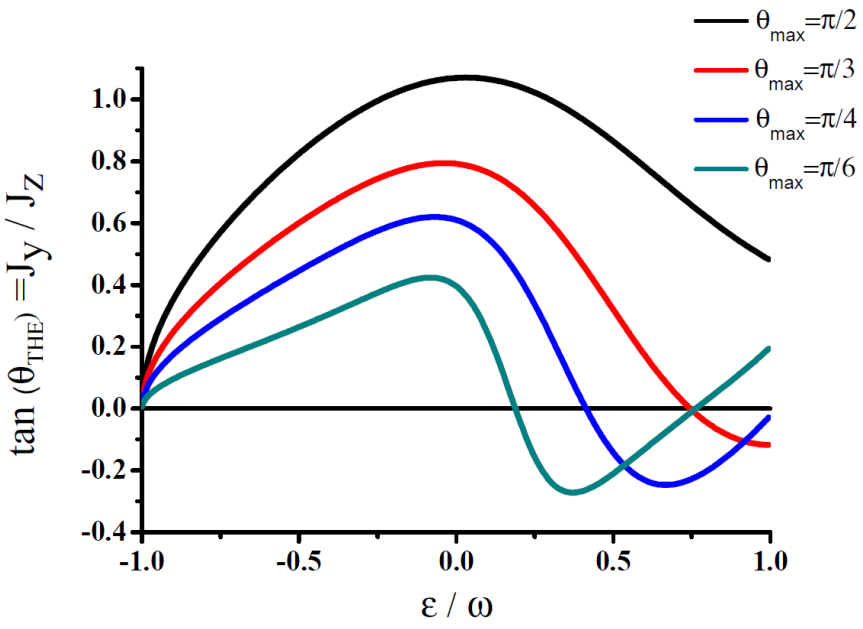

Figure 42: THA *vs.* total energy of carriers calculated in the case of an ideal exchange step discussed in the text for 4 different maximum half opening incident angles ($\pi/6$, $\pi/4$, $\pi/3$, and $\pi/2$). In the best situation, the tunnel Hall angle can reach up to 45° giving rise to a large current parallel to the interface.

The results of the calculations are displayed in Fig. 42. The averaged tunnel Hall angle angle corresponding to several θ_M ($\pi/6$, $\pi/4$, $\pi/3$, and $\pi/2$) is plotted *vs.* the total energy of the incident carrier for an exchange step. It can be seen that a large beam

deviation angle (up to 45°) can be observed throughout a broad energy range leading to a significant conversion from current normal to the plane to current parallel to plane.

The tunnel Hall effect may be observed in some physical situations described at the end of the manuscript corresponding to a quantum well contacted by one ferromagnetic electrode (*e.g.* ferromagnetic semiconductor) and measure the in-plane charge current propagating in the quantum well upon rotating the magnetization from the out-of-plane direction to the in-plane direction.

5.1.7 Barrier engineering and resonant structures.

In the model case of the exchange step where both analytical and numerical calculations can be performed, the universal asymmetry $\mathcal{A}$ is large but the transmission is rather small (Fig. 41). Note however (Eq. 95) that the energy (η) dependence is polynomial and not exponential like the transmission coefficient through tunnel barriers. It is possible to tailor more complicated structures involving resonant tunneling to increase the transmission up to a fraction of unity while keeping extremely high asymmetries. Such structures would be suitable for application. An example is given in Fig. 43: the structure consists of a magnetic quantum well sandwiched between two magnetic electrodes and separated by non-magnetic barriers of different thicknesses. The magnetization of each layer can be independently reversed. It can be seen that this structure possesses 4 different transmission states ($\uparrow\uparrow\uparrow$, $\uparrow\downarrow\uparrow$, $\uparrow\uparrow\downarrow$, and $\uparrow\downarrow\downarrow$) and is a paradigm for a 4 state-memory. The transmission T and transmission asymmetry $\mathcal{A}$ (for opposite parallel wavevector components $\pm\xi$) are plotted in Fig. 43. It can be seen that the peak transmission reaches values close to unity at the peak transmission whereas $\mathcal{A}$ is close to 100%. An experimental confirmation of these predictions would yield a fingerprint of THE. We will describe in more detail possible transport experiments in the last chapter of the present manuscript.

In the systems corresponding to an asymmetric magnetic configuration and giving rise to a strong forward scattering asymmetry, a charge current along the quantum well direction, *i. e.*, along the film plane is expected to take place under normal current injection. This may be detected by transverse voltage measurements (Hall-like geometry). The same qualitative feature (occurrence of a transverse charge current) can be measured in a more simple situation of a non-magnetic quantum well contacted by a single ferromagnetic electrode as previously discussed.

5.2 Case of Rashba interaction in a thin tunnel barrier

We consider now the alternate case of Rashba-SOI terms in a thin tunneling barrier structure. This can mimic the presence of an electric field in the barrier originating from certain structural asymmetry or potential gradient within the heterostructure (structural

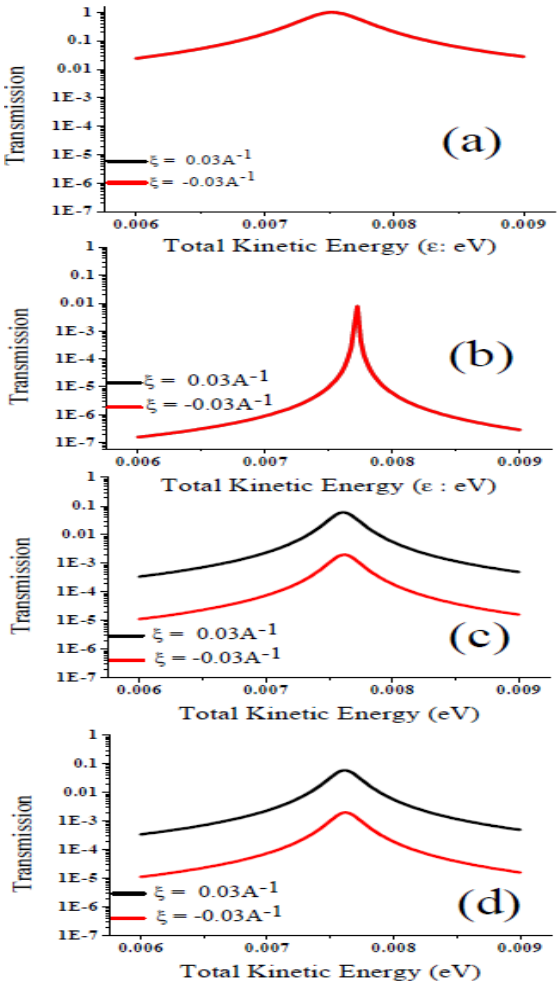

Figure 43: Transmission coefficient calculated for the two opposite incident wavevectors $\xi = \pm 0.3$ nm^{-1} at the first resonant peak of a magnetic quantum well (thickness 20 nm) with ferromagnetic electrodes for the different magnetic configurations *resp.* $\uparrow\uparrow\uparrow$ (a), $\uparrow\downarrow\uparrow$ (b), $\uparrow\uparrow\downarrow$ (c), and $\uparrow\downarrow\downarrow$ (d) corresponding to left magnetic electrode/2 nm thick barrier/20 nm thick magnetic quantum well/2 nm thick barrier/right magnetic electrode. For the symmetric situation, the transmission for $\pm\xi$ are exactly the same whereas different for the non-symmetric configuration. The **k**.**p** material parameters of the whole heterostructure correspond to those of GaSb of high spin-orbit coupling. The barrier thickness is 2 nm and the barrier height is 0.5 eV.

or chemical through charge transfer). This case departs from the previous Dresselhaus case by the fact that the Rashba interaction generally introduces an effective electric field which makes the barrier profile nonsymmetric (structure inversion asymmetry or SIA). A consequence is that

(i) the tunneling structure under consideration lacks of some symmetry properties compared to the Dresselhaus case;

(ii) the properties of the S-matrix also differ from the previous case. We are then going to make the connection with some results preliminary given in the second chapter.

We consider the specific case of Rashba interactions in a thin tunnel barrier. The electron asymmetry transport caused by the interplay of bulk SOI and exchange interaction is already considered. In this part, the SOI in the bulk has been replaced by the SOI due to the structure inversion asymmetry. The inversion symmetry is then broken along the growth the z direction by an existing electric field applied in the barrier, $\overrightarrow{E} = E_z \overrightarrow{z}$. The spin subbands are split in energy like explained by Rashba and Bychkov [95] who have shown that the electric field results in an effective SOI of the form

$$\hat{H}_R = \alpha_R \left(\overrightarrow{z} \times \overrightarrow{p} \right) . \boldsymbol{\sigma} = \alpha_R \left(k_x \sigma_y - k_y \sigma_x \right), \tag{99}$$

where α_R is called the Rashba-Bychkov constant and the $\boldsymbol{\sigma}$ is the Pauli operator.

5.2.1 In-plane wavevector parallel to the magnetization direction

The in-plane wavevector is taken parallel to the x direction, with $\mathbf{k} = (\xi, 0, k)$, then the Rashba Hamiltonian in Eq. 99 has the simple form:

$$\hat{H}_R = \alpha_R \xi \sigma_y.$$

*5.2.1.1 **PA (↑↑)***

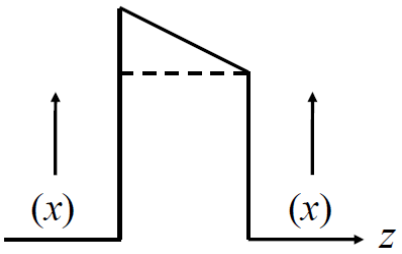

Figure 44: Tunnel junction grown along the z direction with Rashba SOI in the barrier under PA configuration, $\overrightarrow{M} \parallel x$, $\overrightarrow{k_\parallel} = (\xi, 0)$.

The electron Hamiltonian writes:

$$\hat{H}_\xi = \begin{cases} \gamma_c \left(\xi^2 + k^2 \right) + w\sigma_x \ , & \text{if } z < 0 \text{ or } z > a \\ \gamma_c (\xi^2 + k^2) + \alpha_R \xi \sigma_y \ + V, & \text{if } 0 < z < a \end{cases} \tag{100}$$

where γ_c represents the effective mass of electron in the crystal, w is magnitude of exchange interaction, and V is the barrier height.

Let us introduce the expression of the wave functions in the three different regions of space

$$\Psi_\xi(z) = \begin{cases} \Psi_I(z) & \text{for } z < a \\ \Psi_{II}(z) & \text{for } 0 < z < a \\ \Psi_{III}(z) & \text{for } z > a \end{cases} .$$

Taking the complex conjugate of the Hamiltonian in Eq. 100, we obtain

$$\hat{H}^*_\xi = \begin{cases} \gamma_c\left(\xi^2 + k^2\right) + w\sigma_x & \text{if } z < 0 \text{ or } z > a \\ \gamma_c(\xi^2 + k^2) - \alpha_R \xi \sigma_y \ + V & \text{if } 0 < z < a \end{cases} = \hat{H}_{-\xi}.$$

If $\Psi_\xi(z)$ is solution of the Schrödinger equation $\hat{H}_\xi \Psi_\xi(z) = \mathcal{E}\Psi_\xi(z)$, $\Psi^*_\xi(z)$ is also a particular solution of the Schrödinger equation with opposite in-plane wavevector and corresponding to the same magnetization direction in the electrodes. It results that $\hat{H}_{-\xi}\Psi^*_\xi(z) = \mathcal{E}\Psi^*_\xi(z)$. Note that when we take the complex conjugate, we turn from ingoing to outgoing waves and vice versa

In other words from the scattering matrix point of view

$$\begin{aligned} \{b\} &= [S]_\xi \{a\} \\ \{b^*\} &= [S^*]_\xi \{a^*\} . \end{aligned} \tag{101}$$

However,

$$\{a^*\} = [S]_{-\xi} \{b^*\} ,$$

and

$$\{b^*\} = \left[S^+\right]_{-\xi} \{a^*\} . \tag{102}$$

From Eqs. 101 and 102, we obtain:

$$[S^*]_\xi = \left[S^+\right]_{-\xi} . \tag{103}$$

or

$$\begin{bmatrix} r^* & (t')^* \\ t^* & (r')^* \end{bmatrix}_\xi = \begin{bmatrix} r & t \\ t' & r' \end{bmatrix}_{-\xi} . \tag{104}$$

Taking squared magnitude of both siles of Eq. 104, we observe that electrons with positive and negative in-plane wavevectors posses equal transmission coefficients. No asymmetry of transmission is expected in this case. This situation is similar to the case of Dresselhaus interaction with in-plane incident wavevector parallel to the magnetization in the PA magnetic configuration.

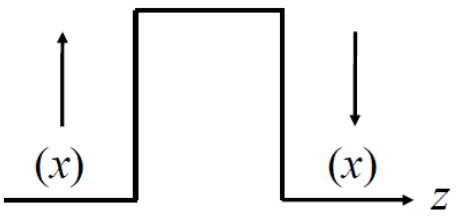

Figure 45: Tunnel junction grown along the z direction with Rashba SOI in the barrier under AP configuration, $\overrightarrow{M} \parallel x$, $\overrightarrow{k_{\parallel}} = (\xi, 0)$.

5.2.1.2 ***AP (↑↓) (see Appendix A)***

In this case, the structure is symmetrical so that it follows the results and conclusions introduced in Appendix A**.**

The electron Hamiltonian now writes:

$$\hat{H}_{\xi} = \begin{cases} \gamma_c \left(\xi^2 + k^2\right) + w\sigma_x & \text{if } z < 0 \\ \gamma_c(\xi^2 + k^2) - \alpha_R \xi \sigma_y \ + V & \text{if } 0 < z < a \\ \gamma_c \left(\xi^2 + k^2\right) - w\sigma_x & \text{if } z > a \end{cases} . \tag{105}$$

This is similar to the PA configuration except that the eigenvectors in the region $z > a$ are now interchanged.

In this case, we also observe that

$$\hat{H}_{\xi}^{*} = \hat{H}_{-\xi}. \tag{106}$$

As a consequence of Eq. 106, the result is that in the AP magnetic configuration, no transport asymmetry *vs.* in-plane incidences is expected upon tunneling. This situation is quite similar to the case of the absence of the out-of-plane components for Dresselhaus interaction.

5.2.2 In-plane wavevector perpendicular to the magnetization direction

Now, the in-plane wavevector is taken parallel to the x direction, $\mathbf{k} = (0, \xi, k)$, so that the Rashba Hamiltonian in Eq. 99 becomes:

$$\hat{H}_R = -\alpha_R \xi \sigma_x,$$

with $\hat{H}_{\xi}^{*} \neq \hat{H}_{-\xi}$.

5.2.2.1 ***PA (↑↑)***

The structure is asymmetric, (see Fig. 46), so that it does not follow the result shown in Appendix A.

The electron Hamiltonian writes:

$$\hat{H}_\xi = \begin{cases} \gamma_c\left(\xi^2 + k^2\right) + w\sigma_x & \text{if } z < 0 \text{ or } z > a \\ \gamma_c(\xi^2 + k^2) - \alpha_R \xi \sigma_x \ + V & \text{if } 0 < z < a \end{cases}.$$

In the electrodes, the upper energy level is $\mathcal{E} = \gamma_c(\xi^2 + k^2) + w$ whereas the lower one is $\mathcal{E} = \gamma_c(\xi^2 + \tilde{k}^2) - w$. The respective eigenvectors are $\frac{1}{\sqrt{2}}\binom{1}{1} = |\uparrow\rangle$ and $\frac{1}{\sqrt{2}}\binom{1}{-1} = |\downarrow\rangle$. The incident energy is smaller than the barrier height so that the relevant wavevectors are purely imaginary. The energy of the upper level is $\mathcal{E} = \gamma_c(\xi^2 - \tilde{q}^2) + \alpha_R\xi + V$, whereas the lower one is $\mathcal{E} = \gamma_c(\xi^2 - q^2) - \alpha_R\xi + V$ where q and $\tilde{q}$ are pure real numbers. The respective eigenvectors are $|\downarrow\rangle$ and $|\uparrow\rangle$.

The corresponding wave functions in each region of the space are given by:

$$\Psi_I(z) = A_1 |\uparrow\rangle e^{ikz} + B_1 |\uparrow\rangle e^{-ikz} + \tilde{A}_1 |\downarrow\rangle e^{i\tilde{k}z} + \tilde{B}_1 |\downarrow\rangle e^{-i\tilde{k}z}, \tag{107}$$

$$\Psi_{II}(z) = A_2 |\uparrow\rangle e^{-qz} + B_2 |\uparrow\rangle e^{qz} + \tilde{A}_2 |\downarrow\rangle e^{-\tilde{q}z} + \tilde{B}_2 |\downarrow\rangle e^{\tilde{q}z}, \tag{108}$$

and

$$\Psi_{III}(z) = A_3 |\uparrow\rangle e^{ikz} + \tilde{A}_3 |\downarrow\rangle e^{i\tilde{k}z}.$$

Using the BDD matching condition for the $\downarrow$ spin at $z = 0$, one obtains:

$$\begin{cases} |\downarrow\rangle + \tilde{B}_1 |\downarrow\rangle = \tilde{A}_2 |\downarrow\rangle + \tilde{B}_2 |\downarrow\rangle, \\ i\tilde{k} |\downarrow\rangle - i\tilde{k}\tilde{B}_1 |\downarrow\rangle = -\tilde{q}\tilde{A}_2 |\downarrow\rangle + \tilde{q}\tilde{B}_2 |\downarrow\rangle; \end{cases}$$

whereas at $z = a$

$$\begin{cases} \tilde{A}_2 |\downarrow\rangle e^{-\tilde{q}a} + \tilde{B}_2 |\downarrow\rangle e^{\tilde{q}a} = \tilde{A}_3 |\downarrow\rangle e^{i\tilde{k}a}, \\ -\tilde{q}\tilde{A}_2 |\downarrow\rangle e^{-\tilde{q}a} + \tilde{q}\tilde{B}_2 |\downarrow\rangle e^{\tilde{q}a} = i\tilde{k}a\tilde{A}_3 |\downarrow\rangle e^{i\tilde{k}a}. \end{cases}$$

Solving this linear system, the amplitude of transmission, A_3, for the $\downarrow$ spin channel takes the form:

$$A_3 = \left[\cosh \tilde{q}a + \frac{i}{2}\left(\frac{\tilde{q}}{\tilde{k}} - \frac{\tilde{k}}{\tilde{q}}\right)\sinh \tilde{q}a\right]^{-1},$$

and, the transmission coefficient of the $\downarrow$ spin follows:

$$T_\downarrow(\xi) = \left[\cosh^2 \tilde{q}a + \frac{1}{4}\left(\frac{\tilde{q}}{\tilde{k}} - \frac{\tilde{k}}{\tilde{q}}\right)^2 \sinh^2 \tilde{q}a\right]^{-1}.$$

Similarly, the transmission coefficient of the $\uparrow$ spin is:

$$T_\uparrow(\xi) = \left[\cosh^2 qa + \frac{1}{4}\left(\frac{q}{k} - \frac{k}{q}\right)^2 \sinh^2 qa\right]^{-1}.$$

We first consider an incident energy smaller than the exchange energy, $-w < \mathcal{E} < w$. The incident $\downarrow$ spin wave is propagative and it can transport the current through the barrier whereas the $\uparrow$ spin wave is an evanescent wave carrying no current. Therefore, the total transmission is equal to the transmission of the $\downarrow$ spin wave.

The total transmission coefficient is then

$$\begin{aligned} T(\xi) &= T_{\downarrow}(\xi) \\ &= \left[\cosh^2 \tilde{q}a + \frac{1}{4}\left(\frac{\tilde{q}}{\tilde{k}} - \frac{\tilde{k}}{\tilde{q}}\right)^2 \sinh^2 \tilde{q}a\right]. \end{aligned} \tag{109}$$

Equation 109 is equivalent to Eq. 3.3 in Ref. [25] describing the spin-polarization transport involving a nonmagnetic tunneling barrier separating two ferromagnetic conductors in the case of a single propagative wave.

If the electron impinges the barrier with an opposite in-plane wavevector, the wave functions in the electrodes remain unchanged whereas the spin in the barrier is reversed. This is equivalent to interchange $\tilde{q} \longleftrightarrow q$ in Eq. 108, so that we deduce the respective wave function in the barrier together with the total transmission coefficient:

$$T(-\xi) = \left[\cosh^2 qa + \frac{1}{4}\left(\frac{q}{\tilde{k}} - \frac{\tilde{k}}{q}\right)^2 \sinh^2 qa\right]^{-1}. \tag{110}$$

The transmission asymmetry of ingoing electrons with opposite in-plane wavevectors is then:

$$\begin{aligned} A &= \frac{T(\xi) - T(-\xi)}{T(\xi) + T(-\xi)} \\ &= \frac{\left[1 + \frac{1}{4}\left(\frac{q}{\tilde{k}} - \frac{\tilde{k}}{q}\right)^2 \tanh^2 qa\right] - \left[1 + \frac{1}{4}\left(\frac{\tilde{q}}{\tilde{k}} - \frac{\tilde{k}}{\tilde{q}}\right)^2 \tanh^2 \tilde{q}a\right]}{\left[1 + \frac{1}{4}\left(\frac{q}{\tilde{k}} - \frac{\tilde{k}}{q}\right)^2 \tanh^2 qa\right] + \left[1 + \frac{1}{4}\left(\frac{\tilde{q}}{\tilde{k}} - \frac{\tilde{k}}{\tilde{q}}\right)^2 \tanh^2 \tilde{q}a\right]} \\ &\approx \tanh(a\delta q). \end{aligned} \tag{111}$$

We recover in Eq. 12 of Chapter 2 devoted to the spin filtering effect. It is possible to say that Eq. 111 characterizes the spin filtering effect caused by a Rashba interaction term in the thin barrier.

In the case of two incident propagative waves of both $\downarrow$ and $\uparrow$ spin channels, the total transmission coefficient is the sum of $T_{\downarrow}$ and $T_{\uparrow}$, and we still obtain spin filtering effect. Moreover, on the condition that the difference of the wavevectors between $\downarrow$ and $\uparrow$ spin channels in the barrier is small, we will recover the total transmission coefficient calculated with two propagative waves in Ref. [25].

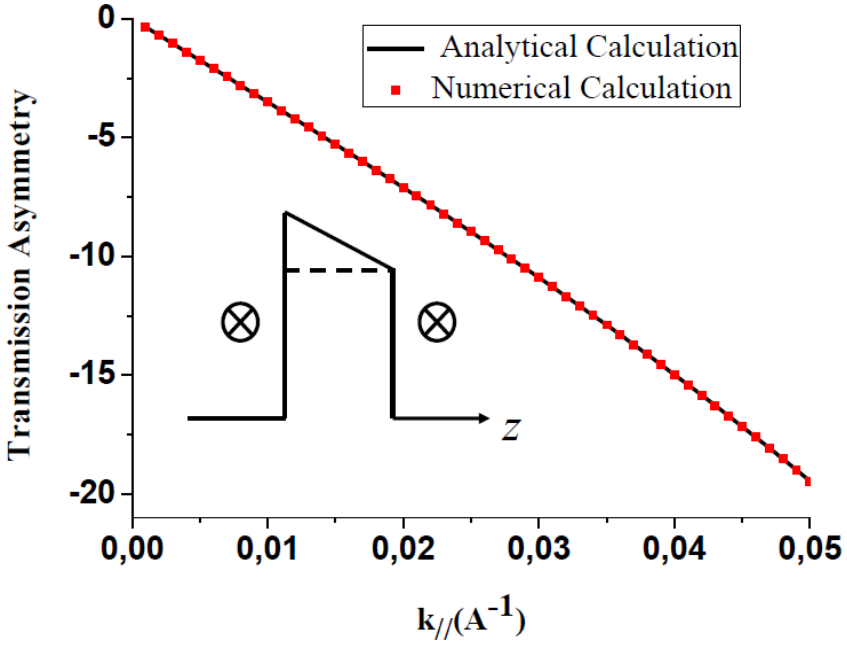

Figure 46: The spin-filter effect caused by the Rashba term in the 1 nm thin barrier *vs.* in-plane wavevector in tunnel junction GaAs/GaAs/GaAs; $m^* = 0.067m_0$, Rashba constant 2 eVÅ, incident energy $\mathcal{E} = 0.1$ eV, exchange interaction 0.18 eV.

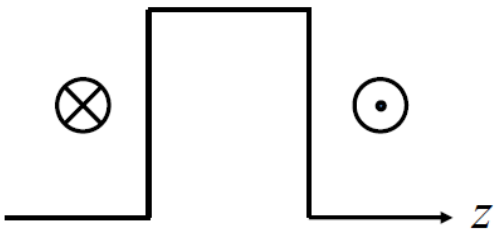

Figure 47: Tunnel junction grown along the z direction with Rashba SOI in the barrier under AP configuration, $\overrightarrow{M} \parallel x$, $\overrightarrow{k_\parallel} = (0, \xi)$.

5.2.2.2 ***AP (↑↓)***

The electron Hamiltonian writes in this case:

$$\hat{H}_\xi = \begin{cases} \gamma_c\left(\xi^2 + k^2\right) + w\sigma_x & \text{if } z < 0 \\ \gamma_c(\xi^2 + k^2) - \alpha_R \xi \sigma_x \ + V & \text{if } 0 < z < a \\ \gamma_c\left(\xi^2 + k^2\right) - w\sigma_x & \text{if } z > a \end{cases}$$

This case is similar to the PA magnetic configuration except that the eigenvectors in the region $z > a$ are reversed. Therefore, $\Psi_I(z)$ and $\Psi_{II}(z)$ are kept unchanged whereas

$$\Psi_{III}(z) = A_3 \left|\downarrow\right\rangle e^{ikz} + \tilde{A}_3 \left|\uparrow\right\rangle e^{i\tilde{k}z}.$$

To transport the current from the left to the right electrode, the electrons must possess an energy larger than the exchange step because they cannot be transmitted from a pure $\downarrow$ state into a pure $\uparrow$ state, and vice versa without SOI. Here, the wave functions are similar to the ones corresponding to the Dresselhaus term in a barrier with an in-plane wavevector parallel to the magnetization direction in the AP configuration. We have demonstrated that the transmission coefficient is now independent of the sign of the in-plane wavevector.

The conclusion about the transport asymmetry arising from the interplay between exchange interaction and Rashba SOI for the electron is the following: Anomalous tunnel Hall effect does not exist in these structures because the Rashba SOC term does not possess any out-of-plane component in the Hamiltonian. Only the spin filtering effect may exist in the case of an in-plane wavevector perpendicular to the magnetization in the PA configuration.

CHAPTER VI

PERTURBATIVE SCATTERING APPROACH TO SPIN-DEPENDENT TUNNELING INCLUDING SPIN-ORBIT INTERACTIONS

6.1 Introduction in the frame of the spin Hall effects

The physical principles of the anomalous Hall effects and related spin-Hall effects, largely revisited since the beginning of the 2000's, follow the first proposal by Dyakonov and Perel in 1971 [8]. It originates from an inequivalent probability for a given spin to be scattered or moved on the left or on the right in a plane containing the trajectory and perpendicular to its spin direction. This asymmetry in the trajectory originates in the action of the spin-orbit force operating during a certain time lapse, either during a scattering event within the collision time, *e.g.* extrinsic spin-Hall mechanism occurring in random impurity alloys or between two collisions (intrinsic SHE) in the host material. From pure symmetry considerations, the asymmetry of deflection (often called Mott's scattering as long as the extrinsic skew scattering mechanisms is concerned) only occurs in the trajectory plane perpendicular to the spin direction. The particular plane is a specific symmetry plane which makes possible to observe such an imbalance of spin diffusion and spin current. Adding an incoming non-zero spin current by exchange forces emanating from a ferromagnet makes the two spin currents being deflected with a different amplitude generating a non-zero transverse charge-current associated to an anomalous Hall effect in the ferromagnet. This has been largely debated in the literature in the past few years as well as in a couple of recent papers [123, 124].

The intrinsic mechanism of the SHE, *e.g.* occurring in GaAs, Pt, Ta, or W, is related to the host spin-orbit Hamiltonian during the accelerating-carrier trajectory and must be described by the full temporal evolution of the carrier wave function between two collisions (source terms). These source terms, calculated via Kubo, Keldysh or Berry'phase formalisms [146] to derive the transverse spin-dependent conductivity or the spin-Hall conductivity, may be afterwards integrated in a semi-classical Boltzmann equation in a non-equilibrium formalism. The extrinsic SHE phenomena can be divided into two parts: the skew scattering terms which become nonzero to the third order of the perturbation calculation and the side-jump terms which represent the lateral space deviation of the carrier wavepacket during the interaction process (effective first order of perturbation in the SOI contribution). Among these contributions to the spin-Hall processes

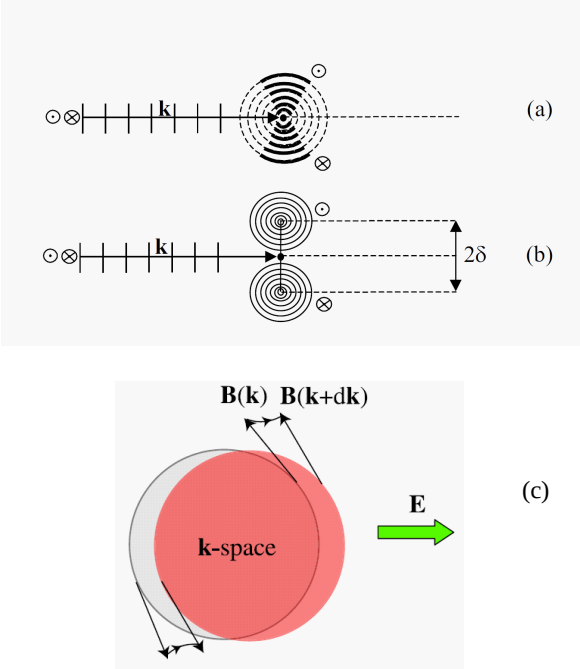

Figure 48: Mechanism of SHE effect: (a) skew scattering, (b) side jump, (c) intrinsic spin Hall effect.

whose more physical details are largely given in some reference articles obtained both in diagrammatic schemes or in semi-empirical Boltzmann pictures [125, 126, 127], the skew-scattering mechanism generally provides the dominant source of the transverse spin current in the limit of dilute alloys. The reason is the linear scaling of the skew-scattering driven transverse conductivity σ_{xy} with the diagonal one σ_{xx} in the limit of vanishing scattering, the scaling factor being the so-called SHA.

The skew-scattering mechanism for the SHE arises because of the non-equal interference between the different parts of the diffused wave (by the Coulomb potential and the related spin-orbit terms) as can be explained through detailed phase-shift analyses in a spherical-symmetry potential picture (partial wave) [147]. This occurs to the third order of perturbation calculations involving, at least, two perturbation terms arising from the Coulombic potential of the impurity (V_C) and one from the central spin-orbit perturbation $V_{S.O.}$ occurring in an effective 3^{rd}-order T matrix scattering operator, asymmetrical with respect to the left and right outgoing waves [128]. In a partial wave decomposition approach (the spin-polarized angular moment being conserved), the effect of the Coulomb potential is entirely reduced to the scattering phase-shift to all orders whereas the spin-orbit interactions enter to the first perturbation order in $V_{S.O.}$. This is then a general way, in the community of ab-initio, to consider calculations to the first order of spin-orbit perturbation $V_{S.O.}$, and the properties of spin-transport from the general Kubo formula [148, 149, 150]. In the geometry of the "dilute alloy regime", this is made by calculating the effect of the spherical symmetry of the spin-orbit terms once

the properties of the overall scattering wave are known, *e.g.* from phase-shift analyses. The investigations of the properties of the SHE in various $3d$, $4d$, and $5d$ transitions metals, involving perturbation calculations techniques are numerous and in particular since the end of the 2000's and the beginning of the 2010's [129].

Our philosophy concerning the treatment of the tunneling-Hall or scattering-Hall effects we propose in the present manuscript can be developed in a same spirit than the KKR formalism extensively used in the ab-initio density functional theory community. Our approach takes also benefit of the perfect 2-dimensionality of the model system under investigations to consider the case of evanescent waves in the diffusion process.

The physical processes of scattering or tunneling transmission in a perfect 2-dimensional system (characterized by a translation invariance or conserved $k_{\|}$) have to be known before the branching of the SOI. One interest of this perturbation method lies in the fact that the SOI may be delocalized in a wide region (*e.g.* the electrodes) or localized in a small region of space like in the case of a thin tunnel junction at the nanometer scale. The case of a thin tunnel junction is then particularly interesting because it mimics the action of the spin-orbit forces, of a given symmetry, on the conductivity, either longitudinal or transverse (longitudinal or spin-Hall for instance). This kind of perturbative scattering approach may then be generalized to any kind of physical systems where we look for the effects of the SOI and possibly exchange on the respective diffusion probability or transmission coefficient (for a tunnel junction) when needed. This method becomes more and more favorable in certain situations, like investigated here, where the transmission is zero before branching the SOI term when the electrodes are made of highly spin-polarized compounds, close to possess a half-metallicity character (GaMnAs or heusler alloys). One can investigate, like demonstrated afterwards, the effect of the SOI in host (contacts) as well as the effect of SOI in the diffusion centers (tunnel barrier) like encountered in skew-scattering Hall effects. The 2-dimensional character of our chosen heterostructures helps that way in both numerical and analytical treatments compared to spherically-symmetric diffusive centers involving spin-orbit contrast potentials.

In the present chapter, we expose the fundamentals of the investigation methods through a large number of examples before tackling the problem of the tunneling-Hall effect by performing perturbation calculations with spin-orbit involved in the electrodes (exchange step) or confined in a small region of the space (tunnel barrier). This method will be demonstrated to be particularly relevant for the case of the perpendicular transport (interface crossing) like proposed in this manuscript. However, it could be used in the treatment of in-plane conduction, *e. g.* in a 2-dimensional-Rashba gas which is a seat of spin-orbit assisted diffusions, possibly responsible for a new kind of anomalous magnetoresistance like described in a series of recent papers [130].

6.2 The Green function method

The single-particle Green function (GF) is a very useful tool for studying the electronic properties of materials and transport phenomena because it can be used to express all the observable properties of the system of interest [131] and because it has many other advantages including the following ones:

(i) It allows to treat complex systems efficiently, starting from idealized ones to *e.g.* interfaces and multilayered systems by handling the complexity as a perturbation from bottom to up. Moreover, in order to obtain the electronic structure of a periodic system, first, with a localized impurity or defect, one can start from the GF method to treat the impurity and subsequent SOI and spin-dependent electronic diffusion as perturbations to increasing order. Similarly, the presence of a surface can be considered to be a perturbation to the GF of an infinite medium. That way, we will introduce a GF treatment for mixed propagative-evanescent waves of tunnel junctions considering the spin-orbit interactions in a localized volume (tunnel junctions) or in half-spaces (exchange step) as perturbations to investigate the properties of the scattered spin-polarized electronic waves taken to the zero-order. This provides us with a generalization of the work dealing with GMR systems [132] to the spin-orbit case.

(ii) More generally, the GF is very useful for calculating the response of a system to external fields *e.g.* the transport properties in the linear response regime (*i.e.*, the conductivity) [133].

For all these reasons, the ability to calculate the GF of a multilayered system or a single interface with an arbitrary potential shaped barrier is very important. For a finite system, the GF may be evaluated locally using unperturbed wave functions as a basis and calculated quite simply as a function of the inverse of the Hamiltonian in the real space. Similarly, the GF for an infinite periodic system may be obtained by this way in the reciprocal space. Nevertheless, in the case of semi-infinite systems, *e.g.* an infinite periodic system with a surface or an interface, one encounters the problem of the matching conditions for the GFs which have been largely discussed and debated in a series of relevant contributions [134, 135, 132, 136]. These papers deal with finding the proper general expressions depending on the exact shape of the GF in each part (material) and describing the multilayer structures with relevant transmissions and reflections at each interface. In the present case, we will start from the well-known expression of the spin-polarized GF corresponding to a simple potential step in the energy range of an evanescent transmission from pure spin-up channel to pure spin-down channel without SOI.

Although we are mostly concerned with the development of the GF methods adapted to our situation of spin-orbit-assisted skew tunneling for an interface or a tunnel junction, it is worth to mention a few applications even without being able to give a full

comprehensive view. In that physical issues, the GF formalism has been used with great success to study transport through mesoscopic devices, exchange coupling, GMR [133] as well as tunneling magnetoresistance [137], surface and interface states, as well as spin-Hall effect of heavy-metal based transition metal alloys [138].

6.3 Green's function and Lippman-Schwinger equation

The scattering theory is essentially a time-independent perturbation theory applied to the case of a continuous spectrum. That means that we know that it exists eigenstates of the full Hamiltonian for every possi vccccv
energy, $\mathcal{E}$. Then we just pick any $\mathcal{E}$, and try to find the perturbed eigenstates $|\Psi(\mathcal{E})\rangle$. There are usually some degenerate eigenstates for any given energy. So, the question becomes which of the presumably infinitely degenerate full-eigenstates we are trying to compute? The answer comes from the causality; we want to be able to completely specify the probability current amplitude incoming in from $\overrightarrow{r} \longrightarrow \infty$, and we want the theory to give us the corresponding outgoing current amplitude. The way we do this is picking an unperturbed eigenstate which has the desired incoming current amplitude (at this stage we do not need to worry what the outgoing current amplitude of the unperturbed state is). The second step is to make sure that our perturbation theory generates no contribution and no changes on the incoming currents, which we accomplish by putting this condition by hand, under the mantra of causality. As we will see, this means that the resulting *full eigenstates* will have desired incoming current amplitudes. We recall that solving a partial differential equation requires first specifying the boundary conditions, which is exactly what the standard scattering theory formalism is designed to do.

Typically, the scattering formalism is described in the following way: an incident particle in the state $|\Psi_0\rangle$ is scattered by the potential V, resulting in a scattered state $|\Psi_s\rangle$. The incident state $|\Psi_0\rangle$ is assumed to be an eigenstate of the background Hamiltonian $\hat{H}_0$, with the eigenvalue $\mathcal{E}$. This is mathematically expressed as:

$$\left(\mathcal{E} - \hat{H}_0\right)|\Psi_0\rangle = 0, \tag{112}$$

The potential $\hat{V}(\mathbf{r})$ is assumed to be *localized* (without however being always a necessary condition), so that

$$\lim_{r\longrightarrow\infty} \hat{V}(\mathbf{r}) = 0. \tag{113}$$

The goal of the scattering theory is then to solve the full eigenvalues problem

$$\left(\mathcal{E} - \hat{H}_0 - \hat{V}\right)|\Psi\rangle = 0, \tag{114}$$

where $|\Psi\rangle$ is the eigenstate of the full Hamiltonian $\hat{H} = \hat{H}_0 + \hat{V}$ of the system with the energy $\mathcal{E}$. It should be clear that there is a different $|\Psi_0\rangle$ and correspondingly a different $|\Psi\rangle$ for each energy $\mathcal{E}$, even though our notation does not indicate this explicitly. We start by defining the scattered state $|\Psi_s\rangle$ *via*

$$|\Psi_s\rangle = |\Psi\rangle - |\Psi_0\rangle \,. \tag{115}$$

The full Schrödinger equation (Eq. 114) may be written as

$$\left(\mathcal{E} - \hat{H}_0\right) |\Psi\rangle = \hat{V} |\Psi\rangle \,, \tag{116}$$

which, after substituting $|\Psi\rangle = |\Psi_s\rangle + |\Psi_0\rangle$ and making use of Eq. 112, gives:

$$\left(\mathcal{E} - \hat{H}_0\right) |\Psi_s\rangle = \hat{V} |\Psi\rangle \,, \tag{117}$$

otherwise,

$$|\Psi_s\rangle = \left(\mathcal{E} - \hat{H}_0\right)^{-1} \hat{V} |\Psi\rangle \,, \tag{118}$$

by adding $|\Psi_0\rangle$ to both sides of Eq. 118, one obtains:

$$|\Psi\rangle = |\Psi_0\rangle + \left(\mathcal{E} - \hat{H}_0\right)^{-1} \hat{V} |\Psi\rangle \,. \tag{119}$$

This is well known as the Lippman-Schwinger equation. It is often expressed in a slightly more compact notation by introducing the concept of Green's function, defined as:

$$G_0^{\pm} = \lim_{\epsilon \longrightarrow 0} \left(\mathcal{E} - \hat{H}_0 \pm i\epsilon\right)^{-1} . \tag{120}$$

G_0^+ (G_0^-) is called retarded (advanced) Green's function. The term $i\epsilon$ is added to enforce causality by making sure that $|\Psi_s\rangle$ has no incoming probability current associated with it. It makes sense that scattered waves propagate away from the source, and not other way around. In our work, as we only consider the retarded Green function, for simplicity we use G_0 instead of G_0^+. Using this definition, the Lippman-Schwinger equation takes its standard form:

$$|\Psi\rangle = |\Psi_0\rangle + G_0 \hat{V} |\Psi\rangle \,. \tag{121}$$

Solving the Lippman-Schwinger equation for $|\Psi\rangle$ is formally very simple, yielding:

$$|\Psi\rangle = \left(1 - G_0 \hat{V}\right)^{-1} |\Psi_0\rangle \,.$$

The Born series give:

$$|\Psi\rangle = |\Psi_0\rangle + G_0 \hat{V} |\Psi_0\rangle + G_0 \hat{V} G_0 \hat{V} |\Psi_0\rangle + ... $$

and to the first order

$$|\Psi\rangle = |\Psi_0\rangle + G_0\hat{V}\,|\Psi_0\rangle\,. \tag{122}$$

Written as an integral equation, Eq. 122 becomes

$$\Psi(\overrightarrow{r}) = \Psi_0(\overrightarrow{r}) + \int G_0(\overrightarrow{r},\overrightarrow{r}')_0\hat{V}(\overrightarrow{r}')\Psi_0(\overrightarrow{r}')d\overrightarrow{r}', \tag{123}$$

where $\langle\overrightarrow{r}\,|\Psi\rangle = \Psi(\overrightarrow{r})$, and $G_0(\overrightarrow{r},\overrightarrow{r}') = \langle\overrightarrow{r}|\,G_0\,|\overrightarrow{r}'\rangle$. The GF, $G_0(\overrightarrow{r},\overrightarrow{r}')$, is a solution of Eq. 120.

$$\left(\mathcal{E} - \hat{H}_0\right) G_0(\overrightarrow{r},\overrightarrow{r}') = \delta\,(\overrightarrow{r} - \overrightarrow{r}')\,. \tag{124}$$

The respective retarded and advanced Green's functions $G_0^{\pm}$ for homogeneous host materials of respective eigenvalues $\mathcal{E}$ and eigenvectors Ψ_k, with a certain translational invariance involving Bloch **k** states, and satisfying $(\mathcal{E} - \hat{H}_0)\Psi_k(r) = 0$ at the energy $\mathcal{E}$, is generally determined according to the general formula:

$$G_0^{\pm}(\mathcal{E},\ r, r') = \sum_k \frac{\Psi_k(r)\Psi_k^*(r')}{\mathcal{E} - \mathcal{E}_k \pm i\eta},$$

to find the bulk or in heterostructures where η ($\eta > 0$) represents an infinitesimal value needed for convergence; η ensures that the electronic waves coming from the left (right) side remains finite over the whole host volume after a given propagation time τ. The equivalent Green's function $G_0^{\pm}$ to be derived for a junction composed of two semi-infinite media or for a tunnel junction is generally more complex to obtain. We present here a general method developed for spin-unpolarized particles based on some references [132, 134, 135, 136] before its generalization to spin-polarized particles.

6.4 Interfacial Green's function for spinless particles

As an example, we first consider the solution of Eq. 124 for a scalar (or spinless) particle in a homogenous potential U_1 for $z < 0$, and U_2 for $z > 0$. *In this part, we have deliberately decided to detail the whole mathematical developments to find the correct description of the GF for a single interface*. The GF satisfies the equation:

$$\begin{aligned} \left(\mathcal{E} - \hat{H}_0\right) G_0(z,z') &= \delta\,(z - z')\,, \\ \text{or } \left(\mathcal{E} + \frac{\hbar^2}{2}\frac{\partial}{\partial z}\frac{1}{m^*(z)}\frac{\partial}{\partial z} - U(z)\right) G_0(z,z') &= \delta\,(z - z')\,, \end{aligned} \tag{125}$$

where $\hat{H}_0 = (\hbar^2/2)\,\frac{\partial}{\partial z}\frac{1}{m^*(z)}\frac{\partial}{\partial z} - U(z)$. Equation. 125 is an ordinary differential equation, the method to find the GF has been well mentioned in mathematical textbooks,

normally it has three main steps. We use this procedure in a particular case, *i.e.,* Eq. 125, with the boundary conditions at $z = \pm\infty$.

The strategy is:

(i) To find a fundamental system $\{\Psi_L^0, \Psi_R^0\}$ of the homogenous Schrödinger equation $\left(\mathcal{E} - \hat{H}_0\right)\Psi = 0$.

(ii) To find a suitable linear combinations of Ψ_L^0 and Ψ_R^0 and find solutions y_1 and y_2 of the equation $\left(\mathcal{E} - \hat{H}_0\right) y = 0$ where $y_1(z)$ is non-infinite at $z = -\infty$, whereas $y_2(z)$ is non-infinite at $z = +\infty$.

(iii) To define the correct GF we make use of the formula

$$G_0(z,z') = \begin{cases} \frac{y_1(z)y_2(z')}{W(y_1,y_2)(z')} \text{if} -\infty < z < z' < +\infty \\ \frac{y_1(z')\,y_2(z)}{W(y_1,y_2)(z')} \text{ if } -\infty < z' < z < +\infty \end{cases}, \tag{126}$$

where $W(z') = \frac{\hbar^2}{2m^*(z')}\left[y_1(z')\frac{\partial y_2(z')}{\partial z'} - \frac{\partial y_1(z')}{\partial z'}y_2(z')\right]$ is the Wronskian potential. In the case $\mathcal{E} > U_1 > U_2$, Eq. 125 has a solution Ψ_L^0 which is finite at $z = -\infty$, and Ψ_R^0 finite at $z = +\infty$,

As well-known, at an energy larger than the potential step, the homogenous Schrödinger equation, $\left(\mathcal{E} - \hat{H}_0\right)\Psi = 0$, admits the solutions:

$$\Psi_L^0 = e^{-ik_2 z_>} + r_L e^{ik_2 z_>} + t_L e^{-ik_1 z_<},$$

$$\Psi_R^0 = e^{ik_1 z_<} + r_R e^{-ik_1 z_<} + t_R e^{ik_2 z_>},$$

where we write $z_<$ instead of $z < 0$, and $z_>$ instead of $z > 0$. Concerning their physical meaning: Ψ_R^0 is the wave transmitted from the left to the right and Ψ_L^0 is the wave transmitted from the right to the left at the same energy. They satisfy the matching conditions at the left and right sides respectively.

By using the BDD matching conditions at $z = 0$, one obtains:

$$\begin{aligned} t_L &= \frac{2k_2}{k_2 + k_1}, t_R = \frac{2k_1}{k_2 + k_1}, \\ r_L &= \frac{k_2 - k_1}{k_2 + k_1}, r_R = \frac{k_1 - k_2}{k_2 + k_1}. \end{aligned}$$

if one chooses $y_1 \equiv \Psi_L^0$, and $y_2 \equiv \Psi_R^0$ satisfying the boundary conditions at $z = \pm\infty$.

Therefore, Eq. 125 possesses a solution of the form:

$$G_0(z,z') = \frac{\Psi_L^0(z')\Psi_R^0(z)\Theta(z - z') + \Psi_L^0(z)\Psi_R^0(z')\Theta(z' - z)}{W(z')}, \tag{127}$$

with the Wronskian potential:

$$W(z') = \frac{\hbar^2}{2m^*(z')}\left[\Psi_L^0(z')\frac{\partial}{\partial z'}\Psi_R^0(z') - \Psi_R^0(z')\frac{\partial}{\partial z'}\Psi_L^0(z')\right]. \tag{128}$$

If we assume, for simplicity and without a big loss of generality, that the effective mass remains unchanged in the layers, one obtains $m^*(z') = m^*$. It is easy to derive $\partial W(z')/\partial z' = 0$ to prove that the Wronskian is independent of the coordinate (z and z'). In this case, we obtain:

$$W = \frac{\hbar^2}{2m^*}\frac{4ik_1k_2}{k_2+k_1}.$$

Following Eq. 127, we recover the *retarded* GF introduced in Refs. [132, 135]

$$G_0(z,z') = \frac{2m^*}{\hbar^2}\frac{t_R}{2ik_1}e^{-ik_1z}e^{ik_2z'};\ z<0,\ z'>0,$$

$$G_0(z,z') = \frac{2m^*}{\hbar^2}\frac{t_L}{2ik_2}e^{-ik_1z'}e^{ik_2z};\quad z>0,\ z'<0,$$

$$G_0(z,z') = \frac{2m^*}{\hbar^2}\frac{1}{2ik_1}\left[e^{ik_1|z-z'|}+r_Re^{-ik_1(z+z')}\right],\ z<0,\ z'<0,$$

$$G_0(z,z') = \frac{2m^*}{\hbar^2}\frac{1}{2ik_2}\left[e^{ik_2|z-z'|}+r_Le^{-ik_2(z+z')}\right],\ z>0,\ z'>0.$$

Note that the *advanced* GF is generally constructed by inversion of the respective left and right incoming wave functions in the expression of the retarded GF.

6.5 *Interfacial Green's function for spin-polarized particle without orbital degeneracy.*

6.5.1 General expression of the Green function.

In order to demonstrate the power of the perturbation methods adapted to the spin-transport case, one first considers the simpler case of the CB, free of any orbital degeneracy, and described by a single $S-$type orbital. Choosing the orthogonal basis functions $|S\rangle \otimes \{|\uparrow\rangle,\ |\downarrow\rangle\}$ allows one to obtain the zeroth-order unperturbed *diagonal* Hamiltonian according to:

$$\hat{H}_0 = \begin{array}{c} \begin{array}{cc} |S\uparrow\rangle & |S\downarrow\rangle \end{array} \\ \begin{bmatrix} \hat{H}_0^{\uparrow\uparrow} & 0 \\ 0 & \hat{H}_0^{\downarrow\downarrow} \end{bmatrix} \end{array}.$$

$\Psi_R^0 = \begin{bmatrix} \Psi_R^{0\uparrow} \\ \Psi_R^{0\downarrow} \end{bmatrix}$ and $\Psi_L^0 = \begin{bmatrix} \Psi_L^{0\uparrow} \\ \Psi_L^{0\downarrow} \end{bmatrix}$ are solutions of the homogenous Schrödinger equation satisfying the boundary conditions for the respective left and right incoming waves,

$$\left(\mathcal{E}\hat{\mathbb{I}} - \hat{H}_0\right)\begin{bmatrix} \Psi_R^{0\uparrow} \\ \Psi_R^{0\downarrow} \end{bmatrix} = 0,$$

and

$$\left(\mathcal{E}\hat{\mathbb{I}} - \hat{H}_0\right)\begin{bmatrix} \Psi_L^{0\uparrow} \\ \Psi_L^{0\downarrow} \end{bmatrix} = 0.$$

where $\hat{\mathbb{I}}$ is the 2×2 unitary matrix. Note that $\left(\mathcal{E}\hat{\mathbb{I}} - \hat{H}_0\right)$ is diagonal.

Now, the spin-polarized GF in the CB is a solution of the following equation

$$\left(\mathcal{E}\hat{\mathbb{I}} - \hat{H}_0\right) G_0(z, z') = \hat{\mathbb{I}}\delta(z - z'), \tag{129}$$

The 2×2 GF admits a diagonal form, due to the orthogonality (no spin mixing) between the basis functions, *i.e.,* $|S\uparrow\rangle$ and $|S\downarrow\rangle$. This makes the treatment rather similar to the spinless case. The diagonal GF then writes:

$$G_0(z, z') = \begin{bmatrix} G_0^{\uparrow\uparrow}(z, z') & 0 \\ 0 & G_0^{\downarrow\downarrow}(z, z') \end{bmatrix},$$

with

$$G_0^{\uparrow\uparrow}(z, z') = \frac{\Psi_R^{0\uparrow}(z)\Psi_L^{0\uparrow}(z')\Theta(z - z') + \Psi_R^{0\uparrow}(z')\Psi_L^{0\uparrow}(z)\Theta(z' - z)}{W^{\uparrow\uparrow}(z')},$$

and

$$G_0^{\downarrow\downarrow}(z, z') = \frac{\Psi_R^{0\downarrow}(z)\Psi_L^{0\downarrow}(z')\Theta(z - z') + \Psi_R^{0\downarrow}(z')\Psi_L^{0\downarrow}(z)\Theta(z' - z)}{W^{\downarrow\downarrow}(z')}.$$

The spin-dependent Lippman-Schwinger equation for the Ψ_R state then writes:

$$\begin{bmatrix} \Psi_R^{\uparrow}(z) \\ \Psi_R^{\downarrow}(z) \end{bmatrix} = \begin{bmatrix} \Psi_R^{0\uparrow}(z) \\ \Psi_R^{0\downarrow}(z) \end{bmatrix} + \int \begin{bmatrix} G_0^{\uparrow\uparrow}(z, z') & 0 \\ 0 & G_0^{\downarrow\downarrow}(z, z') \end{bmatrix} \begin{bmatrix} \hat{V}^{\uparrow\uparrow}(z') & \hat{V}^{\uparrow\downarrow}(z') \\ \hat{V}^{\downarrow\uparrow}(z') & \hat{V}^{\downarrow\downarrow}(z') \end{bmatrix} \begin{bmatrix} \Psi_R^{0\uparrow}(z') \\ \Psi_R^{0\downarrow}(z') \end{bmatrix} dz',$$

where $\hat{V}^{\sigma\sigma'}$ is the matrix element of the perturbed potential in the basis, $|S\uparrow\rangle$ and $|S\downarrow\rangle$.

We then obtain the correction to the overall wave function within the heterostructure according to:

$$\begin{bmatrix} \delta\Psi_R^{\uparrow}(z) \\ \delta\Psi_R^{\downarrow}(z) \end{bmatrix} = \begin{bmatrix} \int G_0^{\uparrow\uparrow}(z, z')\hat{V}^{\uparrow\uparrow}(z')\Psi_R^{0\uparrow}(z')dz' + \int G_0^{\uparrow\uparrow}(z, z')\hat{V}^{\uparrow\downarrow}(z')\Psi_R^{0\downarrow}(z')dz' \\ \int G_0^{\downarrow\downarrow}(z, z')\hat{V}^{\downarrow\uparrow}(z')\Psi_R^{0\uparrow}(z'dz' + \int G_0^{\downarrow\downarrow}(z, z')\hat{V}^{\downarrow\downarrow}(z')\Psi_R^{0\downarrow}(z')dz' \end{bmatrix} \tag{130}$$

6.5.2 Example: perturbative scattering method adapted to electron tunneling through a T_d [110] semiconductor barrier

In order to review this method, we will first describe the approach developed by the IOFFE institute [15] involving SOI in the barrier via such a perturbative method. In this present work, the free electron tunnels through an heterostructure with a symmetric potential profile grown along the $z \parallel [110]$ axis, with the in-plane axes $x \parallel [1\bar{1}0]$, $y \parallel [00\bar{1}]$. The barrier is made of a T_d-group semiconductor, as introduced in the preceding chapters, and the lack of inversion center leads to the appearance of the Dresselhaus k-cubic terms, $\hat{H}_D$, in the Hamiltonian.

6.5.2.1 ***Physical issues***

Along the $[110]$ direction, the Dresselhaus Hamiltonian contains the derivative of the third, second, first, and zeroth order. In perturbative treatment, we are interested in the derivative of the third order term like:

$$\hat{H}_D = \frac{\sigma_x}{2}\left\{\gamma(z)k_z^3 + \left(k_z^3\right)^+\gamma(z)\right\}. \tag{131}$$

Indeed, the presence of the third-derivative term makes the current discontinuous at the interface [31]. To avoid this problem, the authors considered the *k*-cubic term as the perturbation term $V(z)$ in the above part in order to calculate the correction to the transmission coefficient for $\uparrow$ and $\downarrow$ spin channels.

One chooses here orthogonal basis functions with spin-quantization being the eigenvecctors of σ_x according to: $|S\rangle \otimes \{|\uparrow\rangle\,,\ |\downarrow\rangle\}$ with $|\uparrow\rangle = \frac{1}{\sqrt{2}}\binom{1}{1}$, and $|\downarrow\rangle = \frac{1}{\sqrt{2}}\binom{1}{-1}$.

The unperturbed Hamiltonian possesses then the following block form:

$$\hat{H}_0 = \begin{bmatrix} \hat{H}_0^{\uparrow\uparrow} & 0 \\ 0 & \hat{H}_0^{\downarrow\downarrow} \end{bmatrix},$$

with:

$$\hat{H}_0^{\uparrow\uparrow} = \hat{H}_0^{\downarrow\downarrow} = \begin{cases} -\frac{\hbar^2}{2}\frac{\partial}{\partial z}\frac{1}{m_*(z)}\frac{\partial}{\partial z} & \text{for } z<0 \text{ or } z>a \\ -\frac{\hbar^2}{2}\frac{\partial}{\partial z}\frac{1}{m_*(z)}\frac{\partial}{\partial z} + V_0 & \text{for } 0<z<a \end{cases}, \tag{132}$$

and where a is the barrier thickness and V_0 the barrier height. As is well known, the solutions of the homogenous Schrödinger equation at the same incident energy $\mathcal{E} < V_0$ are respectively:

$$\Psi_R^{0\uparrow} = \Psi_R^{0\downarrow} = \begin{cases} e^{ikz} + r_k e^{-ikz}, & z<0 \\ A_k e^{-qz} + B_k e^{qz}, & 0<z<a \\ t_k e^{ik(z-a)}, & z>a \end{cases},$$

$$\Psi_L^{0\uparrow} = \Psi_L^{0\downarrow} = \begin{cases} t_k e^{-ikz}, & z<0 \\ A_k e^{q(z-a)} + B_k e^{-q(z-a)}, & 0<z<a \\ e^{-ik(z-a)} + r_k e^{ik(z-a)}, & z>a. \end{cases},$$

where $t_k = \left[\cosh qa + \frac{i}{2}\left(\frac{q}{k} - \frac{k}{q}\right)\sinh qa\right]^{-1}$ is the transmission amplitude, $r_k = \left[-\frac{i}{2}\left(\frac{q}{k} + \frac{k}{q}\right)\sinh qa\right]t_k$ the reflection amplitude, A_k and B_k are the amplitudes in the barrier, $A_k = \frac{t_k}{2}\left(1 + i\frac{k}{q}\right)e^{-qa}$, $B_k = \frac{t_k}{2}\left(1 - i\frac{k}{q}\right)e^{qa}$; $k = \sqrt{2m\mathcal{E}/\hbar^2} > 0$ is the initial wavevector, $q = \sqrt{2m\left(V_0 - \mathcal{E}\right)/\hbar^2}$, with the same effective masses inside and outside the barrier. The Wronskian potential is independent of the z' coordinate. We choose $z > a$ to calculate its value.

$$W^{\uparrow\uparrow} = \frac{\hbar^2}{2m^*}\left\{\Psi_L^{\uparrow}(z'>a)\frac{\partial\Psi_R^{\uparrow}(z'>a)}{\partial z} - \frac{\partial\Psi_L^{\uparrow}(z'>a)}{\partial z}\Psi_R^{\uparrow}(z'>a)\right\} = i\frac{\hbar^2 k}{m^*}t_k.$$

Note that the Wronskian for the $\downarrow$ spin particle remains unchanged,

$$W^{\downarrow\downarrow} = i\frac{\hbar^2 k}{m^*}t_k.$$

6.5.2.2 *Expression for the SOI potential (Dresselhaus)*

We consider now the properly symmetrized Dresselhaus SOI Hamiltonian in the barrier. Because of

$$\langle\downarrow|\,\sigma_x\,|\downarrow\rangle = -1, \langle\uparrow|\,\sigma_x\,|\uparrow\rangle = 1, \tag{133}$$

$$\langle\uparrow|\,\sigma_x\,|\downarrow\rangle = \langle\downarrow|\,\sigma_x\,|\uparrow\rangle = 0, \tag{134}$$

the perturbed potential can be expressed in a diagonal form according to:

$$\hat{V}(z) = \begin{bmatrix} V^{\uparrow\uparrow}(z) & 0 \\ 0 & V^{\downarrow\downarrow}(z) \end{bmatrix},$$

with

$$V^{\uparrow\uparrow}(z) = \langle\uparrow|\,\hat{H}_D\,|\uparrow\rangle = \frac{1}{2}\left\{\gamma(z)k_z^3 + \left(k_z^3\right)^+\gamma(z)\right\},$$

and

$$V^{\downarrow\downarrow}(z) = \langle\downarrow|\,\hat{H}_D\,|\downarrow\rangle = \frac{-1}{2}\left\{\gamma(z)k_z^3 + \left(k_z^3\right)^+\gamma(z)\right\}.$$

Following Eq. 130, the correction to the zeroth order $\uparrow$-spin wave function within the heterostructure is then:

$$\begin{aligned}\delta\Psi_R^{\uparrow}(z) &= \int_0^a G_0^{\uparrow\uparrow}(z,z')V^{\uparrow\uparrow}(z')\Psi_R^{0\uparrow}(z')dz' \text{ for } \uparrow\text{-spin incidence,} \qquad (135)\\ &= \frac{-im^*e^{ik(z-a)}}{\hbar^2 k}\int_0^a \Psi_L^{0\uparrow}(z')\frac{1}{2}\left\{\gamma(z)k_z^3 + \left(k_z^3\right)^+\gamma(z)\right\}\Psi_R^{0\uparrow}(z')dz',\end{aligned}$$

whereas

$$\begin{aligned}\delta\Psi_R^{\downarrow}(z) &= \int_0^a G_0^{\downarrow\downarrow}(z,z')V^{\downarrow\downarrow}(z')\Psi_R^{0\downarrow}(z')dz' \text{ for } \downarrow\text{-spin incidence} \qquad (136)\\ &= \frac{im^*e^{ik(z-a)}}{\hbar^2 k}\int_0^a \Psi_L^{0\downarrow}(z')\frac{1}{2}\left\{\gamma(z)k_z^3 + \left(k_z^3\right)^+\gamma(z)\right\}\Psi_R^{0\downarrow}(z')dz'.\end{aligned}$$

From Eqs. 135 and 136, we can find the correction to the transmission amplitude for the $\uparrow$- and $\downarrow$- spin channels respectively, according to:

$$\delta t^{\uparrow\uparrow} = -\delta t^{\downarrow\downarrow} = \frac{-im^*}{\hbar^2 k}\int_0^a \Psi_L^{0\uparrow}(z')\frac{i}{2}\left\{\gamma(z)\frac{\overrightarrow{\partial}^3}{\partial z^3} - \frac{\overleftarrow{\partial}^3}{\partial z^3}\gamma(z)\right\}\Psi_R^{0\uparrow}(z')dz'$$

because $\Psi_L^{0\downarrow}$ and $\Psi_L^{0\uparrow}$ possess the same orbital character as $\Psi_R^{0\downarrow}$ and $\Psi_R^{0\uparrow}$, where $\frac{\overrightarrow{\partial}}{\partial z}$ acts to the right, whereas $\frac{\overleftarrow{\partial}}{\partial z}$ acts to the left. This is Eq. (A5) in Ref. [15] . The authors finally obtained:

$$\begin{aligned}
\delta t^{\uparrow\uparrow} &= -\delta t^{\downarrow\downarrow} = \frac{-im^*}{\hbar^2 k}\int_0^a \Psi_L^{0\uparrow}(z')\frac{i}{2}\left\{\gamma(z)\frac{\overrightarrow{\partial}^3}{\partial z^3} - \frac{\overleftarrow{\partial}^3}{\partial z^3}\gamma(z)\right\}\Psi_R^{0\uparrow}(z')dz' \\
&= \frac{-im^*}{\hbar^2 k}\frac{i}{2}\gamma\int_0^a \left\{\Psi_L^{0\uparrow}(z')\frac{\partial^3\Psi_R^{0\uparrow}(z')}{\partial z^3} - \Psi_R^{0\uparrow}(z')\frac{\partial^3\Psi_L^{0\uparrow}(z')}{\partial z^3}\right\}dz' \\
&= \frac{\gamma m^* q^2 a}{2\hbar^2}t_k.
\end{aligned}$$

The conclusion is that the correction to the transmission coefficient is independent of the incoming spin direction, $\left|\delta t^{\uparrow\uparrow}\right|^2 = \left|\delta t^{\downarrow\downarrow}\right|^2$, in the present situation. It means that there is no particular spin filtering effect with normal electron ingoing but only spin-dephasing or spin-rotation effects along the [110] direction like demonstrated by Nguyen *et al.* [31].

6.6 Scattering at spin-orbit-split and exchange-split interfaces; connection to Chapter 5 [Present work]

After having discussed the perturbative scattering methods used, we now consider the properties of the scattering asymmetry and the anomalous tunnel Hall effect we have developed in Chapter 5 and which constitutes our main task. Before having presented the general expression of the transmission coefficient adapted to the present issues, we will consider the respective cases of:

(i) The perturbative scattering asymmetry and tunneling Hall effect introduced by the in-plane and the out-of-plane Dresselhaus *SOI components at left for left incoming waves*.

(ii) The perturbative scattering asymmetry and tunneling Hall effect introduced by *SOI at right with left incoming waves*.

(iii) The perturbative scattering asymmetry and tunneling Hall effect introduced by *SOI at left and right with left incoming waves* before analyzing the resulting effect from symmetry arguments.

We have deliberately chosen here to leave some analytical developments in Appendix B for readers who are interested in the detail of the calculations. We refer the structure to the x, y, and z are cubic axes; $x\|[100]$, $y\|[010]$, and $z\|[001]$ and consider the properties of electron scattering at the interface $z = 0$ between two identical T_d ferromagnetic semiconductors (GaMnAs,...) grown along the z axis. The magnetizations are anti-parallel and are fixed along the x direction. The incident wavevector is $\mathbf{k} = (0,\ \xi,\ k)$.

We first detail the analytical derivation of the corresponding system Green's function before discussing the properties of transmission and asymmetry of transmission

when one considers respectively spin-orbit at left and at right and both in left and right contacts. Of course, some transmissions are linked among some general symmetry properties of the S-matrix derived in Appendix A2.

6.6.1 Reflection, transmission and perturbating potential

The unperturbed Hamiltonian is:

$$\hat{H}_0 = \frac{\hbar^2}{2m^*}\left(k^2+\xi^2\right)\hat{\mathbb{I}} + \epsilon w\sigma_x, \tag{137}$$

where $\epsilon = 1$ in the left region and $\epsilon = -1$ in the right region. The SOI is introduced as a perturbating potential:

$$\begin{aligned}\hat{H}_D &= \left[\frac{\xi^2\sigma_z}{2}\left(\gamma(z)k + k^+\gamma(z)\right) - \frac{\xi\sigma_y}{2}\left(\gamma(z)k^2 + \left(k^+\right)^2\gamma(z)\right)\right] \\ &= -\frac{i\xi^2\sigma_z}{2}\left(\gamma(z)\overrightarrow{\frac{\partial}{\partial z}} - \overleftarrow{\frac{\partial}{\partial z}}\gamma(z)\right) + \frac{\xi\sigma_y}{2}\left(\gamma(z)\overrightarrow{\frac{\partial^2}{\partial z^2}} + \overleftarrow{\frac{\partial^2}{\partial z^2}}\gamma(z)\right),\end{aligned}$$

The unperturbed Hamiltonian in Eq. 137 possesses the following eigenvalues

$$\mathcal{E} = \frac{\hbar^2}{2m^*}\left(k_1^2+\xi^2\right) - w, \text{ and } \mathcal{E} = \frac{\hbar^2}{2m^*}\left(k_2^2+\xi^2\right) + w\,;$$

with the respective eigenvectors

$$|\uparrow\rangle = \frac{1}{\sqrt{2}}\begin{pmatrix}1\\1\end{pmatrix}, \text{ and } |\downarrow\rangle = \frac{1}{\sqrt{2}}\begin{pmatrix}1\\-1\end{pmatrix}.$$

In this new basis $|S\rangle \otimes \{|\downarrow\rangle\,,\ |\uparrow\rangle\}$, this Hamiltonian writes:

$$\hat{H}_0 = \begin{array}{c} \\ \\ \end{array}\begin{array}{c} \begin{array}{cc} |S\downarrow\rangle & \qquad |S\uparrow\rangle \end{array} \\ \begin{bmatrix} \frac{\hbar^2}{2m^*}\left(k_1^2+\xi^2\right) - w & 0 \\ 0 & \frac{\hbar^2}{2m^*}\left(k_2^2+\xi^2\right) + w \end{bmatrix} \end{array}.$$

We now consider the electron transmission within an incident energy range in the exchange step, $-w < \mathcal{E} < w$, where the transmission asymmetry takes place, so that k_1 is real whereas k_2 is pure imaginary. It is then quite convenient to replace k_2 by ik_2. The two solutions of the homogeneous Schrödinger equation, Ψ_R^0 and Ψ_L^0, are given by:

$$\left(\mathcal{E}\hat{\mathbb{I}} - \hat{H}_0\right)\begin{bmatrix}\Psi_R^{0\uparrow}\\ \Psi_R^{0\downarrow}\end{bmatrix} = 0,$$

and

$$\left(\mathcal{E}\hat{\mathbb{I}} - \hat{H}_0\right)\begin{bmatrix}\Psi_L^{0\uparrow}\\ \Psi_L^{0\downarrow}\end{bmatrix} = 0,$$

to obtain:

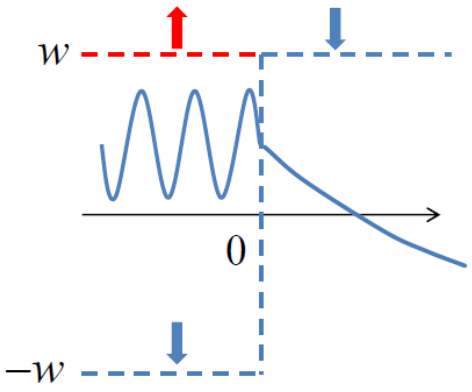

Figure 49: Scheme of a ↓-spin electron, $\Psi_R^{\downarrow 0}$, tunneling through an exchange step of height $2w$ from the left to the right side.

$$\Psi_R^{\downarrow 0}(z) = \left(e^{ik_1 z_<} + r_{R\downarrow} e^{-ik_1 z_<} + t_{R\downarrow} e^{-k_2 z_>}\right), \tag{138}$$

and

$$\Psi_R^{\uparrow 0}(z) = \left(e^{-k_2 z_<} + r_{R\uparrow} e^{k_2 z_<} + t_{R\uparrow} e^{ik_1 z_>}\right) \tag{139}$$

together with

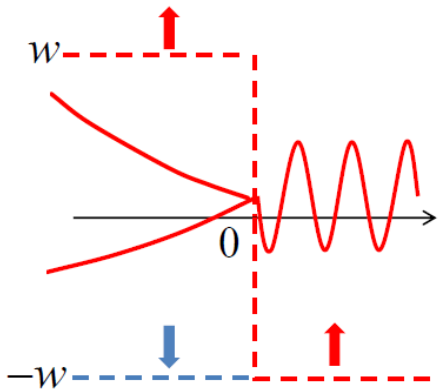

Figure 50: Scheme of an ↑-spin electron, $\Psi_R^{\uparrow 0}$, tunneling through an exchange step of heigh $2w$ from the left to the right side.

$$\Psi_L^{\downarrow 0}(z) = \left(e^{k_2 z_>} + r_{L\downarrow} e^{-k_2 z_>} + t_{L\downarrow} e^{-ik_1 z_<}\right), \tag{140}$$

and

$$\Psi_L^{\uparrow 0}(z) = e^{-ik_1 z_>} + r_{L\uparrow} e^{ik_1 z_>} + t_{L\uparrow} e^{k_2 z_<}. \tag{141}$$

The reflection and transmission amplitudes are then found via the matching conditions at $z = 0$ with possible transmission from propagative to evanescent states ($t_{R\downarrow}$ and $t_{L\uparrow}$) and vice-versa ($t_{L\uparrow}$ and $t_{L\downarrow}$). In details, the matching conditions at $z = 0$ for $\Psi_R^{\downarrow 0}$ are

$$\begin{cases} 1 + r_{R\downarrow} = t_{R\downarrow}, \\ ik_1 - ik_1 r_{R\downarrow} = -k_2 t_{R\downarrow}, \end{cases} \tag{142}$$

thus giving:

$$t_{R\downarrow} = t_{L\uparrow} = \frac{2k_1}{k_1 + ik_2} \text{ and } r_{R\downarrow} = r_{L\uparrow} = \frac{k_1 - ik_2}{k_1 + ik_2}. \tag{143}$$

The matching conditions at $z = 0$ for $\Psi_R^{\uparrow 0}$ are

$$\begin{cases} 1 + r_{R\uparrow} = t_{R\uparrow}, \\ -k_2 + k_2 r_{R\uparrow} = ik_1 t_{R\uparrow}, \end{cases} \tag{144}$$

to give:

$$t_{R\uparrow} = t_{L\downarrow} = \frac{2k_2}{k_2 - ik_1}. \tag{145}$$

We now derive the perturbed potential $\hat{V} = \hat{H}_{SO}$ and show that it will acquire a pure non-diagonal form like:

$$\hat{V} = \begin{bmatrix} 0 & V^{\uparrow\downarrow} \\ V^{\downarrow\uparrow} & 0 \end{bmatrix},$$

where the details of the SOI Hamiltonian form can be found in Appendix B1.

$$\begin{aligned} V^{\uparrow\downarrow} &= \langle\uparrow|\hat{H}_D|\downarrow\rangle, \\ &= \langle\uparrow| \left\{ -\frac{i\xi^2\sigma_z}{2} \left(\gamma(z)\overrightarrow{\frac{\partial}{\partial z}} - \overleftarrow{\frac{\partial}{\partial z}}\gamma(z) \right) + \frac{\xi\sigma_y}{2} \left(\gamma(z)\overrightarrow{\frac{\partial^2}{\partial z^2}} + \overleftarrow{\frac{\partial^2}{\partial z^2}}\gamma(z) \right) \right\} |\downarrow\rangle, \\ &= \frac{-i\xi^2}{2} \left(\gamma(z)\overrightarrow{\frac{\partial}{\partial z}} - \overleftarrow{\frac{\partial}{\partial z}}\gamma(z) \right) + \frac{i\xi}{2} \left(\gamma(z)\overrightarrow{\frac{\partial^2}{\partial z^2}} + \overleftarrow{\frac{\partial^2}{\partial z^2}}\gamma(z) \right), \\ &= \left(\frac{-i\xi^2}{2}\gamma(z)\overrightarrow{\frac{\partial}{\partial z}} + \frac{i\xi}{2}\gamma(z)\overrightarrow{\frac{\partial^2}{\partial z^2}} \right) + \left(\frac{i\xi^2}{2}\overleftarrow{\frac{\partial}{\partial z}}\gamma(z) + \frac{i\xi}{2}\overleftarrow{\frac{\partial^2}{\partial z^2}}\gamma(z) \right), \end{aligned}$$

and

$$\begin{aligned} V^{\downarrow\uparrow} &= \frac{-i\xi^2}{2} \left(\gamma(z)\overrightarrow{\frac{\partial}{\partial z}} - \overleftarrow{\frac{\partial}{\partial z}}\gamma(z) \right) - \frac{i\xi}{2} \left(\gamma(z)\overrightarrow{\frac{\partial^2}{\partial z^2}} + \overleftarrow{\frac{\partial^2}{\partial z^2}}\gamma(z) \right) \\ &= \left(\frac{-i\xi^2}{2}\gamma(z)\overrightarrow{\frac{\partial}{\partial z}} - \frac{i\xi}{2}\gamma(z)\overrightarrow{\frac{\partial^2}{\partial z^2}} \right) + \left(\frac{i\xi^2}{2}\overleftarrow{\frac{\partial}{\partial z}}\gamma(z) - \frac{i\xi}{2}\overleftarrow{\frac{\partial^2}{\partial z^2}}\gamma(z) \right). \end{aligned}$$

As mentioned before, we stress again on the particular point that the incident energy value is chosen to be smaller that the exchange step. It results that, in the right contact, the $\uparrow$-spin state admits a pure propagative character whereas the $\downarrow$-spin state is purely evanescent. Following Eq. 130, the correction to the transmitted wave function for the $\uparrow$-spin state writes:

$$\begin{aligned} \delta\Psi_R^{\uparrow}(z) &= \int G_0^{\uparrow\uparrow}(z, z') V^{\uparrow\downarrow}(z') \Psi_R^{0\downarrow}(z') dz' \\ &= \Psi_R^{0\uparrow}(z) \int \frac{\Psi_L^{0\uparrow}(z')\, V^{\uparrow\downarrow}(z') \Psi_R^{0\downarrow}(z') dz'}{W^{\uparrow\uparrow}(z')}. \end{aligned}$$

The host materials at left and right contacts are made identical and free of SOI so that the Wronskian potential is independent of the z' axis. We then obtain:

$$W^{\uparrow\uparrow} = \frac{\hbar^2}{2m^*} 2ik_1 t_{R\uparrow} = i\frac{\hbar^2 k_1}{m^*} t_{R\uparrow},$$

and

$$\delta\Psi_R^{\uparrow}(z) = \frac{-im^*}{\hbar^2 k_1} e^{ik_1 z} \int \Psi_L^{0\uparrow}(z')\, V^{\uparrow\downarrow}(z') \Psi_R^{0\downarrow}(z') dz'.$$

The correction to the amplitude of transmission is therefore calculated to be:

$$\begin{aligned} \delta t^{\uparrow\downarrow} &= \frac{m^*}{i\hbar^2 k_1} \int \Psi_L^{0\uparrow}(z')\, V^{\uparrow\downarrow}(z') \Psi_R^{0\downarrow}(z') dz' \\ &= \frac{m^*}{i\hbar^2 k_1} \int_{-\infty}^{+\infty} \Psi_L^{0\uparrow}(z') \left[-\frac{i\xi^2}{2}\gamma(z)\frac{\partial \Psi_R^{\downarrow 0}(z')}{\partial z} + \frac{i\xi}{2}\gamma(z)\frac{\partial^2 \Psi_R^{\downarrow 0}(z')}{\partial z^2} \right] dz' \\ &\quad + \frac{m^*}{i\hbar^2 k_1} \int_{-\infty}^{+\infty} \left[\frac{i\xi^2}{2}\gamma(z)\frac{\partial \Psi_L^{0\uparrow}(z')}{\partial z} + \frac{i\xi}{2}\gamma(z)\frac{\partial^2 \Psi_L^{0\uparrow}(z')}{\partial z^2} \right] \Psi_R^{\downarrow 0}(z') dz. \end{aligned} \tag{146}$$

We are now going to calculate the properties of the carrier transmission for the different SOI configurations possibly including SOI to the left, SOI to the right, and SOI in both contacts for the incoming left electrons. We will compare the resulting transport asymmetry in each case.

6.6.1.1 ***Case of SOI on the left for incoming left electrons***

We first note that the zeroth-order transmission coefficient, $\tau_0 = 0$, from left-to-right (or equivalently right-to-left) without involving spin-orbit is zero without spin-mixing interactions. Then, from Eq. 146, the transmission amplitude, τ_L, only involving SOI on the left electrode, is given by:

$$\begin{aligned} \tau_L &= \frac{m^*}{i\hbar^2 k_1} \int_{-\infty}^{0} \Psi_L^{0\uparrow}(z') \left[-\frac{i\gamma\xi^2}{2}\frac{\partial}{\partial z'} + \frac{i\gamma\xi}{2}\frac{\partial^2}{\partial z'^2} \right] \Psi_R^{\downarrow 0}(z') dz' \\ &\quad + \frac{m^*}{i\hbar^2 k_1} \int_{-\infty}^{0} \left[\frac{i\gamma\xi^2}{2}\frac{\partial \Psi_L^{0\uparrow}(z')}{\partial z'} + \frac{i\gamma\xi}{2}\frac{\partial^2 \Psi_L^{0\uparrow}(z')}{\partial^2 z'} \right] \Psi_R^{\downarrow 0}(z') dz'. \end{aligned} \tag{147}$$

After lengthy calculations introduced in Appendix B. 2.1, with the following notations $k_1 = K$ (incoming propagative wavevector) and $k_2 = \lambda K$ (imaginary transmitted wavevector), one obtains:

$$\tau_L = \frac{1}{2w} \frac{\gamma\xi K^2}{(1+i\lambda)^2} \left\{ \frac{\xi}{K}(3\lambda^2 - 1) + 2\lambda\left(\lambda^2 - 1\right) \right\} = \frac{C(\xi, K, \lambda)}{2} \tag{148}$$

with $C(\xi, K, \lambda)$ as introduced in Chapter 5.

6.6.1.2 *Case of SOI at right for incoming left electrons*

One now considers the case of SOI at right with incoming left electrons. *We note that the zeroth-order transmission coefficient, $\tau_0 = 0$ from left-to-right (or equivalently right-to-left) without involving spin-orbit is zero without spin-mixing interactions.*

The amplitude of transmission writes in this case:

$$\begin{aligned}\tau_R &= \frac{m^*}{i\hbar^2 k_1}\int_0^{+\infty}\Psi_L^{0\uparrow}(z')\left[-\frac{i\gamma\xi^2}{2}\frac{\partial}{\partial z'}+\frac{i\gamma\xi}{2}\frac{\partial^2}{\partial z'^2}\right]\Psi_R^{\downarrow 0}(z')dz' \\ &+\frac{m^*}{i\hbar^2 k_1}\int_0^{+\infty}\left[\frac{i\gamma\xi^2}{2}\frac{\partial\Psi_L^{0\uparrow}(z')}{\partial z'}+\frac{i\gamma\xi}{2}\frac{\partial^2\Psi_L^{0\uparrow}(z')}{\partial^2 z'}\right]\Psi_R^{\downarrow 0}(z')dz'.\end{aligned}$$

The calculation detail is shown in Appendix B. 2.2. We obtain

$$\tau_R = \tau_L.$$

This equation agrees with the consequence of the scattering matrix developed in Eq. 87 in Chapter 4.

6.6.1.3 *Case of spin-orbit interactions on the left and right side for left incoming electrons.*

We consider here the case of SOI interactions in the whole heterostructure in the both left and right contacts. To first order of perturbation, the transmission coefficient is simply the sum of the two transmission coefficients τ_L and τ_R from simple argument of the linear response theory. We then derive that the transmission coefficient writes $\tau = \tau_L + \tau_R = 2\tau_L$ thus giving:

$$\begin{aligned}\tau &= \frac{m^*}{i\hbar^2 k_1}\int_{-\infty}^{+\infty}\Psi_L^{0\uparrow}(z')\left[-\frac{i\xi^2}{2}\gamma(z)\frac{\partial\Psi_R^{\downarrow 0}(z')}{\partial z}+\frac{i\xi}{2}\gamma(z)\frac{\partial^2\Psi_R^{\downarrow 0}(z')}{\partial z^2}\right]dz' \\ &+\frac{m^*}{i\hbar^2 k_1}\int_{-\infty}^{+\infty}\left[\frac{i\xi^2}{2}\gamma(z)\frac{\partial\Psi_L^{0\uparrow}(z')}{\partial z}+\frac{i\xi}{2}\gamma(z)\frac{\partial^2\Psi_L^{0\uparrow}(z')}{\partial z^2}\right]\Psi_R^{\downarrow 0}(z')dz' \\ &= \tau_L+\tau_R = 2\tau_L = \left(\frac{\gamma\xi K^2}{w}\right)\frac{\frac{\xi}{K}(3\lambda^2-1)+2\lambda\left(\lambda^2-1\right)}{\left(1+i\lambda\right)^2}.\end{aligned}$$

By perturbative scattering methods, we thus recover the formula derived from the application of the pure matching conditions at the interface (Chapter. 5 and Eq. 7 of our article [18]). This proves the power of this methodology for the calculation of transport properties involving mixed propagative and evanescent electronic states. This perturbative scattering approach is often used to treat the issue of spin-transport like spin-assisted diffusions and spin Hall effects in heavy transition metals and their impurity

alloys. However, it has hardly been employed to investigate the role of the evanescent waves in physical phenomena like skew-tunneling phenomena. We will now use it for the calculation of spin-orbit assisted tunneling transport in the case of a thin tunnel junction where the SOI perturbation is localized in a finite volume (localized electron diffusion equivalent to extrinsic SHE in diluted alloys).

6.6.2 Magnetic tunnel junction with SOI in the barrier: case where SOI is located in a confined region of the space as a spin-orbit diffusive center

6.6.2.1 Calculation of the SOI-assisted transmission coefficient and transmission asymmetry

In the case of a thin tunnel junction, the electron scatters at two different interfaces separated by a barrier and this makes the problem different from the previous treatment. To illustrate this particular issue, we consider the case of a tunnel barrier made of a semiconductor belonging to the T_d -symmetry group separating two ferromagnetic contacts, free of any SOI, still in an antiparallel magnetic configuration (AP). The incident energy lies in the range of the exchange step, $-w < \mathcal{E} < w$, also corresponding to a single incident propagative wave of a pure $\downarrow$ spin character.

The zeroth-order unperturbed Hamiltonian (the back ground Hamiltonian) in the basis $S \otimes \left\{ |\uparrow\rangle = \frac{1}{\sqrt{2}}\binom{1}{1},\ |\downarrow\rangle = \frac{1}{\sqrt{2}}\binom{1}{-1} \right\}$ writes:

$$\hat{H}_0 = \begin{cases} \begin{bmatrix} \gamma_C(k^2+\xi^2) - \epsilon w & 0 \\ 0 & \gamma_C(k^2+\xi^2) + \epsilon w \end{bmatrix} & \text{for } z > 0 \text{ or } z > a \\ \begin{bmatrix} \gamma_C(k^2+\xi^2) + V_0 & 0 \\ 0 & \gamma_C(k^2+\xi^2) + V_0 \end{bmatrix} & \text{for } 0 < z < a \end{cases} . \tag{149}$$

where $\epsilon = 1$ on the left and $\epsilon = -1$ on the right, respectively, and we introduce SOI as a perturbating potential.

In order to simplify the calculation and without loosing generality, we have chosen a particular value for the barrier height, equal to the exchange potential, $V_0 = |w|$, in order to avoid any tunneling scattering for the evanescent wave inside the barrier. By this way, the tunnel transport only involves a single evanescent wave without supplementary reflected waves inside the barrier. The calculation of the more general shape of the GF is given in the article of Aguiar *et al.* [135].

To the first order of the perturbation series of the Lippman-Schingwer equation, the

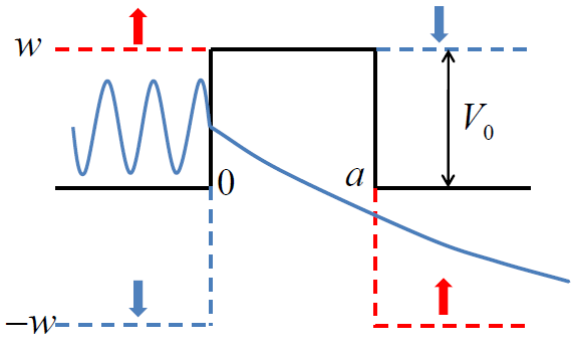

Figure 51: A ↓-spin electron tunnels through a barrier grown along the [001] direction with $V_0 = |w|$ from the left to the right side.

amplitude of transmission, $\delta t^{\downarrow\uparrow}$, is then:

$$\delta t^{\uparrow\downarrow} = \frac{m^*}{i\hbar^2 k_1}\int_0^a \Psi_L^{0\uparrow}(z')\left[-\frac{i\gamma\xi^2}{2}\frac{\partial\Psi_R^{\downarrow 0}(z')}{\partial z}+\frac{i\gamma\xi}{2}\frac{\partial^2\Psi_R^{\downarrow 0}(z')}{\partial z^2}\right]dz' \qquad (150)$$
$$+\frac{m^*}{i\hbar^2 k_1}\int_0^a \left[\frac{i\gamma\xi^2}{2}\frac{\partial\Psi_L^{0\uparrow}(z')}{\partial z}+\frac{i\gamma\xi}{2}\frac{\partial^2\Psi_L^{0\uparrow}(z')}{\partial z^2}\right]\Psi_R^{\downarrow 0}(z')dz',$$

The coefficient of the wave functions $\Psi_R^{0\downarrow}$, and $\Psi_L^{0\uparrow}$, without SOI, are found from the relevant matching condition in a similar way to the case of the exchange step. One then obtains:

$$\Psi_R^{0\downarrow} = t_{R\downarrow}e^{-k_2 z} = \frac{2k_1}{k_1+ik_2}e^{-k_2 z},\ \text{for } z>0 \qquad (151)$$

as well as

$$\Psi_L^{0\uparrow} = t_{L\uparrow}e^{k_2(z-a)} = \frac{2k_1}{k_1+ik_2}e^{k_2(z-a)},\ \text{for } z<a. \qquad (152)$$

The detailed calculations in Appendix B.2.3 give:

$$\delta t^{\uparrow\downarrow} = \frac{e^{-k_2 a}}{\gamma_c}\frac{2\gamma\xi k_2 k_1 a}{(k_1+ik_2)^2}(\xi+k_2). \qquad (153)$$

Without SOI perturbation, the transmission coefficient is also zero in the present situation of incoming/outgoing pure spin states, and consequently, $T^{\uparrow\downarrow} = \left|\delta t^{\uparrow\downarrow}\right|^2$. If one defines again the following parameters $\tan\theta = \xi/K$ ($\Longrightarrow$ $\xi = K\tan\theta$) for the carrier incident angle upon the barrier, and $\eta = \frac{1-\lambda^2}{1+\lambda^2} = \frac{\varepsilon}{w}$ $\left(\Longrightarrow \lambda = \sqrt{\frac{1-\eta}{1+\eta}}\right)$ for the reduced incident kinetic energy like introduced in Chapter 5, we find the asymmetry of transmission for the tunnel barrier case according to:

$$Asymmetry = A = \frac{|\xi+k_2|^2-|-\xi+k_2|^2}{|\xi-k_2|^2+|-\xi-k_2|^2} = 2\frac{\sqrt{(1-\eta)(1+\eta)}\tan\theta}{\tan^2\theta(1+\eta)+(1-\eta)}. \qquad (154)$$

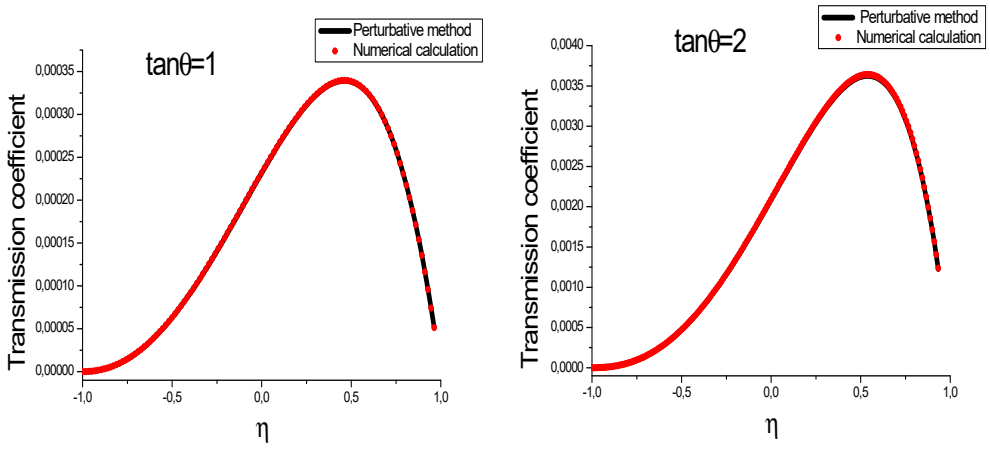

Figure 52: Transmission coefficient for an electron scattering at the interface between GaAs/GaAs in AP configuration calculated by Eq. 153 (black line) and numerical code (red line) with $m^* = 0.067m_{0,}\, \gamma = 24$ eVÅ^3, $w = 150$ meV, barrier thickness 2 nm.

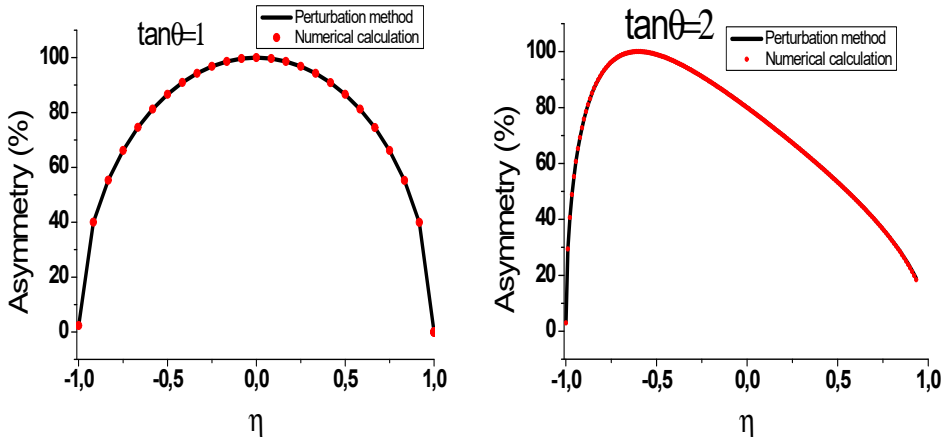

Figure 53: Repective asymmetry transmission in Fig. 52 calculated by Eq. 154 (black line) and 2×2 numerical code (red line).

A first conclusion is that we obtain a very good agreement between the perturbative scattering method and our numerical calculation for the transmission coefficient in Fig. 52 and the asymmetry transmission in Fig. 53. This proves the power of the present method developed to first order. In more details:

The transmission coefficient for an incoming propagative spin-down electron into an outgoing propagative spin-up electron, possible *via* a spin-orbit assisted mechanism (Dresselhaus in the present case), is non-zero after perturbation However, the electronic transmissivity *vs.* incident kinetic energy and incident angle is non-trivial, passing through a maximum located at an energy smaller than the barrier height. This is a peculiarity of the Dresselhaus symmetry. The maximum of transmission depends on the incidence angle ($\tan\theta$ parameter) [see Fig. 52].

In the case of Dresselhaus interaction, like considered here, the maximum of the asymmetry of transmission reaches 100% in any case, which means that the transmission is possible for given electron incidences and fully quenched for the opposite incidence. This particular point in the Brillouin zone (BZ) in the k-space depends on the electron incidence. The **k**.**p** theory gives a maximum of asymmetry when the evanescent wavevector (λ) equals in magnitude the parallel incoming wavevectors in the CB S-band picture. This is another peculiarity of the Dresselhaus interaction. In the case of holes in the VB discussed hereafter in the next chapter, the asymmetry of transmission mediated in the VB by pure core spin-orbit interactions will be associated with the same condition which could be more easily related to the coupling between average orbital moments in the barrier via the p-character orbitals of the VB. One of the very interesting conclusions suggests to infer a pseudo orbital moment for the S-CB electrons experiencing a Dresselhaus potential.

From these whole developments, one can give a general expression for the change of the spin-flip transmitted amplitude for a propagative $\downarrow$ spin S-wave submitted to SOI in a confined region of the space and transmitted into a propagative $\uparrow$-spin S-wave according to the following expression:

$$\delta t^{\sigma\sigma'} = \frac{-im^*}{\hbar^2 k}\int_0^a \Psi_{out}^{0\sigma}(z')V^{\sigma\sigma'}(z')\Psi_{in}^{0\sigma'}(z')dz',$$

where the subscripts (*in*) and (*out*) refer respectively to the unperturbed incoming wave from left with reflection at the left side, and the outgoing wave at right with reflection at the right side (scattering wave, see Ref. [139]).

In Chapter 7, we will give an extension of the perturbation calculations to the case of multiband transport (case of holes in the VB) involving orbital degeneracy like occurring in p-symmetry orbital bands.

CHAPTER VII

PERTURBATIVE SCATTERING APPROACH TO THE SPIN-ORBIT DEPENDENT TUNNELING IN THE VALENCE BAND

7.1 Perturbative scattering methods adapted to orbitally-degenerated valence bands

In this part, we will proof by analytical and numerical methods that the scattering asymmetry process and related anomalous tunnel Hall effect exist also in the VB of semiconductor junctions, only involving core atomic SOI like appearing in a 6-band **k**.**p** Luttinger approach. This is presently a new result that we will show to be connected to some spin-orbit dependent chirality effects in the interaction region with SOI.

This scattering asymmetry process, like previously described in the case of the CB, may be then generalized in the valence band to some *intrinsic* phenomena without invoking necessary odd-potential spin-orbit assistance like Rashba or Dresselhaus SOC terms. We develop, here, the same kind of perturbative scattering approach in a tunnel junction geometry involving *p*-type ferromagnetic semiconductors and spin-polarized holes. The goal is to demonstrate that the forward scattering asymmetry involving mixed propagative (parallel incident wavevector and current) and evanescent tunneling character arise from chirality phenomena (orbital moments). This scattering asymmetry process has been considered in a very recent work dealing with USMR in topological insulator [140] with in-plane current. This new phenomena can also explain the USMR results in an in-plane current geometry involving the GaMnAs compound [77] when the Boltzmann equation for transport is developed up to the second order.

Another interesting experimental situation to explore would be to revisit the case of giant Hall effects observed a decade ago on Ge/GeMn systems characterized by Mn-rich magnetic nanocolumns embedded in a Ge-rich highly conductive phase [141, 142]. The present work puts in evidence a very large anomalous Hall effect of the order of 60% in this kind of systems characterized by a typical distance between nanocolumns of the order of several tens of nms of the order or shorter than the MFP in the Ge-rich phase.

The spin-dependent diffusions and scattering of the p-type carriers on the Mn-rich nanocolumns, like described in this manuscript in the case of 2-dimensionnal

translational systems (2-dimensional multilayers), may explain the same kind of asymmetry of the specular reflection/transmission of carriers on the circumference of the nanocolumns. In order to demonstrate such effects, an analytical calculation should be performed for a cylindrical geometry.

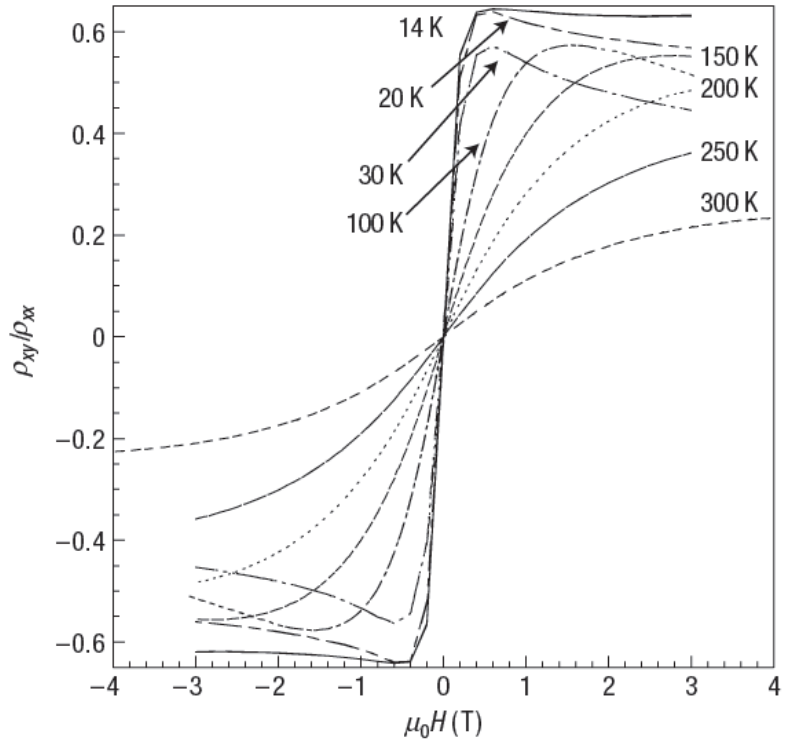

Figure 54: Hall angle ρ_{xy}/ρ_{xx} versus magnetic field recorded at different temperatures [141]**.**

However, the case of spin-polarized carriers in the VB (holes) differs from the case of the CB by several points which makes the treatment of the VB case specific:

(i) The calculations have shown that the intrinsic core SOI of the *p*-type symmetry orbital provides, by itself, properties of skew-tunneling or asymmetry of tunneling transmission *vs.* in-plane wavevectors. This exists without involving supplementary linear Rashba or cubic-Dresselhaus SOC terms, however existing for the T_d symmetry group [44]. The asymmetry of tunneling transmission may then appear in an interaction region of finite volume (tunnel junction) *via intrinsic atomic spin-orbit effects.*

(ii) In addition to spin orbit arising from the *p*-type orbital symmetry, the VB treatment brings a supplementary complexity in term of orbital degeneracy involving light-hole (LH), heavy-hole (HH) and spin-orbit (SO) bands, each of them twice degenerated.

(iii) In the VB of III-V heterostructures, it is well known that, under oblique incidence like considered in this manuscript, LH and HH bands generally mix together on reflection/transmission at interfaces making analytical calculations heavier than the CB case.

(iv) The calculation of spin-orbit perturbative transport in the VB can be undertaken in the same way that the one developed for the CB. By extension to the CB case, the general expression of the correction to the amplitude of the transmission coefficient to the multiband case may be proposed in a form like:

$$\delta t_{(nm)}^{\sigma\sigma'} = \frac{-im_n^*}{\hbar^2 k_n} \sum_l \int_0^d \left[\Psi_{out(n)}^{0\sigma}(z')\right]^* V_{nm}^{\sigma\sigma'}(z') \Psi_{in(m)}^{0\sigma'}(z')\, d\,(z')\,,$$

where now (n) and (m) are the subscript corresponding to the multiband structure of holes in the incoming and outgoing waves to consider, σ and σ' are spin of the wave functions.

It results that the correction to the transmitted wave should be linked to the coupling between corresponding (*in*) and (*out*) wave function and orbital moments of the waves and then to a new kind of chirality phenomena involved in tunnel barriers. This is what we will investigate now in much more details.

To see this, we consider the case of tunneling transport of holes in the VB under some assumptions to make easier analytical calculations in terms of Green's function method. We first work at the limit of almost normal incidence. Second, the most drastic assumption is to consider no spin-orbit Hamiltonian in the contacts, in 6×6 Kane approach, and with SOI only present in the barrier and playing the role of a perturbation potential. We then extend by numerical calculations, in a second part, the $\mathbf{k}.\mathbf{p}$ calculations to a more physical system by including SOI also in electrodes. However, calculations will show that the assumption made while neglecting with SOI in the contacts gives the main results departing not too far from the exact numerical calculations, and thus catching the main trends of the physical processes involved.

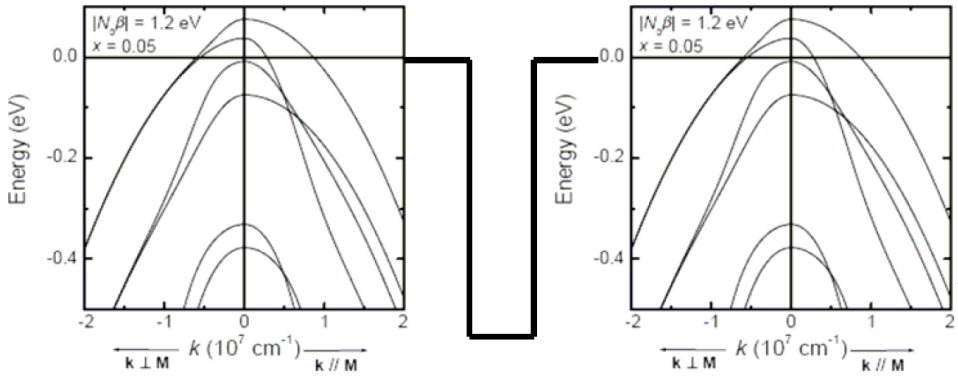

Figure 55: Transmission of electrons through tunnel barrier in the VB with the magnetization direction perpendicular to the wavevector in the contacts.

As an example, we consider a rectangular tunnel barrier grown along the x direction, with respective left and right ferromagnetic contacts in the antiparallel magnetic magnetization with direction along z, and with in-plane incidence along y (x, y, z represent the

cubic axes). To simplify the calculations, we first assume in Chapter 7 corresponding to the perturbation techniques, that the core SOI, $\hat{H}_{SO} = \frac{\hbar}{4m_0^2c^2}\left(\boldsymbol{\nabla}\mathfrak{U} \times \hat{\mathbf{p}}\right).\hat{\boldsymbol{\sigma}}$, is totally neglected in the contacts and is introduced, afterwards, as a perturbation potential in the barrier. This can mimic the case of GaAs barrier sandwiched between two GaMnAs ferromagnetic contacts. Moreover, without loss of generality, we consider that the effective masses remain equal inside and outside the barrier. The true physical situation of SOI in the electrodes (case of GaMnAs electrodes in the real situation) and in the barrier will be treated numerically in a second step, without invoking any perturbative treatment.

In the whole section 7.1, we chose the $6\times6\,\{X, Y, Z\}\bigotimes\{\uparrow, \downarrow\}$ Kane basis functions free of any SOC. By rotation, this basis can be made equivalent to the 6×6 **k.p** Luttinger basis involving the core SOC.

We start by finding the corresponding eigenvectors and eigenvalues before deriving the multiband Green's function as well as the spin-orbit assisted transport properties of SOI-included tunnel barrier junctions in terms of orbital coupling in the barrier.

7.1.1 Hamiltonian, eigenenergies and eigenvectors in the valence bands

7.1.1.1 ***Hypothesis***

In the present calculations, we assume that $k_y \ll k_x$ so that second-order k_y terms can be neglected. Like in the CB, the incident energy lies in an energy range corresponding to the exchange step region, $-w < \mathcal{E} < w$, and the barrier height is equal to the exchange constant energy, $V_0 = |w|$ to make continuous the evanescent character of the tunneling wave functions inside the barrier (we then neglect the scattering of the evanescent wave on the second barrier/right electrode interface for electrons coming from left).

7.1.1.2 ***Description of the Hamiltonian***

Under previous assumption we use the unperturbed 6×6 **k.p** Hamiltonian in the three different regions (left electrode, barrier and right electrode):

$$\hat{H}_0 = \begin{cases} \hat{H}_{kp} + \hat{H}_{exc} & \text{for } x < 0 \text{ or } x > a, \\ \hat{H}_{kp} - V_0 & \text{for } 0 < x < a, \end{cases} \tag{155}$$

where $\hat{H}_{kp}$ represents the kinetic energy, $\hat{H}_{exc}$ the exchange potential, and V_0 is the barrier height (band discontinuity).

$$\hat{H}_{k.p} = \begin{bmatrix} \hat{H}_{k.p}^{\uparrow\uparrow} & 0 \\ 0 & \hat{H}_{k.p}^{\downarrow\downarrow} \end{bmatrix}, \tag{156}$$

with $\hat{H}^{\uparrow\uparrow}_{k.p} = \hat{H}^{\downarrow\downarrow}_{k.p}$, and

$$H^{\uparrow\uparrow}_{k.p} = \frac{\hbar^2}{2m_0} \begin{array}{c} \begin{matrix} |X\uparrow\rangle & |Y\uparrow\rangle & |Z\uparrow\rangle \end{matrix} \\ \begin{bmatrix} (k_x^2+k_y^2) & -k_xk_y\left(\frac{E_{P_X}}{E_{5C}-E_8}+\frac{E_P}{E_6-E_8}\right) & 0 \\ -\frac{E_{P_X}}{E_{5C}-E_8}k_y^2-\frac{E_P}{E_6-E_8}k_x^2 & & \\ -k_xk_y\left(\frac{E_{P_X}}{E_{5C}-E_8}+\frac{E_P}{E_6-E_8}\right) & (k_x^2+k_y^2) & 0 \\ & -\frac{E_{P_X}}{E_{5C}-E_8}k_x^2-\frac{E_P}{E_6-E_8}k_y^2 & \\ 0 & 0 & (k_x^2+k_y^2) \\ & & -\frac{E_{P_X}}{E_{5C}-E_8}(k_x^2+k_y^2) \end{bmatrix} \end{array} \tag{157}$$

We then introduce the M and L parameters according to the notation of Ref [22]

$$\begin{aligned} M &= \left(\frac{E_P}{E_6-E_8}+\frac{E_{PX}}{E_{5C}-E_8}\right), \\ L &= \left(\frac{E_P}{E_6-E_8}-\frac{E_{PX}}{E_{5C}-E_8}\right). \end{aligned}$$

With the definition of these parameters $(1-(M-L)/2)^{-1}$ is the effective mass of the HH (in unit of $\frac{2m_0}{\hbar^2}$) whereas $(1-(M+L)/2)^{-1}$ is the effective mass of the LH. For simplicity, we have chosen the parameters to make *the HH dispersion nearly flat*, $1 \approx (M-L)/2$. Within this approach, under oblique incidence, the LH and HH bands weakly mix together upon the reflection/transmission processes and this makes the analytical development easier. Consequently, without SOI, the HH and LH states can be almost transmitted like free carriers with respective effective masses m^*_{HH}, and $m^*_{LH} = -L^{-1}$ with a predominance for the LH transmission (tunneling).

The exchange Hamiltonian in these basis is written:

$$\hat{H}_{exc} = \begin{array}{c} \begin{matrix} |X\uparrow\rangle & |Y\uparrow\rangle & |Z\uparrow\rangle & |X\downarrow\rangle & |Y\downarrow\rangle & |Z\downarrow\rangle \end{matrix} \\ \begin{bmatrix} \epsilon w & 0 & 0 & 0 & 0 & 0 \\ 0 & \epsilon w & 0 & 0 & 0 & 0 \\ 0 & 0 & \epsilon w & 0 & 0 & 0 \\ 0 & 0 & 0 & -\epsilon w & 0 & 0 \\ 0 & 0 & 0 & 0 & -\epsilon w & 0 \\ 0 & 0 & 0 & 0 & 0 & -\epsilon w \end{bmatrix} \end{array}, \tag{158}$$

where $\epsilon = 1$ at left, and $\epsilon = -1$ at right contacts (opposite magnetizations).

The atomic SOI to consider in the first order of perturbation calculation, $\hat{H}_{SO} = \frac{\hbar}{4m_0^2c^2}\left(\boldsymbol{\nabla}\mathfrak{U}\times\hat{\mathbf{p}}\right).\hat{\boldsymbol{\sigma}}$, writes in the present basis:

$$\hat{H}_{SO} = \begin{array}{c} \begin{array}{cccccc} |X\uparrow\rangle & |Y\uparrow\rangle & |Z\uparrow\rangle & |X\downarrow\rangle & |Y\downarrow\rangle & |Z\downarrow\rangle \end{array} \\ \begin{bmatrix} 0 & -i\Delta/3 & 0 & 0 & 0 & \Delta/3 \\ i\Delta/3 & 0 & 0 & 0 & 0 & -i\Delta/3 \\ 0 & 0 & 0 & -\Delta/3 & i\Delta/3 & 0 \\ 0 & 0 & -\Delta/3 & 0 & i\Delta/3 & 0 \\ 0 & 0 & -i\Delta/3 & -i\Delta/3 & 0 & 0 \\ \Delta/3 & i\Delta/3 & 0 & 0 & 0 & 0 \end{bmatrix} \end{array}, \tag{159}$$

7.1.1.3 ***Eigenvalues and eigenvectors in the left electrode***

We consider also the situation of a minimum mixing between LH and HH under quasi normal incidence. However, one cannot totally avoid the band mixing between LH and HH bands on transmission, and reflection processes as we will see hereafter. In order to compute such transmission, one needs both eigenvectors and eigenvalues.

The eigenvectors and respective eigenvalues of the unperturbed Hamiltonian at the left contact, H_L, are respectively:

Eigenvalues	Eigenvectors	States, k_x
$\mathcal{E} = \frac{\hbar^2}{2m_0}\left(1-\frac{M-L}{2}\right)k_x^2 + w = \frac{\hbar^2 k_x^2}{2m^*_{HH}} + w$	$Z\uparrow$	Propagative, $k_x = k_1$
$\mathcal{E} = \frac{\hbar^2}{2m_0}\left(1-\frac{M-L}{2}\right)k_x^2 + w = \frac{\hbar^2 k_x^2}{2m^*_{HH}} + w$	$HH\uparrow = -\frac{Mk_y}{Lk_x}X\uparrow + Y\uparrow \approx Y\uparrow$ (because $\frac{Mk_y}{Lk_2} \ll 1$)	Propagative, $k_x = k_2$
$\mathcal{E} = \frac{\hbar^2}{2m_0}\left(1-\frac{M+L}{2}\right)k_x^2 + w = \frac{\hbar^2 k_x^2}{2m^*_{LH}} + w$	$LH\uparrow = X\uparrow + \frac{Mk_y}{Lk_x}Y\uparrow$	Propagative, $k_x = k_3$
$\mathcal{E} = \frac{\hbar^2}{2m_0}\left(1-\frac{M-L}{2}\right)k_x^2 - w = \frac{\hbar^2 k_x^2}{2m^*_{HH}} - w$	$Z\downarrow$	Evanescent, $k_x = iK_1$
$\mathcal{E} = \frac{\hbar^2}{2m_0}\left(1-\frac{M-L}{2}\right)k_x^2 - w = \frac{\hbar^2 k_x^2}{2m^*_{HH}} - w$	$HH\downarrow = Y\downarrow$	Evanescent, $k_x = iK_2$
$\mathcal{E} = \frac{\hbar^2}{2m_0}\left(1-\frac{M+L}{2}\right)k_x^2 - w = \frac{\hbar^2 k_x^2}{2m^*_{LH}} - w$	$LH\downarrow = X\downarrow + \frac{Mk_y}{Lk_x}Y\downarrow$	Evanescent, $k_x = iK_3$

,

where m^*_{LH}, m^*_{HH}, $m^*_Z = m^*_{HH}$ are the effective masses in the LH, HH and Z bands, respectively. From the hypothesis we used, the eigenvectors are described by *pure spin states* (no SOI in the leads). Moreover, we find that the orbital character of the eigenvectors are provided by the pure Z and Y waves (z and y are the two in-plane directions) for the two HH bands. The LH orbital eigenvector mixes the X and Y orbitals according to $|LH\rangle = \left|X + \frac{Mk_y}{Lk_x}Y\right\rangle$.

A first important conclusion is that none of these bands, of propagative (contact) or evanescent (barrier) character admits an orbital moment except the LH-band. Indeed, the $|LH\rangle = \left|X + \frac{Mk_y}{Lk_x}Y\right\rangle$ band must be associated with a value of the orbital moment in the barrier equal to

$$\langle LH|\,\hat{L}_z\,|LH\rangle = \frac{\frac{Mk_y}{LK_3}}{1+\left(\frac{Mk_y}{LK_3}\right)^2}\mu_B, \tag{160}$$

where μ_B is the Bohr magneton. The same will occur at the right electrode by symmetry. This is clearly an important feature to consider for the following.

7.1.1.4 ***Eigenvalues and eigenvectors in the right electrode***

In the same way, the eigenvalues and respective eigenvectors of the unperturbed Hamiltonian at the right contact, $\hat{H}_R$, are equivalent to those of the left contact Hamiltonian provided that the $\downarrow$- spin is now reversed into $\uparrow$- spin to give:

Eigenvalues	Eigenvectors	States, k_x
$\mathcal{E} = \frac{\hbar^2 k_x^2}{2m^*_{HH}} + w$	$Z\downarrow$	Propagative, $k_x = k_1$
$\mathcal{E} = \frac{\hbar^2 k_x^2}{2m^*_{HH}} + w$	$HH\downarrow = -\frac{Mk_y}{Lk_x}X\downarrow + Y\uparrow \approx Y\downarrow$	Propagative, $k_x = k_2$
$\mathcal{E} = \frac{\hbar^2 k_x^2}{2m^*_{LH}} + w$	$LH\downarrow = X\downarrow + \frac{Mk_y}{Lkx}Y\downarrow$	Propagative, $k_x = k_3$
$\mathcal{E} = \frac{\hbar^2 k_x^2}{2m^*_{HH}} - w$	$Z\uparrow$	Evanescent, $k_x = iK_1$
$\mathcal{E} = \frac{\hbar^2 k_x^2}{2m^*_{HH}} - w$	$HH\uparrow = Y\uparrow$	Evanescent, $k_x = iK_2$
$\mathcal{E} = \frac{\hbar^2 k_x^2}{2m^*_{HH}} - w$	$LH\uparrow = X\uparrow + \frac{Mk_y}{Lkx}Y\uparrow$	Evanescent, $k_x = iK_3$

Note that $k_1 = k_2$, and $K_1 = K_2$, and that these values are much larger than k_3, and K_3 because of the almost zero dispersion of the HH band we chose.

In the new basis $\{LH\uparrow,\ LH\downarrow, HH\uparrow, HH\downarrow, Z\uparrow,\ Z\downarrow\}$, the bare unperturbed Hamiltonian possesses a block diagonal form according to:

$$\hat{H}_0 = \begin{bmatrix} \hat{H}_{0,\,LH} & 0 & 0 \\ 0 & \hat{H}_{0,\,HH} & 0 \\ 0 & 0 & \hat{H}_{0,\,Z} \end{bmatrix},$$

where

$$\hat{H}_{0,\,LH} = \begin{array}{c} \begin{array}{cc} |LH\uparrow\rangle & |LH\downarrow\rangle \end{array} \\ \begin{bmatrix} \hat{H}_{0,\,LH\uparrow} & 0 \\ 0 & \hat{H}_{0,\,LH\downarrow} \end{bmatrix} \end{array},$$

$$\hat{H}_{0,\,HH} = \begin{array}{c} \begin{array}{cc} |HH\uparrow\rangle & |HH\downarrow\rangle \end{array} \\ \left[\begin{array}{cc} \hat{H}_{0,\,LH\uparrow} & 0 \\ 0 & \hat{H}_{0,\,LH\downarrow} \end{array}\right] \end{array},$$

and

$$\hat{H}_{Z} = \begin{array}{c} \begin{array}{cc} |Z\uparrow\rangle & |Z\downarrow\rangle \end{array} \\ \left[\begin{array}{cc} \hat{H}_{0,\,Z\uparrow} & 0 \\ 0 & \hat{H}_{0,\,Z\downarrow} \end{array}\right] \end{array}$$

with

$$\hat{H}_{0,\,\alpha\uparrow} = \begin{cases} \frac{\hbar^2 k_x^2}{2m_\alpha^*} + w \text{ for } x < 0 \\ \frac{\hbar^2 k_x^2}{2m_\alpha^*} - w \text{ for } x > 0 \end{cases},$$

$$\hat{H}_{0,\,\alpha\downarrow} = \begin{cases} \frac{\hbar^2 k_x^2}{2m_\alpha^*} - w \text{ for } x < a \\ \frac{\hbar^2 k_x^2}{2m_\alpha^*} + w \text{ for } x > a \end{cases}$$

and where the notation α is used for $\{LH,\ HH,\ Z\}$. One important point to note is that the basis are exactly the same for the different layers constituting the junctions. We consider this common basis as the starting point of the perturbation calculation.

7.1.1.5 ***Spin-orbit Hamiltonian and Green's functions***

In the $\{LH,\ HH,\ Z\} \otimes \{\uparrow,\ \downarrow\}$ new basis, with the atomic SOI being switched on in the barrier, and using in the perturbative scattering treatment, the Hamiltonian is :

$$\hat{H}_{SOI} = \begin{array}{c} \begin{array}{cccccc} |LH\uparrow\rangle & |LH\downarrow\rangle & |HH\uparrow\rangle & |HH\downarrow\rangle & |Z\uparrow\rangle & |Z\downarrow\rangle \end{array} \\ \left[\begin{array}{cccccc} 0 & 0 & \frac{-i\Delta}{3} & 0 & 0 & \frac{\Delta}{3}\left(1 - \frac{Mk_y}{LK_3}\right) \\ 0 & 0 & 0 & \frac{-i\Delta}{3} & -\frac{\Delta}{3}\left(1 + \frac{Mk_y}{LK_3}\right) & 0 \\ \frac{i\Delta}{3} & 0 & 0 & 0 & 0 & \frac{-i\Delta}{3} \\ 0 & \frac{-i\Delta}{3} & 0 & 0 & \frac{-i\Delta}{3} & 0 \\ 0 & \frac{\Delta}{3}\left(-1 + \frac{Mk_y}{LK_3}\right) & 0 & \frac{i\Delta}{3} & 0 & 0 \\ \frac{\Delta}{3}\left(1 + \frac{Mk_y}{LK_3}\right) & 0 & \frac{i\Delta}{3} & 0 & 0 & 0 \end{array}\right] \end{array} \quad (161)$$

.

7.1.2 Green's function

As mentioned before, the bare unperturbed Hamiltonian is diagonal in the basis $\{LH,\ HH,\ Z\} \otimes \{\uparrow,\ \downarrow\}$. By extending the GF in the CB to the degenerated basis, we obtain the GF in the VB, satisfying:

$$\left[G_0\left(\mathcal{E}, z, z'\right)\right]_{ml} = \sum_{j,k} \frac{\Psi_m^{0*}\left(k_j, z'\right)\Psi_l^0\left(k_j, z'\right)}{\mathcal{E} - \mathcal{E}\left(k_j\right) + i\eta}\delta_{ml}, \quad (162)$$

where $(j,m,n) = \{LH\uparrow, LH\downarrow, HH\uparrow, HH\downarrow, Z\uparrow, Z\downarrow\}$, in the case of an orthogonal basis $\langle \Psi_m^0(k_j)|\ \Psi_l^0(k_j)\rangle = \delta_{ml}$ like one consider here.

The expression of the GF, of a diagonal form, is:

$$G_0(x,x') = \begin{array}{c} \begin{array}{cccccc} |LH\uparrow\rangle & |LH\downarrow\rangle & |HH\uparrow\rangle & |HH\downarrow\rangle & |Z\uparrow\rangle & |Z\downarrow\rangle \end{array} \\ \left[\begin{array}{cccccc} G_{LH}^{\uparrow\uparrow} & 0 & 0 & 0 & 0 & 0 \\ 0 & G_{LH}^{\downarrow\downarrow} & 0 & 0 & 0 & 0 \\ 0 & 0 & G_{HH}^{\uparrow\uparrow} & 0 & 0 & 0 \\ 0 & 0 & 0 & G_{HH}^{\downarrow\downarrow} & 0 & 0 \\ 0 & 0 & 0 & 0 & G_{Z}^{\uparrow\uparrow} & 0 \\ 0 & 0 & 0 & 0 & 0 & G_{Z}^{\downarrow\downarrow} \end{array}\right] \end{array}.$$

As developed in the same way than in CB, the diagonal components of the GF write:

$$\left(\mathcal{E} - \hat{H}_{0,\alpha\sigma}\right) G_\alpha^{\sigma\sigma}(x,\ x') = \delta(x-x'), \tag{163}$$

with α being band index. The GF $G_\alpha^{\sigma\sigma}(x,\ x')$ can be formed via the expression of the ingoing wave on the left $\Psi_{R,\,\alpha}^{0\sigma}$ and the ingoing wave on the right $\Psi_{L,\,\alpha}^{0\sigma}$. The functions $\Psi_{R,\,\alpha}^{0\sigma}$ and $\Psi_{L,\,\alpha}^{0\sigma}$ satisfy the homogenous Schrödinger equation.

We consider $G_{LH}^{\downarrow\downarrow}(x,\ x')$ for down-spin electrons left coming from as an example,

$$G_{LH}^{\downarrow\downarrow}(x,\ x') = \frac{\Psi_{R,\,LH}^{0\downarrow}(x)\Psi_{L,\,LH}^{0\downarrow}(x')\Theta(x-x') + \Psi_{R,\,LH}^{0\downarrow}(x')\Psi_{L,\,LH}^{0\downarrow}(\ x)\Theta(x'-x)}{W_{LH}^{\downarrow\downarrow}(x')}, \tag{164}$$

As mentioned before, the mixing between HH and LH is small and neglected in our calculations in the limit of an almost normal incidence . The wave functions $\Psi_{R,\,LH}^{0\downarrow}$ and $\Psi_{L,\,LH}^{0\downarrow}$ satisfy the homogenous Schrödinger equation for the $LH\downarrow$ state according to:

$$\begin{cases} \left(\mathcal{E} - \frac{\hbar^2 k_x^2}{2m_{LH}^*} - w\right)\Psi_{LH}^{0\downarrow}(x) = 0 & \text{for } x < a, \\ \left(\mathcal{E} - \frac{\hbar^2 k_x^2}{2m_{LH}^*} + w\right)\Psi_{LH}^{0\downarrow}(x) = 0 & \text{for } x > a\ , \end{cases}$$

One obtains:

$$\Psi_{L,\,LH}^{0\downarrow}(x) = \begin{cases} e^{-ik_3(x-a)} + r_{L,\,LH\downarrow}e^{ik_3(x-a)} & \text{for } x > a \\ t_{L,\,LH\downarrow}e^{K_3(x-a)} & \text{for } x < a \end{cases}$$

with

$$t_{L,\,LH\downarrow} = \frac{-2ik_3}{K_3 - ik_3} = t_{R,\,LH\uparrow},$$

representing the transmission coefficient for left incoming down-spin electrons.

For the following calculation, one introduces

$$t_{R,\,LH\uparrow} = \frac{2ik_3}{ik_3 - K_3}.$$

On the other hand, at the right interface, one has

$$\Psi^{0\downarrow}_{R,\,LH}(x) = \begin{cases} e^{-K_3(x-a)} + r_{R,\,LH\downarrow} e^{K_3(x-a)} & \text{for } x < a \\ t_{R,\,LH\downarrow} e^{ik_3(x-a)} & \text{for } x > a \end{cases}.$$

with

$$t_{R,\,LH\downarrow} = \frac{-2K_3}{-K_3 + ik_3}.$$

We do similarly to find the other diagonal components $G^{\downarrow\downarrow}_{LH}$, $G^{\uparrow\uparrow}_{HH}, G^{\downarrow\downarrow}_{HH}$, $G^{\uparrow\uparrow}_{Z}$, and $G^{\downarrow\downarrow}_{Z}$.

7.1.3 Spin-dependent Lippman-Schwinger equation in the valence bands

The spin-dependent Lippman-Schwinger equation in the valence band is:

$$\Psi_R(x) = \Psi^0_R(x) + \int G_0\,(x, x')\,\hat{H}_{SO}\Psi^0_R(x')dx', \tag{165}$$

where

$$\Psi_R(x) = \begin{pmatrix} \Psi^{\uparrow}_{R,\,LH}(x) & \Psi^{\downarrow}_{R,\,LH}(x) & \Psi^{\uparrow}_{R,\,HH}(x) & \Psi^{\downarrow}_{R,\,HH}(x) & \Psi^{\uparrow}_{R,\,Z}(x) & \Psi^{\downarrow}_{R,\,Z}(x) \end{pmatrix},$$

and $\Psi^0_R(x)$ is a solution of the homogenous Schrödinger equation,

$$\Psi^0_R(x) = \begin{pmatrix} \Psi^{0\uparrow}_{R,\,LH}(x) & \Psi^{0\downarrow}_{R,\,LH}(x) & \Psi^{0\uparrow}_{R,\,HH}(x) & \Psi^{0\downarrow}_{R,\,HH}(x) & \Psi^{0\uparrow}_{R,\,Z}(x) & \Psi^{0\downarrow}_{R,\,Z}(x) \end{pmatrix}.$$

In the region of interest $-w < \mathcal{E} < w$, we have three propagative ingoing waves in the left contact $\Psi^{0\uparrow}_{R,\,LH}$, $\Psi^{0\uparrow}_{R,\,HH}$, and $\Psi^{0\uparrow}_{R,\,Z}$, whereas one has three propagative outgoing waves $\Psi^{0\downarrow}_{R,\,LH}$, $\Psi^{0\downarrow}_{R,\,HH}$, and $\Psi^{0\downarrow}_{R,\,Z}$ in the right contact . However, the atomic SOI which is considered as a perturbating potential only couples $|Z\uparrow\rangle$ to $|LH\downarrow\rangle$ and $|HH\downarrow\rangle$ and vice versa, whereas $\langle LH\uparrow|\,\hat{H}_{SOI}\,|HH\downarrow\rangle = \langle HH\uparrow|\,\hat{H}_{SOI}\,|LH\downarrow\rangle = 0$. In addition, with our hypothesis, the HH is nearly flat so that the relevant evanescent sates are very quickly vanishing in the barrier. This implies that the coupling between the HH-pure Y orbital and the HH-pure Z orbital is small enough to be neglected in the barrier. According to the Lippman-Schwinger equation for the valence band, Eq. 165, the possible couplings between the left ingoing and the right outgoing waves are shown in Fig. 56.

7.1.4 Ingoing $Z\uparrow$ in the left contact

According to the Lippman-Schwinger equation for the valence band, Eq. 165, one obtains:

$$\delta\Psi^{0\downarrow}_{R,\,LH}(x) = \int_0^a G^{\downarrow\downarrow}_{LH}(x,\,x')\left(\frac{-\Delta}{3}\right)\left(1 + \frac{Mk_y}{LK_3}\right)\Psi^{0\uparrow}_{R,\,Z}(x')dx' \tag{166}$$

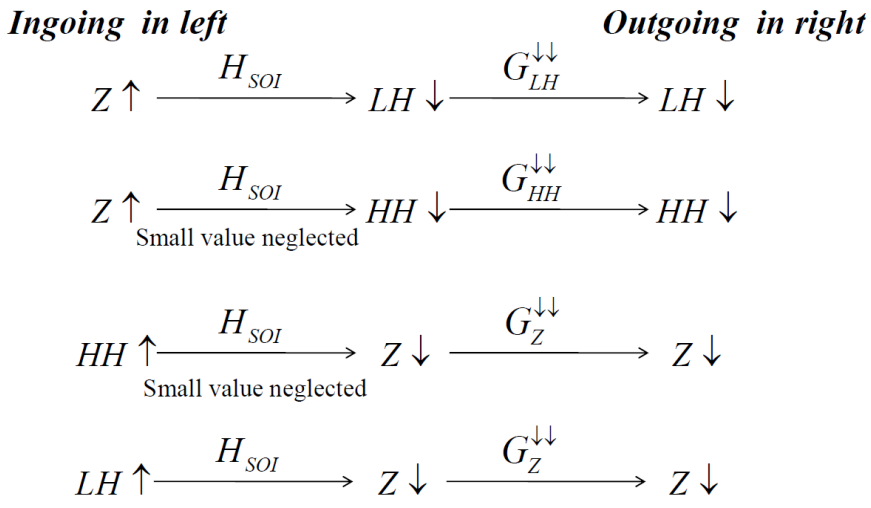

Figure 56: Sketch of different transmission amplitude corresponding to up-spin electrons coming from left.

where $G^{\downarrow\downarrow}_{LH}(x,x')$ was introduced before

$$G^{\downarrow\downarrow}_{LH}(x,\ x') = \frac{\Psi^{0\downarrow}_{R,\,LH}(x)\Psi^{0\downarrow}_{L,\,LH}(x')\Theta(x-x') + \Psi^{0\downarrow}_{R,\,LH}(x')\Psi^{0\downarrow}_{L,\,LH}(\ x)\Theta(x'-x)}{W^{\downarrow\downarrow}_{LH}(x')}, \tag{167}$$

The Wronskian $W^{\downarrow\downarrow}_{LH}(x')$ writes in this case

$$W^{\downarrow\downarrow}_{LH}(x') = \frac{\hbar^2}{2m^*_{LH}}\left[\Psi^{0\downarrow}_{L,\,LH}\frac{\partial\Psi^{0\downarrow}_{R,\,LH}}{\partial x'} - \frac{\partial\Psi^{0\downarrow}_{L,\,LH}}{\partial x'}\Psi^{0\downarrow}_{R,\,LH}\right] = i\frac{\hbar^2 k_3}{m^*_{LH}}t^{\downarrow}_{R,LH}.$$

because the effective masses are kept unchanged in the layers.

With the results that, from Eqs. 166, and 167, the correction to the wave function of the $LH\downarrow$ band is given by

$$\delta\Psi^{0\downarrow}_{R,\,LH}(x) = \frac{\Psi^{0\downarrow}_{R,\,LH}(x)}{W^{\downarrow\downarrow}_{LH}}\left(\frac{-\Delta}{3}\right)\left(1+\frac{Mk_y}{LK_3}\right)\int_0^a \Psi^{0\downarrow}_{L,\,LH}(x')\Psi^{0\uparrow}_{R,\,Z}(x')dx'. \tag{168}$$

Similarly to the the CB, the correction to the transmission amplitude for $\Psi^{0\downarrow}_{R,\,LH}$ in the right contact can then be put in the following form:

$$\delta t^{\downarrow\uparrow}_{LH} = \frac{m^*_{LH}}{i\hbar^2 k_3}\left(\frac{-\Delta}{3}\right)\left(1+\frac{Mk_y}{LK_3}\right)\int_0^a \Psi^{0\downarrow}_{L,\,LH}(x')\Psi^{0\uparrow}_{R,\,Z}(x')dx'. \tag{169}$$

with

$$\Psi^{0\uparrow}_{R,\,Z} = \begin{cases} e^{ik_1x} + r_{R,\,Z\uparrow}e^{-ik_1x} & \text{for } x<0 \\ t_{R,\,Z\uparrow}e^{-K_1x} & \text{for } x>0 \end{cases}.$$

The matching conditions at $x=0$ give us:

$$t_{R,\,Z\uparrow} = \frac{2ik_1}{ik_1 - K_1}.$$

The integral in Eq. 169 is calculated:

$$\begin{aligned}
\int_0^a \Psi^{0\downarrow}_{L,\,LH}(x')\Psi^{0\uparrow}_{R,\,Z}dx' &= t_{R,\,LH\uparrow}t_{R,\,Z\uparrow}e^{-K_3 a}\int_0^a e^{(K_3-K_1)x}dx \\
&= \frac{t_{R,\,LH\uparrow}t_{R,\,Z\uparrow}e^{-K_3 a}\left[e^{(K_3-K_1)a}-1\right]}{K_3-K_1} \\
&= \frac{t_{R,\,LH\uparrow}t_{R,\,Z\uparrow}\left[e^{-K_1 a}-e^{-K_3 a}\right]}{K_3-K_1}.
\end{aligned}$$

to give *in fine,*

$$\delta t^{\downarrow\uparrow}_{LH} = \frac{m^*_{LH}}{i\hbar^2 k_3}\left(\frac{-\Delta}{3}\right)\left(1+\frac{Mk_y}{LK_3}\right)\frac{t_{R,\,LH\uparrow}t_{R,\,Z\uparrow}\left[e^{-K_1 a}-e^{-K_3 a}\right]}{K_3-K_1} \quad (170)$$

$$= \frac{ik_3}{2\left(\mathcal{E}-w\right)}\left(\frac{\Delta}{3}\right)\left(1+\frac{Mk_y}{LK_3}\right)\frac{t_{R,\,LH\uparrow}t_{R,\,Z\uparrow}\left[e^{-K_1 a}-e^{-K_3 a}\right]}{K_3-K_1}, \quad (171)$$

because $\frac{m^*_{LH}}{\hbar^2 k_3} = \frac{k_3}{2(\mathcal{E}-w)}$.

7.1.5 Ingoing $LH\uparrow$ band in the left contact

We consider now the case of ingoing $LH\uparrow$ in the left contact. The Lippman-Schwinger equation for the $Z\downarrow$, Eq. 165, gives:

$$\delta\Psi^{0\downarrow}_{R,\,Z}(x) = \int_0^a G^{\downarrow\downarrow}_Z(x,\,x')\left(\frac{\Delta}{3}\right)\left(1+\frac{Mk_y}{LK_3}\right)\Psi^{0\uparrow}_{R,\,LH}(x')dx' \quad (172)$$

$G^{\downarrow\downarrow}_Z(x,\,x')$ satisfies the following equation:

$$\left(\mathcal{E}-\hat{H}_{0,Z\downarrow}\right)G^{\downarrow\downarrow}_Z(x,x') = \delta(x-x').$$

It can be written:

$$G^{\downarrow\downarrow}_Z(x,\,x') = \frac{\Psi^{0\downarrow}_{R,\,Z}(x)\Psi^{0\downarrow}_{L,\,Z}(x')\Theta(x-x') + \Psi^{0\downarrow}_{R,\,Z}(x')\Psi^{0\downarrow}_{L,\,Z}(\,x)\Theta(x'-x)}{W^{\downarrow\downarrow}_Z(x')},$$

where $\Psi^{0\downarrow}_{R,\,Z}$, and $\Psi^{0\downarrow}_{L,\,Z}(\,x)$ satisfy the homogenous Schrödinger equation for the Z state:

$$\left(\mathcal{E}-\hat{H}_{0,Z\downarrow}\right)\Psi^{0\downarrow}_{R,\,Z}(x) = 0, \text{ and } \left(\mathcal{E}-\hat{H}_{0,Z\downarrow}\right)\Psi^{0\downarrow}_{L,\,Z}(x) = 0.$$

Similarly to Sec. 7.1.4, the correction to the transmission amplitude of the $Z\downarrow$ state in the right contact is:

$$t^{\downarrow\uparrow}_Z = \frac{m^*_Z}{i\hbar^2 k_1}\left(\frac{\Delta}{3}\right)\left(1+\frac{Mk_y}{LK_3}\right)\int_0^a \Psi^{0\downarrow}_{L,\,Z}(x')\Psi^{0\uparrow}_{R,\,LH}(x')dx'. \quad (173)$$

with

$$\Psi^{0\downarrow}_{L,\,Z}(x) = \begin{cases} e^{-ik_1(x-a)} + r_{L,\,Z\downarrow}e^{ik_1(x-a)} & \text{for } x > a \\ t_{L,\,Z\downarrow}e^{K_1(x-a)} & \text{for } x < a \end{cases},$$

and

$$\Psi^{0\uparrow}_{R,\,LH}(x) = \begin{cases} e^{ik_3x} + r_{R,\,LH\uparrow}e^{-ik_3x} & \text{for } x < 0 \\ t_{R,\,LH\uparrow}e^{-K_3x} & \text{for } x > 0 \end{cases},$$

The matching conditions at $z = a$ for $\Psi^{0\downarrow}_{L,\,Z}(x)$ give

$$t_{L,\,Z\downarrow} = \frac{-2ik_1}{-ik_1 + K_1} = \frac{2ik_1}{ik_1 - K_1} = t_{R,\,Z\uparrow},$$

an the matching conditions at $z = a$ for $\Psi^{0\uparrow}_{R,\,LH}(x)$ give

$$t_{R,\,LH\uparrow} = \frac{2ik_3}{ik_3 - K_3}.$$

The integral in Eq. 173 is then calculated to be

$$\begin{aligned} \int_0^a \Psi^{0\downarrow}_{L,\,Z}(x')\Psi^{0\uparrow}_{R,\,LH}(x')dx' &= t_{R,\,LH\uparrow}t_{R,\,Z\uparrow}e^{-K_1a}\int_0^a e^{(K_1-K_3)x'}dx' \\ &= \frac{t_{R,\,LH\uparrow}t_{R,\,Z\uparrow}e^{-K_1a}\left[e^{(K_1-K_3)a} - 1\right]}{K_1 - K_3} \\ &= \frac{t_{R,\,LH\uparrow}t_{R,\,Z\uparrow}\left[e^{-K_3a} - e^{-K_1a}\right]}{K_1 - K_3}. \end{aligned}$$

The correction to the transmission amplitude of the $Z\downarrow$:

$$\begin{aligned} \delta t^{\downarrow\uparrow}_Z &= \frac{m^*_Z}{i\hbar^2k_1}\left(\frac{\Delta}{3}\right)\left(1 + \frac{Mk_y}{LK_3}\right)\int_0^a \Psi^{0\downarrow}_{L,\,Z}(x')\Psi^{0\uparrow}_{R,\,LH}(x')dx', \\ &= \frac{m^*_Z}{i\hbar^2k_1}\left(\frac{\Delta}{3}\right)\left(1 + \frac{Mk_y}{LK_3}\right)\frac{t_{R,\,LH\uparrow}t_{R,\,Z\uparrow}\left[e^{-K_3a} - e^{-K_1a}\right]}{K_1 - K_3} \\ &= \frac{ik_1}{2\left(\mathcal{E}-w\right)}\left(\frac{\Delta}{3}\right)\left(1 + \frac{Mk_y}{LK_3}\right)\frac{t_{R,\,LH\uparrow}t_{R,\,Z\uparrow}\left[e^{-K_3a} - e^{-K_1a}\right]}{K_3 - K_1}. \end{aligned}$$

because $\frac{m^*_Z}{\hbar^2k_1} = \frac{k_1}{2(\mathcal{E}-w)}$.

7.1.6 Scattering asymmetry in the valence band

Neglecting the SOI in the barrier, the unperturbed transmission coefficient is zero so that the total transmission coefficient is equal to the correction according to:

$$
\begin{aligned}
\left|\delta t\left(k_y\right)\right|^2 &= \left|\delta t_{LH}\right|^2 \frac{\left\langle \hat{J}_{x>a}(LH\uparrow)\right\rangle}{\left\langle \hat{J}_{x<0}(Z\uparrow)\right\rangle} + \left|\delta t_Z\right|^2 \frac{\left\langle \hat{J}_{x>a}(Z\downarrow)\right\rangle}{\left\langle \hat{J}_{x<0}(LH\uparrow)\right\rangle} \\
&= \left|\delta t_{LH}\right|^2 \frac{k_1}{k_3} + \left|\delta t_Z\right|^2 \frac{k_3}{k_1} \\
&\quad \frac{k_1}{k_3}\left\{\frac{k_3}{2\left(\mathcal{E}-w\right)}\left(\frac{\Delta}{3}\right)\left(1+\frac{Mk_y}{LK_3}\right)\frac{t_{LH}t_Z\left[e^{-K_1a}-e^{-K_3a}\right]}{K_3-K_1}\right\}^2 + \\
&\quad \frac{k_3}{k_1}\left\{\frac{k_1}{2\left(\mathcal{E}-w\right)}\left(\frac{\Delta}{3}\right)\left(1+\frac{Mk_y}{LK_3}\right)\frac{t_Zt_{LH}\left[e^{-K_3a}-e^{-K_1a}\right]}{K_3-K_1}\right\}^2 \\
&= \frac{k_1k_3}{2\left(\mathcal{E}-w\right)^2}\left(\frac{\Delta}{3}\right)^2\left\{\frac{t_{LH}t_Z\left[e^{-K_1a}-e^{-K_3a}\right]}{K_3-K_1}\right\}^2\left(1+\frac{Mk_y}{LK_3}\right)^2,
\end{aligned}
$$

where

$$
\frac{\left\langle \hat{J}_R(Z\downarrow)\right\rangle}{\left\langle \hat{J}_L(LH\uparrow)\right\rangle} = \frac{k_3}{k_1}, \text{ and} \frac{\left\langle \hat{J}_R(LH\downarrow)\right\rangle}{\left\langle \hat{J}_L(Z\uparrow)\right\rangle} = \frac{k_1}{k_3},
$$

$$
\left\langle \hat{J}_R(Z\downarrow)\right\rangle = \frac{\hbar^2k_1}{m_Z^*} = \frac{2\left(\mathcal{E}-w\right)}{k_1}, \ \left\langle \hat{J}_L(LH\uparrow)\right\rangle = \frac{\hbar^2k_3}{m_{LH}^*} = \frac{2\left(\mathcal{E}-w\right)}{k_3}.
$$

When the in-plane wavevector changes its sign, $k_y \longrightarrow -k_y$, one obtains

$$
\left|\delta t\left(-k_y\right)\right|^2 = \frac{k_1k_3}{2\left(\mathcal{E}-w\right)^2}\left(\frac{\Delta}{3}\right)^2\left\{\frac{t_{LH}t_Z\left[e^{-K_1a}-e^{-K_3a}\right]}{K_3-K_1}\right\}^2\left(1-\frac{Mk_y}{LK_3}\right)^2.
$$

Which leads to the transmission asymmetry, A, for holes having opposite in-plane wavevector components:

$$
\begin{aligned}
A &= \frac{\left|\delta t\left(k_y\right)\right|^2 - \left|\delta t\left(-k_y\right)\right|^2}{\left|\delta t\left(k_y\right)\right|^2 + \left|\delta t\left(-k_y\right)\right|^2} \\
&= \frac{2\frac{Mk_y}{LK_3}}{1+\left(\frac{Mk_y}{LK_3}\right)^2} = 2\left\langle LH\right|\hat{L}_z\left|LH\right\rangle.
\end{aligned} \tag{174}
$$

This is the central result of this section devoted to the perturbation calculation analysis concerning the VB.

The correction to the amplitude of transmission is then shown to be linked to the orbital momentum of the evanescent states of the LH-band in the tunneling barrier as previously suggested. From the comparison with the calculations, we observe a very good agreement between these results calculated by GF method and the transfer matrix

calculation using 6×6 **k**.**p** Hamiltonian with parameters chosen to make the HH nearly flat (see Fig. 57). The results obtained are, however, somewhat different, in some energy range, from the calculations obtained via the true Luttinger-parameter tunnel junction showing that an advanced numerical platform is mandatory. This is performed in the next section.

7.2 Anomalous tunnel Hall effect and giant transport asymmetry in the valence band

We will now extend these analytical results to the case of real systems including SOI in both contacts and barriers which may be played by GaMnAs ferromagnetic semiconductors in contacts. The results shown in Fig. 58 were obtained in a 6-band approach (we have checked that the 14-; and 30-band models give similar results); the lower curve displays the asymmetry $\mathcal{A}$ *vs.* hole energy $\mathcal{E}$ in the case of a 3-nm-thick tunnel barrier. The energy range covers the valence spin subbands, namely, starting from the highest energy, the up-spin heavy-hole band ($HH\uparrow$), the up-spin light-hole band ($LH\uparrow$), the down-spin light-hole band ($LH\downarrow$), the down-spin heavy-hole band ($HH\downarrow$), the up-spin–split-off band ($SO\uparrow$), and the down-spin split-off band ($SO\downarrow$). We refer to points (1) to (6) marked by vertical arrows for discussing the contribution from holes emitted from the different spin subbands in Region I to the current injected in Region II. For instance, with these parameters, the energy of the $HH\uparrow$ [$HH\downarrow$] maximum, corresponds to 0.15 eV [-0.15 eV], the energy origin being taken at the top of the valence band of the non-magnetic material, and is indicated by point (1) [(4)]. Correspondingly, one observes an almost fully negative transmission asymmetry in this energy range for predominant majority spin-up injection, that is, as far as $HH\downarrow$ does not contribute to the current. At more negative energy [$\mathcal{E}<-0.15$ eV: point (4)], a sign change of $\mathcal{A}$ occurs at the onset of $HH\downarrow$ (in the upper left inset, see the step in the transmission coefficient, which reaches almost +50%). The asymmetry $\mathcal{A}$ remains positive after crossing $SO\uparrow$ [point (5)] before turning negative again once crossing $SO\downarrow$ [point (6)]. Note that $\mathcal{A}$ changes sign two times at characteristic energy points corresponding to a sign change of the injected particle spin. We have performed the same kind of calculation for a simple contact (*i.e.*, $d=0$; right upper inset in Fig. 58, black curve). It is remarkable that $\mathcal{A}$, although smaller, keeps the same trends as for the 3-nm tunnel junction, except for a change of sign, showing a subtle dependence of the exchange coupling on the barrier thickness. Without tunnel junction, $\mathcal{A}$ abruptly disappears as soon as $SO\downarrow$ contributes to tunneling [circle region] *i.e.*, when evanescent states disappear. In the case of tunnel junction, $\mathcal{A}$, although small, subsists in this energy range and this should be related to the evanescent character of the tunneling wave function in the barrier.

Figure 59 shows very good agreement of the results calculated by 6-; 14-; 30-band.

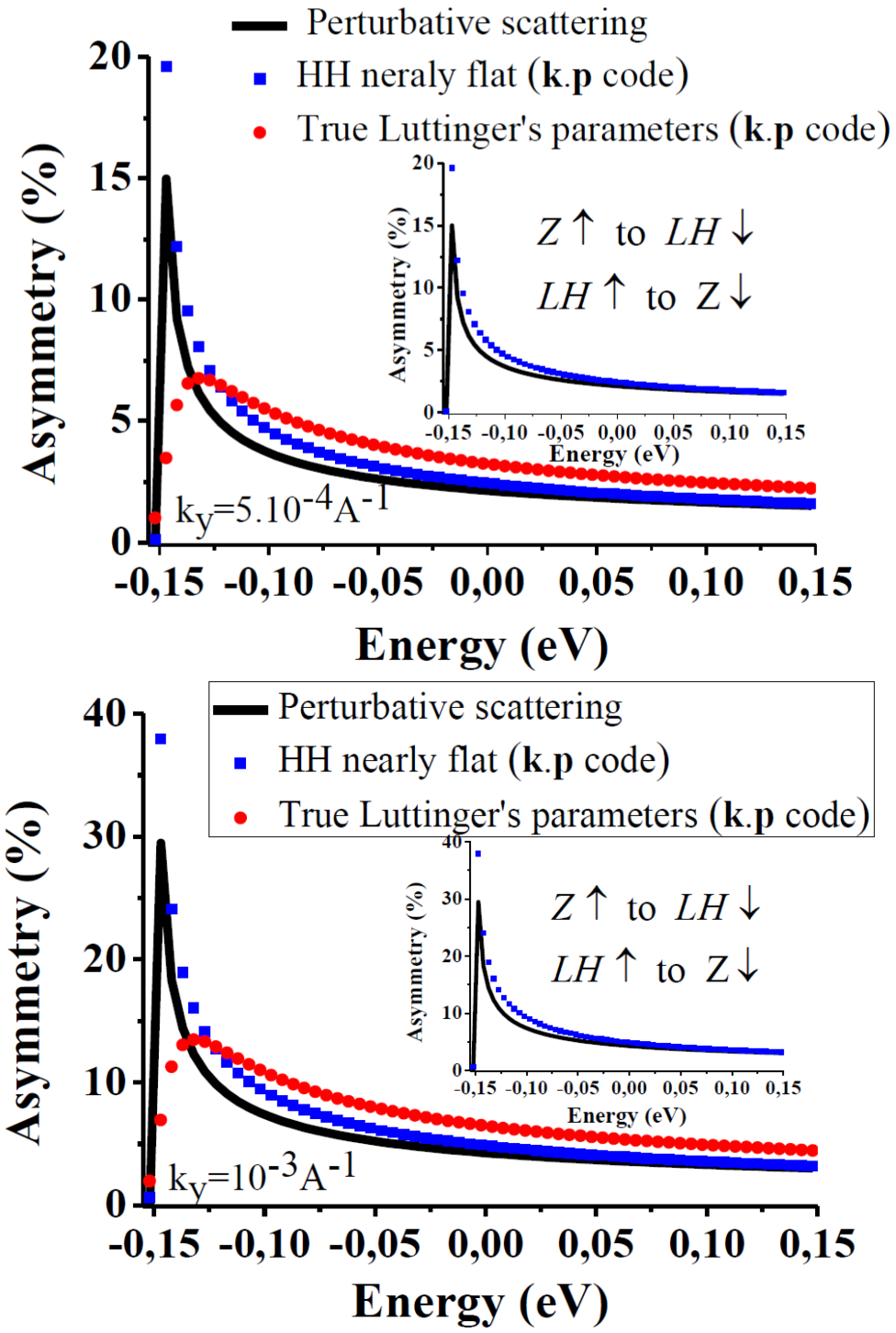

Figure 57: Asymmetry *vs.* incident energy calculated from Eq. 174 (black line), 6-band **k.p** with HH nearly flat (blue line), $\gamma_1 = 4.5$, $\gamma_2 = 2.1$, $\gamma_3 = 2.9$, barrier height -0.15 eV, barrier thickness 10 nm, M=2($\gamma_1 + \gamma_2 + 1$), $L = 6\gamma_2$; and real case (red line) $\gamma_1 = 6.85$: (upper) $k_y = 5.10^{-4}$ A^{-1}; (lower) $k_y = 10^{-3}$ A^{-1}. The energy is counted from the top of the VB.

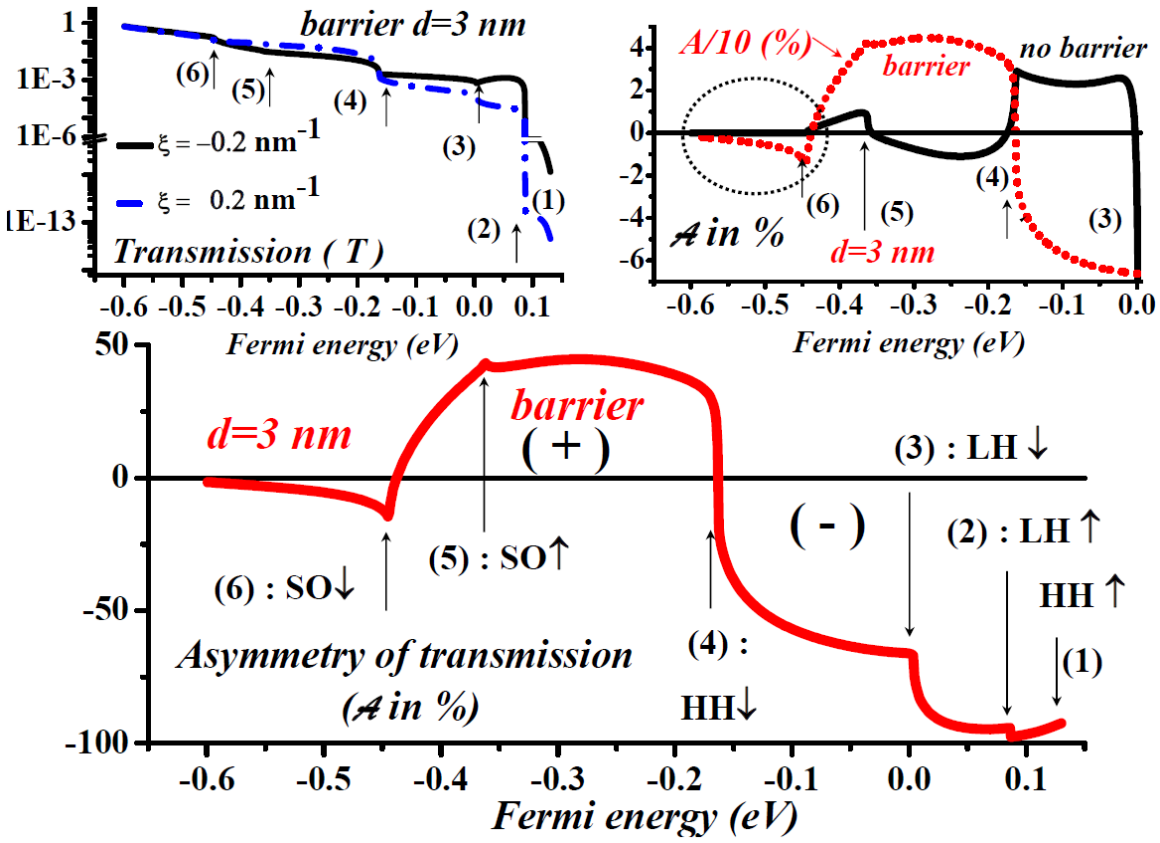

Figure 58: (*Bottom*): Transmission asymmetry $\mathcal{A}$ *vs. total* energy $\mathcal{E}$ for a magnetic tunnel junction in the AP state. The parameters are: $2w = 0.3$ eV, parallel wavevector $\xi = 0.2$ nm^{-1}, barrier thickness $d = 3$ nm, and barrier height 0.6 eV. The energy zero corresponds to the non-magnetic upper-valence-band maximum. (*Upper left inset*): transmission T calculated in the AP state; (*Upper right inset*): Asymmetry $\mathcal{A}$ without tunnel barrier ($d = 0$; black) compared to the case of the tunnel junction (dotted red).

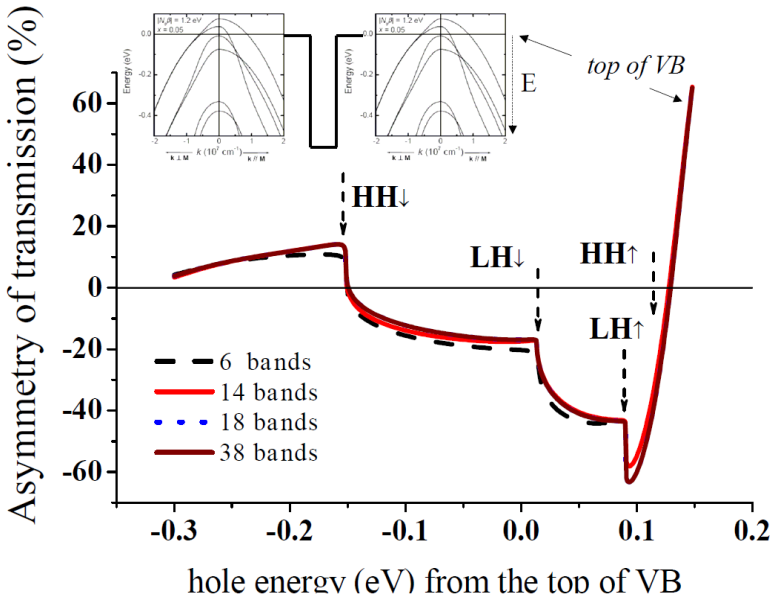

Figure 59: Transmission asymmetry $\mathcal{A}$ $vs.$ total energy $\mathcal{E}$ calculated in the VB for a p-type magnetic tunnel junction in the AP state by respective 6×6, 14×14, 18×18 (14-ghost-band) and 30×30 ghost band **k.p** method. The parameters are: $2w = 0.3$ eV, parallel wavevector $\xi = k_{||} = 0.005$ Å^{-1}, barrier thickness $d = 3$ nm, and barrier height 0.3 eV. The energy zero corresponds to the non-magnetic upper-valence-band maximum

Moreover, we have checked that the asymmetry appears to be robust and persists even when a single electrode is magnetic, (Fig. 60). In 6×6 **k.p** model, the spin filtering effect does not exist because the cubic term is not included.

We have presented theoretical evidence for a large interfacial scattering asymmetry of carriers *vs.* incidence in semiconducting exchange steps and tunnel barriers. This involves either the Dresselhaus interaction in the conduction band of electrodes or spin-orbit hybridization.

7.3 Tunneling transmission asymmetry and tunneling anisotropy

The tunneling asymmetry calculated in the present work manifests itself by a large difference of transmission coefficient between the two opposite $k_{||} = \pm\xi$ incidences. The forward scattering asymmetry should also be associated to a change in the average transmission coefficient between opposite incidence angles $T = (1/2)[T(+\xi)+T(-\xi)]$ so that it also affects the total sum of the transmission channels $T = \sum_{k_{||}} T(k_{||})$ responsible for the overall conduction through the Landauer-Buttiker formula. We emphasize that this effect may predominantly contribute to the TAMR signal in the VB, in the AP magnetic configuration of a magnetic tunnel junction as well as in the case of a single ferromagnetic contact. The resistance change originating from the "chirality-assisted" tunneling process is expected to be large in the VB (compared to the CB).

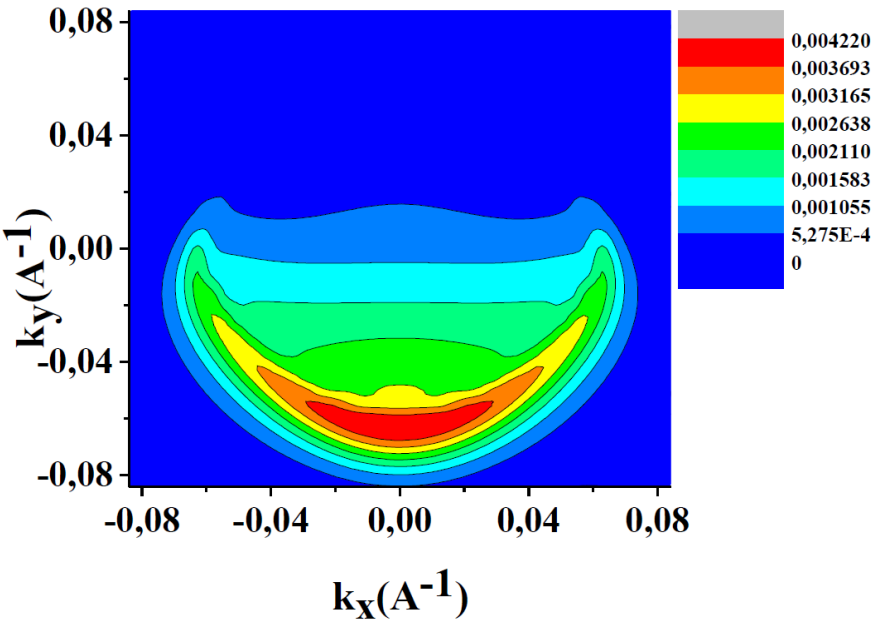

Figure 60: Transmission coefficient T in a 6×6 $\mathbf{k}.\mathbf{p}$ model for a tunnel junction when only the left electrode is magnetic; the parameters are: exchange energy $2w = 0.3$ eV, barrier thickness 3 nm, barrier height 0.6 eV, and total kinetic energy -0.1 eV.

We have checked that the electronic transmission is quasi isotropic when the magnetization is out-of-plane. On the contrary, for an in-plane magnetization, the electronic tunneling beam is strongly deflected and the resistance drops. Figure. 61 displays the change of resistance observed on a tunnel junction with a ferromagnetic GaMnAs/AlAs(3 nm)/GaAs:Be structure with a higher resistance state (smaller transmission coefficient) corresponding to the direction of the magnetization along the normal of the film plane. A resistance change as large as 40% can be observed on such junction (Fig. 61) which may reveal the major role of this tunneling asymmetry process on the conductance itself. Presently, the in-plane orientation of the magnetization does only lead to a small change of resistance of the order of 2% due to the in-plane strain anisotropy field.

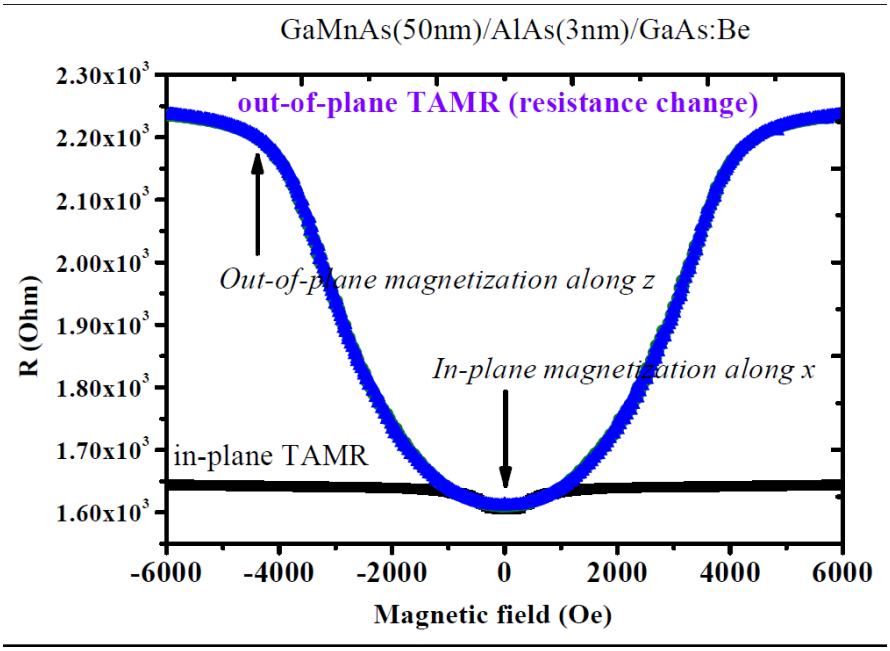

Figure 61: Tunneling anisotropy magnetoresistance (TAMR) of GaMnAs(50 nm)/ AlAs/ GaAs:Be 128 μm^2 junctions. Change of the tunneling Resistance *vs.* magnetization orientation from in-plane to out-of-plane (TAMR). The resistance is higher by 30% when the magnetization is aligned along the direction z normal to the plane.

CHAPTER VIII

CONCLUSION

We provide here the main conclusions and propose future possible experiments to evidence the interfacial skew tunneling effects demonstrated in the present manuscript.

The interfacial skew transmission and skew tunneling effects we have demonstrated in this work via advanced **k**.**p** methods had never been investigated up to now and result in several specific properties which clearly depart from any known existing properties dealing with spin-Hall effects or galvanic or Inverse Edelstein effects. The first novel property is a prediction of a strong asymmetry of transmission at ferromagnetic / spin-orbit interfaces experimented by carriers, electrons or holes with a marked evanescent character crossing such interfaces, at opposite incidences, *i.e.*, characterized by positive or negative incoming in-plane parallel wavevectors normal to the magnetization. This is due to a particular combination of the matching properties of the wave functions submitted to both exchange and SO interactions or by selective tunneling branching of the orbital moment in the barrier. These results have been derived by considering different possible Hamiltonian terms describing SOI, that are bulk Dresselhaus terms, bulk or interfacial Rashba terms, and more surprisingly, core SOI terms in the VB of semiconductors. The particular properties of the transmission asymmetry have been calculated to be strong in much cases once one considers that the exchange interactions could be strong enough compared to the kinetic energy or Fermi energy in order to favor an incoming single spin channel (*e.g.* the majority one) which has to be transmitted into opposite spin-channels (*e.g.* minority one). The expected almost zero transmission in the situation of a half-metallic material, which is nearly the case of a lightly-doped ferromagnetic semiconductor (GaMnAs or GeMn) is enhanced via the spin-flip processes mediated by the spin-orbit terms which make possible spin-mixing and spin-flip during the coherent transmission or tunneling processes. However, whereas the transmission from majority to minority spin channels is made possible via SOI, as it can be easily observed through perturbation calculations to first order, the SOC also makes that the transmission differs for opposite carrier incidences. This originates from a new type of chirality phenomena which promotes a difference in the probability of transmission when one considers both propagative (parallel wavevectors) and evanescent (tunneling along the current flow) characters of the overall electronic wave function. This makes the phenomenon we describe truly new. This new type of chirality phenomena has been

particularly well described in this work by considering advanced perturbation investigations involving the role of the SOC on both the transmission properties as well as its impact on the deviation of the electronic flux (Chapter 5).

8.1 ARPES spectroscopy

Such strong difference of $+\mathbf{k}_{\|}$ and $-\mathbf{k}_{\|}$ transmission that we expect for carriers when the spin splitting is large compared to the kinetic energy (electrons or holes or electrons and holes in the case of magnetic Esaki diodes such as GaMnAs /n^{++}-GaAs), can hardly been observed in solid-state devices at the length scale where the mean-free path before isotropization processes take place (through the angular-dependence of the Boltzmann equation) except in the situation of a thin tunnel-junction electrode. A first possibility to consider in a real experimental situation is the measurement of the difference in the intensity collected in angular-resolved photoelectron spectroscopy (ARPES), but not necessarily spin-resolved, at the surface of thin magnetic/spin-orbit bilayers owing to the strong in-plane wavevector selectivity of this technique. Such precursor ARPES measurements have been considered in the past in the case of GdO/Gd bilayers [100]. This could be implemented in other situations involving strong exchange-split materials.

8.2 Skew tunneling and anomalous tunnel Hall effects

Nevertheless, the property of skew tunneling described here admits equivalent properties to skew diffusion for an overall carrier flow summed over the Fermi surface. Indeed, an incoming carrier flux along the normal direction of the heterostructure (the so-called z direction) can be divided into different positive and negative carrier incidence angles transmitted differently at the other side of the contact. This asymmetry of transmission leads to an overall parallel interface current along y if the magnetization is directed along x from symmetry properties. This 'anomalous' tunnel Hall current exists at the length scale of the mean free path and may be detected or measured in several situations described hereafter. This tunnel Hall current is proportional to the incoming carrier flux and proportional to the so-called THA reflecting the importance of the deviation of the flux in the same way that the spin-Hall angle (SHA) describes the flux deviation for the spin-Hall effect. The integration of the lateral charge flux along the y direction on a thickness given by the electronic mean-free path then transforms a two-dimensional current density per unit surface into a one-dimensional current density per unit length like in Inverse Edelstein processes [17] when considering Rashba-split interfacial 2-dimensional gas or TI, Fig. 62.

Such anomalous tunnel Hall effects could be investigated in the future in several

experimental situations involving spin-dependent electronic transport.

8.2.1 Tunnel Hall in micronic GaMnAs-based tunnel junctions (normal current injection)

The first series of experiments we can think about is the measurement of possible transverse Hall voltage in skew tunneling devices made of GaMnAs/InGaAs/GaMnAs tunnel junctions in the Anti-Parallel magnetic state with InGaAs thin tunnel barriers (*e.g.* 4 to 6 nm thickness). These kind of magnetic heterostructures have already been investigated by M. Elsen during his PhD thesis [112] for their properties of tunneling Magnetoresistance (TMR) as well as for successful STT experiments. The proposed experiments should consist in injecting a current normal to the stack via a top contact and measuring the transverse hole flow or transverse voltage between two separate contacts located on either side of the junction. One necessary condition for the experimental success is to consider a bottom GaMnAs electrode thickness not largely exceeding the mean free-path in GaMnAs, namely of few nm. A typical 5-10 nm thick GaMnAs should then be considered.

The expected transverse voltage signal is then:

$$\Delta V_{THE} = \theta_{THE} \frac{\lambda W}{t} \frac{V_J}{R_T} \rho_M$$

where θ_{THE} is the THA,V_J the bias applied to the junction, R_T is the tunnel barrier resistance (Ωm^2), λ is the MFP, t the GaMnAs channel thickness and ρ_M the resistivity of GaMnAs, and W the width of the contact. Then, for a THA of 0.2, an applied bias of 0.5 V, a channel thickness and width of respectively 10 nm and 100 μm, a resistivity of 1 mΩ.cm and a tunnel barrier resistance of 100 kΩ.μm^2, we obtain a transverse voltage of 10 μV which is clearly measurable.

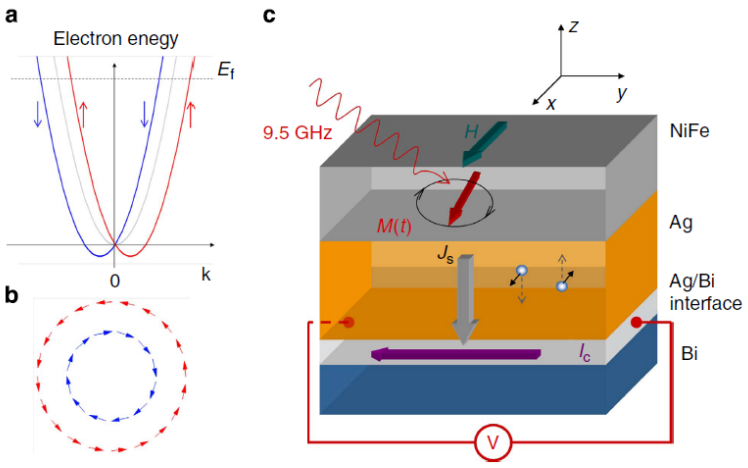

Figure 62: Electronic structure of interface Rashba states and principle of experiments [17].

8.2.2 GaMnAs-based tunnel junctions with in-plane current injection

Owing to some latest experiments published, a second possible tunneling transport geometry is to measure the conductivity of the same kind of GaMnAs-based tunnel junction with thinner InGaAs barriers (1-2 nm thick) in a geometry of in-plane current injection. The role of the InGaAs barrier introduced here is not to promote tunneling although existing also here, but to uncouple the two magnetic states of GaMnAs at its both sides to control a well-defined AP state. The asymmetry of the scattering (or tunneling) rate from one GaMnAs layer to the second GaMnAs layer, Fig. 63, should manifest itself by a measurable difference of conductivity (or resistivity) depending on the direction of the in-plane current flow either $+I$ or $-I$ for the same AP configuration like in recent USMR measurements. Such difference of conductivity between $+I$ and $-I$ experimental configurations is zero in the PA state and becomes opposite in the other AP configuration state. Such non-linearity of conductance in the current and current sign should arise because the probability of scattering (transmission) at interfaces depends on the carrier incidence. This could be quite easily seen in a diffusive picture taking into account a difference in the transmission-reflection rates in the approach of the Fuchs-Sondheimer model for interface diffusion. Such peculiarities of non-linearity in I-V characteristics in metals have already been observed in Cambridge and ETH Zürich on SMR and USMR effects.

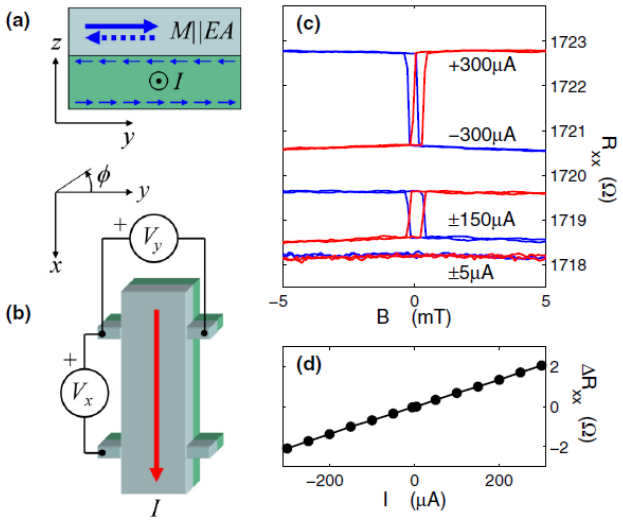

Figure 63: (a) Schematic of the linear spin Hall magnetoresistance phenomenon. The thin arrows represent the SHE-induced spin polarization; the thick arrows represent the easy-axis (EA) magnetization of the ferromagnet. (b) Schematic of the device and measurement geometry. (c) Longitudinal resistance measurements at 130 K and different amplitudes and signs of the applied current as a function of the external magnetic field. The steps correspond to the 180° magnetization reversal. (d) Difference between resistance states for opposite magnetizations, set by sweeping the magnetic field from negative or positive values to the zero field, as a function of the applied current [77].

8.2.3 Unidirectional magnetoresistance in a magnetic topological insulator

In very recent work [140], USMR in magnetic or nonmagnetic topological insulator (TI) heterostructures is considered. These measurements lead to signals of magnitude larger than in other reported systems [77, 80, 81].

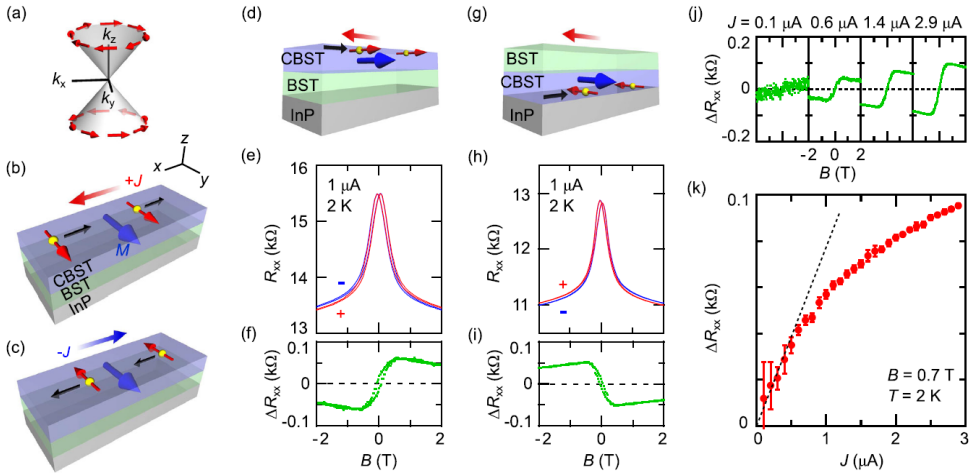

Figure 64: (a) Schematic diagram of spin-momentum locking of the surface Dirac state in TI. (b),(c) Schematic illustration of the concept for UMR in TI heterostructures $(Cr_xBi_{1-y}Sb_y)_2Te_3$ (CBST/BST) on InP substrate under $+J$ (b) and $-J$ (c) dc current. Here, magnetic field, magnetization, and dc current are along the in-plane direction, where dc current is applied perpendicular to the magnetization direction. (d) Schematic illustration of a "normal" CBST/BST heterostructure. (e) Magnetic field dependence of resistance R_{xx} for the sample depicted in (d), measured under $J = +1\ \mu A$ (red) and $J = -1\ \mu A$ (blue) at 2 K. (f) Difference of the resistance ΔR_{xx} of plus and minus current shown in (e). (g)–(i) The same as (d)–(f) for the "inverted" BST=CBST heterostructure. (j) ΔR_{xx} measured under various current for the normal CBST/BST heterostructure. (k) Current J dependence of ΔR_{xx} at 2 K under $B = 0.7T$ for the normal CBST/BST. The black dotted line shows a slope in the low-J region [140].

8.3 Optical spin-pumping experiments on semiconductor/SOC (heavy metal) systems

A last experimental investigation to perform would be to measure a transverse Hall voltage in GaAs/Pt systems after spin-selected optical pumping. The helicity-dependent optical pumping would have for effect to promote well-selected spins in the conduction band of optically active semiconductors (GaAs in the present case) before being transferred to the heavy metal material *e.g.* played by Pt. The optically pumped spin-polarized carriers may experiment an asymmetry of transmission through Pt leading to a transverse lateral current which could be measurable via the transverse voltage. Such kind of experiments have been already been performed in international teams (Italy,

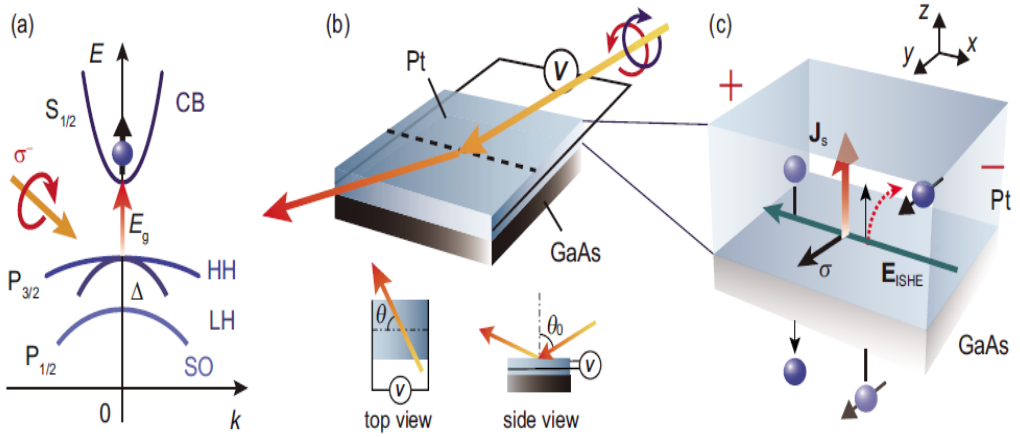

Figure 65: (a) A schematic illustration of the band structure of GaAs and spin-polarized electrons generated by the absorption of circularly polarized light. (b) A schematic illustration of the Pt/GaAs hybrid structure used in this study; θ is the in-plane angle between the incident direction of the illumination and the direction across the two electrodes attached to the Pt layer; θ_0=65° is the angle of the light illumination to the normal axis of the film plane. (c) A schematic illustration of the inverse spin Hall effect induced by photoexcited pure spin currents in the Pt/GaAs system [144].

Japan) on Ge/Pt [143] and GaAs/Pt [144] systems with successful results attributed to Inverse Spin-Hall effects effects of Pt (see Fig. 65) .

APPENDIX A

GEOMETRY OF THE SCATTERING MATRIX WITH MAGNETIZATION INCLUDED: GENERAL ARGUMENTS RELATED TO SCATTERING IN THE PRESENCE OF SOI

As introduced in Sec. 4.7 in the general case, the total transmission coefficients of the left and right incoming waves are equal, $T_{k_\parallel} = T'_{k_\parallel}$ (see Fig. 66). In this work, we deal wiht magnetic semiconductors where the internal magnetization is the local magnetization of the atoms. Let us assume that this local magnetic field is represented by a potential vector, *i.e.*, $\nabla \times \mathbf{A} = \mathbf{M}$, analogous to an external field $\mathbf{B} = \mathbf{M}$.

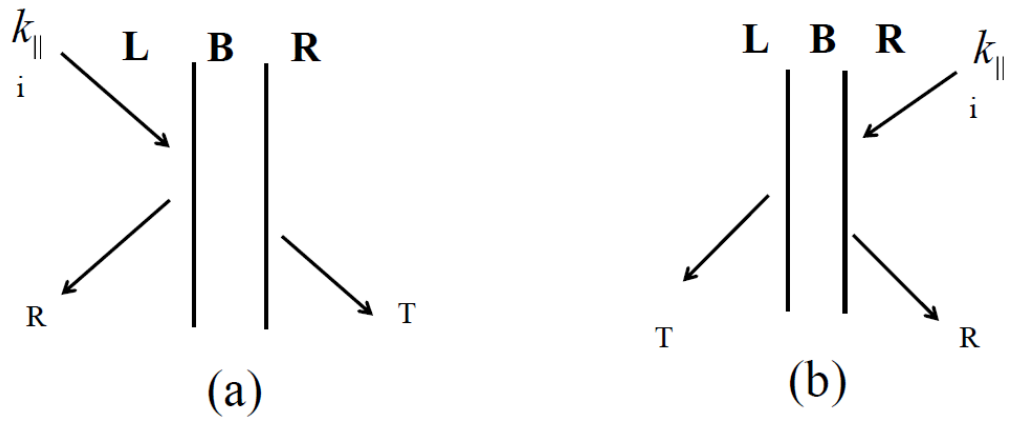

Figure 66: The total transmission coefficient of the incoming wave from the left (a) is equal to the tranmsission coefficient of the incoming wave from the right (b), $T = T'$.

A.1 Without spin-orbit interaction

We first show the reciprocity property of the S-matrix without SOI in an external or internal magnetic field.

Suppose that the electron Hamiltonian is:

$$H = H_{kinetic} + H_M = \frac{(i\hbar\boldsymbol{\nabla} + e\mathbf{A})^2}{2m},$$

where $e < 0$ is the electron charge.

Let us find the solution $\Psi(\mathbf{r})$ of the Schrödinger equation:

$$\frac{(i\hbar\boldsymbol{\nabla}+e\mathbf{A})^2}{2m}\Psi(\mathbf{r}) = E\Psi(\mathbf{r}), \tag{175}$$

to obtain the S-matrix connecting the outgoing amplitude $\{b\}$ to the incoming amplitude $\{a\}$. Taking the complex conjugate of Eq. 175

$$\frac{(-i\hbar\boldsymbol{\nabla}+e\mathbf{A})^2}{2m}\Psi^*(\mathbf{r}) = E\Psi^*(\mathbf{r})$$

and, at the same time, reversing the vector potential $\mathbf{A}$ (and hence the magnetic field $\mathbf{B}$), we obtain

$$\frac{(i\hbar\boldsymbol{\nabla}+e\mathbf{A})^2}{2m}\Psi^*(\mathbf{r}) = E\Psi^*(\mathbf{r}). \tag{176}$$

Comparing Eq. 175 to Eq. 176, we deduce:

$$\Psi^*_{\mathbf{B}}(\mathbf{r}) = \Psi_{-\mathbf{B}}(\mathbf{r}).$$

In other words, if we know the solutions of the Schrödinger equation in a magnetic field $+\mathbf{B}$, we can obtain a solution that is valid for $-\mathbf{B}$ by taking its complex conjugate. Taking the complex conjugate, however, turns an incoming wave into an outgoing wave and vice versa. So if

$$\{b\} = [S]_{+B}\{a\},$$

that is

$$\{b^*\} = [S^*]_{+B}\{a^*\},$$

then we must have

$$\{a^*\} = [S]_{-B}\{b^*\}$$

that is

$$\{b^*\} = \left[S^{-1}\right]_{-B}\{a^*\}.$$

Therefore,

$$\left[S^{-1}\right]_{-B} = [S^*]_{+B}.$$

From the unitary property of the S-matrix, we have

$$\left[S^{-1}\right]_{-B} = \left[S^{+}\right]_{-B}.$$

Finally, we obtain

$$[S^*]_{+B} = \left[S^{+}\right]_{-B},$$

that is

$$[S]_{+B} = \left[S^{T}\right]_{-B},$$

or, in a more detailed form

$$\begin{bmatrix} r_{+B} & t'_{+B} \\ t_{+B} & r'_{+B} \end{bmatrix} = \begin{bmatrix} r_{-B} & t_{-B} \\ t'_{-B} & r'_{-B} \end{bmatrix} \tag{177}$$

We take the squared magnitude of both sides of Eq. 177, and we obtain,

$$|r_{+B}|^2 = |r_{-B}|^2 . \tag{178}$$

Because of conserved current $|t_{+B}|^2 + |r_{+B}|^2 = |t_{-B}|^2 + |r_{-B}|^2 = 1$, one has:

$$|t_{+B}|^2 = |t_{-B}|^2 . \tag{179}$$

This means that in the structure without SOI, the electron transmission coefficient in the magnetic field $+\mathbf{B}$ is equal to the electron transmission coefficient in the magnetic field $-\mathbf{B}$. According to Eq. 177, we also obtain:

$$\left|t'_{+B}\right|^2 = |t_{-B}|^2 . \tag{180}$$

Eqs. 179 and 180 lead to

$$\left|t'_{+B}\right|^2 = |t_{-B}|^2 = |t_{+B}|^2 ,$$

we recover the balance of the total transmission coefficients for left and right incoming waves, $T = T'$ which is a well known property inferred by the scattering matrix formalism.

Taking the magnetic field and the in-plane wavevector along the y direction and applying the C_{2z} symmetry to the structure under the $-\mathbf{B}$ magnetic field to reverse both the magnetization and the in-plane wavevector, we obtain that the transmission coefficient is independent of the sign of the in-plane wavevector. In other structures, it always exists a C_2 operator to reach a similar conclusion: the electron transmission is independent of the sign of in-plane wavevector.

According to the result $|t_{-B}|^2 = |t_{+B}|^2$, then rotating the structure by the C_{2y} operator, we find that the electrons with opposite in-plane wavevectors have the same transmission coefficient in all configurations. Figure. 67 is as an example in the case where the in-plane wavevector is parallel to the magnetization in the PA configuration.

A.2 Case of the spin-orbit interaction

In this part, we consider the scattering of electrons/holes in a tunnel junction grown along the z direction, the exchange interaction is considered as a local magnetic field $\overrightarrow{M} = m_x \overrightarrow{x}$, the in-plane wavevector is parallel or perpendicular to the magnetic field direction. The geometry of the scattering matrix is studied to predict the transmission

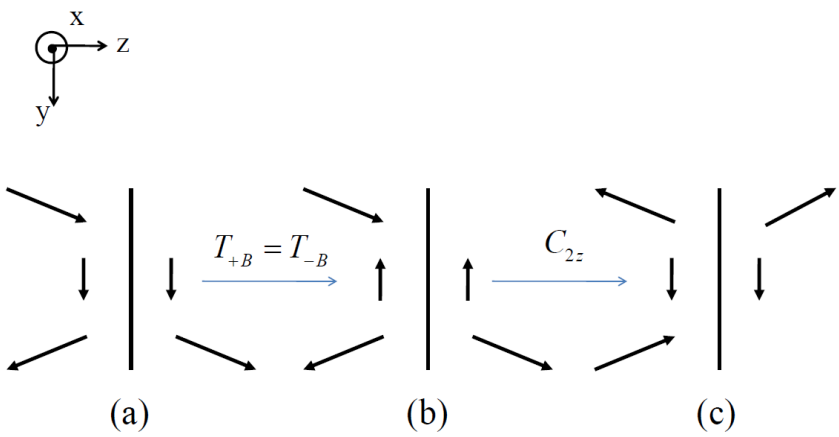

Figure 67: Eq.(179) shows that, as long as SOI is not included, electron scattering at the interface in the magnetic field $+\mathbf{B}$ (a) leads to an equal transmission coefficient in the magnetic field $-\mathbf{B}$ (b). Then the C_{2z} operator reverses both the magnetizations and the in-plane wavevectors (c). Comparing (a) to (c), we find that the transmission coefficient is independent of the signs of the in-plane wavevectors.

coefficient of electrons with a respectively positive $+\overrightarrow{k}_{\parallel}$ and negative $-\overrightarrow{k}_{\parallel}$ in-plane wavevector. The electrodes are made of identical materials with parallel of antiparallel magnetization directions.

A.2.1 In-plane wavevector parallel to the magnetization direction

A.2.1.1 ***PA***

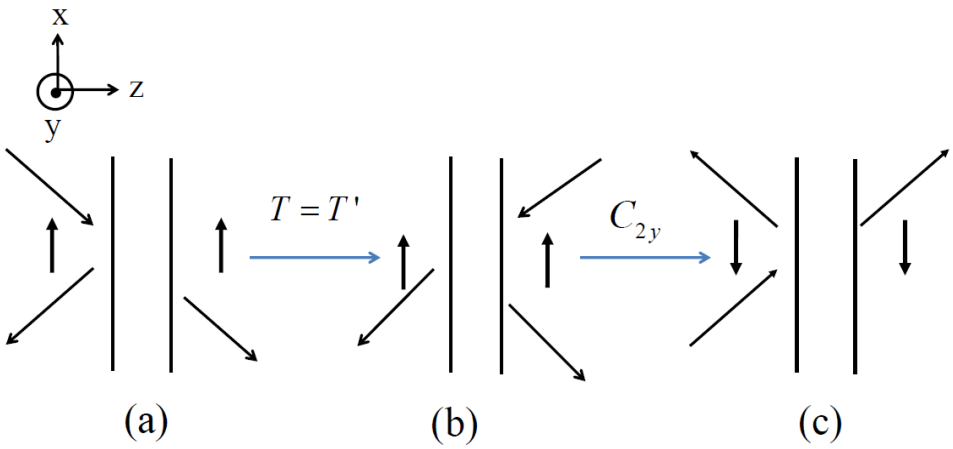

Figure 68: (a) Tunnel junction with PA magnetizations in the electrodes, (b) apply $T = T'$, (c) apply the C_{2y} rotations to structure (b) to obtain the incoming wave from left sign with opposite in-plane wavevectors opposite and opposite magnetizations.

In this case (see Fig. 68), there is no conclusion for possible relationships between

the transmission coefficient for opposite in-plane wavevectors. Therefore, it is necessary to do the analytical or numerical calculation to obtain the transport asymmetry in this case and the particular properties of the asymmetry will depend on the particular Hamiltonian to be considered (*ex.* the spin filtering effect in Chapter 2).

A.2.1.2 ***AP***

See Fig.69.

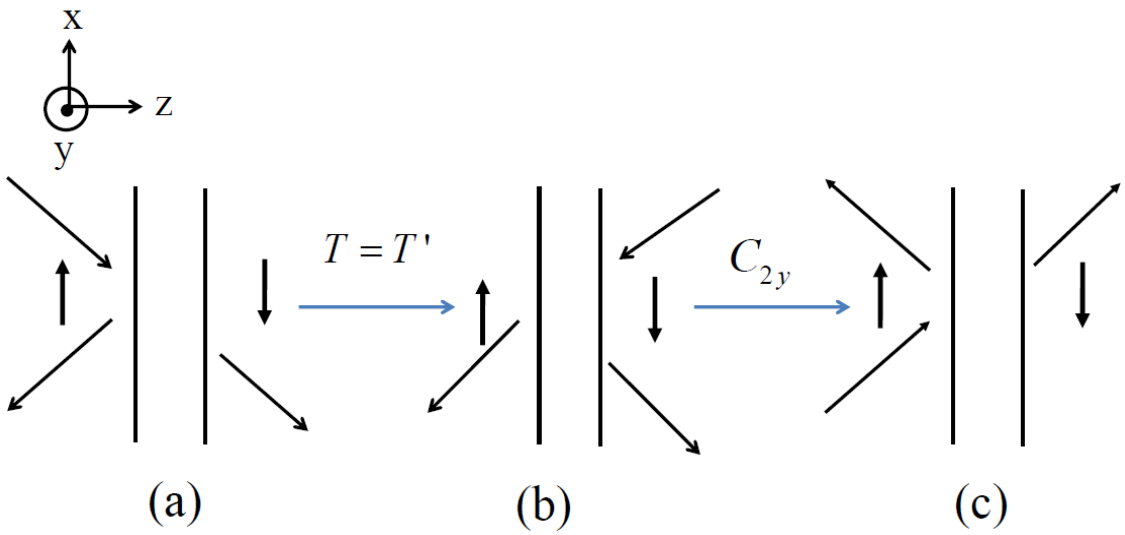

Figure 69: (a) Tunnel junction with AP magnetizations in the electrodes, (b) the scattering matrix formalism leads to $T = T'$, (c) apply the C_{2y} rotation to the structure (b) to recover the inital structure with opposite in-plane wavevectors.

The electron with opposite in-plane wavevectors have the same transmission coefficients.

A.2.2 In-plane wavevector perpendicular to the magnetization direction

A.2.2.1 ***PA***

See Fig. 70.

The electron with opposite in-plane wavevectors have the same transmission coefficients.

A.2.2.2 ***AP***

See Fig. 71

No conclusion concerning the relationships between the transmission coefficient for opposite in-plane wavevectors can be reached.

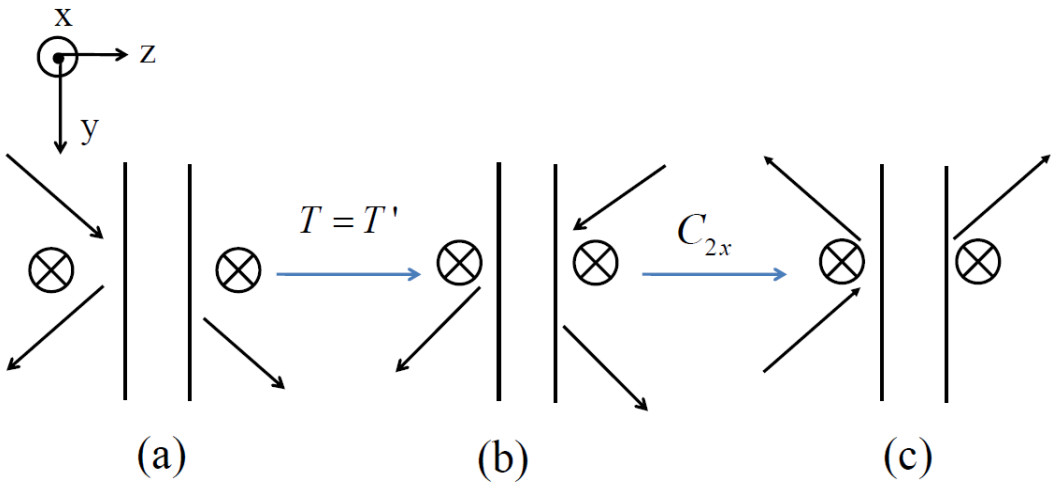

Figure 70: (a) Tunnel junction with PA magnetizations in the electrodes, (b) the scattering matrix formalism leads to $T = T'$, (c) apply the C_{2x} rotation to the structure (b) to recover the inital structure with opposite in-plane wavevectors.

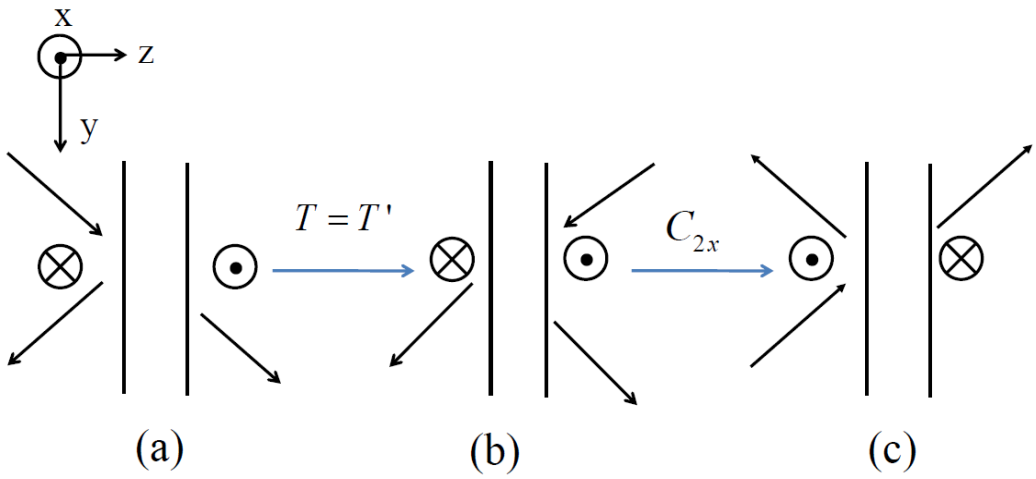

Figure 71: (a) Tunnel junction with AP magnetization in the electrodes, (b) the scattering matrix formalism leads to $T = T'$, (c) apply the C_{2x} rotation to the structure (b) to obtain the incoming wave in the left electrode with opposite in-plane wavevectors and opposite magnetizations.

APPENDIX B

EXPRESSION OF THE SPIN-MATRIX COMPONENTS AND PERTURBATIVE SCATTERING CALCULATIONS IN THE CONDUCTION BAND

B.1 Expression of the spin-matrix components

$$\langle \uparrow | \sigma_z | \uparrow \rangle = \langle \downarrow | \sigma_z | \downarrow \rangle = 0, \tag{181}$$

$$\langle \uparrow | \sigma_z | \downarrow \rangle = \begin{bmatrix} \frac{1}{\sqrt{2}} & \frac{1}{\sqrt{2}} \end{bmatrix} \begin{bmatrix} 1 & 0 \\ 0 & -1 \end{bmatrix} \begin{bmatrix} \frac{1}{\sqrt{2}} \\ -\frac{1}{\sqrt{2}} \end{bmatrix} = 1, \tag{182}$$

$$\langle \downarrow | \sigma_z | \uparrow \rangle = \begin{bmatrix} \frac{1}{\sqrt{2}} & -\frac{1}{\sqrt{2}} \end{bmatrix} \begin{bmatrix} 1 & 0 \\ 0 & -1 \end{bmatrix} \begin{bmatrix} \frac{1}{\sqrt{2}} \\ \frac{1}{\sqrt{2}} \end{bmatrix} = 1, \tag{183}$$

$$\langle \uparrow | \sigma_y | \downarrow \rangle = \begin{bmatrix} \frac{1}{\sqrt{2}} & \frac{1}{\sqrt{2}} \end{bmatrix} \begin{bmatrix} 0 & -i \\ i & 0 \end{bmatrix} \begin{bmatrix} \frac{1}{\sqrt{2}} \\ -\frac{1}{\sqrt{2}} \end{bmatrix} = i,$$

$$\langle \downarrow | \sigma_y | \uparrow \rangle = \begin{bmatrix} \frac{1}{\sqrt{2}} & -\frac{1}{\sqrt{2}} \end{bmatrix} \begin{bmatrix} 0 & -i \\ i & 0 \end{bmatrix} \begin{bmatrix} \frac{1}{\sqrt{2}} \\ \frac{1}{\sqrt{2}} \end{bmatrix} = -i; \tag{184}$$

where $|\uparrow\rangle = \begin{bmatrix} \frac{1}{\sqrt{2}} \\ \frac{1}{\sqrt{2}} \end{bmatrix}$, $|\downarrow\rangle = \begin{bmatrix} \frac{1}{\sqrt{2}} \\ -\frac{1}{\sqrt{2}} \end{bmatrix}$ are eigenvectors of σ_x.

B.2 Perturbative scattering calculations in the conduction band

B.2.1 Case of spin-orbit interactions on the left for incoming left electrons (Equation 147)

$$\begin{aligned} \tau_L &= \frac{m^*}{i\hbar^2 k_1} \int_{-\infty}^{0} \Psi_L^{0\uparrow}(z') \left[-\frac{i\gamma\xi^2}{2} \frac{\partial}{\partial z'} + \frac{i\gamma\xi}{2} \frac{\partial^2}{\partial z'^2} \right] \Psi_R^{\downarrow 0}(z') dz' \\ &+ \frac{m^*}{i\hbar^2 k_1} \int_{-\infty}^{0} \left[\frac{i\gamma\xi^2}{2} \frac{\partial \Psi_L^{0\uparrow}(z')}{\partial z'} + \frac{i\gamma\xi}{2} \frac{\partial^2 \Psi_L^{0\uparrow}(z')}{\partial^2 z'} \right] \Psi_R^{\downarrow 0}(z') dz'. \end{aligned}$$

One may introduce the respective A_{L1}, and A_{L2} parameters according to:

$$A_{L1} = \int_{-\infty}^{0} \Psi_L^{\uparrow 0}(z') \left[-\frac{i\gamma\xi^2}{2}\frac{\partial}{\partial z'} + \frac{i\gamma\xi}{2}\frac{\partial^2}{\partial z'^2} \right] \Psi_R^{\downarrow 0}(z')dz', \tag{185}$$

and

$$A_{L2} = \int_{-\infty}^{0} \left[\frac{i\gamma\xi^2}{2}\frac{\partial \Psi_L^{0\uparrow}(z')}{\partial z'} + \frac{i\gamma\xi}{2}\frac{\partial^2 \Psi_L^{0\uparrow}(z')}{\partial^2 z'} \right] \Psi_R^{\downarrow 0}(z')dz',$$

so that:

$$\tau_L = \frac{m^*}{i\hbar^2 k_1}\left(A_{L1} + A_{L2}\right).$$

We then calculate A_{L1}, and A_{L2}.

$$\begin{aligned}
2A_{L1} &= \int_{-\infty}^{0} \Psi_L^{0\uparrow}(z') \left(-i\xi^2\gamma\frac{\partial}{\partial z} + i\xi\gamma\frac{\partial^2}{\partial z^2} \right) \Psi_R^{\downarrow 0}(z')dz' \qquad (186)\\
&= \int_{-\infty}^{0} t_{L\uparrow} e^{k_2 z'} \left\{ -i\gamma\xi^2\frac{\partial}{\partial z'} + i\gamma\xi\frac{\partial^2}{\partial z'^2} \right\} \left(e^{ik_1 z'} + r_{R\downarrow} e^{-ik_1 z'} \right) dz'\\
&= \int_{-\infty}^{0} t_{L\uparrow} e^{k_2 z'} \left\{ -i\gamma\xi^2\frac{\partial}{\partial z'} \right\} \left(e^{ik_1 z'} + r_{R\downarrow} e^{-ik_1 z'} \right) dz'\\
&\quad + \int_{-\infty}^{0} t_{L\uparrow} e^{k_2 z'} \left\{ i\gamma\xi\frac{\partial^2}{\partial z'^2} \right\} \left(e^{ik_1 z'} + r_{R\downarrow} e^{-ik_1 z'} \right) dz'\\
&= \int_{-\infty}^{0} t_{L\uparrow} e^{k_2 z'} \left(-i\gamma\xi^2 \right) (ik_1)(e^{ik_1 z'} - r_{R\downarrow} e^{-ik_1 z'})dz'\\
&\quad + \int_{-\infty}^{0} t_{L\uparrow} e^{k_2 z'} (i\gamma\xi)(-k_1^2) \left(e^{ik_1 z'} + r_{R\downarrow} e^{-ik_1 z'} \right) dz'\\
&= \int_{-\infty}^{0} t_{L\uparrow}\gamma\xi^2 k_1 e^{k_2 z'} (e^{ik_1 z'} - r_{R\downarrow} e^{-ik_1 z'})dz'\\
&\quad + \int_{-\infty}^{0} -it_{L\uparrow}\gamma\xi k_1^2 e^{k_2 z'} \left(e^{ik_1 z'} + r_{R\downarrow} e^{-ik_1 z'} \right) dz'
\end{aligned}$$

If one defines (I) as:

$$\begin{aligned}
(I) &= \int_{-\infty}^{0} t_{L\uparrow}\gamma\xi^2 k_1 e^{k_2 z'} (e^{ik_1 z'} - r_{R\downarrow} e^{-ik_1 z'})dz' \qquad (187)\\
&= \int_{-\infty}^{0} t_{L\uparrow}\gamma\xi^2 k_1 \left(e^{(k_2+ik_1)z'} - r_{R\downarrow} e^{(k_2-ik_1)z'} \right) dz'\\
&= t_{L\uparrow}\gamma\xi^2 k_1 \left\{ \frac{1}{k_2+ik_1} - \frac{r_{R\downarrow}}{k_2-ik_1} \right\} = \frac{t_{L\uparrow}\gamma\xi^2 k_1}{k_1^2+k_2^2}\left\{ (k_2 - ik_1) - r_{R\downarrow}(k_2+ik_1) \right\}\\
&= \frac{t_{L\uparrow}\gamma\xi^2 k_1}{k_1^2+k_2^2}\frac{2(k_2^2-k_1^2)}{k_2-ik_1} = \frac{2t_{L\uparrow}\gamma\xi^2 k_1(k_2^2-k_1^2)}{(k_1^2+k_2^2)(k_2-ik_1)}
\end{aligned}$$

with

$$
\begin{aligned}
k_2 - ik_1 - r_{R\downarrow}(k_2 + ik_1) &= (k_2 - ik_1) - \frac{k_1 - ik_2}{k_1 + ik_2}(k_2 + ik_1) \\
&= (k_2 - ik_1) + \frac{(k_2 + ik_1)(k_2 + ik_1)}{k_2 - ik_1} \\
&= \frac{(k_2 - ik_1)^2 + (k_2 + ik_1)^2}{k_2 - ik_1} = \frac{2(k_2^2 - k_1^2)}{k_2 - ik_1}
\end{aligned}
$$

and

$$
\begin{aligned}
(II) &= \int_{-\infty}^{0} -it_{L\uparrow}\gamma\xi k_1^2 e^{k_2 z'} \left(e^{ik_1 z'} + r_{R\downarrow} e^{-ik_1 z'} \right) dz' \qquad (188) \\
&= \int_{-\infty}^{0} -it_{L\uparrow}\gamma\xi k_1^2 (e^{(k_2 + ik_1)z'} + r_{R\downarrow} e^{(k_2 - ik_1)z'}) dz' \\
&= -it_{L\uparrow}\gamma\xi k_1^2 \left(\frac{1}{k_2 + ik_1} + \frac{r_{R\downarrow}}{k_2 - ik_1} \right) \\
&= \frac{-it_{L\uparrow}\gamma\xi k_1^2}{(k_1^2 + k_2^2)} \left\{ (k_2 - ik_1) + r_{R\downarrow}(k_2 + ik_1) \right\} \\
&= \frac{-it_{L\uparrow}\gamma\xi k_1^2}{(k_1^2 + k_2^2)} \frac{-4ik_1 k_2}{(k_2 - ik_1)} = \frac{-4t_{L\uparrow}\gamma\xi k_1^3 k_2}{(k_1^2 + k_2^2)(k_2 - ik_1)}
\end{aligned}
$$

with

$$
\begin{aligned}
(k_2 - ik_1) + r_{R\downarrow}(k_2 + ik_1) &= (k_2 - ik_1) + \frac{k_1 - ik_2}{k_1 + ik_2}(k_2 + ik_1) \\
&= (k_2 - ik_1) - \frac{(k_2 + ik_1)(k_2 + ik_1)}{k_2 - ik_1} \\
&= \frac{(k_2 - ik_1)^2 - (k_2 + ik_1)^2}{k_2 - ik_1} = \frac{-4ik_1 k_2}{k_2 - ik_1}
\end{aligned}
$$

$$
\begin{aligned}
2A_{L1} &= (I) + (II) \qquad (189) \\
&= \frac{2t_{L\uparrow}\gamma\xi^2 k_1 (k_2^2 - k_1^2)}{(k_1^2 + k_2^2)(k_2 - ik_1)} - \frac{4t_{L\uparrow}\gamma\xi k_1^3 k_2}{(k_1^2 + k_2^2)(k_2 - ik_1)}
\end{aligned}
$$

$$
\begin{aligned}
2A_{L2} &= \left\{ \int_{-\infty}^{0} \left(i\xi^2\gamma \frac{\partial \Psi_L^0(z')}{\partial z'} + i\xi\gamma \frac{\partial^2 \Psi_L^0(z')}{\partial z'^2} \right) \Psi_R^0(z') dz' \right\} \qquad (190) \\
&= \int_{-\infty}^{0} \left(e^{ik_1 z'} + r_{R\downarrow} e^{-ik_1 z'} \right) \left(i\gamma\xi^2 \frac{\partial}{\partial z'} + i\gamma\xi \frac{\partial^2}{\partial z'^2} \right) t_{L\uparrow} e^{k_2 z'} dz' \\
&= \int_{-\infty}^{0} \left(e^{ik_1 z'} + r_{R\downarrow} e^{-ik_1 z'} \right) \left(i\gamma\xi^2 k_2 + i\gamma\xi k_2^2 \right) t_{L\uparrow} e^{k_2 z'} dz' \\
&= i\gamma\xi k_2 t_{L\uparrow} (\xi + k_2) \int_{-\infty}^{0} (e^{(ik_1+k_2)z'} + r_{R\downarrow} e^{(k_2 - ik_1)z'}) dz' \\
&= i\gamma\xi k_2 t_{L\uparrow} (\xi + k_2) \left\{ \frac{1}{ik_1 + k_2} + r_{R\downarrow} \frac{1}{k_2 - ik_1} \right\} \\
&= \frac{i\gamma\xi k_2 t_{L\uparrow}}{k_2^2 + k_1^2} (\xi + k_2) \left\{ (k_2 - ik_1) + r_{R\downarrow} ik_1 + k_2 \right\} \\
&= \frac{i\gamma\xi k_2 t_{L\uparrow}}{k_2^2 + k_1^2} (\xi + k_2) \frac{-4ik_1 k_2}{k_2 - ik_1} = \frac{4t_{L\uparrow}\gamma\xi k_1 k_2^2 (\xi + k_2)}{(k_2^2 + k_1^2)(k_2 - ik_1)}
\end{aligned}
$$

$$
\begin{aligned}
\tau_L &= \frac{m^*}{i\hbar^2 k_1} (A_{L1} + A_{L2}), \\
&= \frac{m^*}{i\hbar^2 k_1} \left[\frac{t_{L\uparrow}\gamma\xi^2 k_1 (k_2^2 - k_1^2)}{(k_1^2 + k_2^2)(k_2 - ik_1)} - \frac{2t_{L\uparrow}\gamma\xi k_1^3 k_2}{(k_1^2 + k_2^2)(k_2 - ik_1)} + \frac{2t_{L\uparrow}\gamma\xi k_1 k_2^2 (\xi + k_2)}{(k_2^2 + k_1^2)(k_2 - ik_1)} \right] \\
&= \frac{m^*}{i\hbar^2 k_1} \frac{t_{L\uparrow}\gamma\xi k_1}{(k_1^2 + k_2^2)(k_2 - ik_1)} \left[\xi(k_2^2 - k_1^2) - 2k_1^2 k_2 + 2k_2^2 (\xi + k_2) \right] \\
&= \frac{m^*}{i\hbar^2 k_1} \frac{2k_1}{k_1 + ik_2} \frac{\gamma\xi k_1}{(k_1^2 + k_2^2)(k_2 - ik_1)} \left[\xi(3k_2^2 - k_1^2) + 2k_2 \left(k_2^2 - k_1^2 \right) \right] \\
&= \frac{2m^*}{\hbar^2} \frac{\gamma\xi k_1}{(k_1 + ik_2)^2 (k_1^2 + k_2^2)} \left\{ \xi(3k_2^2 - k_1^2) + 2k_2 \left(k_2^2 - k_1^2 \right) \right\}.
\end{aligned}
$$

With the following notations, $k_1 = K$ (incoming propagative wavevector) and $k_2 = \lambda K$ (imaginary transmitted wavevector), one obtains:

$$
\begin{aligned}
\tau_L &= \frac{2m^*}{\hbar^2} \frac{\gamma\xi K}{(K + i\lambda K)^2 (K^2 + \lambda^2 K^2)} \left\{ \xi(3\lambda^2 K^2 - K^2) + 2\lambda K \left(\lambda^2 K^2 - K^2 \right) \right\} \\
&= \frac{2m^*}{\hbar^2} \frac{\gamma\xi K}{K^4 (1 + i\lambda)^2 (1 + \lambda^2)} K^3 \left\{ \frac{\xi}{K} (3\lambda^2 - 1) + 2\lambda \left(\lambda^2 - 1 \right) \right\} \\
&= \frac{1}{\gamma_C} \frac{\gamma\xi}{(1 + i\lambda)^2 (1 + \lambda^2)} \left\{ \frac{\xi}{K} (3\lambda^2 - 1) + 2\lambda \left(\lambda^2 - 1 \right) \right\} \\
&= \frac{1}{\gamma_C K^2 (1 + \lambda^2)} \frac{\gamma\xi K^2}{(1 + i\lambda)^2} \left\{ \frac{\xi}{K} (3\lambda^2 - 1) + 2\lambda \left(\lambda^2 - 1 \right) \right\} \\
&= \frac{1}{2w} \frac{\gamma\xi K^2}{(1 + i\lambda)^2} \left\{ \frac{\xi}{K} (3\lambda^2 - 1) + 2\lambda \left(\lambda^2 - 1 \right) \right\}.
\end{aligned}
$$

B.2.2 Case of spin-orbit interactions on the right for incoming left electrons

$$\begin{aligned}\tau_R &= \frac{m^*}{i\hbar^2 k_1}\int_0^{+\infty}\Psi_L^{0\uparrow}(z')\left[-\frac{i\gamma\xi^2}{2}\frac{\partial}{\partial z'}+\frac{i\gamma\xi}{2}\frac{\partial^2}{\partial z'^2}\right]\Psi_R^{\downarrow 0}(z')dz' \\ &+\frac{m^*}{i\hbar^2 k_1}\int_0^{+\infty}\left[\frac{i\gamma\xi^2}{2}\frac{\partial\Psi_L^{0\uparrow}(z')}{\partial z'}+\frac{i\gamma\xi}{2}\frac{\partial^2\Psi_L^{0\uparrow}(z')}{\partial^2 z'}\right]\Psi_R^{\downarrow 0}(z')dz'.\end{aligned}$$

Let us introduce the notations A_{R1}, and A_{R2}.

$$\begin{aligned}A_{R1} &= \int_0^{+\infty}\left(e^{-ik_1 z'_>}+r_{L\uparrow}e^{ik_1 z'_>}\right)\left\{-i\gamma\xi^2\frac{\partial}{\partial z'}+i\gamma\xi\frac{\partial^2}{\partial z'^2}\right\}t_{R\downarrow}e^{-k_2 z'_>}dz' \\ &= \int_0^{+\infty}\left(e^{-ik_1 z'_>}+r_{L\uparrow}e^{ik_1 z'_>}\right)(i\gamma\xi)(\xi k_2+k_2^2)t_{R\downarrow}e^{-k_2 z'_>}dz' \\ &= i\gamma\xi k_2(\xi+k_2)t_{R\downarrow}\int_0^{+\infty}(e^{-(ik_1+k_2)z'}+r_{L\uparrow}e^{(ik_1-k_2)z'})dz' \\ &= -i\gamma\xi k_2(\xi+k_2)t_{R\downarrow}\int_0^{-\infty}(e^{(ik_1+k_2)z'}+r_{L\uparrow}e^{(k_2-ik_1)z'})dz' \\ &= i\gamma\xi k_2(\xi+k_2)t_{R\downarrow}\int_{-\infty}^{0}(e^{(ik_1+k_2)z}+r_{L\uparrow}e^{(k_2-ik_1)z})dz' \\ &= i\gamma\xi k_2(\xi+k_2)t_{R\downarrow}\left\{\frac{1}{(ik_1+k_2)}+r_{L\uparrow}\frac{1}{(k_2-ik_1)}\right\} \\ &= \frac{i\gamma\xi k_2(\xi+k_2)t_{R\downarrow}}{(k_1^2+k_2^2)}\left\{(k_2-ik_1)+r_{L\uparrow}(ik_1+k_2)\right\} \\ &= \frac{i\gamma\xi k_2(\xi+k_2)t_{R\downarrow}}{(k_1^2+k_2^2)}\frac{-4ik_1k_2}{k_2-ik_1} \\ &= \frac{4\gamma\xi k_1k_2^2(\xi+k_2)t_{R\downarrow}}{(k_1^2+k_2^2)(k_2-ik_1)}\end{aligned} \tag{191}$$

$(k_2-ik_1)+r_{L\uparrow}(ik_1+k_2)=(k_2-ik_1)+\frac{k_1-ik_2}{k_1+ik_2}(ik_1+k_2)=\frac{-4ik_1k_2}{k_2-ik_1}$

$$\begin{aligned}A_{R2} &= \int_0^{+\infty}\left\{i\gamma\xi^2\frac{\partial\left(e^{-ik_1z'}+r_{L\uparrow}e^{ik_1z'}\right)}{\partial z'}+i\gamma\xi\frac{\partial^2\left(e^{-ik_1z'}+r_{L\uparrow}e^{ik_1z'}\right)}{\partial z'^2}\right\}t_{R\downarrow}e^{-k_2z'}dz' \\ &= \int_0^{+\infty}t_{R\downarrow}e^{-k_2z'}(i\gamma\xi^2)\left(-ik_1e^{-ik_1z'}+ik_1r_{L\uparrow}e^{ik_1z'}\right)dz' \\ &\quad -\int_0^{+\infty}t_{R\downarrow}e^{-k_2z}(i\gamma\xi k_1^2)\left(e^{-ik_1z_>}+r_{L\uparrow}e^{ik_1z_>}\right)dz' \\ &= \int_0^{+\infty}t_{R\downarrow}\gamma\xi^2k_1(e^{-(ik_1+k_2)z'}-r_{L\uparrow}e^{-(k_2-ik_1)z'})dz' \\ &\quad -\int_0^{+\infty}t_{R\downarrow}(i\gamma\xi k_1^2)\left(e^{-(ik_1+k_2)z'}+r_{L\uparrow}e^{-(k_2-ik_1)z'}\right)dz' \\ &= \frac{2t_{R\downarrow}\gamma\xi^2k_1(k_2^2-k_1^2)}{(k_1^2+k_2^2)(k_2-ik_1)}-\frac{4t_{R\downarrow}\gamma\xi k_1^3k_2}{(k_1^2+k_2^2)(k_2-ik_1)}\end{aligned} \tag{192}$$

Therefore,

$$\begin{aligned}\tau_R &= \frac{m^*}{i\hbar^2 k_1}\left[\frac{A_{R1}+A_{R2}}{2}\right] \\ &= \frac{m^*}{i\hbar^2 k_1}\left[\frac{2\gamma\xi k_1 k_2^2(\xi+k_2)t_{R\downarrow}}{(k_1^2+k_2^2)(k_2-ik_1)} + \frac{t_{R\downarrow}\gamma\xi^2 k_1(k_2^2-k_1^2)}{(k_1^2+k_2^2)(k_2-ik_1)} - \frac{2t_{R\downarrow}\gamma\xi k_1^3 k_2}{(k_1^2+k_2^2)(k_2-ik_1)}\right].\end{aligned}$$

Because $t_{R\downarrow} = t_{L\uparrow}$, one can observe that $\tau_R = \tau_L$.

B.2.3 Case of SOI located in the barrier

$$\begin{aligned}\delta t^{\uparrow\downarrow} &= \frac{m^*}{i\hbar^2 k_1}\int_0^a \Psi_L^{0\uparrow}(z')\left[-\frac{i\gamma\xi^2}{2}\frac{\partial\Psi_R^{\downarrow 0}(z')}{\partial z} + \frac{i\gamma\xi}{2}\frac{\partial^2\Psi_R^{\downarrow 0}(z')}{\partial z^2}\right]dz' \\ &\quad + \frac{m^*}{i\hbar^2 k_1}\int_0^a \left[\frac{i\gamma\xi^2}{2}\frac{\partial\Psi_L^{0\uparrow}(z')}{\partial z} + \frac{i\gamma\xi}{2}\frac{\partial^2\Psi_L^{0\uparrow}(z')}{\partial z^2}\right]\Psi_R^{\downarrow 0}(z')dz',\end{aligned} \tag{193}$$

We use the first term in Eq. 193

$$\begin{aligned}2A_1 &= \int_0^a \Psi_L^{\uparrow 0}(z')\left(-i\xi^2\gamma\frac{\partial}{\partial z'} + i\xi\gamma\frac{\partial^2}{\partial z'^2}\right)\Psi_R^{\downarrow 0}(z')dz' \\ &= \int_0^a t_{_{L\uparrow}} e^{k_2(z'-a)}\left\{-i\gamma\xi^2\frac{\partial}{\partial z'} + i\gamma\xi\frac{\partial^2}{\partial z'^2}\right\}t_{R\downarrow}e^{-k_2 z}dz' \\ &= \int_0^a t_{_{L\uparrow}} e^{k_2(z'-a)}\left\{i\gamma\xi^2 k_2 + i\gamma\xi k_2^2\right\}t_{R\downarrow}e^{-k_2 z}dz' \\ &= \int_0^a e^{-k_2 a}t_{_{L\uparrow}}t_{R\downarrow}i\gamma\xi k_2(\xi+k_2)dz' \\ &= e^{-k_2 a}t_{_{L\uparrow}}t_{R\downarrow}i\gamma\xi k_2(\xi+k_2)a\end{aligned} \tag{194}$$

and the second term

$$\begin{aligned}2A_2 &= \int_0^a \left(i\xi^2\gamma\frac{\partial\Psi_L^{\uparrow 0}(z')}{\partial z'} + i\xi\gamma\frac{\partial^2\Psi_L^{\downarrow 0}(z')}{\partial z'^2}\right)\Psi_R^{\downarrow 0}(z')dz' \\ &= \int_0^a t_{R\downarrow}e^{-k_2 z'}\left\{i\gamma\xi^2\frac{\partial}{\partial z'} + i\gamma\xi\frac{\partial^2}{\partial z'^2}\right\}t_{_{L\uparrow}}e^{k_2(z'-a)}dz' \\ &= \int_0^a t_{R\downarrow}e^{-k_2(z'+a)}\left\{i\gamma\xi^2 k_2 + i\gamma\xi k_2^2\right\}t_{_{L\uparrow}}e^{k_2 z}dz' \\ &= e^{-k_2 a}t_{_{L\uparrow}}t_{R\downarrow}i\gamma\xi k_2(\xi+k_2)a\end{aligned} \tag{195}$$

One obtains:

$$
\begin{aligned}
\delta t^{\uparrow\downarrow} &= \frac{m^*}{i\hbar^2 k_1}\left(A_1 + A_2\right) \qquad (196)\\
&= e^{-k_2 a}\frac{m^*}{i\hbar^2 k_1}\left(t_{_{L\uparrow}} t_{R\downarrow}\right) i\gamma\xi k_2(\xi + k_2)a\\
&= e^{-k_2 a}\frac{m^*}{i\hbar^2 k_1}\left[\frac{2k_1}{k_1 + ik_2}\frac{2k_1}{k_1 + ik_2}\right] i\gamma\xi k_2(\xi + k_2)a\\
&= e^{-k_2 a}\frac{2m^*}{\hbar^2}\frac{2k_1\gamma\xi k_2(\xi + k_2)a}{\left(k_1 + ik_2\right)^2}\\
&= \frac{e^{-k_2 a}}{\gamma_c}\frac{2\gamma\xi k_2 k_1 a}{\left(k_1 + ik_2\right)^2}(\xi + k_2).
\end{aligned}
$$

REFERENCES

[1] M. N. Baibich, J. M. Broto, A. Fert, F. Nguyen Van Dau, F. Petroff, P. Etienne, G. Creuzet, A. Friederich, and J. Chazelas, Phys. Rev. Lett. **61**, 2472 (1988).

[2] G. Binasch, P. Griinberg, F. Saurenbach, and W. Zinn, Phys. Rev. B **39** (1998).

[3] M. Jullière, Phys. Lett. **54A**, 225 (1975).

[4] S. Datta, B. Das, Appl. Phys. Lett. **56**, 665 (1990).

[5] S. Murakami, N. Nagaosa, S.-Ch. Zhang, Sci. **5**, 301 (2003).

[6] J. Sinova, D. Culcer, Q. Niu, N. A. Sinitsyn, T. Jungwirth, and A. H. MacDonald, Phys. Rev. Lett. **9** (2004).

[7] J.E. Hirsch . Phys. Rev. Lett. **83** (1999).

[8] M.I. Dyakonov and V.I. Perel. Phys. Lett. A. **35** (1971).

[9] L. K. Zou, S. H. Wang, Y. Zhang, J. R. Sun,1 J. W. Cai, and S. S. Kang, Phys. Rev. B **93**, 014422 (2016).

[10] G. Dresselhaus, Phys. Rev. **100**, 580 (1956).

[11] V. I. Perel', S. A. Tarasenko, and I. N. Yassievich, Phys. Rev. B **67**, 201304 (R) (2003).

[12] Nguyen Thi Lam Hoai, Spin properties of evanescent states and tunneling in semiconductors, PhD thesis Ecole Polytechnique (2010).

[13] S. A. Tarasenko, V. I. Perel', and I. N. Yassievich, Phys. Rev. Lett. **93**, 056601 (2004).

[14] M. M. Glazov, P. S. Alekseev, M. A. Odnoblyudov, V. M. Chistyakov, S. A. Tarasenko, and I. N. Yassievich, Phys. Rev B **71**, 155313 (2005).

[15] P. S. Alekseev, M. M. Glazov, and S. A. Tarasenko, Phys. Rev. B **89**, 155306 (2014).

[16] A. Matos-Abiague and J. Fabian, Phys. Rev. Lett **115**, 056602 (2015).

[17] J.C. Rojas-Sánchez, L. Vila, G. Desfonds, S. Gambarelli, J. P. Attané, J. M. De Teresa, C. Magén, and A. Fert, Nat. Comm (2013).

[18] T. Huong Dang, H. Jaffrès, T. L. Hoai Nguyen, and H.-J. Drouhin, Phys. Rev. B **92**, 060403 (2015).

[19] T. Huong Dang, E. Erina, T. L. Hoai Nguyen, H. Jaffrès, and H.-J. Drouhin, SPIE proceedings 9931-78 (2016) (invited paper).

[20] M. Elsen, H. Jaffrès, R. Mattana, L. Thevenard, A. Lemaitre, and J.-M. George, Phys. Rev. B **76**, 144415 (2007).

[21] G. F. Koster, J. O. Dimmock, R. G. Wheeler, and H. Statz, Properties of the Thirty-Two Point Groups (M.I.T Press, Cambridge, Massachusetts, U.S.A, (1963).

[22] Guy Fishman "Semi-conducteurs les bases de la theorie k.p", édition de l'École Polytechnique (2010).

[23] J. Bardeen, Phys. Rev. Lett. **6**, 57 (1961).

[24] W. A. Harrison, Phys. Rev. **123**, 85 (1961).

[25] J. C. Slonczewski, Phys. Rev. B **39**, 6995 (1989).

[26] T. Dietl, H. Ohno and F. Matsukura, Phys. Rev. B **63**, 195205 (2001).

[27] M. Abolfath, A. H. MacDonald, and Leo Radzihovsky, Phys. Rev. B **68**, 155318 (2003).

[28] A.Voskoboynikov et al, Phys. Rev. B **59**, 12514 (1999).

[29] E. A. de Andrada et all, E. A. de Andrada e Silva and G. C. La Rocca, Phys. Rev. B **59**(R), 15583 (1999).

[30] A. Zakharova, K. Nilsson, K. A. Chao, and S. T. Yen, Phys. Rev. B **72**, 115329 (2005).

[31] T. L. Nguyen, H.-J. Drouhin, J.-E. Wegrowe, and G. Fishman, Phys. Rev. B **79**, 165204 (2009).

[32] M. I. D'yakonov and V. I. Perel', Sov. Phys. Solid State **13**, 3023 (1972).

[33] D. J. BenDaniel and C. B. Duke, Phys. Rev. **152**, 683, 121202(R) (1966).

[34] J.-M. Jancu, R. Scholz, E. A. de Andrada e Silva, and G. C. La Rocca, Phys. Rev. B **72**, 193201 (2005).

[35] H. Ohno, H. Munekata, T. Penney, S. von Moln r, and L. L.Chang, Phys. Rev. Lett. **68**, 2664 (1992).

[36] H. Ohno, A. Shen, F. Matsukura, A. Oiwa, A. Endo, S. Katsumoto, and Y. Iye, Appl. Phys. Lett. **69**, 363 (1996).

[37] A. Haury, A. Wasiela, A. Arnoult, J. Cibert, S. Tatarenko, T.Dietl, and Y. Merle d'Aubigné, Phys. Rev. Lett. **79**, 511 (1997).

[38] D. Ferrand, C. Bourgognon, J. Cibert, A. Wasiela, S. Tatarenko, Y. Merle d'Aubigné, A. Bonnani, D. Stifter, H. Sitter, V.K Le, S. Koleśnik , J. Jaroszyński, M. Sawicki, T. Andrearczyk, and T. Dietl, Physica B **1177** (2000).

[39] F. Matsukura, H. Ohno, A. Shen, and Y. Sugawara, Phys. Rev. B **57**, R2037 (1998).

[40] A. Oiwa, S. Katsumoto, A. Endo, M. Hirasawa, Y. Iye, H. Ohno, F. Matsukura, A. Shen, and Y. Sugawara, Solid State Commun. **103**, 209 (1997).

[41] A. Van Esch, L. Van Bockstal, J. De Boeck, G. Verbanck, A. S.van Steenbrgen, P. J. Wellmann, B. Grietens, R. Bogaerts, F.Herlach, and G. Borghs, Phys. Rev. B **56**, 13 103 (1997).

[42] H. Shimizu, T. Hayashi, T. Nishinaga, and M. Tanaka, Appl.Phys. Lett. **74**, 398 (1999).

[43] M. Cardona and F. Pollak, Phys. Rev. **142**, 530 (1966).

[44] M. Cardona, N. E. Christensen, and G. Fasol, Phys. Rev. B **38**, 1806 (1988).

[45] R. K. Hayden, D. K. Maude, L. Eaves, E. C. Valadares, M. Henini, F. W. Sheard, O. H. Hughes, J. C. Portal, and L. Cury, Phys. Rev. Lett. **66**, 1749 (1991).

[46] I. Vurgaftman, J. R. Meyer, and L. R. Ram-Mohan, J. Appl. Phys. **89**, 5815 (2001).

[47] E.O. Kane: J. Phys. Chem. Solids **1**, 249 (1957)

[48] E.O. Kane: "The **k**.**p** method", in Semiconductors and Semimetals, ed. by R.K. Willardson, A.C. Beer, Vol. **1** (Academic Press, New York) (1966).

[49] E.O. Kane: "Energy band theory", in Handbook on Semiconductors, ed. by T.S. Moss, W. Paul, Vol. **1** (North-Holland, Amsterdam, 1982).

[50] A. Elçi and E. D. Jones, Phys. Rev. B **34**, 8611, (1986).

[51] G. Dresselhaus, A.F. Kip, C. Kittel: Phys. Rev. **98(2)**, 368–384 (1955).

[52] G.F. Koster: "Space groups and their representations", in Solid State Phys.,ed. by F. Seitz, D. Turnbull, Vol. **5** (Academic Press, New York), (1957).

[53] R. Winkler, ISSN :0081-3869, Springer-Verlag Berlin Heidelberg (2003).

[54] J. M. Luttinger, Phys. Rev. **102**, 1030 (1956).

[55] J. M. Luttinger and W. Kohn, Phys. Rev. **97**, 869 (1955).

[56] M. V. Durnev, M. M. Glazov, and E. L. Ivchenko, Phys. Rev. B **89**, 075430 (2014).

[57] S. Richard, F. Aniel, and G. Fishman, Phys. Rev. B **70**, 235204 (2004).

[58] N. A. Cukaric, M. Z . Tadic, B. Partoens, and F. M. Peeters, Phys. Rev. B **88**, 205306 (2013).

[59] B. A. Foreman, Phys. Rev. Lett **80**, 3823, (1998).

[60] K. I. Kolokolov, J. Li, and C. Z. Ning, Phys. Rev. B **68**, 161308R, (2003).

[61] S. Vajna, E. Simon, A. Szilva, K. Palotas, B. Ujfalussy, and L. Szunyogh, Phys. Rev. B **85**, 075404 (2012).

[62] E. Simon, A. Szilva, B. Ujfalussy, B. Lazarovits, G. Zarand, and L. Szunyogh, Phys. Rev. B **81**, 235438 (2010).

[63] D. L. Smith, C. Mailhiot, Phys. Rev. B **33**, 8345 (1986).

[64] F. Szmulowicz, Phys. Rev. B **54**, 11539 (1996).

[65] M.F.H. Schuurmans and G.W. 't Hooft, Phys. Rev. B **31**, 8041 (1985).

[66] R. Eppenga, M.F.H. Schuurmans, and S. Colak, Phys. Rev. B **36**, 1554 (1987).

[67] R. Winkler and U. Ro¨ssler, Phys. Rev. B **48**, 8918 (1993).

[68] A.T. Meney, Besire Gonul, and E.P. O'Reilly, Phys. Rev. B **50**, 10 893 (1994).

[69] Soline Richard, Modélisation physique de la structure électronique, du transport et de l'ionisation par choc dans les matériaux IV-IV massifs, contraints et dans les puits quantiques, PhD thesis Université Paris XI Orsay (2005).

[70] M. Abolfath, T. Jungwirth, J. Brum, and A. H. MacDonald, Phys. Rev. B **63**, 054418 (2001).

[71] D. Wortmann, H. Ishida,and S. Blügel, Phys. Rev. B **65**, 165103 (2002).

[72] D. Wortmann, H. Ishida,and S. Blügel, Phys. Rev. B **66**, 075113 (2002).

[73] H. Ishida, D. Wortmann, and T. Ohwaki, Phys. Rev. B **70**, 085409 (2004).

[74] N. Cavassilas, F. Aniel, K. Boujdaria, and G. Fishman, Phys. Rev. B **64**, 115207 (2001).

[75] P. Vogl, J. Hjalmarson, and J.D. Dow, J. Phys. Chem. Solids **44**, 365 (1983).

[76] P. M. Haney, H.-W Lee, K.-J Lee, A. Manchon, and M. D. Stiles, Phys. Rev. B **87**, 174411 (2013).

[77] K. Olejník, V. Novák, J. Wunderlich, and T. Jungwirth, Phys. Rev. B **91**, 180402(R) (2015).

[78] V. P. Amin, M. D. Stiles, Phys. Rev. B **94**, 104419 (2016).

[79] V. P. Amin, M. D. Stiles, Phys. Rev. B **94**, 104420 (2016).

[80] C. O. Avci, K. Garello, A. Ghosh, M. Gabureac, S. F.Alvarado, and P. Gambardella, Nat. Phys. **11**, 570 (2015).

[81] C. O. Avci, K. Garello, J. Mendil, A. Ghosh, N. Blasakis, M.Gabureac, M. Trassin, M. Fiebig, and P. Gambardella, Appl. Phys. Lett. **107**, 192405 (2015).

[82] J. Kim, P. Sheng, S. Takahashi, S. Mitani, and M. Hayashi, Phys. Rev. Lett. **116**, 097201 (2016).

[83] E. L. Ivchenko and A. Yu. Kaminski, U. Rössler, Phys. Rev. B **54**, 8 (1996).

[84] R. Wessel, M. Altarelli, Phys. Rev. B **37**, 17 (1989).

[85] A .G. Petukhov, A. N. Chantis, and D. O. Demchenko, Phys. Rev. Lett. **89**, 107205 (2002).

[86] P. M. Haney and M. D. Stiles, Phys. Rev. Lett. **105**, 126602 (2010).

[87] A. Kalitsov, M. Chshiev, I. Theodonis, N. Kioussis, and W. H. Butler, Phys. Rev. B **79**, 174416 (2009).

[88] W. H. Butler, Sci. Technol. Adv. Mater. **9**, 014106 (2008).

[89] S. Datta "Electronic transport in Mesoscopic Systems", Cambridge Univ. Press, Cambridge, (1995).

[90] R. Pérez-Alvarez, F. Garcia-Moliner, Transfer matrix, Green function and related techniques, Universitat Jaume I (2004).

[91] A. Hoffmann, IEEE Trans. Magn. **49**, 5172-5193 (2013).

[92] L. Liu, O. J. Lee, T.J. Gudmundsen, D. C. Ralph, and R. A. Buhrman, Phys. Rev. Lett. **109**, 096602 (2012).

[93] I. M. Miron, G. Gaudin, S. Auffret, B. Rodmacq et al., Nat. Mat. **9**, 230-234 (2010).

[94] K. Garello, I. M. Miron, C. O. Avci, F. Freimuth et al., Nat. Nano. **8**, 587-593 (2013).

[95] Y. A. Bychkov and E. I. Rashba, Sov. Phys. JETP Lett. **39**, 78 (1984).

[96] K. Shen, G. Vignale, and R. Raimondi, Phys. Rev. Lett. **112**, 096601 (2014).

[97] E. Lesne et al., Nat. Comm. **5** (2014).

[98] J.-C. Rojas-Sánchez, N. Reyren, P. Laczkowski, W. Savero, J.-P. Attané, C. Deranlot, M. Jamet, Phys. Rev. Lett. **112**, 106602 (2014).

[99] Y. Liu, Z. Yuan, R. J. H. Wesselink, A. A. Starikov, and P. J. Kelly, Phys. Rev. Lett. **113**, 207202 (2014).

[100] O. Krupin, G. Bihlmayer, K. Starke, S. Gorovikov, J. E. Prieto, K. Döbrich, S. Blügel, and G. Kaindl, Phys. Rev. B **71**, 201403(R) (2005).

[101] G. Bihlmayer, Y. Koroteev, Y. M. Echenique et al., surface science **600**, 3888-3891 (2006).

[102] O. Krupin, G. Bihlmayer, K. M. Dobrich, J. E. Prieto, K. Starke, S. Gorovikov, S. Blügel, S. Kevan, and G Kaindl, New. Journ. of Physics **11**, 013035 (2009).

[103] W. H. Butler, X.-G. Zhang, and T. C. Schulthess, Phys. Rev. B **63**, 054416 (2001).

[104] B. Scharf, A. Matos-Abiague, J. E. Han, E. M. Hankiewicz, and I. Žutić, Phys. Rev. Lett. **117**, 166806 (2016).

[105] A. Vedyayev, N. Ryzhanova, N. Strelkov, and B. Dieny, Phys. Rev. Lett. **110**, 247204 (2013).

[106] P. S. Alekseev, JETP Lett. **92**, 788 (2010).

[107] P. C. van Son, H. van Kempen, and P. Wyder, Phys. Rev. Lett. **58**, 2271 (1987).

[108] T. Valet and A. Fert, Phys. Rev. B **48**, 7099 (1993).

[109] An asymmetry also occurs when a single magnetic electrode is considered (Region I) and a paramagnet in Region II, both in AP and PA configurations or when two different ferromagnets are considered. This would lead to four different resistance states. On the other hand, the case of Rashba interactions *via* an external electric field leading to a curvature of the band profile is excluded from this discussion. This can lead to asymmetry of scattering in the parallel case.

[110] H.-J. Drouhin, G. Fishman, and J.-E. Wegrowe, Phys. Rev. B **83**, 113307 (2011).

[111] F. Bottegoni, H.-J. Drouhin, G. Fishman, and J.-E. Wegrowe, Phys. Rev. B **85**, 235313 (2012).

[112] Marc Elsen, Magnétorésistances et transfert de spin dans des hétérostructures tunnel à base de (Ga,Mn)As, PhD thesis Universite Paris VI (2007).

[113] M. Elsen, O. Boulle, J.-M. George, H. Jaffrès, R. Mattana, V. Cros, A. Fert, A. Lemaitre, R. Giraud, and G. Faini, Phys. Rev. B **73**, 035303 (2006).

[114] M. Elsen, H. Jaffrès, R. Mattana, M. Tran, J.-M. George, A. Miard, and A. Lemaitre, Phys. Rev. Lett. **99**, 127203 (2007).

[115] This fact immediatly proves that the effect we describe does not exist in the spin filtering asymmetry considered in Refs. 10 and 11, where the DP spin-orbit Hamiltonian reduces to $\gamma\left(\widehat{\sigma}_x k_x - \widehat{\sigma}_y k_y\right)\partial^2/\partial z^2$, the term proportional to $\widehat{\sigma}_z$ being neglected.

[116] Transport now involves the $D\left(\xi, k_1, k_2\right)$ coefficient which can be deduced from $C\left(\xi, k_1, k_2\right)$ by interchanging k_1 and k_2 as well as ξ to $-\xi$, resulting in the change of $\mathcal{A}\left(t, \eta\right)$ into $\mathcal{A}\left(-t, \eta\right) = -\mathcal{A}\left(t, \eta\right)$ (this can also be simply checked by symmetry considerations).

[117] P. Pfeffer and W. Zawadzki, Phys. Rev. B **41**, 1561 (1990).

[118] The boundary conditions at interfaces are: *i*) the continuity of the components of the envelope function, $\psi_n^+ + \sum_{\overline{n}} r_{n,\overline{n}}\psi_{\overline{n}}^- = \sum_{n'} t_{n,n'}\psi_{n'}^+$ where $(+)$ $[(-)]$ refer to wave functions propagating to the right (to the left), and $t_{n,n'}$ ($r_{n,\overline{n}}$) is the amplitude of the transmitted (reflected) wave in band n' ($\overline{n}$) for a normalized incident wave in band n; *ii*) the continuity of the components of the current wave, $\widehat{J}\psi_n^+ + \sum_{\overline{n}} r_{n,\overline{n}}\widehat{J}\psi_{\overline{n}}^- = \sum_{n'} t_{n,n'}\widehat{J}\psi_{n'}^+$. With conservation of $k_\parallel$, the multiband transmission writes $T_{n,n'}\left(\xi\right) = \left[t_{n,n'}\right]^* \, t_{n,n'} \left\langle \psi_{n'} \left| \widehat{J} \right| \psi_{n'} \right\rangle / \left\langle \psi_n \left| \widehat{J} \right| \psi_n \right\rangle$.

[119] Supplemental Material, Phys. Rev. B **92**, 060403 (2015).

[120] It can be checked that the THE voltage is of the order of $\rho/\delta L\left(\ell\right) t\mathcal{A}\left(t, \eta\right) J_z$, where$L$ is the lateral size of the junction and δ the thickness of the collecting channel.

[121] The relationship $\eta = \left(-t^2 + \mathcal{E}/w\right) / \left(1 + t^2\right)$ relates η to the reduced total energy $\mathcal{E}/w$ and the angular averaging is performed with $d\theta = dt/\left(1 + t^2\right)$.

[122] S. Sangiao, J. M. De Teresa, L. Morellon, I. Lucas, M. C. Martinez-Velarte, and M. Viret, Appl. Phys. Lett. **106**, 172403 (2015).

[123] B. Zimmermann, K. Chadova, D. Ködderitzsch, S. Blügel, H. Ebert, and D. V. Fedorov, Phys. Rev. B **90**, 220403(R) (2014).

[124] B. Zimmermann, H. L. Nguyen, P. Mavropoulos, S. Blügel, and Y. Mokrousov, Phys. Rev. B **94**, 060406(R) (2016).

[125] N. A. Sinitsyn, A. H. MacDonald, T. Jungwirth, V. K. Dugaev, and J. Sinova, Phys. Rev. B **75**, 045315 (2007).

[126] N. Nagaosa, J. Sinova, S. Onoda, A. H. MacDonald, N. P. Ong, Rev. Mod. Phys. **82,** No. 2, (2010).

[127] J. Sinova, S. O. Valenzuela, J. Wunderlich, C. H. Back, T. Jungwirth, Rev. Mod. Phys. **87,** (2015).

[128] S. Maekawa, S. O. Valenzuela, E. Saitoh, and T. Kimura, Spin Current (Vol. **17**). Oxford University Press. (2012).

[129] M. Gradhand, D. V. Fedorov, P. Zahn, and I. Mertig, Phys. Rev. Lett **104**, 186403 (2010).

[130] W. Zhang, M. B. Jungfleisch, W. Jiang, J. E. Pearson, and A. Hoffmann, J. Appl. Phys. **117**, 17C727 (2015).

[131] J. W. Negele, H. Orland, Quantum many particle systems, New York (1998).

[132] D. A. Stewart, W. H. Butler, X.-G. Zhang, and V. F. Los, Phys. Rev. B **68**, 014433 (2003).

[133] W. H. Butler, X.-G. Zhang, D. M. C. Nicholson, and J. M. MacLaren, Phys. Rev. B **52**, 13399 (1995).

[134] A. A. Lucas , H. Morawitz, G. R. Henry, J. P.Vigneron, P. Lambin, P. H. Cutler, and T. E. Feuchtwang, Phys. Rev. B, **37**, 10708, (1988).

[135] M. A. M. de Aguiar, Phys. Rev. A **48**, (1993**).**

[136] V. F. Los, and A. V. Los, Phy. Rev. B **77**, 024410 (2008).

[137] E. Y.Tsymbal, O. N. Mryasov, and P. R. LeClair, Condensed Matter, **15**(**4**), R109 (2003).

[138] S. Lowitzer, M. Gradhand, D. Ködderitzsch, V. F. Dmitry, I. Mertig, and H. Ebert, Phys. Rev. Lett **106**, 056601 (2011).

[139] Ph. Mavropoulous, Lecture Notes, 45th IFF Springschool, Jülich Forschungszentrum (2014).

[140] K. Yasuda, A. Tsukazaki, R. Yoshimi, K. S. Takahashi, M. Kawasaki, and Y. Tokura, Phys. Rev. Lett **117**, 127202 (2016).

[141] M. Jamet *et al.* Nature. Mat 1686 (2006).

[142] T. Devillers, M. Jamet, A. Barski, V. Poydenot, P. Bayle-Guillemaud, and E. Bellet-Amalric, Phys. Rev. B **76**, 205306 (2007).

[143] F. Bottegoni, A. Ferrari, F. Rortais, C. Vergnaud, A. Marty, G. Isella,1 M. Finazzi, M. Jamet, and F. Ciccacci, Phys. Rev. B **92**, 214403 (2015).

[144] K. Ando, M. Morikawa, T. Trypiniotis, Y. Fujikawa, C. H. W. Barnes, and E. Saitoh, App. Phys. Lett. **96**, 082502 (2010).

[145] A. Kalitsov, I. Theodonis, N. Kioussis, M. Chshiev, W. H. Butler, and A. Vedyayev, J. Appl. Phys **99**, 08G501 (2006).

[146] Y. Mokrousov, Lecture Notes, 40th IFF Springschool, Jülich Forschungszentrum (2009).

[147] P. Strange, Relativistic Quantum Mechanics: with applications in condensed matter and atomic physics. Cambridge University Press (1998).

[148] R. Kubo, J. Phys. Soc. Jpn. **12**, 570–586 (1957).

[149] G. Rickayzen, Green's functions and condensed matter, Academic Press, London (1980).

[150] G. D. Mahan, Physics of Solids and Liquids, 3rd ed. (Kluwer Academic, 2000).

Titre : Effet Tunnel Hall Anormal à l'interface de semi-conducteurs contrôlé par les interactions d'échange et spin-orbite. Etude dans le cadre d'une approche k.p étendue

Mots clés : transport tunnel dépendant du spin, spin-orbit, effet tunnel Hall, théorie **k**.**p**

Nous avons étudié par des méthodes numériques et en théorie **k.p** avancée les propriétés tunnel d'électrons et de trous dans des systèmes modèles et hétérostructures composés de semi-conducteurs impliquant des interactions spin-orbite de volume. Nous démontrons que le couplage entre les interactions spin-orbite et d'échange à l'interface de jonctions tunnel résulte en un fort contraste de transmission de porteurs selon le signe de la composante de leur vecteur d'onde dans le plan de la jonction. Cet effet conduit à un effet tunnel anormal d'interface que nous appelons « Effet Hall Tunnel Anormal » (ATHE). De façon similaire, des processus tunnel non-conventionnels se manifestant sur des isolants topologiques ont été prédits par d'autres auteurs. Alors que l'ensemble de ces effets Hall anormaux sont liés aux interactions spin-orbite, les effets tunnel anormaux diffèrent des effets Hall tunnel, des effets Hall et des effets Hall de spin par la forte amplitude prédite ainsi que par des phénomènes de chiralité. Ces propriétés possèdent un lien non-trivial avec la symétrie du système. L'ensemble de ces résultats démontre l'existence d'une nouvelle classe d'effets tunnel qui devaient être étudiés expérimentalement dans un futur proche. En ce qui concerne la bande de valence, nous démontrons, en utilisant un Hamiltonien 14x14 prolongeant un modèle 2x2, que le calcul décrivant l'ATHE repose sur un traitement subtil des états dits « spurious » (états non-physiques) et nous donnons quelques éléments d'amélioration et de compréhension. Dans ce mémoire de thèse, nous développons deux méthodes numériques pour résoudre le problème des états spurious en développant en parallèle des méthodes **k.p** respectivement à 14 bandes et 30 bandes afin de décrire des matériaux semi-conducteurs à gap indirect. Les calculs menés dans la bande de valence d'hétérostructures semi-conductrice incluant interfaces et barrières tunnel (approches 6x6 et 14x14) sans centre de symétrie d'inversion mettent en évidence des propriétés d'asymétrie équivalente à celles obtenues dans la bande de conduction. De tels effets sont interprétés, dans le cadre de calculs de perturbation en transport basés sur des techniques de fonctions de Green, par des effets chiraux orbitaux lors du branchement tunnel des fonctions évanescentes dans la barrière.

Titre : Interfacial skew tunneling in group III-V and group IV semiconductors driven by exchange and spin-orbit interactions; Study in the frame of an extended k.p theory

Key words: spin-dependent tunneling, spin-orbit, tunnel Hall effect, skew tunneling, **k**.**p** theory

The interplay of spin-orbit (SOI) and exchange interactions at interfaces and tunnel junctions results in spectacular transmission asymmetries and Anomalous Tunnel Hall Effects for electrons *and* holes (ATHE). Related tunneling phenomena in topological insulators have been predicted. While they all originate from the SOI anisotropy, ATHE differs from the tunneling Hall effect, spontaneous anomalous and spin Hall effects, or spin-galvanic effect, previously reported by its giant forward asymmetry and its chiral nature. All the results presented in this PhD report show that a new class of tunneling phenomena can now be investigated and experimentally probed. When valence bands (VB) are involved, we show - using by accurate 6x6, 14x14 or 30x30 **k.p** (indirect bandgap semiconductor) and a 2x2 toy model - that ATHE rely on a subtle treatment of the spurious (unphysical) states.Calculations performed in the valence bands, without inversion asymmetry, more astonishingly highlight the same trends in the asymmetry A which appears to be related to the difference of orbital chirality and to the related branching (overlap) of the corresponding evanescent wave functions responsible for the tunneling current. Besides, we built an analytical model and developed scattering perturbative techniques based on Green's function method to analytically deal with electrons and holes and to compare the output with numerical calculations. The agreement between the different approaches is very good. In the case of holes, the asymmetry appears to be robust and persists even when a single electrode is magnetic.